2014

Soil Chemical Insights Provided through Vibrational Spectroscopy

Sanjai J. Parikh
University of California Davis, sjparikh@ucdavis.edu

Keith W. Goyne
University of Missouri

Andrew J. Margenot
University of California Davis

Fungai N.D. Mukome
University of California Davis

Francisco J. Calderón
USDA-ARS, Central Great Plains Research Station

CHAPTER ONE

Soil Chemical Insights Provided through Vibrational Spectroscopy

Sanjai J. Parikh*,[1], Keith W. Goyne†, Andrew J. Margenot*, Fungai N.D. Mukome* and Francisco J. Calderón‡

*Department of Land, Air and Water Resources, University of California Davis, Davis, CA, USA
†Department of Soil, Environmental and Atmospheric Sciences, University of Missouri, Columbia, MO, USA
‡USDA-ARS, Central Great Plains Research Station, Akron, CO, USA
[1]Corresponding author: e-mail address: sjparikh@ucdavis.edu

Contents

Advances in Agronomy, Volume 126
ISSN 0065-2113, http://dx.doi.org/10.1016/B978-0-12-800132-5.00001-8

Abstract

Vibrational spectroscopy techniques provide a powerful approach to the study of environmental materials and processes. These multifunctional analytical tools can be used to probe molecular vibrations of solid, liquid, and gaseous samples for characterizing materials, elucidating reaction mechanisms, and examining kinetic processes. Although Fourier transform infrared (FTIR) spectroscopy is the most prominent type of vibrational spectroscopy used in the field of soil science, applications of Raman spectroscopy to study environmental samples continue to increase. The ability of FTIR and Raman spectroscopies to provide complementary information for organic and inorganic materials makes them ideal approaches for soil science research. In addition, the ability to conduct in situ, real time, vibrational spectroscopy experiments to probe biogeochemical processes at mineral interfaces offers unique and versatile methodologies for revealing a myriad of soil chemical phenomena. This review provides a comprehensive overview of vibrational spectroscopy techniques and highlights many of the applications of their use in soil chemistry research.

1. INTRODUCTION

Fourier transform infrared (FTIR) and Raman spectroscopies provide scientists with powerful analytical tools for studying the organic and inorganic components of soils and sediments. In addition to their utility for investigating sample mineralogy and organic matter (OM) composition, these techniques provide molecular-scale information on metal and organic sorption processes at the solid–liquid interface. As such, both mechanistic and kinetic studies of important biogeochemical processes can be

conducted. It is the versatility and accessibility of these vibrational spectroscopy techniques that make them a critical tool for soil scientists. In this review FTIR and Raman spectroscopy approaches are introduced and a comprehensive discussion of their applications for soil chemistry research is provided.

The primary objective of this review is to provide a synopsis of vibrational spectroscopy applications with utility for soil chemistry research. In doing so, FTIR and Raman spectroscopy will be presented, their sampling techniques introduced, and relevant studies discussed. Due to the large number of FTIR studies in the field of soil science and related disciplines far exceeding those for Raman, this review is heavily weighted towards FTIR. Additionally, emphasis will be placed on applications of vibrational spectroscopy for studying soil minerals, soil organic matter (SOM), bacteria and biopolymers, and various soil amendments (i.e. biochar, compost, biosolids). Particular attention is given to the analysis of OM in whole soils, fractions, and extracts. Molecular-scale analysis at the mineral–liquid interface and approaches for analyzing soil samples will also be discussed.

Vibrational spectroscopy approaches for studying soil, and the chemical processes occurring within, are some of the most versatile and user-friendly tools for scientists. Today, computer hardware and software capabilities continue to grow and the vast literature of vibrational spectroscopy studies is correspondingly expanding. As highlighted in this review, there is a wealth of information that can be garnered from these analysis techniques and the future of vibrational spectroscopy holds great promise for scientists working in the fields of soil and environmental sciences.

1.1 FTIR Spectroscopy

The development of the FTIR spectrometer relied on the prior invention of the Michelson interferometer by Albert Abraham Michelson in 1880 (Livingston, 1973). With the Michelson interferometer it became possible to accurately measure wavelengths of light. Although Jean Baptiste Joseph Fourier had previously developed the Fourier transform (FT), the calculations to convert the acquired interferograms to spectra remained cumbersome—even following the advent of computers. It was not until the development of the Cooley–Tukey Algorithm in 1965 (Cooley and Tukey, 1965) that computers could rapidly perform FT and modern FTIR spectroscopy became possible. The FTIR spectrometers that soon developed have remained relatively unchanged in recent decades, though advances in computer science have enabled new

methods for data collection, processing, and analysis. Today the methods of data acquisition are becoming increasingly sophisticated and the applications for FTIR continue to grow. Specific collection techniques, such as transmission, diffuse reflectance infrared Fourier transform spectroscopy (DRIFTS), and attenuated total reflectance (ATR) will be discussed later in this review.

Infrared microspectroscopy (IRMS) is a FTIR spectroscopy technique that is developing rapidly and providing exciting new experimental capabilities for soil scientists. The first documentation of combining infrared (IR) spectroscopy with microscopy are several studies from 1949 where the technique was applied to analyze tissue sections and amino acids (Barer et al., 1949; Blout and Mellors, 1949; Gore, 1949). This promising new technique offered imaging and chemical information of samples at a new level of resolution. However, as the two instruments were not integrated and computer technology was still in its infancy, the combination suffered from low signal to noise ratios and slow data processing (Katon, 1996; Shearer and Peters, 1987). Those interested in the early difficulties of these techniques are referred to Messerschmidt and Chase (1989) for details on the theory and causes of design failures in the early instruments. After about two decades, advances in computerization and IR spectroscopy instrumentation (i.e. interferometer, Fourier transformation, detectors) greatly increased the use and applicability of this analytical technique (Carr, 2001; Heymann et al., 2011; Hirschfeld and Chase, 1986; Liang et al., 2008). Despite the extensive use of IRMS in biomedical and material science through the 1980s and 1990s, similar analyses in soils were challenged by appropriate sample preparation (i.e. ~10 μm thin sections). In addition, due to the heterogeneous nature of soil, the spatial resolution of the microscopes used in the instruments was insufficient to characterize most soil samples. For discussion and details on the component setup of IR microscopes the reader is directed to several excellent articles (Katon, 1996; Lang, 2006; Stuart, 2000; Wilkinson et al., 2002). Improvements in microprocessor and computational technologies, and direct coupling of the microscope with IR spectrophotometer improved spatial resolution (typically 75–100 μm) and enabled a new scale of differentiation (Holman, 2010). IRMS can be used with the IR spectrometer in transmission, reflectance, grazed incidence, and ATR modes (Brandes et al., 2004).

FTIR spectroscopy uses polychromatic radiation to measure the excitation of molecular bonds whose relative absorbances provide an index of the abundance of various functional groups (Griffiths and de Haseth, 1986). Molecules with dipole moments are considered to be IR detectable. Dipole

moments can be permanent (e.g. H_2O) or induced through molecular vibration (e.g. CO_2). Absorption of IR light occurs when photon transfer to the molecule excites it to a higher energy state. These "excited states" result in vibrations of molecular bonds, rotations, and translations. The IR spectra contain peaks representing the absorption of IR light by specific molecular bonds as specific frequencies (i.e. wavenumbers) due to stretching (symmetric and asymmetric), bending (or scissoring), rocking, and wagging vibrations. An excellent introduction to FTIR theory and instrumentation is provided by Smith (2011). While not all molecules lend themselves to FTIR analysis, the majority of inorganic and organic compounds in the environment are IR active. In soils and environmental sciences much of the FTIR literature focuses on the mid-infrared (MIR) region of light (approximately 4000 to 400 cm^{-1}).

1.2 Raman Spectroscopy

Raman spectroscopy was first observed experimentally by Raman and Kirishnan in 1928 as a technique using secondary radiation concurrent with the discovery of IR spectroscopy (Raman and Krishnan, 1928). Due to a greater difficulty in perfecting the technique, Raman spectroscopy initially lagged behind and suffered from less experimental and instrumental development. Significantly hampered by fluorescence, it was not until the early light source used by Raman and Kirishnan (sunlight) was replaced that the technique gained popularity. Initially several different modifications of mercury lamps [including water cooled (Kerscchbaum, 1914), mercury burner (Hibben, 1939), and cooled mercury burner (Rank and Douglas, 1948; Spedding and Stamm, 1942)] were used but these were affected by sample photodecomposition.

The introduction of lasers by Porto and colleagues (Leite and Porto, 1966; Porto et al., 1966) paved the way for modern day instruments. The use of a near-infrared (NIR) excitation laser source (Nd:YAG at 1064 nm) in FT-Raman analysis in the late 1980s, coupled with advances in other parts of the instrumentation [detectors (Epperson et al., 1988; Pemberton et al., 1990) and scattering suppression filters (Otto and Pully, 2012)], overcame the aforementioned major limitation of Raman spectroscopy—fluorescence (Hirschfeld and Chase, 1986). For a more detailed account of the history of Raman spectroscopy, readers are directed to Ferraro (1967). Novel techniques such as surface-enhanced Raman spectroscopy (SERS) and confocal Raman microspectroscopy have elevated the importance of Raman spectroscopy in the field of soil chemistry (Corrado et al., 2008; Dickensheets et al., 2000;

Francioso et al., 2001; Leyton et al., 2008; Sanchez-Cortes et al., 2006; Szabó et al., 2011; Vogel et al., 1999; Xie and Li, 2003; Yang and Chase, 1998).

In contrast to IR spectroscopy, in which vibrational spectra are measured by the absorption of incident photons, Raman spectroscopy utilizes the scattering of incident photons to observe the transitions between the quantized rotational and vibrational energy states of the molecules. When a monochromatic light source interacts with matter, photons can traverse, absorb, or scatter. Photon scattering can be elastic (Rayleigh) or inelastic (Raman).

In Rayleigh scattering, the frequency of the emitted photons does not change relative to the incident light frequency. This type of scattering arises from approximately 10^{-4} of incident photons and is thus more intense (Smith and Dent, 2005) relative to the inelastic scattering of 10^{-8} of incident photons in Raman scattering (Petry et al., 2003). Inelastic scattering can result from (1) excitation of molecules in the ground state (v_0) to a higher energy vibrational state (Stokes) and (2) return of molecules in an excited vibrational state to the ground state (anti-Stokes) (Popp and Kiefer, 2006). The different transition schemes are illustrated in Figure 1.1. Due to the small population of molecules in the excited vibrational state at room temperature (calculated from the Boltzmann distribution),

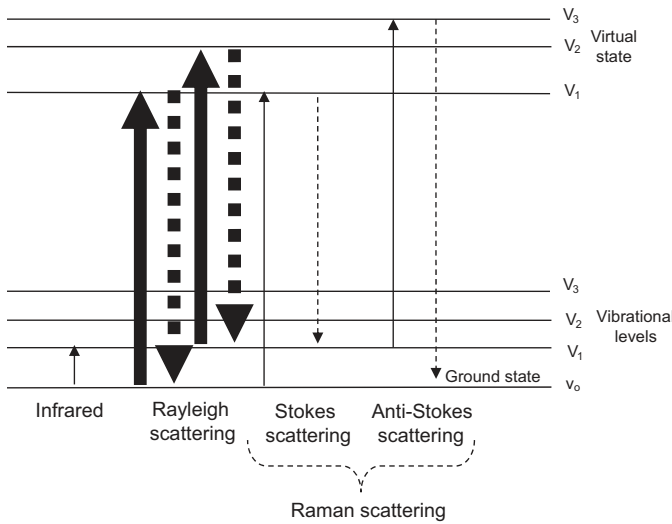

Figure 1.1 Energy level transitions of infrared and Raman spectroscopy. Larger arrows for Rayleigh scattering signify greater abundance. *Adapted with permission from Smith and Dent (2005).*

anti-Stokes bands are not usually considered important in Raman spectra. The energy of emitted photons is relative to the incident light and hence, although plotted like IR spectra, Raman spectra display the wavenumbers shift in the energy of the incident radiation. For a more comprehensive explanation of the principle, theory and instrumentation of Raman spectroscopy the reader is directed to several resources (Colthup et al., 1990; Ferraro, 2003; Lewis and Edwards, 2001; Long, 1977, 2002; Lyon et al., 1998; Pelletier, 1999; Popp and Kiefer, 2006; Smith, 2005).

The change in polarizability of a molecular bond measured by Raman spectroscopy is more intense in pi bonds of symmetric molecules (e.g. olefinic and aromatic C═C) compared to sigma bonds of atoms of different electronegativity (e.g. O–H, C–N and C–O) (Sharma, 2004). As the latter type of bonds (asymmetric) are more intensely IR active, Raman spectroscopy provides complementary information on symmetric bonds. Additionally, the weakness of Raman bands of asymmetric bonds, particularly O–H, limits spectral interference of water, one of the major limitations of FTIR analysis (Li-Chan et al., 2010). Figure 1.2 shows positions of Raman bands for generalized inorganic and organic samples. As Raman and FTIR are both vibrational spectroscopies, combining these complementary approaches can provide thorough molecular bond characterization of samples. A comparison of Raman and IR spectroscopy pertaining to soil chemistry is summarized in Table 1.1.

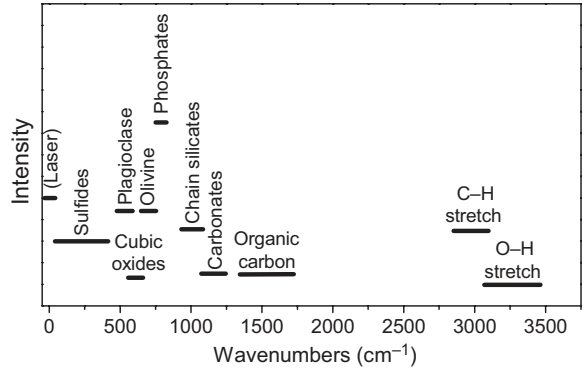

Figure 1.2 Diagram showing general positions of Raman shifts of certain types of minerals and organic matter. Overlapping of bands is minimal, allowing detection of components of complex heterogeneous matrices like soil. *Adapted with permission from Fries and Steele (2011).*

Table 1.1 Comparison of Raman and Infrared Spectroscopic Analysis for Soil Chemical Analysis

	Raman Spectroscopy	Infrared Spectroscopy
Spectral interference from water	No	Yes
Spectral interference from glass containers	No	Yes
Sample preparation	No	Yes (minimal)
Overlapping of spectral bands	Yes (minimal)	Yes
Intensity of band is quantitative	Yes	Yes (limited)
Sensitive to composition, bonding, chemical environment, phase, and crystalline structure	Yes	No
In situ analysis	Yes	No

2. FTIR SAMPLING TECHNIQUES

There are a variety of sampling approaches that are conducive for analysis of environmental samples. The most common methods of collecting FTIR spectra are transmission, DRIFTS, and ATR. The basic sampling principles for these spectroscopic approaches are illustrated in Figure 1.3. In recent years, FTIR-microspectroscopy (IRMS) is being used more commonly in soil science research. The greatest advances with IRMS have been made by utilizing the energy beam from synchrotron (SR) source to enhance spatial resolution of FTIR.

2.1 Transmission

The simplest method for collecting FTIR data is via transmission (Figure 1.3(A)). This is a relatively inexpensive sampling technique, which has been used extensively since the invention of the FTIR. In transmission, the sample is placed directly in the path of the IR beam and the transmitted light is recorded by the detector. Liquid samples are dried onto IR windows (e.g. ZnSe, Ge, CdTe), and solid samples are ground and mixed with KBr and pressed into pellets or wafers. Transmission is often considered a bulk IR measurement because all components of the sample (e.g. exterior, interior) encounter the beam. Samples must be sufficiently thin (~1–20 μm for solid samples, or 0.5–1 mm for KBr pellets) and sufficient light must reach the detector. Soil and mineral samples can be analyzed following careful sample preparation, which can be labor intensive and involves grinding, mixing with KBr, and pressing of pellets or wafers. Since sample desiccation

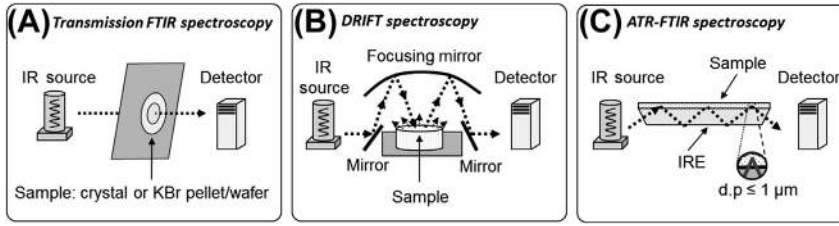

Figure 1.3 Representative illustration of common FTIR sampling approaches including: (A) transmission, (B) diffuse reflectance infrared Fourier transform spectroscopy (DRIFTS), and (C) attenuated total reflectance (ATR)-FTIR. (FTIR, Fourier transform infrared.) *Adapted with permission from Parikh and Chorover (2005).*

is required for transmission analysis, artifacts such as the dehydration of surface complexes may result.

2.2 Diffuse Reflectance Infrared Fourier Transform Spectroscopy

In DRIFTS, IR radiation penetrates the sample to a depth, which is dependent on the reflective and absorptive characteristics of the sample (e.g. Figure 1.3(B)). This partially absorbed light is then diffusely re-emitted from the sample and collected on a mirror that focuses energy coming from the sample onto the detector. The resulting spectrum is comparable to that produced in transmission mode, but is more dependent on spectral properties of the sample interface (Griffiths and de Haseth, 1986).

DRIFTS is well suited for soil analysis because the spectra can be obtained directly from the samples with minimal sample preparation. Typically only drying and grinding are required, although, dilution with KBr is sometimes beneficial. Grinding is best done finely and uniformly across the sample set in order to avoid artifacts that could affect the baseline and peak widths (20 mesh should suffice). Coarser soils trap light more effectively than finer soils, resulting in higher overall absorbance and a shifted baseline (Reeves et al., 2012). Also, mineral bands can be affected by particle size due to variations in specular distortion between small and large silica fragments (Nguyen et al., 1991). Fine grinding can additionally improve spectral quality by homogenizing soil samples. MIR radiation does not penetrate soil samples very well, so the volume of soil scanned by diffuse reflectance instruments is limited to a few cubic millimeters.

Similar to transmission analysis of pressed pellets, DRIFTS can be used to analyze soil or sediment samples diluted with KBr (typically 2–10% sample by mass). This approach is particularly useful when only small sample

volumes are available or if the sample is strongly IR absorbing. However, quantitative calibrations with soil samples can only be achieved using spectra from "as is" neat samples not diluted with KBr (Janik et al., 1998; Reeves et al., 2001).

2.3 Attenuated Total Reflectance Fourier Transform Infrared Spectroscopy

ATR-FTIR spectroscopy is a tool that can be used for nondestructive in situ studies of soil minerals, humic substances (HS), bacteria, and other samples. As illustrated in Figure 1.3(C), ATR-FTIR spectra provide information on functional groups near the surface (~1 μm) of an internal reflection element (IRE) (Nivens et al., 1993a, 1993b). One distinct advantage to ATR-FTIR as compared to other sampling techniques is the relative ease of collecting quality data in the presence of water. Water absorbs strongly in the MIR range (particularly at 1640 cm^{-1} and 3300 cm^{-1}) common to vibrational frequencies of many functionalities (Suci et al., 1998). ATR-FTIR avoids water interference by sending IR light through a highly refractive index prism (IRE). The refracted IR light travels beyond the IRE surface in evanescent waves, probing the solid–liquid interface without penetrating into the bulk solution (Suci et al., 1998). Due to the ability to conduct experiments in the presence of water, ATR-FTIR techniques can be used to examine sorption of aqueous species at crystal and mineral-coated crystal interfaces (Arai and Sparks, 2001; Borer et al., 2009; Goyne et al., 2005; Jiang et al., 2010; Parikh et al., 2011; Peak et al., 1999). ATR-FTIR is a particularly powerful approach for studying sorption because it is can provide information on the speciation of bound molecules and differentiate between inner- and outer-sphere complexes. Since FTIR can be used to probe distinct vibrations arising from biomolecules and inorganic solids, ATR-FTIR is additionally useful for investigating processes at the bacteria–mineral and biomolecule–mineral interfaces (Benning et al., 2004; Deo et al., 2001; Omoike et al., 2004; Parikh and Chorover, 2006, 2008).

ATR-FTIR is limited in that only a few crystal materials can be used effectively. Some of the most common IRE's used include ZnSe, Ge, and KRS-5. When choosing an IRE, consideration must be given to the refractive index (RI) of both crystal and sample, wavenumbers range of interest, solubility of the IRE, and acidity of the experiment. Information on various ATR crystals can be easily found from FTIR spectrometer manufacturers and the literature (e.g. Lefèvre, 2004; Smith, 2011). In recent years, the development of single bounce ATR has led to the commonplace use of diamond as

an IRE. Diamond has the advantage of being very durable and resistant to most solution chemistries. Regardless of the crystal used, the IRE must have a high RI such that IR light passing through the crystal is refracted within the crystal. The light traveling from the optically dense medium (IRE) into the rare medium (bacteria/liquid medium) will totally reflect at the interface if the angle of incidence is greater than the critical angle (Chittur, 1998b). The critical angle is calculated using the following equation:

$$\theta_{\text{critical}} = \sin^{-1} \frac{\text{RI of rare medium}}{\text{RI of dense medium}} \tag{1.1}$$

where θ is the incident angle (Chittur, 1998a). A high RI of the IRE and increasing θ will result in a decreased depth of penetration (Schmitt and Flemming, 1998). The IR beam is able to penetrate into the rare medium allowing a sample spectrum to be acquired from the thin layer attached to the crystal surface (Schmitt and Flemming, 1998).

The RI of the IRE (n_1) and sample (n_2) governs the depth of beam penetration. The depth of penetration (d_p) is calculated using the following equation (Mirabella, 1985):

$$d_p = \frac{\lambda}{2\pi \left[\left(\sin^2 \theta \right) - \left(\frac{n_1}{n_2} \right)^2 \right]^{\frac{1}{2}}} \tag{1.2}$$

where λ is the wavelength (cm) and θ is the angle of incidence. The intensity of reflected light traveling through the IRE will be reduced through interactions with IR absorbing material in the rare medium (Chittur, 1998a). IR light is absorbed by the sample on the IRE surface and the IR detector records the amount of light absorbed from the original IR source, thus producing IR absorption bands and an IR spectrum (Nivens et al., 1993a, 1993b).

As shown in Eqn (1.2), the depth of penetration is dependent on θ. Variable angle ATR (VATR)-FTIR permits depth profiling of samples at the IRE–liquid interface by varying θ of the IR beam into the sample to alter the d_p. This technique provides information on the spatial arrangement of samples at the IRE interface on small length scales. The effective angle of incidence (θ_{eff}) is determined using the following equation (Pereira and Yarwood, 1994):

$$\theta_{\text{eff}} = \theta_{\text{fix}} - \sin^{-1} \left[\frac{\sin \left(\theta_{\text{fix}} - \theta_{\text{var}} \right)}{n_1} \right] \tag{1.3}$$

where θ_{fix} is angle of the crystal face (commonly 45°), and θ_{var} is the scale angle set on the VATR accessory. As an example of how d_p varies as a function of θ_{eff} the depth of penetration for bacteria on a ZnSe IRE is shown in Figure 1.4. For more information on ATR-FTIR, a number of review papers are suggested (Hind et al., 2001; Madejová, 2003; Strojek and Mielczar, 1974).

2.4 IR Microspectroscopy

IRMS is another approach for nondestructive in situ studies of soil components, but with the additional advantage of high spatial resolution. IRMS analysis can be performed in several measurement modes: transmission, diffuse reflection, reflection–absorption, grazing incidence reflection, and attenuated total reflection (Garidel and Boese, 2007). Sample preparation of soil samples is perhaps the most important factor for effectively applying this technique. For example, for IRMS analysis in transmission mode, thin sections of <10 μm thickness are required to avoid total light adsorption (Gregoriou and Rodman, 2002). This can be achieved by embedding the soil (typically air- or freeze-dried) in an epoxy resin and then microtoming with a diamond or glass knife. In some instances, samples may be better

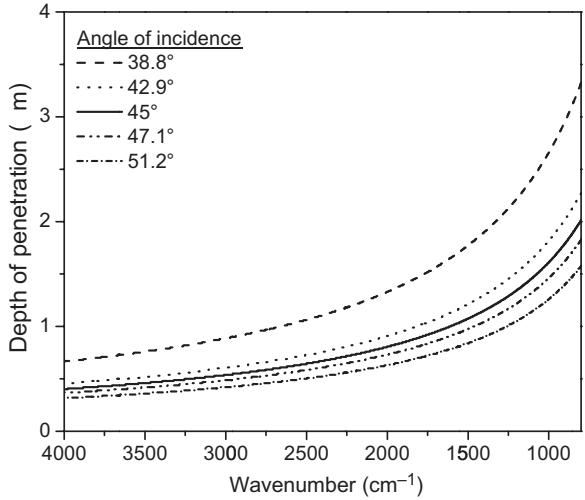

Figure 1.4 Calculated plot of the effect of altering the angle of incidence into an ATR internal reflection element (IRE) on the depth of penetration into the sample. In this case the refractive index (RI) for the IRE was $n_1 = 2.4$ (e.g. ZnSe or diamond) and the RI for the sample was $n_2 = 1.38$ (e.g. organic biopolymer or bacteria). (ATR, attenuated total reflectance.)

suited to drying in liquid nitrogen and cryomicrotoming at subzero temperatures. Cryomicrotoming has been successfully used to analyze OM stability in intact soil microaggregates (Lehmann et al., 2007; Wan et al., 2007). After slicing, the mode of analysis determines the surface to mount the thin sections. For example, transmission electron microscopy grids are used in transmission mode or gold reflective microscope slides for reflection modes.

To obtain high quality spectra, the selected resin must not have adsorption bands that overlap with the sample and the sample surface must be even (Brandes et al., 2004). Polishing or thin sectioning can be used to avoid spectral "fringing". Fringing occurs from interference between light that has been transmitted directly through the sample and light that has been internally reflected (Griffiths and de Haseth, 2006). The resultant sinusoidal patterns of this phenomenon are not easily subtracted from the spectra, making interpretation difficult (Holman et al., 2009).

Most resins are carbon based, presenting a unique sample preparation challenge for analysis of carbonaceous soil material. This has been overcome through use of noncarbon embeddings such as sulfur (Hugo and Cady, 2004; Lehmann et al., 2005; Solomon et al., 2005). For reflection mode, smooth sample surfaces are required to avoid collection inefficiency arising from excessive scattering of the reflected light. This mode is not favored for analysis of soils because it has a high signal to noise ratio suited to homogenous samples. For more information regarding sample preparation in other modes, the reader is directed elsewhere (Brandes et al., 2004).

The capability of simultaneously obtaining biochemical information and high-resolution images of soil features using IRMS is currently unmatched. However, the applicability of IRMS to soil science research is limited by several factors including water adsorption and spatial resolution. Intense absorption in the MIR region associated with water is a major challenge for real time and in situ IR analyses. Spatial resolution is typically limited to 3–10 μm due to the diffraction limit of the IR source (Garidel and Boese, 2007). Details on the relationship between the diffraction limit and the wavelength of the IR source are explained in the reference.

2.5 SR-FTIR Spectromicroscopy

The motivation for combining SR radiation with an IR spectrophotometer arises from a desire to improve the signal to noise ratio and to overcome the diffraction limit of conventional IRMS (smallest practical spot size is approximately 20 μm) mainly due to the low brightness of the thermal IR source and use of an aperture (Carr, 2001). SR radiation is electromagnetic

radiation emitted when electrons, moving at velocities close to the speed of light, are forced to move in a high energy electron storage ring and produce a light source that has an intrinsic brilliance 100–1000 times that of light source used in IRMS (Lombi et al., 2011; Martin and McKinney, 2001; Solomon et al., 2012). At present, there are more than 50 light source facilities worldwide dedicated to the production of this radiation for research purposes. The electromagnetic radiation is nonthermal and highly polarized resulting in a reduced S/N ratio and improved spectral and spatial resolution. Another benefit of this technique is that despite the high intensity of the radiation, it does not degrade or change the chemical composition of the sample and elevates the sample temperature by only 0.5 K (Wilkinson et al., 2002). Figure 1.5 presents a schematic layout of the IR spectromicroscope highlighting its key components.

The hybrid technique affords high resolution (down to a few microns in the MIR region) that is no longer limited by the aperture size, but by

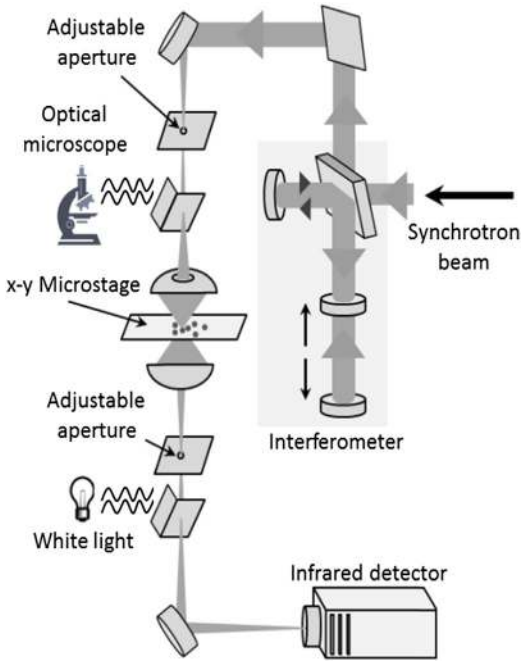

Figure 1.5 Schematic layout of key components of the synchrotron microspectroscope. The microstage (where sample is mounted) is computer controlled, enabling precision mapping. (For color version of this figure, the reader is referred to the online version of this book.) *Adapted with permission from Wilkinson et al. (2002).*

the optical system's numerical aperture and the wavelength of light, as explained by Carr (2001). The attainable spot size is 0.7 times the diameter of the wavelength of the IR beam, which is a spot size of 2–20 μm in the MIR region (Holman, 2010; Levenson et al., 2008). Until recently, intense absorption in the mid IR region associated with water was a major obstacle to real time and in situ analyses via SR-FTIR but has since been overcome using open channel microfluidics (Holman et al., 2010, 2009).

Several good reviews on the application of SR-FTIR with a focus on soils have been written (Holman, 2010; Holman and Martin, 2006; Lawrence and Hitchcock, 2011; Lombi et al., 2011; Raab and Vogel, 2004). In particular, the excellent review by Holman (2010) was a key resource in compiling this chapter. However, in a recent review comparing advanced in situ spectroscopic techniques and their applications in environmental biogeochemistry research, it is evident that there is opportunity for more studies in this field using this technique (Lombi et al., 2011). Numerous closely related applications of SR-FTIR can be found in literature: surface and environmental science (Hirschmugl, 2002; Sham and Rivers, 2002); biology and biomedicine (Dumas and Miller, 2003; Dumas et al., 2007); fossils (Foriel et al., 2004); fate and organic contaminants transport of pollutants in plants (Dokken et al., 2005a,b), and location and characterization of contaminants in sediments (Ghosh et al., 2000; Song et al., 2001).

3. RAMAN SAMPLING TECHNIQUES

3.1 Dispersive Raman Spectroscopy

Dispersive Raman spectroscopy, commonly referred to as Raman spectroscopy, utilizes visible laser radiation, as the source of incident light (Figure 1.6(A)). As the intensity of the Raman scatter is proportional to $1/\lambda^4$, shorter excitation laser wavelengths result in greater Raman signal (Lyon et al., 1998; Schrader et al., 1991). This technique requires only a few grams of sample with minimal to no sample preparation. Most liquid and solid samples can be analyzed without removal of atmospheric gases and water vapor as required for FTIR analysis. Solid samples can be finely ground to ensure homogeneity of the sample while liquid samples can be analyzed glass tubes or cuvettes. Particle size, although typically not considered to matter, may induce changes in the Raman spectra. In a recent study of several samples (i.e. silicon, quartz graphite, and charcoal, basalt and silicified volcanic sediments) comparing crushed and bulk samples, Foucher et al. (2013) showed differences in the spectra of the silicon and silicified

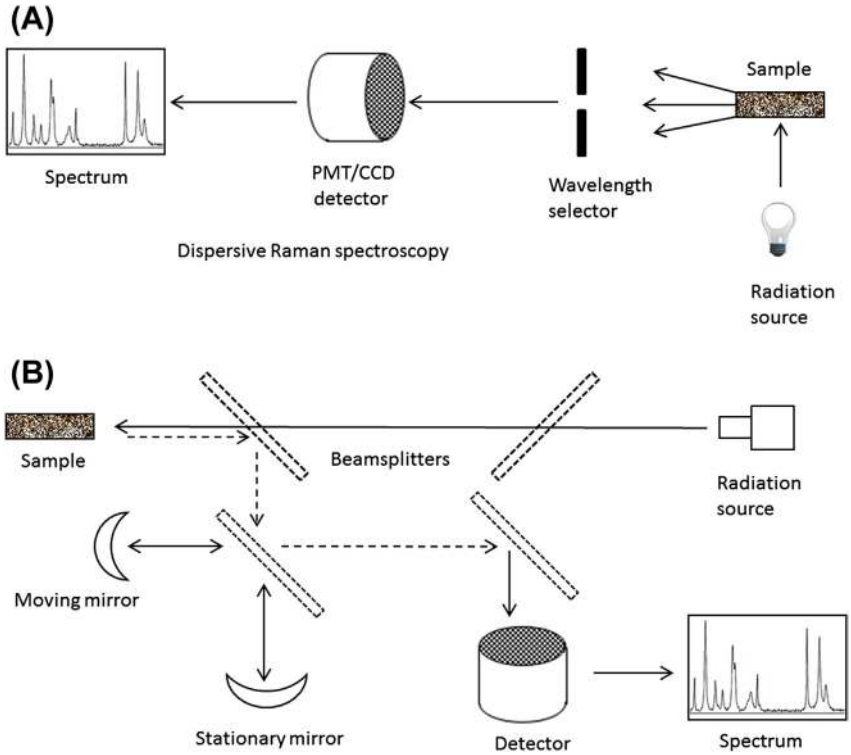

Figure 1.6 Schematic of instrument setup showing difference between (A) Dispersive and (B) Fourier transform Raman spectroscopy. (PMT, Photomultiplier tube; CCD, charged coupled detector.) (For color version of this figure, the reader is referred to the online version of this book.) *Adapted with permission from Das and Agrawal (2011).*

volcanic sediments, and fewer differences in the others. The authors suggested that crushing results in an increase in the background signal level and peak width, and a slight shift in peak position, due to localized heating from the Raman laser. Interferences from the media and container glass are minimal and only become important for samples that produce a weak Raman signal. This enables analysis of samples to be performed within packaging, reducing the risk of sample contamination and loss. For analyses in polymer containers, greater consideration of potential interference from the container is required.

Despite the ease of sample preparation, this technique is hindered by several effects arising from the analysis process (Bowie et al., 2000). Firstly, the intensity of the incident light may result in heating of the sample leading to structural modifications, thermal degradation, and background thermal

radiation (Yang et al., 1994). For whole soil analysis, this technique can be severely limited by fluorescence depending on the sample and the wavelength utilized due to saturation of the silicon charged coupled detector typically used in this type of instrument. This limitation has been partially overcome through the use of software and by varying the wavelength of the incident light, as fluorescence is excitation wavelength-dependent. Oxidative pretreatment of soils with chemicals such as hydrogen peroxide (for removal of unsaturated aliphatic and aromatic compounds) has also been used to minimize sample fluorescence, enabling Raman analysis of soil mineral phases (Edwards et al., 2012). Fluorescence interferences when attempting Dispersive Raman were principally responsible for the development of FT-Raman. Early attempts to perform Dispersive Raman analysis on 50% of all "real samples" (including soils and clays) suffered from severe fluorescence interference and lack of resolution (Ewald et al., 1983; Hirschfeld and Chase, 1986).

3.2 Fourier Transformed Raman Spectroscopy (FT-Raman)

Improvements in Raman instrumentation, particularly incorporation of Fourier spectroscopy (detector signal enhancement), use of NIR excitation lasers of either yttrium vanadate (Nd:YVO_4) and neodymium-doped yttrium aluminum garnet (Nd:YAG) emitting light at a wavelength of 1064 nm (approximately 9400 cm^{-1}), and use of optical filters with very low transmission at the Rayleigh line wavelength have reduced interference by reflecting the interfering light (Hirschfeld and Chase, 1986; Schrader et al., 2000; Zimba et al., 1987). FT-Raman, as Dispersive Raman, requires small amounts of sample and minimal sample preparation. For solid samples, finely ground neat samples can be analyzed. In analysis of inorganic salts, Raman spectral intensity has been shown to increase as sample particle size decreases (Pellow-Jarman et al., 1996). The use of FT-Raman with post spectral processing has been advantageous for overcoming additional shortfalls (e.g. background thermal radiation) associated with Dispersive Raman spectroscopy (Yang et al., 1994) and resulted in improved spectral quality for a number of previously problematic samples, such as HS (Yang and Wang, 1997).

Due to the high wavelength used in FT-Raman, intensity of the Raman signal is very weak [Intensity = 1/(wavelength)^4] but fluorescence is negligible. Interferometers convert the Raman signal into a single interferogram and the sensitive NIR detectors [e.g. germanium (Ge) and indium gallium arsenide (InGaAs)] used in conjunction, greatly enhance the signal–noise ratio of the resultant signal. FT-Raman has wide applications and several

good reviews detailing the application of this technique to a diverse range of fields are available (Brody et al., 1999a,b; Lewis and Edwards, 2001), including FT-Raman use in soil chemistry (Bertsch and Hunter, 1998; Hayes and Malcolm, 2001; Kizewski et al., 2011). This technique has been adapted to obtain quality data from the soil components: humic and fulvic acids (Yang and Wang, 1997) and clay minerals (Aminzadeh, 1997; Coleyshaw et al., 1994; Frost et al., 2010b; Frost and Palmer, 2011; Frost et al., 1997). However, few studies on more complex samples such as whole soils have been performed (Francioso et al., 1996). The technique has long been touted as an effective astrobiological tool in the exploration of Mars (Bishop and Murad, 2004; Ellery et al., 2004; Popp and Schmitt, 2004). For example, FT-Raman was recently included in the instrumentation of the ExoMars rover. FT-Raman has proven to be a versatile analytical tool, which is opening new scientific frontiers, including inclusion of this instrument on the MARS Rover.

3.3 Raman Microspectroscopy

First introduced in 1990, Raman microspectroscopy combines the robustness of Dispersive Raman spectroscopy with the resolution of optical microscopy to analyze single living cells and chromosomes (Puppels et al., 1990). Since then, the technique has been widely used in many disciplines to study bacteria (Huang et al., 2004; Xie and Li, 2003), fish (Ikoma et al., 2003), ceramics (Durand et al., 2012), and soils (Lanfranco et al., 2003). While, no sample preparation is required. However, due to the small spot size utilized in this technique, homogeneity of the sample and analysis of more than one position is paramount to acquiring a representative spectrum. Raman microspectroscopy offers several advantages over Dispersive and FT-Raman, including smaller minimum quantities of analyte, depth profiling via confocal microscopy, and improved spatial resolution with mapping and correlated imaging.

3.4 Surface-Enhanced Raman Scattering Spectroscopy

SERS was inadvertently first observed in 1974 by Fleischmann et al. (1974) and later explained by Jeanmaire and Van Duyne (1977) and Albrecht and Creighton (1977). This technique essentially incorporates a solution of the analyte into an electrochemical cell (Figure 1.7). When incident radiation is shone on the surface metal, of which the nature and roughness of the surface are critical, surface plasmons are generated from oscillation of the electron density (arising from conduction electrons held in the metal lattice) laterally (at a few microns/nanometers) to the metal surface. For scattering to be observed, the oscillation of the plasmons must be perpendicular to

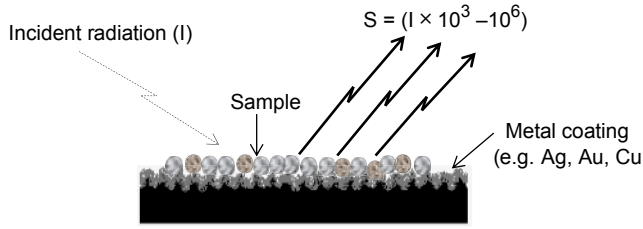

Figure 1.7 Schematic illustration of signal enhancing achieved in surface enhanced Raman scattering (S = enhanced signal). (For color version of this figure, the reader is referred to the online version of this book.)

the metal surface hence the requirement of a rough surface with peaks and valleys (smooth surfaces are inactive). These plasmons generate an enhanced electromagnetic field experienced by the analyte resulting in a scattered Raman signal that is greatly enhanced (Smith, 2005—Modern Raman Spectroscopy).

SERS greatly improves the sensitivity of Dispersive Raman spectroscopy by overcoming the challenge of a low-intensity sample signal. The greatest signal enhancement has been observed using metals such as silver, copper, and gold as coatings and aggregated colloidal suspensions, metal films, and beads as roughened substrates (Huang et al., 1999; Moskovits, 1985; Otto et al., 1992). The Raman signal is increased by up to 10^3–10^6 times when compared to the unenhanced signal and two explanations have been used to describe the enhancement (Moskovits, 1985). The first, and likely more important, involves direct electromagnetic interaction of the analyte with the roughened metal surface resulting in scattering from oscillations of surface metal plasmons perpendicular to the metal surface (Campion and Kambhampati, 1998; Das and Agrawal, 2011; Smith, 2005). The second theory involves chemical enhancement from charge transfer from the metal surface to the analyte due to analyte/metal surface binding (Moskovits, 1985; Otto et al., 1992).

Due to its sensitivity and ability to quench fluorescence, SERS has found a number of applications in soil chemistry research. Examples of these applications include: characterization of carbon in soil (Corrado et al., 2008; Francioso et al., 2000, 2001; Francioso et al., 1996); investigation of humic binding mechanisms (Corrado et al., 2008; Francioso et al., 2001; Francioso et al., 1996; Leyton et al., 2008; Liang et al., 1999; Sánchez-Cortés et al., 1998; Sanchez-Cortes et al., 2006; Vogel et al., 1999; Yang and Wang, 1997; Yang and Chase, 1998). In a series of studies, Francioso et al. successfully used

SERS to study different molecular weight humic and fulvic acids extracted from Irish peat using silver as the metal coating. Advances in SERS instrumentation and improvements of the technique have enabled in situ monitoring of soil carbon sequestration (Stokes et al., 2003; Wullschleger et al., 2003) and application to the qualitative investigation of metal contaminants (e.g. Zn) in soil (Szabó et al., 2011). Several reviews and texts discussing the technique and its application have been written in recent years (Campion and Kambhampati, 1998; Corrado et al., 2008; Etchegoin and Le Ru, 2010; Huang et al., 2010; Katrin et al., 2002; Lombardi and Birke, 2009; Moskovits, 2005; Otto et al., 1992; Stiles et al., 2008).

4. SOIL MINERAL ANALYSIS

Vibrational spectroscopy has many utilities associated with soil mineral studies due to the ability of FTIR and Raman spectroscopies to elucidate local structures and composition changes within samples. Application of these spectroscopic techniques ranges from basic confirmation of mono-mineral samples to pedogenic studies of mineral formation. Additionally, vibrational spectroscopy can be applied solely or in conjunction with other instruments, most notably X-ray diffraction (XRD), for soil mineral confirmation and investigations. Although the utility of vibrational spectroscopy for mineral studies is hampered by similar energies produced from specific bond types (e.g. Si–O and Al–O) commonly found in similar environments within many minerals, FTIR and Raman spectroscopy are well suited for identifying and characterizing amorphous minerals and minerals with hydroxyl, carbonate, and sulfate groups (Amonette, 2002). A variety of FTIR techniques can be employed for mineral analyses, depending on available equipment and study objectives, including transmission with KBr pressed pellets, DRIFTS, and ATR techniques (Madejová, 2003). The wide range of applicable techniques and information obtained makes vibrational spectrometers very useful tools for investigating minerals. There are a number of excellent reviews and resources regarding application of vibrational spectroscopy to minerals including Farmer (1974b), McMillan and Hofmeister (1988), Russell and Fraser (1994), Johnston and Aochi (1996), Madejová and Komadel (2001), and Madejová (2003).

Micro-Raman and FT-Raman are the two Raman techniques most applied to soil mineral analysis. Removal of highly florescent OM is a necessary sample pretreatment step (e.g. combustion, chemical oxidation,

and solvent extraction) to ensure applicability of these techniques. Separation of the mineralogical and water-soluble organic fractions in soil samples enabled differentiation between ten different English soils using both fractions (Edwards et al., 2012). The authors utilized differing amounts of hydrogen peroxide (10, 25, and 50%) to remove incremental amounts of the nonparticulate organic matter from the soils. Analysis of the organic and inorganic sections of the Raman spectra of these samples showed differences in the OM (e.g. fulvic and humic fractions and long-aliphatic carbon chains) as well as mineralogy (e.g. calcite, hematite, and gypsum). Similarly, solvent extraction enabled applicability of Raman spectroscopy to perform speciation studies in the solid phases of natural and anthropogenic compounds present in river and estuarine sediments with appreciable clay and OM contents (Villanueva et al., 2008).

4.1 Phyllosilicates

Phyllosilicates, or layer silicates, are the most common minerals in soils. They are composed of one or two sheets of Si in tetrahedral coordination with O, with varying isomorphically substituted Al tetrahedra, fused to cations in octahedral coordination with O or OH. IR spectroscopy has been used to study clay minerals for a great number of years (Farmer, 1958). The utility of this technique is that it can be employed to distinguish between types of clay minerals (1:1 vs. 2:1 layer silicates) and further distinguish minerals within each structural grouping (e.g. kaolinite vs dickite). Structural details (di- vs trioctahedral nature) and compositional information (octahedral layer cations) of samples can be obtained as well.

Differentiation and characterization of layer silicates using FTIR is primarily based on vibrations associated with constituent units of the minerals (the hydroxyl functional group, the silicate anion, and cations residing in the octahedral layer and interlayer) as described by Farmer (1974c). The stretching vibrations of structural hydroxyl groups (OH) are found between 3750 and 3400 cm^{-1} and the bending bands are located between 950 and 600 cm^{-1}. Silicon bonded to oxygen (Si–O) stretching vibrations appear in the 1200–700 cm^{-1} region, and are also observed from 700 to 400 cm^{-1} along with octahedral cation vibrations. Vibrations from interlayer cations are found outside the MIR range between 150 and 70 cm^{-1} (Farmer, 1974c). Major portions of the IR spectrum used to fingerprint clay minerals are illustrated in Figure 1.8 from Madejová (2003). Notable differences in the 1:1 and 2:1 layer silicate spectra (Figure 1.8(A)a–c and d–g, respectively) are observed in OH stretching and Si–O stretching regions.

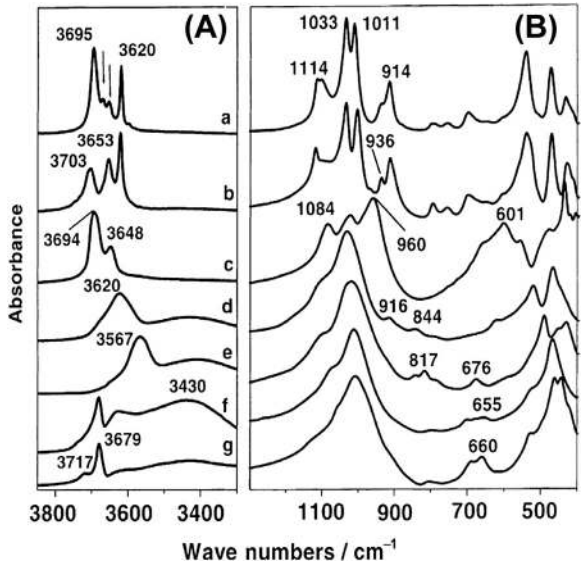

Figure 1.8 Transmission infrared spectra of pressed KBr discs containing samples of the 1:1 layer silicates (a) kaolinite, (b) dickite, (c) chrysotile, and the 2:1 layer silicates (d) SAz-1 montmorillonite, (e) nontronite, (f) hectorite, and (g) saponite for (A) the O-H stretching region and (B) the Si–O stretching and OH bending region. *From Madejová (2003), reprinted with permission.*

The 1:1 layer silicates exhibit two or more OH stretching vibrations from 3700 to 3620 cm^{-1} (kaolinite—4, dickite—3, chrysotile—2); whereas, the 2:1 minerals contain only a single OH stretching band. The number and location of the OH stretching bands in the 1:1 layer silicates can further identify the minerals. The absorption band at 3630–3620 cm^{-1} in kaolinite, dickite, and nacrite (1:1 layer silicates; spectra not shown) is attributed to internal OH groups between the tetrahedral and octahedral sheets. The band at 3700 cm^{-1} for these three minerals is associated with internal surface OH groups located on the octahedral layer surface that are involved in hydrogen bonding to oxygen atoms of the underlying tetrahedral layer surface (Madejová, 2003; Russell and Fraser, 1994). The remaining OH stretching bands in kaolinite and dickite are also associated with internal surface OH groups (Farmer, 2000), and the assignment of OH bands in chrysotile is unresolved (Madejová, 2003). Presence of the single OH stretching vibration in 2:1 layer silicates is attributed to OH coordinated with octahedral cations. The single broad band is attributed to isomorphous substitution within the mineral that disrupts crystalline order and increases structural imperfections (Russell and Fraser, 1994), and exact location of

this band in the spectrum is dependent upon the cation(s) to which OH is bonded (Farmer, 1974(C)). For example, the Al_2OH vibration at 3620 cm^{-1} in montmorillonite (Figure 1.8(A)d) is common for smectites with high Al content in the octahedral layer, whereas the band at 3567 cm^{-1} in Figure 1.8(A)e is indicative of Fe_2OH associated with Fe octahedra in nontronites (Madejová, 2003). In the trioctahedral minerals hectorite and saponite (Figure 1.8(A)f–g), OH stretching of Mg (Mg_3OH) in the octahedral layer appears at 3680 cm^{-1}. Číčel and Komadel (1997) describe the use of deconvoluting OH stretching frequencies in IR spectra to quantify the composition of octahedral cations. In micas and smectites, the method provides a fair degree of accuracy (2.5–10% relative error) for determining cation structural formula coefficients when compared to data derived from chemical analyses.

The Si–O stretching and OH bending region (Figure 1.8(B)) can also be quite informative for differentiating between the layer silicates. The 1:1 minerals shown in Figure 1.8(B)a–c and nacrite (spectrum not shown) exhibit three strong Si–O frequencies between 1120 and 950 cm^{-1} (Madejová, 2003; Russell and Fraser, 1994). In contrast, Si–O stretching in the 2:1 layer silicates (Figure 1.8(B)d–g) is noted by a single broad peak residing at 1030–1010 cm^{-1}. The di- or trioctahedral nature of a mineral apparently influences where the Si-O stretching band appears within a spectrum, as bands for the trioctahedral minerals which appear are higher wavenumbers (1030–1020 cm^{-1}) than the dioctahedral minerals (~1010 cm^{-1}) (Madejová, 2003).

Vibrations from OH bending, referred to as librational frequencies of OH by Farmer (1974b), can also be evaluated for identifying structure of the octahedral layer. The OH bending vibrations in di- and trioctahedral 1:1 layer silicates are noted at 950–800 cm^{-1} and 700–600 cm^{-1}, respectively (Madejová, 2003). The OH bending portion of the spectrum has particular utility for elucidating the composition of dioctahedral 2:1 layer silicates due to frequency changes with octahedral cation composition (Farmer, 1974b). The following list of vibrational OH frequencies from Farmer (1974c) notes these changes quite well: Al_2OH, 950–915 cm^{-1} in all dioctahedral 2:1 species; FeAlOH, ~890 cm^{-1} in montmorillonites; MgAlOH, ~840 cm^{-1} in montmorillonites; and Fe_2OH, ~818 cm^{-1} in nontronites. Several of these bands (Al_2OH, AlMgOH, and Fe_2OH) are readily observed in Figure 1.8(B)d–e. Presence of Al_2OH (916 cm^{-1}) and AlMgOH (844 cm^{-1}) vibrations in the SAz-1 montmorillonite spectrum is indicative of isomorphous substitution within the octahedral layer of this mineral (Madejová, 2003).

Greater details about the detailed structure of clay minerals or "nanoscale architecture" (Johnston, 2010) can also be investigated using vibrational spectroscopy. For example, low-temperature (<30 K) FTIR has been employed for detailed studies of OH stretching vibrations of kaolin group minerals (Balan et al., 2010; Bish and Johnston, 1993; Johnston et al., 2008; Prost et al., 1989). Reductions in temperature enhance resolution of OH stretching vibrations in IR spectra by shifting high frequency bands to higher frequencies (i.e. greater wavenumbers) and low frequency bands to lower frequencies (Prost et al., 1989). Prost et al. (1989) applied this approach to study crystalline kaolinite, dickite, and nacrite, and compared spectra of these minerals to poorly crystalline kaolinites. Their work demonstrated that the relative amounts of dickite-like and nacrite-like structures within poorly crystalline kaolinite increases as crystallinity of the sample decreases.

Johnston et al. (2008) expanded upon the low-temperature work of Prost et al. (1989) by conducting a more detailed study of OH stretching vibrations as a function of temperature. In kaolin group minerals, octahedral layer OH groups and the O of silicon tetrahedra found on opposing sides of the interlayer interact through hydrogen bonding (O(H)···O). Using FTIR data collected at 15 and 300 K, Johnston et al. (2008) demonstrated a linear correlation between OH stretching vibrations of kaolin group polytypes (kaolinite, dickite, and nacrite) and the corresponding distances of O(H)···O interlayer pairings. Interestingly, the correlation indicates that a 0.001 nm change in distance results in a 4 cm^{-1} shift in band position (Johnston, 2010), and more importantly the relationship provides clear identification of the three polytypes or the degree of disorder within a kaolin group mineral sample. Using this relationship, Johnston et al. (2008) identified structural disorders (dickite- or nacrite-like features) in 9 out of the 10 kaolinite samples analyzed, even in samples considered to be well ordered. Similar to the findings of Prost et al. (1989), the presence of dickite- and nacrite-like features increased with increasing disorder in the crystal structure. Low-temperature FTIR was unable to distinguish whether features represented discrete particles of dickite or nacrite or stacking mistakes in sample, but selected area electron diffraction patterns for Capim kaolinite indicate that the features were due to interstratified stacking mistakes. Thus, the use of low-temperature FTIR appears to be sufficiently sensitive for assessing structural disorders in kaolin group minerals (Johnston et al., 2008). The reader is referred to Johnston (2010) for additional examples regarding the application of FTIR and low-temperature FTIR for the detailed study of clay minerals.

There are numerous other applications of vibrational spectroscopy for the study of clay minerals, and the following studies illustrate the breadth and depth of information that can be gained with FTIR spectroscopy. Johnston et al. (1992) and Schuttlefield et al. (2007) used FTIR to study water interactions and uptake, respectively, onto clay minerals. Komadel et al. (1996) monitored HCl and temperature-induced structural changes in reduced-charge montmorillonites via FTIR analyses. Octahedral sheet evolution with progressive kaolinization was studied by Cuadros and Dudek (2006) using mixed kaolinite–smectite samples and transmission FTIR spectroscopy. Petit and colleagues (Petit et al., 1998, 2006) have developed FTIR-based methodology to quantitatively measure the layer charge properties of clay minerals through evaluation of NH_4^+ deformation vibrations. In addition to these more common bulk FTIR analysis approaches, a number of studies have utilized the spatial resolution provided by FTIR microspectroscopy to investigate in situ changes in clay minerals (Beauvais and Bertaux, 2002; Johnston et al., 1990; Rintoul and Fredericks, 1995). For example, Beauvais and Bertaux (2002) characterized in situ differentiation of kaolinite in lateritic weathering profiles from sample thin sections (30 μm thick). Changes observed in the four O–H stretching bands (between 3550 and 3750 cm^{-1}) were used as a proxy to differentiate among different kaolin species. More recently, Katti and Katti (2006) employed FTIR microscopy and micro-ATR spectroscopy to understand the influence of clay swelling on the misorientation and physical breakdown of montmorillonite platelets. Drying-induced acidity on smectite and kaolinite surfaces was studied using ATR-FTIR by Clarke et al. (2011).

Although less common than FTIR, Raman spectroscopy can also provide important information for the study of phyllosilicates. Abrupt shifts in the three Raman v(OH) bands of dickite, combined with XRD analysis, provided evidence for the first documented occurrence of a pressure-induced phase transformation in a 1:1 phyllosilicate (Johnston et al., 2002b). The reversible structural phase transitions occurred between 2.0 and 2.5 GPa as evidenced by shifts in the layers and significant changes in the stacking sequence and interlayer hydrogen bonding structure. In another study, kaolinite-like layered phyllosillicates, bismutoferrite $BiFe_3^{2+}(Si_2O_8)(OH)$, and chapmanite $SbFe_3^{2+}(Si_2O_8)(OH)$ were characterized through Raman and IR spectroscopy. The spectra were related to the molecular structure of the minerals with characteristic Raman bands attributed to the Si-O-Si stretching and bending vibrations and the (Si–O terminal) stretching vibration (Frost et al., 2010a; Rinaudo et al., 2004). Raman miscrospectroscopy

has also utilized to show water sorption in both the lattice and interlayers of vermiculite and muscovite (Haley et al., 1982).

4.2 Allophane and Imogolite

Allophane and imogolite are hydrated aluminosilicate minerals that exhibit short-range order crystallinity. Most commonly these minerals are found in Andisols or Spodosols (Dahlgren, 1994); however, allophane and imogolite can be precipitated from solution in any soil with sufficiently high concentrations of Si^{4+} and Al^{3+} in soil solution (Harsh et al., 2002). These minerals can be indicative of important pedogenic processes (Chadwick and Chorover, 2001) and they can strongly influence soil chemical processes (Harsh et al., 2002). Thus, identification and quantification of these minerals may be particularly useful for soil chemical and pedogenic studies.

IR spectroscopy is one technique that has application for identifying and quantifying allophane and imogolite in soils (Dahlgren, 1994; Farmer et al., 1977). The spectra of allophane and imogolite contain OH stretching vibrations (3800–2800 cm^{-1}), H–O–H deformation vibrations from absorbed water (1700–1550 cm^{-1}), Si–O stretching and OH vibrations (1200–800 cm^{-1}), and a band at 348 cm^{-1} that may be applicable for quantitative or semiquantitative determination of allophane and imogolite (Harsh et al., 2002). A primary difference between allophane and imogolite IR spectra can be found at 1050–900 cm^{-1}. Imogolite and protoimogolite contain two absorption maxima at ~940 and ~1000 cm^{-1}; the former is attributed to an unshared hydroxyl in the orthosilicate group and the latter to Si–O vibrations (Harsh et al., 2002; Russell and Fraser, 1994). In contrast, allophane shows only a single Si–O band in this region that varies in location with changes in the Si/Al ratio (Figure 1.9) (Harsh et al., 2002); band position (1020–975 cm^{-1}) decreases in wavenumbers as Si/Al decreases. Differences in this spectral region of allophane and imogolite are attributed to changes in Si–O polymerization; silicon tetrahedra in imogolite are not polymerized and polymerization increases in allophane with increasing Si/Al ratio (Harsh et al., 2002).

Utilizing the absorbance band at 348 cm^{-1}, quantification of allophane and imogolite content in soils was first proposed by Farmer et al. (1977) and the method is detailed by Dahlgren (1994). There are several challenges associated with using IR spectroscopy to quantify these minerals (Dahlgren, 1994). Obtaining appropriate reference materials for use in developing a standard curve may be challenging, as IR absorption at 348 cm^{-1} varies among allophane samples used as standards (Farmer et al., 1977). Allophane

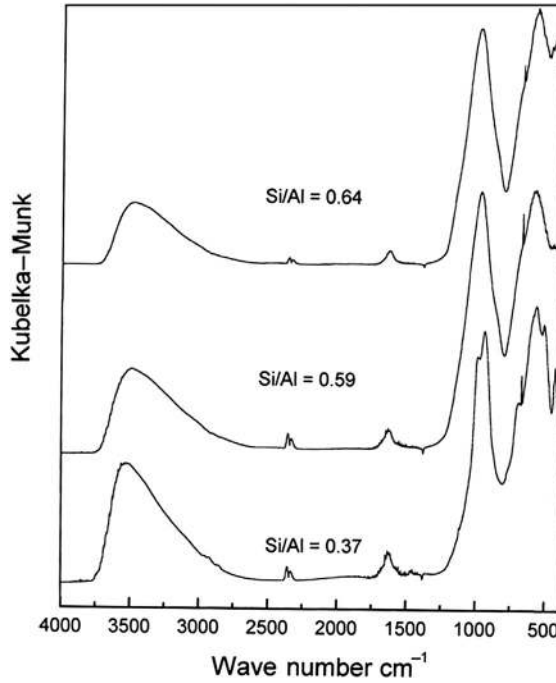

Figure 1.9 Diffuse reflectance Fourier transform infrared (DRIFTS) spectra of allophanes with decreasing Si/Al molar ratio. *From Harsh et al. (2002), reprinted with permission.*

and imogolite are not the only minerals to express a vibration band at 348^{-1} cm^{-1}; many common layer silicates and metal oxides absorb IR radiation at this wavelength as well (Farmer et al., 1977). Concern about the latter issue has led some to discourage the use of IR spectroscopy for quantifying allophane and imogolite (Joussein et al., 2005), although acquisition of difference spectra for samples before and after varying treatments may mitigate this concern.

Dahlgren (1994) outlines three methods for using IR spectroscopy to quantify allophane/imogolite content in samples (allophane/imogolite is used here to indicate that the methods cannot separate quantities of one mineral or the other when both minerals are present in a sample). Although the methods outlined in Dahlgren (1994) specifically employ transmission analysis of pressed pellets, DRIFTS and ATR-FTIR analysis of powder samples may also be appropriate after additional method development. The first technique involves simple analysis of samples mixed with KBr diluent and heated to 150 °C overnight, followed by mineral quantification based on absorption at 348 cm^{-1}. This approach suffers most greatly from

interferences at 348 cm^{-1}, as it does not adequately account for interference from other minerals absorbing in this portion of the spectrum. The other two recommended techniques mitigate this concern by employing the development of a difference spectrum. Samples are analyzed to obtain spectra prior to and after selective dissolution of allophane/imogolite using acid oxalate or dehydroxylation of allophane/imogolite at 350 °C. Spectra collection is followed by computer-aided subtraction of one spectrum from the other to develop a difference spectrum that can be used to quantify allophane/imogolite content at 348 cm^{-1}. Calculation of a difference spectrum should effectively remove contributions at the target wavelength to improve quantification of allophane/imogolite content in the sample, thereby minimizing concerns expressed by Joussein et al. (2005).

4.3 Metal Oxides, Hydroxides, and Oxyhydroxides

IR spectroscopy can be employed to identify and study the structures of metal oxides, hydroxides, and oxyhydroxides, collectively referred to as metal oxides hereafter (Farmer, 1974a; Lewis and Farmer, 1986; Russell and Fraser, 1994; Russell et al., 1974). The greatest focus of metal oxide FTIR investigations has been on iron oxide structures and properties. Aluminum and manganese (Mn) oxides can be observed with IR spectroscopy as well, although Mn oxides have been received the least attention. A distinct advantage of IR spectroscopy over XRD for studying metal oxides is the ability to characterize poorly crystalline and crystalline metal oxide phases. The FTIR spectra of hematite (α-Fe_2O_3), goethite (α-FeOOH), gibbsite (γ-$AlOH_3$), and diaspore [α-AlO(OH)] are shown in Figure 1.10. Although similarities exist, the ATR-FTIR and DRIFTS spectra can be quite different in band ratios and peak width, due primarily to the differences in the interaction of the sample with the IR beam and the depth of beam penetration into the sample. This figure is an illustrative reminder that MIR spectra are greatly influenced by the sample collection method and caution should be used in making band assignments from the literature when sampling methods differ.

Gibbsite, a crystalline $Al(OH)_3$ polymorph, is the most commonly occurring crystalline aluminum oxide in soils and bauxite deposits (Allen and Hajek, 1989). The gibbsite structure consists of Al in sixfold coordination with OH that generates dioctahedral sheets stacked upon one another. There are six distinct structural OH groups in gibbsite: three OH groups are oriented perpendicular to the sheet and three OH are oriented parallel to the sheet (pointed toward empty octahedral sites) (Huang et al., 2002). The OH groups oriented parallel to the sheet form intralayer hydrogen bonds

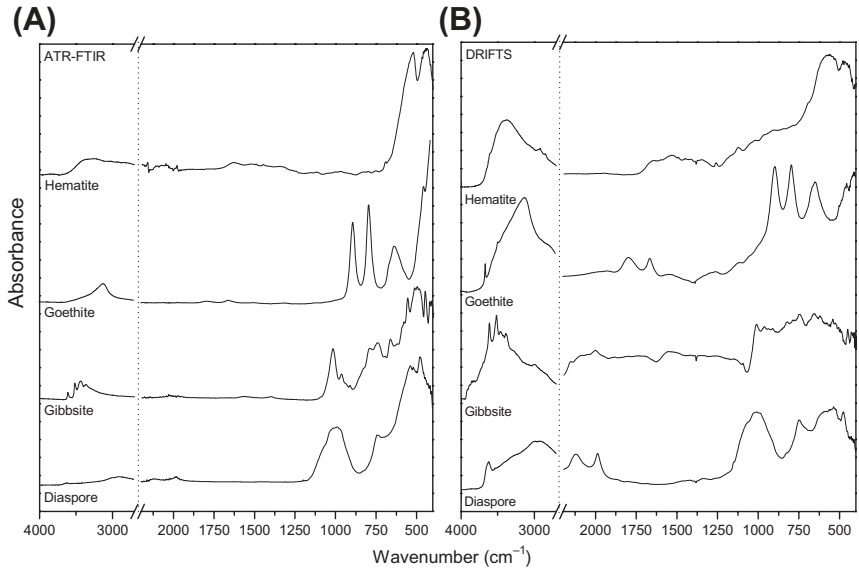

Figure 1.10 Mid-infrared spectra of some common soil minerals collected by (A) ATR-FTIR spectroscopy and (B) DRIFTS. All spectra were collected using a Thermo Nicolet 6700 spectrometer. ATR samples were collected using a single bounce diamond IRE (GladiATR, PIKE Technologies) with no ATR correction performed. Samples for DRIFTS (EasiDiff, PIKE Technologies) were diluted with KBr (10% mineral). (ATR, attenuated total reflectance; FTIR, Fourier transform infrared; IRE, internal reflection element; DRIFTS, diffuse reflectance Fourier transform infrared spectroscopy.)

within a gibbsite sheet, whereas OH oriented perpendicular to the sheet for interlayer hydrogen bonds between gibbsite sheets (Wang and Johnston, 2000). Subsequently, the FTIR spectrum of gibbsite (Figure 1.10) is characterized by OH stretching bands (Russell and Fraser, 1994).

The number of OH stretching bands readily observed in a spectrum of $Al(OH)_3$ polymorphs as well as band frequency is highly dependent upon the crystallinity of the specimen studied (Elderfield and Hem, 1973). In general, Elderfield and Hem (1973) observed that band resolution increased with crystallinity and the two highest frequency OH stretching bands moved to higher frequencies (as much as 30 cm^{-1}). At ambient temperature, IR spectra of well crystallized gibbsite (Figure 1.10) typically exhibit five OH stretching vibrations at 3620, 3527, 3464, and a doublet at 3391/3373 cm^{-1}; Al–O and Al–OH vibrations generally appear in aluminum oxides between 1100 and 400 cm^{-1} (Lu et al., 2012). However, Wang and Johnston (2000) employed low temperature (12 K) to identify a sixth OH band at 3519 cm^{-1} (Figure 1.11(A)). The sixth band was also observed in Raman spectra

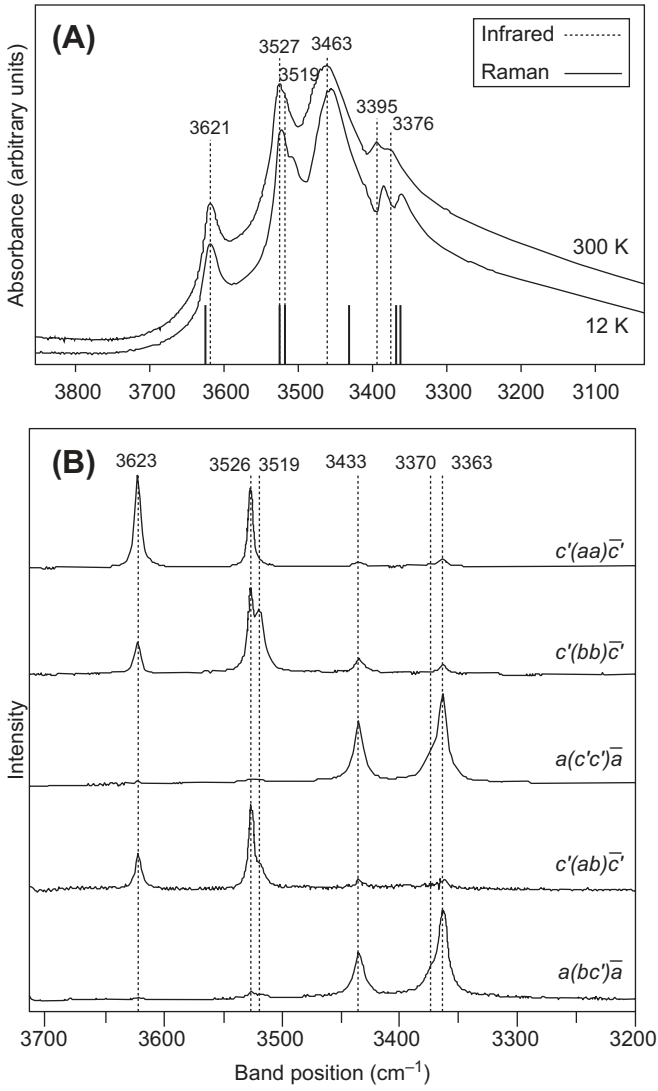

Figure 1.11 (A) FTIR spectra of gibbsite at 12 and 300 K; short vertical lines indicate OH positions in Raman spectrum. (B) Polarized single-crystal Raman spectra of gibbsite at varying Raman scattering geometries (Wang and Johnston, 2000). (FTIR, Fourier transform infrared.) *Reprinted with permission.*

obtained using polarized single-crystal Raman spectroscopy through the collection of data at different crystal orientations and manipulation of polarization analyzer settings (Figure 1.11(B)). Furthermore, the authors applied the Lippincott and Schroeder (LS-1D) model to predict the location of

the OH stretching vibrations based on interatomic O···O distances, thus permitting assignment of individual OH groups in the crystal structure to specific intra- and interlayer OH bands. Intra- and interlayer OH bands were assigned to the three highest and three lowest frequency OH bands, respectively (Wang and Johnston, 2000).

Balan et al. (2006) modeled IR and Raman spectra of gibbsite using ab initio quantum mechanical calculations and collected ambient temperature FTIR spectra of powdered, synthetic gibbsite. Theoretical vibrational spectra of gibbsite in the OH stretching region matched quite well with the experimental spectra collected by Balan et al. (2006) and Wang and Johnston (2000). Proposed OH stretching assignments to bands were similar between the two studies. However, the ability of theoretical IR spectra to match experimental spectra was highly dependent upon the particle shape modeled (e.g. sphere vs plate). At lower frequencies (1200–200 cm^{-1}), theoretical IR spectra did not match experimental spectra due to particle shape challenges and band overlap. The same challenges were reported by Balan et al. (2008) in a similar approach for studying bayerite (β-$Al(OH)_3$). Ferreira et al. (2011) employed molecular modeling and vibrational spectroscopy to determine if spinel-like or nonspinel structures are present in γ-Al_2O_3. Theoretical IR spectra for spinel-like structures agreed most closely with experimental data and the spinel-like structure was predicted to be thermodynamically more stable (19 kJ mol^{-1} per formula unit greater than nonspinel structure from 0 to 1000 K). The work of Balan et al. (2008, 2006) and Ferreira et al. (2011) demonstrate the potential utility of coupling ab initio calculations with experimentally collected vibrational spectra to further understand the nanoscale architecture of minerals, but also indicate that molecular modeling is currently unable to replace experimental spectra.

As noted earlier, Fe oxides have been extensively studied using vibrational spectroscopy due to their widespread occurrence and diversity, high reactivity, and importance as soil coloring agents. Goethite (α-FeOOH) and hematite (α-Fe_2O_3) are two of the more common iron oxides found in soils (Allen and Hajek, 1989), but six other Fe oxides (ferrihydrite, green rust, lepidocrocite, maghemite, magnetite, and schwertmannite) are also present (Bigham et al., 2002). Fe oxides are solely or primarily composed of Fe in sixfold coordination with O and OH, although Fe tetrahedra are found in magnetite and maghemite (Schwertmann and Cornell, 2000). MIR spectra of the more commonly found iron oxides can be found in Russell and Fraser (1994), Schwertmann and Cornell (2000),

and Glotch and Rossman (2009). Here, the ATR and DRIFT spectra of goethite and hematite are shown in Figure 1.10. The hematite spectra display prominent peaks at 525 and 443 cm^{-1} in the ATR-FTIR spectrum (578 and 480 cm^{-1} in the DRIFTS spectrum) corresponding to the Fe-O vibrations of hematite (Schwertmann and Cornell, 1991; Schwertmann and Taylor, 1989).

For goethite, Blanch et al. (2008) assigned the band at 670 cm^{-1} to in-plane OH bending, 633 cm^{-1} to the Fe–O stretch, 497 cm^{-1} to the asymmetric stretch of Fe–O, 450 cm^{-1} was assigned to the Fe(III)–OH stretch, the Fe–OH asymmetric stretch appears at 409 cm^{-1}, and two Fe–O symmetric stretches arise at 361 and 268 cm^{-1}. Easily observed in Figure 1.10 are the peaks associated with OH stretching (3153 cm^{-1}), in-plane OH deformation (839 cm^{-1}), and out-of-plane OH deformation (794 cm^{-1}) (Russell and Fraser, 1994). It is important to note, however, that these bands broaden and shift to higher frequencies as Al content in the sample increases >5.85 mol.%. These shifts are attributed to structural strains within the mineral when additional Al atoms are found in the first cation coordination sphere surrounding a substituted Al atom, perhaps resulting in partial ordering of the Al sites and formation of Al-rich clusters (Blanch et al., 2008). Comparison of vibrations in goethite to the isostructural diaspore (α-AlOOH) provides further comparison for these shifts in frequency (goethite→diaspore): 268→350 cm^{-1}; 290→372 cm^{-1}; 361→518 cm^{-1}; 410→578 cm^{-1}; 450→690 cm^{-1} (Blanch et al., 2008). Similar work investigating the effect of Al substitution on hydroxyl behavior during the dehydroxylation of goethite was conducted by Ruan et al. (2002a). Cambier (1986b) illustrated the influence of crystallinity on the FTIR spectrum of goethite: spectral bands broaden with decreasing crystallinity. This change was attributed to the weakening of H-bonds within the crystal due to changes in Fe-O bonds associated with the tilting of octahedra rows within the goethite structure (Cambier, 1986b). In Cambier (1986a), the influence of particle size on goethite spectra was evaluated. [See Wang et al. (1998) for a detailed description of particle size, shape, and internal structure effects on the FTIR spectrum of hematite.] The work of Blanch et al. (2008) and Cambier (1986a,b) illustrate the need to consider the influence of substituted cations, crystallinity, and particle shape when evaluating and interpreting the spectra of specimens.

As with clay minerals, the abundance of studies on Fe oxides using vibrational spectroscopy makes it difficult to mention or discuss any in great detail. However, the following studies indicate the utility of FTIR for studying Fe oxides. Tejedor-Tejedor and Anderson (1990) used ATR-FTIR with

a cylindrical internal refection (CIR) cell to study changes in the structure of water at the solid–water interface of goethite as a function of pH, ionic strength, and electrolyte anions. Ruan et al. (2001) and Boily et al. (2006) used FTIR to study dehydroxylation of goethite during phase transition to hematite, and Ruan et al. (2002b) applied FTIR microscopy to further study this phenomenon. Similar to Balan et al. (2008, 2006) and Ferreira et al. (2011), Blanchard et al. (2008) employed molecular modeling and FTIR spectroscopy to interpret and assign vibrational bands observed in the spectrum of hematite. Chernyshova et al. (2007) used FTIR and Raman spectroscopy to identify maghemite-like defects in the structure of hematite nanoparticles (7–120 nm) and the role both particle size and growth kinetics have on the formation of structural defects. From the vibrational spectroscopic results, a new general model was developed to describe solid-state transformations of hematite nanoparticles as a function of particle size (Chernyshova et al., 2007).

Mn oxides have not been studied using vibrational spectroscopy to the same extent as Fe and Al oxides, but valuable resources exist for identifying and characterizing Mn oxides. Potter and Rossman (1979) and Julien et al. (2004) captured FTIR and Raman scattering spectra for a large number of Mn oxides. More recently, Zhao et al. (2012a) reported FTIR spectra for six birnessite samples with different mean Mn oxidation states. With respect to other IR applications for Mn oxides, Parikh and Chorover (2005) used four different FTIR techniques to study biogenic Mn oxide formation on *Pseudomonas putida* GB-1. In situ monitoring revealed the development of MnO_x upon addition of $MnSO_4$ and changes in the spectra of extracellular biomolecules. Interestingly, the spectra of biogenic MnO_x was not identical to the spectra of synthetic Mn oxides due to the incorporation of biomolecules within the solid phase.

Thibeau et al. (1978) first reported the Raman spectra of FeO, Fe_3O_4, α-Fe_2O_3 α-FeOOH, and γ-FeOOH. In other work, Hart et al. were able to completely assign the Raman spectra of hematite and magnetite (Hart et al., 1976). Despite these studies, Raman analysis of iron oxidation products has been hampered by their poor light scattering ability (Thibeau et al., 1978), uncertainty over the number of peaks in the spectra (Dünnwald and Otto, 1989), and potential thermal degradation by Raman radiation (Bersani et al., 1999). SERS overcomes these limitations and has been utilized to investigate the structures of hematite (α-Fe_2O_3), magnetite (Fe_3O_4), wustite (FeO), maghemite (γ-Fe_2O_3), goethite (α-FeOOH), lepidocrocite (γ-FeOOH), and δ-FeOOH (de Faria et al., 1997).

4.4 Mineral Weathering and Pedogenesis

Vibrational spectroscopy can be a very useful tool for investigating weathering reactions and pedogenesis, and it can be used independently or in conjunction with XRD, electron microscopy, and other molecular spectroscopy analyses to elucidate changes in a system. FTIR and Raman spectroscopies can be employed to identify changes to mineral surfaces and the development of new mineral phases during weathering reactions in the laboratory, and these changes can be evaluated ex situ or in situ. These approaches are powerful tools for studying mineral transformations and identifying mineral phases within soil samples. Tomić et al. (2010) utilized transmission FTIR and Raman microspectroscopy (with corroboration from XRD analysis) to differentiate between soluble minerals present throughout a morphologically similar vertisol sequence. In this study, the presence of dolomite, aragonite, and calcite in lower soil horizons compared to gypsum was used to explain the surface layer transition of the soils from calcic- to calcimagnesic-vertisols.

Through an ATR-FTIR approach, Cervini-Silva et al. (2005) analyzed powder samples to evaluate the development of new mineral phases following rhabdophane ($CePO_4 \cdot H_2O$) reaction with solutions containing organic acids and chelating agents. FTIR analysis permitted identification of CeO_2 (s) precipitate formation, which explained the lack of Ce^{3+} (aq) in some reaction vessels. Similarly, DRIFTS permitted Goyne et al. (2010) to identify the formation of Ca- and rare earth elements (REE)-oxalate precipitates following reaction of apatite with oxalate at differing aqueous phase concentrations. Goyne et al. (2006) also used DRIFTS analyses to document the formation of Cu precipitates following chalcopyrite ($CuFeS_2$) reaction with organic ligands under anoxic conditions. The formation of precipitates was in agreement with chemical speciation model results predicting oversaturation of covellite (CuS), and these results were used to explain nonstoichiometric chalcopyrite dissolution and the low Cu concentration in solution.

In a study of mica weathering to hydroxyl interlayered vermiculite (Maes et al., 1999), FTIR spectra in conjunction with XRD patterns were used to document biotite transformation after K^+ extraction and oxidation. The DRIFTS data collected by Choi et al. (2005) during a study of clay mineral weathering in caustic aqueous systems revealed the development of nitrate sodalite and nitrate cancrinite secondary precipitates. In addition to demonstrating differences in formation of these nitrate-containing precipitates as a function of the clay mineral reacted, Cs^+ (aq) and Sr^{2+} (aq) concentration

in the reaction vessel, and time, FTIR data were more useful at identifying mineral precipitation at earlier reaction times than XRD (Choi et al., 2005). Although none of these studies were entirely spectroscopy-centered, they illustrate the utility of FTIR for rapid acquisition of additional data that can aid in explaining mineral weathering. FTIR spectroscopy can be extended to the study of soil mineral composition and transformation during pedogenesis (Caillaud et al., 2004; Chorover et al., 2004). When used in this context, FTIR can be particularly useful for identifying the formation of amorphous minerals.

In situ measurements of mineral weathering or change can also be completed using FTIR. Morris and Wogelius (Morris and Wogelius, 2008) developed a multiple internal reflection flow through cell for capturing FTIR spectra, and applied this to study forsteritic glass dissolution in the presence of phthalic acid. This approach permitted in situ observations of phthalate attachment and subsequent changes on the mineral surface that would otherwise not have been observed. Using an ATR flow through circle cell, Parikh and Chorover (2005) monitored biogenic Mn oxide formation on bacteria biofilms through time. Usher et al. (2005) used ATR-FTIR for in situ monitoring of mineral oxidation upon exposure to oxidizing gases, thereby illustrating that in situ analyses need not be restricted to aqueous studies.

The weathering of limestone (i.e. monuments) due to salt formation was investigated by Kramar et al. (2010) using micro-Raman spectroscopy in conjuction with XRD. Gypsum was identified within the sample by its main Raman band at 1008 cm^{-1} and some twin minor doublet bands, at 414, 494 cm^{-1}, and 623, 671 cm^{-1}, assigned to ν_2 symmetric and ν_4 antisymmetric bending of the SO_4 tetrahedra. The XRD analysis also corrobated the presence of gypsum in the weather limestone. Furthermore, micro-Raman enabled the observation of minor differences in the weathering processes arising from specific weathering conditions. Raman peaks signifying the presence of magnesium sulfate hydrates (i.e. hexa- and pentahydrites) and niter were observed only in the efflorescence of structures weathered indoors. The assignment of the magnesium sulfate hydrates was based on the extensive Raman study of this series of hydrates by Wang et al. (2006).

The effectiveness of micro-Raman in the investigation of weathering products is also evident in a study of soils present at an abandoned zinc and lead mine by Goienaga et al. (2011). By analyzing samples from the top 2 cm of soil, they were able to identify the presence of 16 primary (including dolomite, calcite, fluorite, graphite, and rutile) and 23 secondary minerals (zinc, cadmium, and lead minerals) resulting from several processes

including: dissolution–precipitation processes; weathering of superficial mineral phases; percolation of dissolved ions; and precipitation. The impact of the deterioration of guardrails, brake linings, and tires in conjunction with exhaust fumes on heavy metals in urban soils has been investigated using Raman spectroscopy and X-ray fluorescence. Zinc (as hydrozincite and zinc nitrate) and barium (as witherite) were determined to be the main contaminants of the soils (Carrero et al., 2012).

5. SOM SPECTRAL COMPONENTS

FTIR spectroscopy is a well-suited analytical tool for studying organic molecules in soil samples. The presence of dipole moments in organic functional groups allows FTIR to be used for sample identification, quantification, and purity analysis for a myriad of organic compounds. In fact, there is a long history of analyzing pharmaceuticals, pesticides, and other organic compounds using this approach. However, due to the observed fluorescence of organic molecules, Raman spectroscopy is typically not the preferred approach for vibrational spectroscopy analysis of organics.

Although considerably more complex than anthropogenic organic compounds, the chemical composition of SOM makes it a suitable substrate for FTIR analysis. Organic molecule bonds, in SOM commonly C–O, C═O, C–C, C–H, O–H, N–H, N═C, and S–H, absorb in the MIR region, with overtones extending to the NIR region (12,000–4000 cm^{-1}), in particular for O–H and N–H. These molecular bonds collectively constitute SOM and influence its interactions with other soil components (e.g. minerals, bacteria, water). The abundance of oxygen (O), nitrogen (N), and sulfur (S) provide SOM with its high chemical reactivity (e.g. cation and anion-exchange capacity, acidity, binding metals and anthropogenic organic compounds). Of these, O is most abundant and exists primarily in carboxyl form, arguably the single most important functional group given its basis for the majority of SOM properties (Hay and Myneni, 2007). Additional O-containing functional groups can be divided broadly into acidic (i.e. enol, phenol) and neutral (i.e. alcohol, ether, ketone, aldehyde, ester) categories. Important N groups are amines and amides. Aromatics, acids, and sugars are also functionally significant moieties (Sparks, 2002). Common assignments for IR absorbing moieties present within SOM are provided in Table 1.2. A recent review of vis-NIR spectroscopy calibration for predicting soil carbon content provides an excellent summary of fundamental SOM absorbances (Stenberg et al., 2010).

Table 1.2 FTIR Vibrational Assignments for Soil Organic Matter Absorbances

Wavenumbers (cm^{-1})	Assignment	Sample Type	FTIR Method
3700–3200	O–H and N–H stretch	Humic acids and humin of soil[a]	Transmission[a]
3690–3619	Free O–H, N–H stretch	Humic acids[b,c] and fulvic acids of soil[c]	Transmission[b,c]
3450–3300	Hydrogen bonded O–H, N–H stretch; greater N–H contribution at lower range	Humic acids of soil[d,b,e] and pyrophosphate extracts of soil[f]	Transmission[d,f], ATR[e]
3110–3000	Aromatic C–H stretch	Humic acids and humin of soil[a,f,g], pyridine extracts of coals[h]	Transmission[a,f,h], ATR[g]
3000–2800	Aliphatic C–H stretch	Humic acids of soil[b,f]	Transmission[b,f]
2925	Aliphatic C–H antisymmetric stretch	Humic acids of charcoals[i]	Transmission[i]
2855–2850	Aliphatic C–H symmetric stretch	Humic acids of soil[a] and charcoal[i]	Transmission[a,i]
2730	CH_3 deformation	Petroleum-contaminated soil[j]	DRIFTS[j]
2600–2500	H-bonded OH of carboxylic acids	Humic acids of soil[f]	Transmission[f]
1765–1700	Carbonyl C═O stretch[x]	Humic acids of soil[a,d,k] and water-extractable OM of soil[l]	Transmissio[a,d,k,l]
1720	Carboxylic acid C═O stretch	Humic acids of soil[b], peat[m]	Transmission[b], ATR[m]
1710	Free organic acid carboxylic C═O	Peat[m]	ATR[m]
1700	Carboxylic acid, ketone, aldehyde C═O stretch	Humic acids of soil[a]	Transmission[a]
1660–1630	Amide C═O stretch (amide I)	Humic acids of soil[d,e]	Transmission[d,e]
1650	Quinone ketone C═O stretch	Humic acids of soil[a]	Transmission[a]

Continued

Table 1.2 FTIR Vibrational Assignments for Soil Organic Matter Absorbances—cont'd

Wavenumbers (cm^{-1})	Assignment	Sample Type	FTIR Method
1650–1600	Aromatic C=C stretch and/or carboxylate C–O asymmetric stretch and/or conjugated ketone C=O stretch	Humic fractions of soil[b,o], peat[m], soil organic horizons[p]	Transmission[b,o,p], ATR[m,n]
1590–1500	Amide N–H bend and C=N stretch (amide II)	Humic acids of soil[a,d,k]	Transmission[a,d,k]
1570	Aromatic C–H deformation	Humic acids of charcoals[i]	Transmission[i]
1550–1500	Aromatic C=C stretch	Humic acids of soil[a,b]	Transmission[a,b]
1470–1370	Aliphatic C–H bend	Humic acids of soil[d,k], peat[m]	Transmission[a,k], ATR[m]
1410–1380	Phenolic C–O stretch, OH deformation	Humic acids of soil[k], peat[m]	Transmission[k], ATR[m]
1400–1380	Carboxylate C–O symmetric stretch	Humic acids of soil[q,r]	Transmission[q], DRIFTS[r]
1330–1315	Ester C–O	Humic acids of soils[a]	Transmission[a]
1300	C–H overtone	Soil[s]	DRIFTS[s]
1280–1200	Carboxylic acid C–O stretch, OH deformation, ester, phenol C–O asymmetric stretch	Humic acids of soil[d,e]	Transmission[d,e]
1190–1127	Alcohol, ether, phenol C–O–C stretch, poly OH stretch	Humic acids of soil[o] and charcoals[i]	Transmission[i,o]
1170–1120	Aliphatic O–H, C–OH stretch	Humic acids of soil[b]	Transmission[b]
1160–1000	Ester, phenol C–O–C, C–OH stretch, attributed to polysaccharides or polysaccharide-like compounds	Humic acids of soil[k], soil organic horizons[p], and compost[t]	Transmission[k,p], ATR[t]

975–700	Aromatic C–H out-of-plane bend; increasing wavenumbers with increasing degree of substitution	Soil[u], soil organic horizons[u], humic acids of soil[a,b], charcoal[i]	Transmission[a,b,i], DRIFTS[u], ATR[u]
720	CH_2 wag	Coal[v]	Transmission[v]
670	OH bending	Biochar[w]	ATR[w]

FTIR: Fourier transform infrared, ATR: attenuated total reflectance (FTIR) spectroscopy, DRIFTS: diffuse reflectance infrared Fourier transform spectroscopy.
[a]Tatzber et al. (2007).
[b]Senesi et al. (2003).
[c]Scherrer et al. (2010).
[d]Fernández-Getino et al. (2010).
[e]Vergnoux et al. (2011).
[f]Piccolo et al. (1992).
[g]Aranda et al. (2011).
[h]Sobkowiak and Painter (1992).
[i]Ascough et al. (2011).
[j]Forrester et al. (2013).
[k]Olk et al. (2000).
[l]He et al. (2011b).
[m]Artz et al. (2008).
[n]Solomon et al. (2007a).
[o]Sánchez-Monedero et al. (2002).
[p]Haberhauer (1998).
[q]Ellerbrock et al. (1999).
[r]Ding et al. (2002).
[s]Cozzolino and Morón (2006).
[t]Tandy et al. (2010).
[u]Cécillon et al. (2012).
[v]Ibarra et al. (1996).
[w]Mukome et al. (2013).
[x]For a detailed discussion of carboxyl assignments, see (Hay and Myneni, 2007).

Due to the fact that SOM is a complex and heterogeneous mixture of these functional groups, FTIR spectroscopy requires specialized methodologies and data interpretation, in contrast to pure compounds or simple mixtures of known composition. This, however, is not so much a shortcoming of FTIR spectroscopy as a reflection of the inherent chemical diversity of SOM. Indeed, FTIR spectroscopy is well suited to provide molecular insight to this defining aspect of SOM precisely. The major limitation of FTIR for SOM analysis arises from mineral interference, with the implication that sample selection and/or preparation or spectral treatment are key strategies for overcoming this. A detailed description of SOM analysis in whole soils and SOM fractions and extracts is provided later in this review.

Identification of absorbance bands in FTIR spectra can be challenging in heterogeneous samples like SOM. Sample identity (e.g. bulk soil, SOM extract, compost) can be used a priori to narrow possible assignments or make specific claims to the greater structural environment of the bonds assigned. Even for spectra of SOM-rich or extract samples without interfering or overlapping mineral and inorganic absorbances, heterogeneity among SOM fractions [e.g. particulate organic matter (POM), light fraction (LF)] can make assignments difficult (Calderón et al., 2011b; Stenberg et al., 2010). The heterogeneous nature of SOM limits assignments to only be tentatively made, based on the presence of MIR peaks assigned to specific functional groups whose MIR absorbances are well established in the literature. Additionally, the presence of multiple molecular bonds that absorb MIR light within the same frequency range further limit assignments for SOM. For instance, a common assignment for 1650 cm^{-1} band in samples known to contain nitrogenous OM is amide C═O (amide I), and in the context of SOM this may be broadly assigned as an absorbance of peptides or proteins (Calderón et al., 2011b). Knowing the sample type can help discriminate among possible assignments and justify specific molecular environments. For example, in the case of overlaps between C═N (amide II) and aromatic C═C at 1530 cm^{-1}, or polysaccharide type (e.g. lignin, cellulose, pectin) for ν(C–O) absorbance (1160–1020 cm^{-1}).

In cases where identifying SOM composition and/or quantifying functionalities is not necessary, absorbance assignment may be irrelevant. The high sensitivity of FTIR to organic functionalities allows fingerprinting of SOM samples, much in the same way mass spectrometry methods (e.g. py-GC-MS, py-MBMS) can be used to fingerprint soils or OM samples by chemical composition. For instance, FTIR fingerprints of SOM grassland

and forest soils over a 700-m elevation range in France allowed discrimination by canonical variate analysis of sites by vegetation cover, presumably as a result of vegetation influence on SOM composition (Ertlen et al., 2010). Absorbances were collected on bulk soils, which varied significantly in SOM content (4.5–50% soil C); spectra were then corrected for particle size. The potential for overlap of mineral and organic absorbances was not taken into account, but differences in absorption were assumed to be due to SOM (reflecting differing vegetation) given similar mineralogy. Second and third derivatives of absorbances incrementally increased the ability of FTIR to improve discrimination among soil type by SOM.

Arocena et al. (1995) were the first to use IRMS technique to investigate the nature of the organic and mineral components in SOM. The study compared in situ OM spectra with extracted humic acids, showing the effects of the extraction process (appearance of potentially degraded ester band at approximately 1720 cm^{-1} and loss of amide II band at 1520 cm^{-1}). In another application of IR microscopy, DRIFTS mapping was utilized to map the distribution (mm-scale) of OM composition on soil microaggregate surfaces. The authors showed that OM composition was affected by preferential flow-path surfaces arising from earthworm and root activity (Leue et al., 2010a).

SR-FTIR spectroscopy has also shown capabilities of fingerprinting complex materials such as soil organic carbon (SOC). In one study, thin films of humic acids extracted from the silt and clay fractions of natural forests, plantations, and cultivated fields were shown to exhibit qualitative and quantitative differences in aromatic-C, aliphatic-C, phenolic-C, carboxylic-C, and polysaccharide-C (Solomon et al., 2005). Similar humic acid extracts were used to investigate the speciation, composition, and the long-term impact of anthropogenic activities on SOC from soils originating from tropical and subtropical agroecosystems (Solomon et al., 2007a). The use of SR-FTIR spectroscopy with other SR-based techniques, particularly near-edge X-ray absorption fine structure (NEXAFS) spectroscopy, has provided complementary data for microscale analysis of soil components. After overcoming the methodological constraints of sample preparation by embedding their samples in sulfur, Lehmann et al. (2005) determined differences in black and nonblack C from samples analyzed using the two techniques.

The two techniques were also used in the analysis of thin sections of free stable microaggregates. By mapping the spatial distribution of organic carbon in the microaggregates of three soils, Lehmann et al. (2007) showed

the correlation of aliphatic C and the ratio of aliphatic C/aromatic C to kaolinite O–H, in addition to greater microbial-derived OM on the mineral surface, as evidence supporting models of C stabilization in microaggregates. Adsorption of organics on mineral surfaces rather than occlusion of organic debris by adhering clay particles was proposed as the initial dominant process responsible for aggregate formation. Mapping of images using this technique generates considerable data. Overlapping bands, swamping from major bands such as O-H stretching and Si–O–Si stretching, and spectral fringing are a few of the challenges to spectral interpretation that arise (Lawrence and Hitchcock, 2011; Lehmann and Solomon, 2010).

In an early article highlighting the potential application of FT-Raman and SERS to HS, Yang and Chase (1998) highlighted the limitations of Dispersive Raman to the study of HS, namely fluorescence coupled with the dark color of the organic molecules. Utilizing FT-Raman, Yang et al. elucidated the building blocks of HS (through acid hydrolysis to remove labile constituents) to be low, structurally disordered carbon networks with two peaks at ~1600 cm^{-1} and ~1300 cm^{-1} (Yang and Wang, 1997; Yang et al., 1994). Assignment of Raman bands in a complex matrix such as soils is challenging but some of the characteristic peaks are presented in Table 1.3. Due to the variability of samples, this table should be observed only as a guideline for possible assignments. More comprehensive band assignments are available in the literature (Chalmers and Griffiths, 2002; Ferraro, 2003; Smith, 2005). Peaks associated with humic acids are less complex (usually consisting of two broad bands), but show some variation depending on origin (Yang and Wang, 1997).

Due to the significant signal enhancement and quenched fluorescence, more studies have utilized SERS to investigate SOM. Several studies have applied SERS to the characterization of humic acids in soil (Corrado et al., 2008; Francioso et al., 2000, 2001, 1996; Liang et al., 1996; Vogel et al., 1999), including the effect of pH on humic acid structure at different pH values. In a series of studies, Francioso et al. were the first to successfully utilize SERS to ascertain structural and conformational characteristics of humic acids extracted from peat (Francioso et al., 1996). In later work the same authors applied SERS, DRIFTS, and NMR spectroscopy to study humic and fulvic acids extracted from peat, leonardite, and lignite. The peat humic acids had a greater content of oxygenated (COOH, C–OH in carbohydrates and phenols) and aliphatic groups while the humic acids from the leonardite and lignite had a lower content of sugar-like components and polyethers (Francioso et al., 2001).

Table 1.3 Raman Peak Assignments Relevant to Soil Organic Constituents

Raman Shift (cm^{-1})	Assignment	Raman Method
3240	Water, symmetric N–H stretch of 2° amines	Dispersive[a]
3059	C═C–H aromatic stretch	SERS[b]
2950–75	CH_3 symmetric stretch	Dispersive[d], FT-Raman[d], SERS[b,c,d]
2935	C–H stretch	SERS[b,c]
2840–2890	CH_2 asymmetric stretch	Dispersive[d], FT-Raman[d], SERS[b,c,d]
2135	Triple C–C, NH_3 vibrational mode	Dispersive[a]
1735	C═O ester stretch	Dispersive[d], FT-Raman[d], SERS[b,d]
1635–1680	Amide I: C═O, C–N, N–H	FT-Raman[e], SERS[b],
1580–1600	Aromatic C═C stretch	Dispersive[a], FT-Raman[d,e], SERS[f]
1550–1575	Amide II: N-H, C–N	Dispersive[a,d], FT-Raman[d], SERS[b,d]
1530	Graphite C═C (G band)	Dispersive[b,g]
1440–1460	C–H bending vibration	Dispersive[a,d,g], FT-Raman[d], SERS[b,d]
1380	COOH symmetric stretch	Dispersive[a,d], FT-Raman[d], SERS[d,f]
1300–1340	Diamond C═C (D band)	Dispersive[b,g], FT-Raman[e]
1270	CH_2 deformation	Dispersive[d], FT-Raman[d], SERS[b,d]
1145–1160	C–C breathing vibration, C–O asymmetric stretch	FT-Raman[h]
1085	C–O stretch, C–N stretch	Dispersive[d], FT-Raman[d], SERS[b,d],
1061	C–N and C–C stretch	SERS[b]
1030–1130	C–C stretch, C–O stretch, C–O–H deformation	SERS[b]
950–990	Aromatic C–H out-of-plane deformation	Dispersive[a,d], FT-Raman[d], SERS[d]
897	C–O–C stretch	SERS[b]

SERS: surface enhanced Raman scattering spectroscopy, FT-Raman: Fourier transform Raman spectroscopy.
[a]Dollish et al., (1974).
[b]Maquelin et al. (2002).
[c]Vogel et al. (1999).
[d]Yang and Chase (1998).
[e]Yang and Wang (1997).
[f]Roldan et al. (2011).
[g]Edwards et al. (2012).
[h]Schenzel et al. (2001).

Humic binding mechanisms have also generated several SERS studies (Corrado et al., 2008; Leyton et al., 2008; Liang et al., 1999; Roldán et al., 2011; Sánchez-Cortés et al., 1998; Sanchez-Cortes et al., 2006; Vogel et al., 1999; Yang and Chase, 1998). In a recent study, Roldán et al. (2011) utilized SERS and surface-enhanced fluorescence to investigate the interaction of humic acids extracted from a soil amended for over 30 years with cattle manure, cow slurries, crop residues, and a control sample with the herbicide paraquat (1,1′-dimethyl-4,4′-bipyridinium). Binding mechanisms were attributed to the structure of the HS. The polyphenolic aromatic-rich HS, originating from crop residues, interacted through π-π stacking with similar groups of the pesticide. For the cattle manure and cow slurry HS, the interactions were mostly ionic and occurred through the larger amounts of carboxylate groups. Advances in SERS instrumentation and improvements of the technique have enabled in situ monitoring of soil carbon sequestration (Stokes et al., 2003; Wullschleger et al., 2003). By modifying the SERS surface from "passive" silver to an "active/electro" surface using copper, detection of humic acids at 1000 ppm was possible, although not reproducible. Signal reproducibility was improved by using a hybrid electro-SERS surface (electrochemically enhanced adsorption with an alumina-based copper). In another study, SERS was similarly enhanced through the use of a chelating agent (4-(2-pyridylazo) resorcinol) to detect Zn (II) in contaminated industrial soils (Szabó et al., 2011).

6. BACTERIA AND BIOMOLECULES

In soil environments, bacteria and biopolymers are ubiquitous and play a critical role in aggregate stability, nutrient cycling, and bioremediation. All of these processes involve interactions between biopolymers and mineral surfaces, which are dependent on the nature and quantity of reactive biomolecular functional groups. FTIR spectroscopy has emerged as a fundamental tool for evaluating biomolecule and bacterial composition and its utility has been realized for a diversity of disciplines including microbiology, medicine, engineering, and environmental science. In soil science, the development of FTIR as a tool to examine biological samples has been critical for increasing our mechanistic understanding of cell/biomolecule adhesion on mineral surfaces.

FTIR spectroscopy was first suggested as a tool for bacterial identification over 100 years ago (Coblentz, 1911), and over the years has been used extensively to study microorganisms and biomolecules (Brandenburg

and Seydel, 1996; Fringeli and Günthard, 1981; Jiang et al., 2004; Legal et al., 1991; Levine et al., 1953; Naumann et al., 1996; Nivens et al., 1993a, 1993b; Omoike and Chorover, 2004; Riddle et al., 1956; Schmitt and Flemming, 1998; Wang et al., 2010). Common FTIR band assignments corresponding to lipids, nucleic acids, proteins, and polysaccharides of bacteria and biomolecules are presented in Table 1.4. Naumann et al. (1988, 1991) established FTIR spectroscopy as a method to rapidly identify microorganisms through analysis of specific "fingerprint" spectra. Their method utilizes spectral derivatives and correspondence maps to differentiate and identify bacteria. This approach is commonly used for identification of bacteria from pure cultures and extracts (e.g. Schmitt and Flemming, 1998; Yu and Irudayaraj, 2005). Microbial identification via FTIR has also been successful from simple mineral matrices, such as detection of *Bacillus subtilis* spores within bentonite (Brandes Ammann and Brandl, 2011) and *Escherichia coli*

Table 1.4 Pertinent Infrared Assignments for Bacteria and Biopolymer Samples

Wavenumbers (cm^{-1})	IR Band Assignment
2956	$\nu_{as}(CH_3)$[a]
2920	$\nu_{as}(CH_2)$[a]
2870	$\nu_{s}(CH_3)$[a]
2850	$\nu_{s}(CH_2)$[a]
1720–1729	$\nu_{as}(COOH)$[b]
1652–1637	Amide I: C═O, C–N, N–H[b,c,d]
1550–1540	Amide II: N–H, C–N[a–c]
1460–1454	$\delta(CH_2)$[b,c]
1400–1390	$\nu_{s}(COO^-)$[b,c]
1220–1260	$\nu_{as}(PO_2^-)$ of phosphodiesters (hydrated)[b,e,f]
1170	ν(C–O)[d]
1114–1118	ν(C–O–P, P–O–P), aromatic ring vibrations[b,d]
1084–1088	$\nu_{s}(PO_2^-)$ of phosphodiesters,[i] ring vibrations,[b] ν(C–C)[g]
1045, 1052, 1058	ν(C–O–C, C–C) from polysaccharides[b,g]
962–968	$\nu(PO_2^-)$[h,i]
650–450	$\nu(CH_2)$[j]

ν_{as}: asymmetric stretching vibration, ν_s: symmetric stretching vibration, δ: bending vibration.
[a]Schmitt and Flemming (1998).
[b]Brandenburg and Seydel (1996).
[c]Sockalingum et al. (1997).
[d]Nivens et al. (1993a, 1993b).
[e]Brandenburg et al. (1997).
[f]Naumann et al. (1991).
[g]Fringeli and Günthard (1981).
[h]Barja et al. (1999).
[i]Quiles et al. (1999).
[j]Deo et al. (2001).

metabolic products on carbonate minerals (Bullen et al., 2008). For details on the use of FTIR to identify and classify microorganisms, readers are referred to Mariey et al. (2001), who give a thorough review of articles from the 1990s which utilize FTIR spectroscopy for characterization of microorganisms, and papers by Maquelin et al. (2003, 2002) who employ FTIR and Raman spectroscopies to identify medically relevant microorganisms.

Due to the presence of SOM, characterization of bacteria within soil samples is not feasible. The organic nature of bacteria results in similarities of peak locations between SOM and microbial samples. For this reason many IR band assignments are common among these samples. However, stark contrasts in typical spectra can be observed and reflect significant differences in the chemical composition, with bacteria having much lower C:N and C:P than SOM (Horwath, 2007). This difference results in prominent amide I (1650 cm^{-1}), amide II (1550 cm^{-1}), and PO_4^{3-} (1240 cm^{-1}) peaks in FTIR spectra of bacteria. As an illustrative example, spectra for various bacterial species collected using multibounce ATR-FTIR on a ZnSe IRE are shown in Figure 1.12(A). CH_2 and CH_3 bonds of aliphatic chains are also prevalent on bacteria and the corresponding symmetric and asymmetric vibrations can be easily observed as a quartet of IR peaks at approximately 2560,

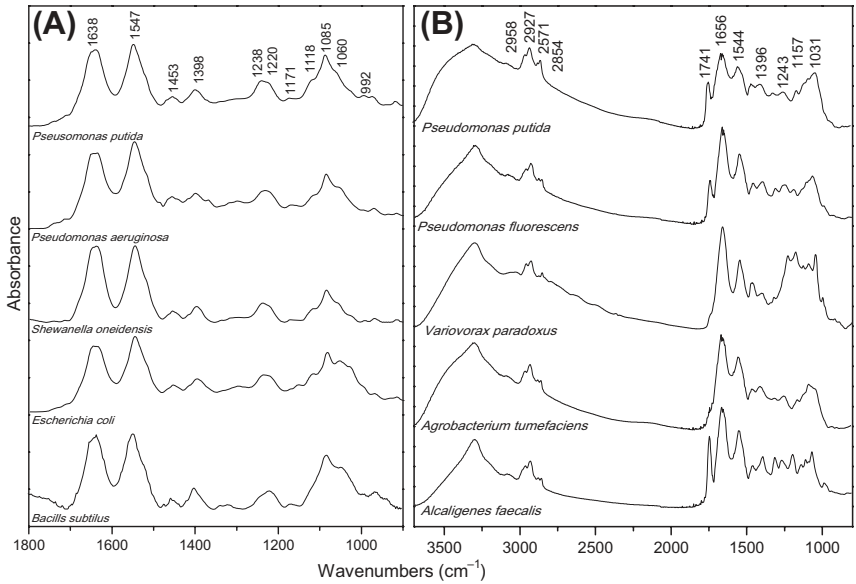

Figure 1.12 FTIR spectra of various bacteria collected by (A) ATR-FTIR on ZnSe and (B) transmission on ZnSe (Thermo Nicolet 6700 spectrometer). (ATR, attenuated total reflectance; FTIR, Fourier transform infrared.)

2930, 2570, and 2855 cm^{-1}. Examples of these peaks are shown in transmission FTIR spectra of various bacteria species in Figure 1.12(B). Although, characterization of in situ soil bacteria is not possible, knowledge regarding the IR spectra of bacteria is very important for understanding processes of bacterial adhesion to mineral surfaces.

A number of studies have used FTIR to characterize and study interactions of specific bacterial components including extracellular polymeric substances (EPS) (Badireddy et al., 2008; Beech et al., 1999; Eboigbodin and Biggs, 2008; Omoike and Chorover, 2004, 2006; Omoike et al., 2004; Wingender et al., 2001), lipopolysaccharides (LPS) (Brandenburg, 1993; Brandenburg et al., 2001, 1997; Brandenburg and Seydel, 1990; Kamnev et al., 1999; Parikh and Chorover, 2007, 2008), phospholipids (Brandenburg et al., 1999; Brandenburg and Seydel, 1986; Cagnasso et al., 2010; Hübner and Blume, 1998), and DNA (Brewer et al., 2002; Falk et al., 1963; Mao et al., 1994; Pershina et al., 2009; Tsuboi, 1961; Zhou and Li, 2004). In addition, ATR-FTIR has emerged as a powerful tool for studying biofilm formation, composition, and structure (Beech et al., 2000; Cheung et al., 2000; Schmitt and Flemming, 1999; Spath et al., 1998).

Although less extensively studied, the nondestructive nature and minimal sample handling of Raman techniques, coupled with the invisibility of water have lent themselves well to application of analysis of bacteria and biomolecules. Raman techniques afford a fast and relatively simple way to identify bacteria compared to the tedious and lengthy conventional and instrumental methods as discussed by Ivnitski et al. (1999). As in soil analysis, the development of FT-Raman overcame florescence, which hindered Raman analysis of cells due to naturally strongly fluorescent constituents such as enzymes and coenzymes (Schrader et al., 2000). In one of the first studies applying FT-Raman to bacterial identification, Naumann et al. (1995) obtained reproducible spectra of *Enterobacteriaceae, Staphylococcus, Bacillus*, and *Pseudomonas* bacterial strains that had no florescence interference even for highly colored bacteria. The Raman spectra gave complementary information (C–H bond stretching of the bacterial membrane phospholipids, amino acids, and RNA/DNA) to the FTIR data (amide I/II bands of proteins and oligo/polysaccharides of cell walls). Confocal Raman microspectroscopy has also been used successfully to rapidly identify microorganisms in blood samples (Maquelin et al., 2003), and similar techniques could likely be applied for environmental analysis. A comparison between Raman and FTIR spectroscopy of bacteria samples from that study is provided in Figure 1.13.

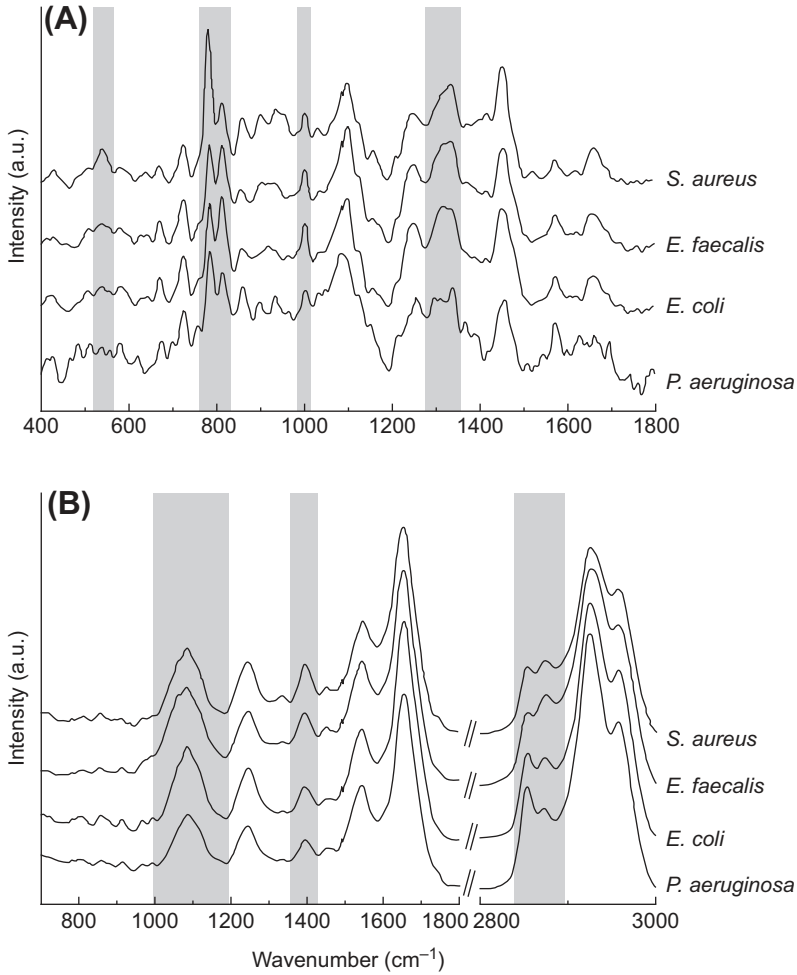

Figure 1.13 Representative Raman (A) and FTIR (B) spectra of four microorganisms (*Staphylococcus aureus*, *Enterococcus faecalis*, *Escherichia coli*, *Pseudomonas aeruginosa*). These spectra demonstrate the complementary and unique information provided by these techniques. Gray boxes have been placed over the spectra to indicate areas of differences. (FTIR, Fourier transform infrared.) *Reprinted with permission Maquelin et al. (2003).*

The high resolution and size scale necessary for these samples have meant ready application for micro-Raman and SERS. The first study to apply SERS to bacterial cell wall research examined impregnated and coated *E. coli* bacteria with silver colloids and observed sharp and intense SERS spectra (Efrima and Bronk, 1998). The resulting spectra were relatively

selective, preferentially showing bands associated with molecules and functional groups in the immediate proximity of the metal surface. Many studies have since used this technique to characterize bacteria with rapid analytical times and reproducible data (Kahraman et al., 2007; Naja et al., 2007). Improvements in the SERS substrate (through use of nanoparticles) has increased homogeneity of the substrate resulting in improved reproducibility of the Raman spectra and afforded greater sensitivity to the technique. Liu et al. were able to use this approach to detect fine-scale changes in the bacterial cell wall of single bacterium (*S. aureus*) during the bacterium's different growth stages and bacterial response to antibiotic treatment during early period of antibiotic exposure (Liu et al., 2009). Similarly, by coating volcanic clinopyroxene rocks with silver colloidal nanoparticles, SERS was utilized as a simple, sensitive technique to detect the presence of biomolecules (adenine, guanine, nucleobases, and micro-RNA) on the rocks (Muniz-Miranda et al., 2010). According to the authors, Martian rocks and sediments, believed to be analogous to pyroxene rocks, could be similarly investigated for evidence of life (extinct or extant) particularly using the sharp SERS adenosine band at 735 cm^{-1}. For additional information on Raman spectroscopy in microbiology, readers are referred to an informative review article by Petry et al. (2003).

7. SOIL AMENDMENTS

Characterization of materials using FTIR and Raman spectroscopies is an established method for scientists and is a common quality control practice in various industries. FTIR spectroscopy can serve as a rapid and informative method for analysis of a variety of soil amendments, including biochar, compost, and biosolids. This information can be utilized for quality control, predicting reactivity, and recalcitrance, or to provide insight into interfacial interactions between the amendment and soil constituents.

7.1 Biochar

Biochar is a byproduct of biomass pyrolysis (or gasification) to produce biofuels, as well as an intentional primary product from the partial pyrolysis of biomass. The produced biochar is highly aromatic and has increased C stability relative to the original feedstock materials (Lehmann and Joseph, 2009). Biochar differs from charcoal in that its primary use is not as a source of fuel, and is commonly applied to agricultural fields as a soil amendment.

The use of biochar, or black carbon, as a soil amendment has received increased attention since the discovery of the Terra Preta de Indio soils (approximately 7000 year old anthropogenic influenced soils) in the Amazon. It is proposed that these soils have received historical applications of charcoal, which provide a number of beneficial properties to the soil today (Glaser and Woods, 2004; Sombroek, 1966). Studies on the Terra Preta de Indio soils have shown that they have greater cation exchange capacity (Liang et al., 2006), fertility, and nutrient retention (Glaser, 2007; Lehmann and Joseph, 2009; Smith, 1980; Sohi et al., 2010), and stable stored carbon (Glaser et al., 2002; Sombroek et al., 2003) compared to nearby pedogenically similar soils. Presently much research is focused on attempting to replicate the conditions in these soils using biochar (Busscher et al., 2010; Case et al., 2012; Joseph et al., 2010; Kookana et al., 2011; Laird et al., 2010; Major et al., 2009; Mulvaney et al., 2004; Novak et al., 2009; Singh et al., 2010; Steinbeiss et al., 2009; Verhejien et al., 2010; Zimmerman et al., 2011).

Today, many growers are considering the use of biochar soil amendments for agronomic benefits and climate change mitigation strategies. The diversity of biochar source materials, pyrolysis methods, soils, and agricultural systems lends complexity to determining the appropriate circumstances for biochar amendments; however, it is becoming increasingly clear that the best use for a given biochar is dependent on its physical and chemical properties (Brewer et al., 2009). A number of recent publications have used FTIR and Raman spectroscopies to evaluate the chemical properties of biochar.

In an attempt to determine the difference between charcoal found within the Terra Preta de Indio soils and modern day manufactured biochars, Jorio et al. (2012) utilized Dispersive Raman to examine the carbon nanostructure within these materials. Their results reveal that the charcoal in these soils had an in-plane crystallite size distribution (La) of 3–8 nm range while that of several analyzed biochars was between 8 and 12 nm. The crystallite size distribution was approximated from intensity of the D and G bands as according to Cançado et al. (2007). Knowledge of the differences in the carbonaceous material increases the potential for improving biochar production methods to produce carbon of similar nanostructure to that of the Amazonian soils (Jorio, 2012).

FTIR spectroscopy has long been used to examine the chemical characteristics of charcoal materials (O'Reilly and Mosher, 1983; Starsinic et al., 1983; Wolf and Yuh, 1984) and the increased prevalence of biochar has resulted in the routine use of FTIR in biochar analysis (e.g. Brewer et al.,

2009; Fuertes et al., 2010; Keiluweit et al., 2010; Lehmann et al., 2005; Mukome et al., 2013). FTIR spectra of biochar provide information regarding the relative contribution of chemical functional groups (Table 1.5) and give a qualitative indication of the aromaticity of samples.

As a tool for characterization, FTIR spectroscopy can be used to elucidate the impact of pyrolysis temperature on the chemical composition of biochar. Increasing pyrolysis temperature and duration resulted in straw feedstock biochars with decreased peak intensities for C–O, O–H, and aliphatic C–H, concomitant with increased aromatic bands (Peng et al., 2011). A similar result was observed when ponderosa pine shavings and grass clippings were pyrolyzed from 100 to 700 °C and analyzed via FTIR (Keiluweit et al., 2010). The results demonstrate dehydration (decreased O–H), followed by increased lignin- and cellulose-derived products (C═C,

Table 1.5 Functional Group Assignments Corresponding to Biochar Samples as Determined by ATR-FTIR Analysis

Wavenumbers (cm^{-1})	Assignment
2924	ν(C–H) vibrations in CH_3 and CH_2[a–f]
2850	ν(C–H) vibrations in CH_3 and CH_2[a–f]
1695	ν(C═O) vibration aromatic carbonyl/carboxyl C═O stretching[a–f]
1640	ν(C═C) vibration, C═C aromatic ring[a–f]
1587	C═C vibration[a–f]
1505–1515	Skeletal C═C vibration (lignin)[a–f]
1460	δ(C–H) vibrations in CH_3 and CH_2[a–f]
1423	C═C vibration[a–f]
1380	ν(C–O) vibration aromatic and δ(C–H) vibrations in CH_3 and CH_{2v}[a–f]
1240–1260	ν(C–O) vibration phenolic[a–f]
1154	Aromatic C–O stretching[a,b,e]
1080–1040	Si–O, C–O stretch of polysaccharides[a]
1029	Aliphatic ether C–O and alcohol C–O stretching[a,b,d,e]
870	1 adjacent H deformation[a,b,d,e]
804	2 adjacent H deformations[a,b,d,e]
750	4 adjacent H deformations[a,b,d,e]
667	γ(OH) bend[a,e]

[a]Hsu and Lo (1999).
[b]Sharma et al. (2004).
[c]Keiluweit et al. (2010).
[d]Özçimen and Ersoy-Meriçboyu (2010).
[e]Wu et al. (2009).
[f]Brewer et al. (2009).

C═O, C–O, C–H), and finally condensation into aromatic ring structures (decrease in number of FTIR bands) for biochars produced at 700 °C. Since FTIR spectroscopy probes chemical bonds with dipole moments, nonpolar materials are not strong IR absorbers; therefore, the FTIR spectra of highly aromatic chars do not have large peaks.

It should be noted that FTIR is not limited to characterization of discrete biochar samples, but can also be used to study and characterize charcoal within soil. For example, the Terra Preta de Indio soils were evaluated using SR ATR-FTIR in order to compare the content of phenolics, aliphatics, aromatics, carboxyls, and polysaccharides in these and adjacent soils having no charcoal added (Solomon et al., 2007b). Analysis of carbon functional groups present in the analyzed samples revealed that the Terra Preta de Indio soils have elevated levels of recalcitrant carbon (aliphatic and aromatic) attributed to historical additions of charcoal and the increased carbon sequestration within these soils.

Although determination of aromaticity and structural disorder of charcoals can be probed with FTIR, Raman spectroscopy provides distinct advantages for determining the structural order of carbonaceous materials. For example, the structural order of carbon nanostructures is routinely evaluated using this approach (Ajayan, 1999; Dresselhaus et al., 2005; Ferrari et al., 2006). Similarly, the amorphous nature of biochars can be determined via Dispersive Raman analysis. Through analysis of the Raman shift at 1500 cm^{-1} (sp^2 carbon), 1150 cm^{-1} (sp^3-hyridized carbon), and 1530 cm^{-1} (sp^2-hydridized carbon) the amorphous nature of biochar can be evaluated (Schmidt et al., 2002). Similar to the pyrolysis temperature effects evaluated with FTIR, Raman spectroscopy has demonstrated that the amorphous carbon components of biochar decrease with increased duration of steam gasification (Wu et al., 2009). During feedstock conversion to biochar, Raman bands associated with the disordered carbon decrease relative to aromatic and recalcitrant carbon. Another study using Dispersive Raman spectroscopy as a biochar characterization tool showed changes that occur in the ratio of sp^2 (G band) to sp^3 C (D band) in the material as a function of pyrolysis temperature (Chia et al., 2012). In addition, Dispersive Raman revealed how the sp^2 to sp^3 ratio changes with biochar feedstock (Jawhari et al., 1995; Mukome et al., 2013). The G or graphite-band arises from vibrations of sp^2 C found in graphitic materials and C═C bonds, while the D-band (diamond band) is linked to the breathing modes of disordered graphite rings (Ferrari and Robertson, 2000; Sadezky et al., 2005). On occasion these two broad peaks have been

further deconvoluted into seven peaks and further structural characterization information determined (Kim et al., 2011; Li et al., 2006). A helpful summary of Raman band assignments for charcoal samples is also presented by Wu et al. (2009).

7.2 Compost

Analysis of compost via vibrational spectroscopy results in spectra similar to those observed for SOM and humic fractions. One notable difference between analyses of these samples is that the humification of compost raw materials can be observed as a function of composting time to study the composting process (Chen, 2003; Inbar et al., 1991; Ouatmane et al., 2000; Smidt and Schwanninger, 2005; Wershaw et al., 1996), and characterize compost materials (Carballo et al., 2008b; Niemeyer et al., 1992). The evolution of FTIR spectra of green-waste samples to compost has shown an increase in etherified and peptidic compounds (bands at 1384, 1034, and 1544 cm^{-1}) with a relative decrease of more labile aliphatic carbon pools (2925 and 1235 cm^{-1}) (Amir et al., 2010). This interpretation of the spectral results are consistent with corresponding analysis of total C, H, N, and O content during the composting process. Other studies examining the composting processes highlight the increase of aromatic content and reduction in oxygen containing functional moieties (e.g. carboxylic, carbonylic groups) with increased humification (Fuentes et al., 2007). An excellent discussion of changes in FTIR spectra through observation of indicator bands for product control during waste material processing can be found in Smidt and Schwanninger (2005). Through a process of calibration with database of compost samples, FTIR has also been shown to hold promise as a rapid and cost-effective tool for estimating total C, total N, lignin, and cellulose content of composts (Tandy et al., 2010).

7.3 Biosolids

Due to the comparable composition of biosolids with compost and SOM, FTIR spectra are similar and band assignments are analogous. Biosolid IR spectra have numerous bands attributed to typical organic functional groups such as OH, CH_2, CH_3, C═O, COOH. Composted biosolids tend to be highly aliphatic and similar to fulvic acids extracted from soil and aquatic samples (Pérez-Sanz et al., 2006; Tapia et al., 2010). The addition of iron salts in wastewater treatments plants to coagulate OM can lead to the production of Fe-rich biosolid materials. Combined analysis of Fe content in biosolid extracted humic fractions and carboxyl content of FTIR spectra showed a

positive relationship, suggesting the formation of carboxyl-Fe complexes. Iron chelation by water-soluble HS has shown to increase Fe uptake by plants (Cesco et al., 2002), thus biosolids may serve as a source of Fe fertilizer (Pérez-Sanz et al., 2006).

8. MOLECULAR-SCALE ANALYSIS AT THE SOLID–LIQUID INTERFACE

Vibrational spectroscopy has proven to be an extremely valuable tool for elucidating binding mechanisms for a variety of compounds on environmental surfaces. These versatile techniques have successfully been employed to probe the soil–liquid interface for studies examining the sorption of inorganic ions, natural OM, anthropogenic organic compounds, biomolecules, and bacteria to clay minerals and metal oxides. In this case ATR-FTIR spectroscopy is the tool of choice for elucidating binding mechanisms at interfaces. In each of these cases it is the ability to use coatings to increase sensitivity and permit evaluation of sorption processes that makes ATR-FTIR analytically powerful. Although advanced X-ray techniques are providing new capabilities and additional insights for studies of mineral interfaces, the relative ease, low cost, and analytical power of FTIR spectroscopy approaches makes it an invaluable tool for researchers.

When it comes to FTIR for analysis at the solid–liquid interface, the use of ATR-FTIR is essential. Although DRIFTS has also been used to examine sorption reactions, this approach can introduce artifacts, which make data interpretation difficult and may yield incorrect results. The use of crystal IRE solves this problem and permits examination in the presence of water. The reason this works is that the IR light traveling through the IRE does not penetrate directly through the aqueous medium, but instead an evanescent wave propagates at each reflection point to provide information regarding the IR absorbance by molecules present at the IRE surface. Through the use of a reference water spectrum, water bands can be effectively subtracted to produce spectra revealing the interactions of species, which may be dissolved or bound to the substratum. For soil science research, one of the most important developments of ATR-FTIR was creating coatings on the IRE with relevant mineral phases to examine sorption to these surfaces. The use of IRE coatings was first developed by Hug et al. (Hug, 1997; Hug and Sulzberger, 1994) and has been widely adapted as a standard approach for evaluating sorption to mineral surfaces. These studies even allow discrimination between inner- and outer-sphere sorption mechanisms.

8.1 Organic Molecule Interactions with Mineral Surfaces

Organic molecules reacting with mineral surfaces may undergo a variety of processes such as surface complexation, oxidation/reduction, transformation, and polymerization. Therefore, evaluating the interactions of organic compounds with mineral surfaces is critical for understanding mineral dissolution, SOM stabilization, alteration of a solid's physicochemical properties, organic pollutant fate and transport in soil and sediment, and the formation of biomolecules on early Earth (Duckworth and Martin, 2001; Gu et al., 1995; Hazen and Sverjensky, 2010; Parikh et al., 2011; Wu et al., 2011; Yoon et al., 2004a). Vibrational spectroscopy provides a means to capture a spatially integrated response of the local bonding environment by measuring energies associated with the motion of bonded atoms, which can then be utilized to determine molecular structure (Amonette, 2002; Sposito, 2004). Therefore, vibrational spectroscopy provides a relatively convenient means to measure changes in the molecular structure of an adsorbed species (adsorbate) relative to an aqueous species (adsorptive) or changes in the adsorbent before and after complexation reactions.

Vibrational spectroscopy studies may employ direct observation of adsorbate interactions with an adsorbent or use alternative strategies. Johnston et al. (1993) and Sposito (2004) discuss two alternative strategies and refer to them as the use of adsorbate surrogates and reporter groups. In the case of adsorbate surrogates, a particular chemical species is used as an in situ probe to identify adsorbate–adsorbent interactions that can then be applied to understand adsorption mechanisms for similar compounds (Sposito, 2004). For example, Axe and Persson (2001) and Yoon et al. (2004b) used oxalate as an adsorbate surrogate to understand the interaction of dicarboxylates with metal oxide surfaces. This is in contrast to the use of reporter units, typically hydroxyl groups when working with mineral adsorbents, on the adsorbent surface. When employing reporter units one investigates changes in mineral spectra before and after reaction with an adsorbate to indicate adsorbate bonding characteristics (Sposito, 2004). Johnston and Stone (1990) used the reporter unit approach to study hydrazine sorption to kaolinite. Upon intercalcation of hydrazine, the intensity of OH stretching and deformation bands in Raman and FTIR spectra was substantially reduced, and the reductions in intensity were attributed to hydrogen bonding between hydrazine and OH groups of kaolinite present in the interlayer.

A variety of FTIR techniques have been used to investigate organic compound–mineral interactions (e.g. transmission, FTIR, DRIFTS, ATR-FTIR, SR-FTIR). Although the interference from water in a spectrum is typically

diminished in transmission FTIR and DRIFTS analyses due to dehydration of the sample, these methods may provide inaccurate representation of interactions on a hydrated mineral surface. Kang and Xing (2007) and Kang et al. (2008) noted that the carboxylic acid function groups of organic acids tend to form outer-sphere complexes with metal centers on minerals when the spectra of pastes were collected using in situ ATR-FTIR. However, inner-sphere complexes were more predominant in the DRIFTS spectra of freeze-dried samples as noted by shifts in the asymmetric COO^- stretch to higher frequencies. The inducement of inner-sphere coordination on a mineral surface is due not only to dehydration but also to significant decreases in pH upon drying. This can be discerned from the observation of Kang and Xing (2007) that inner-sphere complexation was favored at lower pH, and the work of Dowding et al. (2005) and Clarke et al. (2011) illustrating drastic pH decreases (hydrogen ion activity increased 1000-fold) with increased drying. Although the spectra of powders or pressed pellets is applicable for understanding interactions under extremely dry conditions, it may provide false information regarding the types of surface complexes formed under well hydrated conditions. This may be particularly problematic when attempting to apply mechanistic understanding of bonding observed in transmission FTIR or DRIFTS to explain macroscopic data collected under hydrated conditions (i.e. batch test tube sorption experiments). Therefore, it is more appropriate to study organic interactions with minerals under hydrated conditions using saturated pastes obtained from batch experiments or in situ bonding of organics to mineral-coated crystals when practical.

The assignment of molecular vibrations to spectral features observed at particular frequencies can be quite challenging in complex spectra due to: (1) the wide range of frequencies where some vibrations may appear in a spectrum; (2) the overlap of frequencies associated with two or more vibrations; (3) spectral interferences (e.g. water, CO_2); (4) slight differences in band position within spectra collected using differing FTIR techniques; and (5) insufficient or lack of information on band assignments for a particular compound. One means to aid in the assignment of bands within a spectrum is through the study of spectral changes as a function of pH. Examples of this approach can be found in studies of the fluoroquinolone antibiotics ofloxacin (Goyne et al., 2005) (Figure 1.14) and ciprofloxacin (Gu and Karthikeyan, 2005b; Trivedi and Vasudevan, 2007). Through the collection of aqueous ofloxacin spectra (Figure 1.14), Goyne et al. (2005) were able to observe loss of the C═O stretch of the COOH (1710 cm^{-1}) and increased intensity of the COO^- asymmetric (1585 cm^{-1}) and symmetric (1340 cm^{-1}) stretches as pH increased. Decreased intensity of vibration at 1400 cm^{-1} with increased acidity was attributed to protonation of N_4 in

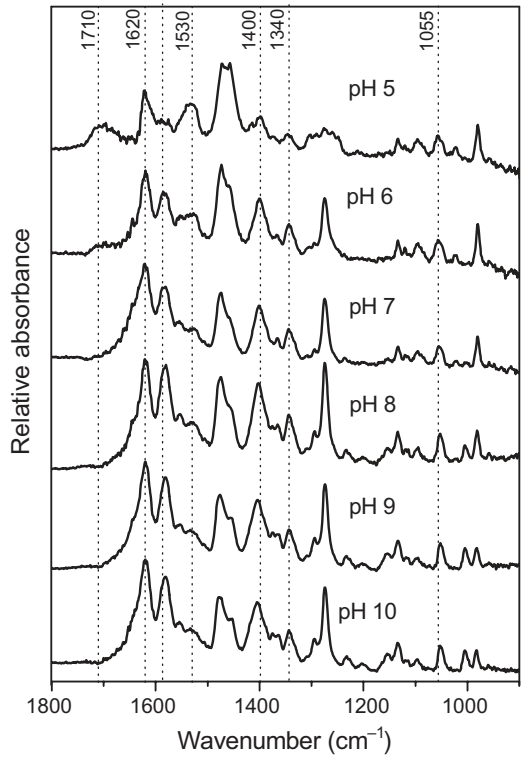

Figure 1.14 ATR-FTIR difference spectra of ofloxacin in 0.02 M $CaCl_2$ background electrolyte solution from pH 5 to 10. *Adapted with permission from Goyne et al. (2005).*

the piperazinyl ring. Trivedi and Vasudevan (2007) used a similar approach; however, they also investigated aqueous spectra of Fe^{3+}-ciprofloxacin complexes as a function of pH, which was useful for interpreting the spectra of ciprofloxacin bound to goethite. In addition, prediction of FTIR and Raman spectra using molecular modeling can help to further elucidate observed vibrational bands (Kubicki and Mueller, 2010).

Indications of inner- and outer-sphere complex formation on mineral surfaces and the types of surface complex structures formed can also be acquired from MIR spectra. Formation of inner-sphere complexes between adsorbates with a carboxylic acid group and mineral surfaces is often indicated by substantial shifts (25–150 cm^{-1}) in the frequency of asymmetric and symmetric COO^- stretching relative to a spectrum of the aqueous adsorptive (e.g. Chorover and Amistadi, 2001; Duckworth and Martin, 2001; Gu et al., 1995; Gu and Karthikeyan, 2005b; Kang and Xing, 2007). With respect to the types of structural complexes formed, there are three common coordination modes developed between

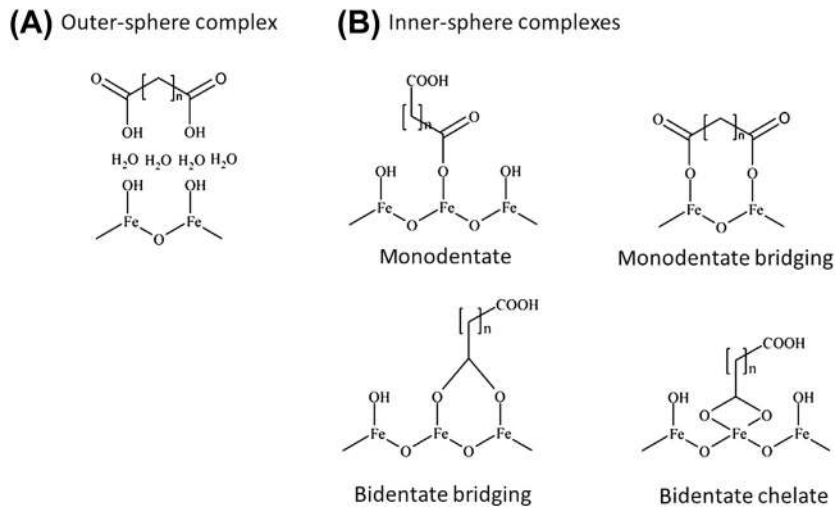

Figure 1.15 Various adsorption complexes between dicarboxylic acids and an iron oxide surface. *Adapted with permission from Kang et al. (2008).*

Table 1.6 General Range of Carboxyl Band Separations ($\Delta\nu$), between Unbound Carboxyl Groups ($\Delta\nu_{ionic}$) and Metal-Carboxyl Complexes ($\Delta\nu_{com}$), and Corresponding Binding Coordination (Dobson and McQuillan, 1999; Hug and Bahnemann, 2006; Kang et al., 2008)

Coordination	COO^- Band Separation ($\Delta\nu$)	$\Delta\nu_{com}$:$\Delta\nu_{ionic}$	Carboxyl Shift
Monodentate	350–500 cm^{-1}	$\Delta\nu_{com} > \Delta\nu_{ionic}$	$\nu_s(COO^-)$ lower
Binuclear bidentate	150–180 cm^{-1}	$\Delta\nu_{com} < \Delta\nu_{ionic}$	$\nu_s(COO^-)$ higher or lower $\nu_{as}(COO^-)$ higher or lower
Mononuclear bidentate	60–100 cm^{-1}	$\Delta\nu_{com} << \Delta\nu_{ionic}$	$\nu_s(COO^-)$ higher ν_{as} (COO^-) lower

a carboxylate group and a cation at the mineral surface: (1) monodentate binding; (2) chelating bidentate; and (3) bridging bidentate (Figure 1.15). The formation of these coordination modes can be distinguished through determination of the separation distance (cm^{-1}) between the asymmetric and symmetric COO^- stretching vibrations ($\Delta\nu = \nu_{as}COO^- - \nu_sCOO^-$) (Alcock et al., 1976; Deacon and Phillips, 1980). As shown in Table 1.6, the range of $\Delta\nu$ for chelating bidentate, bridging bidentate, and unidentate bridging are 60–100 cm^{-1}, 150–180 cm^{-1}, and 350–500 cm^{-1}, respectively

(Dobson and McQuillan, 1999; Kang et al., 2008). It should be noted that these are only typical ranges of $\Delta\nu$ for coordination assignments and analyses can be made on an individual basis by comparing the $\Delta\nu$ of unbound carboxyl groups ($\Delta\nu_{ionic}$) with those representing metal-carboxyl complexes ($\Delta\nu_{com}$) such $\Delta\nu_{com} > \Delta\nu_{ionic}$ for monodentate binding, $\Delta\nu_{com} < \Delta\nu_{ionic}$ for bridging bidentate, and $\Delta\nu_{com} << \Delta\nu_{ionic}$ for chelating bidentate (Hug and Bahnemann, 2006). The differences in $\Delta\nu$ for the various coordination modes arise due to changes in C–O bond lengths and O–C–O angles upon bonding to a cation that subsequently alter the frequency at which a vibration is observed (Nara et al., 1996).

8.1.1 Low Molecular Weight Organic Acids

There has been a considerable amount of research published examining the interaction of low molecular weight organic molecules at the solid–liquid interface using vibrational spectroscopy. The pioneering work by Tejedor-Tejedor et al. (Tejedor-Tejedor and Anderson, 1990; Tejedor-Tejedor et al., 1992) demonstrated how in situ analysis of organic molecules could be carried out using ATR-FTIR in order to elucidate sorption mechanisms to mineral surfaces. In these companion papers, phthlate (PHTH), *p*-hydroxybenzoate (PHB), and 2,4-dihydroxybenzoate (2,4DHB) were reacted with goethite suspensions and analyzed using a cylindrical ZnSe ATR-FTIR IRE. Through comparison of IR spectra before and after reaction with goethite the authors determined that PHTH and PHB both bound to goethite through bidentate–binuclear surface complexes via both oxygens of a carboxyl group to a single iron atom. For 2,4DHB, a bidentate–mononuclear surface complex through one carboxyl oxygen and one phenolic oxygen was formed on goethite. Since the publication of these papers, the use of ATR-FTIR to elucidate sorption mechanisms of small organic molecules has become commonplace.

Due to interference from a heterogeneous background matrix (SOM and various minerals), it is highly challenging to determine binding mechanisms of small organic molecules in soil samples. For this reason, research in this area has been conducted using pure mineral phases such as Fe oxides (e.g. hematite, goethite), Al oxides (e.g. gibbsite, corundum), Ti-oxides (e.g. rutile, anatase), and phyllosilicates (e.g. smectite, montmorillonite) to examine low molecular weight organic molecule (e.g. amino acids, carboxylic acids) sorption mechanisms. Table 1.7 provides a list of selected studies, which have used FTIR spectroscopy to study these processes. Readers are also directed to Lefèvre et al. (2012) for a recent review of carboxylic acid reactions with mineral surfaces.

Table 1.7 Compiled List of Studies Investigating the Sorption of Amino Acids, Carboxylic Acids, and Other Low Molecular Weight Organic Molecules to Mineral Surfaces

References	Sorbate	Mineral	Analysis Method
Axe and Persson (2001)	Oxalate	Boehmite	ATR-FTIR
Axe et al. (2006)	Oxalate, malonate	Goethite	ATR-FTIR
Barja et al. (2001)	Phosphonate	Goethite	ATR-FTIR
Bargar et al. (1999)	Pb(II)-ethylenediaminetetraacetic acid (EDTA)	Goethite	ATR-FTIR, DRIFTS, EXAFS
Benetoli et al. (2007)	Alanine, methionine, glutamine, cysteine, aspartic acid, lysine, histidine	Bentonite, kaolinite	Transmission FTIR, XRD, Mössbauer
Boily et al. (2000)	Benzenecarboxylate	Goethite	ATR-FTIR
Borer et al. (2009)	Desferrioxamine b	Lepidocrocite	ATR-FTIR
Borda et al. (2003)	Oxalate	Goethite	ATR-FTIR
Bowen et al. (1988)	Dimethyl monophosphate	Montmorillonite	Transmission FTIR
Brigatti et al. (1999)	Cysteine	Montmorillonite, beidellite	Transmission FTIR, XRD, DTC
Cagnasso et al. (2010)	L-α-phosphatidylcholine, phosphatidyl-ethanolamine, phosphatidic acid	Goethite, hematite	ATR-FTIR
Dobson and McQuillan (1999)	Formate, acetate, oxalate, succinate, fumarate, malonate	Titanium oxide, aluminum oxide, zirconium oxide, tantalum oxide	ATR-FTIR
Duckworth and Martin (2001)	Oxalate, malonate, glutarate, succinate, adipate	Hematite	ATR-FTIR
Fitts et al. (1999)	Cu(II)-glutamate	γ-Alumina	ATR-FTIR, EXAFS
Kang and Xing (2007)	Succinic acid, glutaric acid, adipic acid, azelaic acid	Kaolinite, montmorillonite	ATR-FTIR, DRIFTS
Kang et al. (2008)	Succinic acid, glutaric acid, adipic acid, azelaic acid	Goethite	ATR-FTIR, DRIFTS

Gu et al. (1995)	Phthalate, catechol, natural organic matter	Hematite	ATR-FTIR, NMR
Gulley-stahl et al. (2010)	Catechol	Manganese oxides, iron oxide, titanium oxides chromium oxide (amorphous nanoparticles)	ATR-FTIR
Ha et al. (2008)	Lactate	Hematite	ATR-FTIR, QCC
Hug and Sulzberger (1994)	Oxalate, acetate	Anatase	ATR-FTIR, SVD
Hug and Bahnemann (2006)	Oxalate, malonate, succinate	Rutile, anatase, lepidocrocite	ATR-FTIR
Hwang and Lenhart (2008)	Maleate acid, fumarate, succinate	Hematite	ATR-FTIR
Johnson et al. (2004)	Maleate	Corundum	ATR-FTIR
Kubicki et al. (1999)	Acetate, oxalate, citrate, benzoate, salicylate, phthalate	Quartz, albite, illite, kaolinite, montmorillonite	ATR-FTIR, MOC
Lackovic et al. (2003)	Citrate	Goethite, kaolinite, illite	ATR-FTIR
Lefèvre et al. (2012)	5-Sulfosalicylic acid	Gibbsite	ATR-FTIR
Mendive et al. (2006)	Oxalate	Anatase, rutile	ATR-FTIR
Norén et al. (2008)	Sarcosine, 5-carboxy-2-methyl-1H-imidazole-4-carboxylate (H_2MIDA^-), ethylenediamine-*N*,*N*-diacetic acid (H_2EDDA)	Goethite	ATR-FTIR
Norén and Persson (2007)	Acetate, benzoate, cyclohexanecarboxylate	Goethite	ATR-FTIR
Parikh et al. (2011)	Glutamate, aspartate	Rutile	ATR-FTIR, QCC
Parikh and Chorover (2006)	Phenylphosphonic acid adenosine 5′-monophosphate, 2′-deoxyadenyl-(3′->5′)-2′-DNA	Hematite	ATR-FTIR

Continued

Table 1.7 Compiled List of Studies Investigating the Sorption of Amino Acids, Carboxylic Acids, and Other Low Molecular Weight Organic Molecules to Mineral Surfaces—cont'd

References	Sorbate	Mineral	Analysis Method
Persson et al. (1998)	Acetate	γ-Alumina	ATR-FTIR
Persson and Axe (2005)	Oxalate, malonate	Goethite	ATR-FTIR
Roddick-Lanzilotta et al. (1998)	Lysine	Anatase, titanium oxide (amorphous)	ATR-FTIR
Roddick-Lanzilotta and Mcquillan (1999)	Lysine peptide, polylysine	Titanium oxide (amorphous)	ATR-FTIR
Roddick-Lanzilotta and McQuillan (2000)	Glutamate, aspartate	Anatase	ATR-FTIR
Rosenqvist et al. (2003)	*O*-phthalate, maleate, fumarate, malonate, oxalate	Gibbsite (nano)	ATR-FTIR
Rotzinger et al. (2004)	Formate, acetate	Rutile	ATR-FTIR
Specht and Frimmel (2001)	Oxalate, malonate, succinate	Kaolinite	ATR-FTIR
Tejedor-Tejedor et al. (1992, 1990)	Phthalate, *p*-hydroxybenzoate, 2,4-dihydroxybenzoate	Goethite	ATR-FTIR
Weisz et al. (2001)	Oxalate, salicylate		ATR-FTIR
Weisz et al. (2002)	Oxalate, salicylate, nicotinate, pyridine-3,4 dicarboxylic acid, pyridine-2,6 dicarboxylic acid, 2,2-bipyridine-4,4 dicarboxylic acid	Titanium oxide	ATR-FTIR
Yoon et al. (2004a)	Oxalate	Boehmite	ATR-FTIR

EXAFS: extended X-ray absorption fine structure spectroscopy, XRD: X-ray diffraction, DTC: differential thermal calorimetry, QCC: quantum chemical calculations, SVD: singular value decomposition, NMR: nuclear magnetic resonance spectroscopy, MOC: molecular orbital calculations, FTIR: Fourier transform infrared, ATR: attenuated total reflectance.

The combined use of vibrational spectroscopy with chemical modeling techniques provides increased assurance in data interpretation of binding mechanisms and surface coordination complexes. Kubicki and Muller (2010) present an excellent review of computational spectroscopy for environmental chemistry studies and details on methods and applications are found within. This synergistic approach is now commonly used to study the interaction for both small organic (e.g. Adamescu et al., 2010; Ha et al., 2008; Kubicki et al., 1999; Parikh et al., 2011) and inorganic (e.g. Baltrusaitis et al., 2007; Bargar et al., 2005; Paul et al., 2005) molecules with mineral surfaces. For example, quantum chemical calculations were used in conjunction with experimental collection of ATR-FTIR spectra to reveal that lactate binds to hematite nanoparticles through both outer-sphere and inner-sphere coordination (Ha et al., 2008). The chemical modeling improved data interpretation to reveal that inner-sphere coordinated lactate formed primarily monodentate, mononuclear complexes with the hydroxyl functional group facing away from hematite surface.

Kubicki et al. (1999) studied the sorption of a number carboxylic acids (i.e. acetic, oxalic, benzoic, salicylic, phthalic) to common soil minerals (i.e. quartz, albite, illite, kaolinite, montmorillonite) using batch experiments, ATR-FTIR spectroscopy, and molecular orbital calculations. The results reveal that inner-sphere coordination of the carboxylic acids does not occur through Si^{4+} on mineral surfaces. In fact, substantial chemisorption of carboxylic acids to clay minerals was only observed for illite, which was believed to contain trace Fe-hydroxide coatings. The modeling component in this study provides verification of ATR-FTIR spectroscopic interpretations and refines surface complexation structures, such as the monodentate or bidentate bridging of oxalic acid on albite, illite, and kaolinite.

In order to determine the influence of solution chemistry (pH, amino acid concentration) on surface structures of glutamic acid at the rutile (α-TiO_2)–water interface, ATR-FTIR experiments were conducted on rutile thin films and quantum chemical calculations were carried out (Parikh et al., 2011). Correlation of experimental and calculated FTIR peak locations indicated the three potential surface configurations of glutamate on rutile. The proposed surface complexations are (1) bridging bidentate through inner-sphere coordination of both carboxyl groups; (2) chelating-monodentate via inner-sphere coordination of the γ-carboxyl; and (3) bridging bidentate with inner-sphere coordination of the α-carboxyl and outer-sphere coordination of the γ-carboxyl. It is only with the inclusion

of sophisticated modeling techniques along with spectroscopic approaches that elucidation of these specific surface complexes is possible. In these studies the synergistic nature of combining computational modeling with experimental spectroscopy can be exploited to yield high benefits.

8.1.2 Herbicides and Pharmaceuticals

Vibrational spectroscopy has been used considerably to evaluate the interactions of agrochemicals and contaminants with layer silicates and metal oxides. Elucidating mechanisms of adsorption between such compounds and minerals is valuable for determining chemical fate and transport in the environment, particularly in subsoil horizons where organic carbon content is generally minimal. Tables 1.8 and 1.9 present a complied list of studies, which probe the sorption of organic herbicides and antibacterial compounds to mineral surfaces using vibrational spectroscopy.

Several studies have illustrated the sorption of neutral organic herbicides to neutral siloxane surface sites in the interlayer of layer silicates, and the dependence of neutral herbicide sorption on the presence of less hydrated interlayer cations (Cs^+ and K^+) and low charge density (Boyd et al., 2011; Li et al., 2003; Sheng et al., 2002). We refer the reader to the review article by Boyd et al. (2011) that thoroughly synthesizes these studies and the application of vibrational spectroscopy for studying neutral organic compound interactions with clay minerals; however, we note below a few interesting applications of FTIR found in several of these studies.

Sheng et al. (2002) collected FTIR spectra of the herbicide 4,6-dinitro-*o*-cresol (DNOC) adsorbed to potassium saturated Wyoming smectites to evaluate orientation of DNOC on the clay surface. The FTIR spectra of oriented clay films collected at 0° and 45° of beam incidence show two in-plane bands associated with asymmetric N–O vibrations at 1550 to 1510 cm^{-1}, symmetric N–O stretching vibrations of NO_2 (1356 and 1334 cm^{-1}), and an out-of-plane NO_2 rocking vibration at ~745 cm^{-1}. Intensity of in-plane vibrations in 0° spectra was greater than the 45° spectra and the opposite trend was observed for the out-of-plane band. Because intensity of the absorption bands varied with increasing angle of beam incidence, the authors were able to apply linear dichroism to determine that the spectra indicated parallel orientation of DNOC to the clay mineral surfaces (Sheng et al., 2002). In a more robust study of DNOC and 4,6-dinitro-2-sec-butylphenol adsorption to clay minerals with differing exchangeable cations, Johnston et al. (2002a) used linear dichroism FTIR to reveal that positions of the N–O bands varied little on three K-saturated clays.

Table 1.8 Compiled List of Studies Investigating the Sorption of Antimicrobial Organic Compounds to Mineral Surfaces

References	Sorbate	Mineral	Analysis Method
Aristilde et al. (2010)	Oxytetracycline	Na-montmorillonite	Transmission FTIR, XRD, NMR, MCMS
Chabot et al. (2009)	p-Arsanilic acid	Hematite, maghemite, goethite	ATR-FTIR
Chang et al. (2012)	Tetracycline	Illite	ATR-FTIR, XRD
Chang et al. (2009a, 2009b)	Tetracycline	Palygorskite	ATR-FTIR, XRD
Chen et al. (2010)	Clindamycin, linomycin	Birnessite	Transmission FTIR
Depalma et al. (2008)	p-Arsanilic acid	Hematite, maghemite, goethite	ATR-FTIR
Goyne et al. (2005)	Ofloxacin	Alumina, silica	ATR-FTIR
Gu and Karthikeyan (2005b)	Ciprofloxacin	Hydrous Al-oxide, hydrous Fe-oxide	ATR-FTIR
Gu and Karthikeyan (2005a)	Tetracycline	Hydrous Al-oxide, hydrous Fe-oxide	ATR-FTIR
Kulshrestha et al. (2004)	Oxytetracycline	Montmorillonite	Transmission FTIR, XRD
Li et al. (2010)	Tetracycline	Na-montmorillonite, Ca-montmorillonite, mica-montmorillonite, hectorite	ATR-FTIR, XRD
Li et al. (2011)	Ciprofloxacin	Kaolinite	ATR-FTIR
Nowara et al. (1997)	Enrofloxacin, ciprofloxacin, levofloxacin	Illite, montmorillonite, vermiculite, kaolinite	Transmission FTIR, XRD, Microcalorimetry,
Paul et al. (2012)	Ofloxacin	Anatase	ATR-FTIR
Pei et al. (2010)	Ciprofloxacin	Montmorillonite, kaolinite	ATR-FTIR
Pusino et al. (2000)	Triasulfuron	Montmorillonite	Transmission FTIR
Peterson et al. (2009)	Cephapirin	Quartz, feldspar	Raman microscopy, transmission FTIR

Continued

Table 1.8 Compiled List of Studies Investigating the Sorption of Antimicrobial Organic Compounds to Mineral Surfaces—cont'd

References	Sorbate	Mineral	Analysis Method
Rakshit et al. (2013a)	Oxytetracycline	Magnetite	ATR-FTIR
Rakshit et al. (2013b)	Ciprofloxacin	Magnetite	ATR-FTIR
Trivedi and Vasudevan (2007)	Ciprofloxacin	Goethite	ATR-FTIR
Wang et al. (2010)	Ciprofloxacin	Montmorillonite	Transmission FTIR, XRD
Wu et al. (2010)	Ciprofloxacin	Montmorillonite	Transmission FTIR
Wu et al. (2013a)	Nalidixic acid	Montmorillonite, kaolinite	Transmission FTIR, XRD
Wu et al. (2013b)	Ciprofloxacin	Kaolinite, montmorillonite	Transmission FTIR, XRD
Yan et al. (2012)	Enrofloxacin	Montmorillonite	ATR-FTIR, 2D-COS
Zhao et al. (2012)	Tetracycline	Montmorillonite	FTIR-PAS, XRD

XRD: X-ray diffraction, NMR: nuclear magnetic resonance spectroscopy, MCMS: Monte Carlo molecular simulations, 2D COS: two dimensional correlation spectroscopy, FTIR-PAS: FTIR photoacoustic spectroscopy, ATR: attenuated total reflectance, FTIR: Fourier transform infrared

Table 1.9 Compiled List of Studies Investigating the Sorption of Organic Pesticide Compounds to Mineral Surfaces

References	Sorbate	Mineral	Analysis Method
Adamescu et al. (2010)	Dimethylarsinic acid	Hematite, goethite	ATR-FTIR, QCC
Barja et al. (1999)	Methylphosphonic acid (glyphosate surrogate)	Goethite	ATR-FTIR
Barja and Afonso (2005)	Glyphosate, aminomethyphosphonic acid	Goethite	ATR-FTIR
Celis et al. (1999)	2,4-Dichlorophenoxyacetic acid (2,4-D)	Montmorillonite, ferrihydrite	Transmission FTIR
Chen, et al. (2009)	1-naphthyl methylcarbamate (carbaryl)	Montmorillonite, kaolinite, goethite	Transmission FTIR
Davies and Jabeen (2002)	Isoproturon, N,N-dimethylurea (model compound), 4-isopropylaniline (model compound)	Bentonite, montmorillonite, kaolinite	Transmission FTIR, TGA, XRD
Davies and Jabeen (2003)	Atrazine, 2-chloropyrimidine, 3-chloropyridine	Bentonite, montmorillonite, kaolinite	Transmission FTIR, TGA, XRD
Goyne et al. (2004)	2,4-Dichlorophenoxyacetic acid (2,4-D)	Alumina, silica	ATR-FTIR
Johnston et al. (2002)	4,6-Dinitro-*o*-cresol, 4,6-dinitro-2-sec-butylphenol	Montmorillonite	Transmission FTIR
Laird et al. (1994)	Atrazine	Soil clay fraction	FTIR-PAS, XRD
Li et al. (2009)	2,4-Dichlorophenoxyacetic acid (2,4-D), acetochlor	Bentonite	Transmission FTIR
de Oliveira et al. (2005)	1-naphthyl methylcarbamate (carbaryl)	Montmorillonite	Transmission FTIR
Pusino et al. (2003)	Quinmerac 7-chloro-3-metbylquinoline-8-carboxylic acid, quinclorac 3,7-dichloroquinoline-8-carboxylic acid	Montmorillonite	Transmission FTIR

Continued

Table 1.9 Compiled List of Studies Investigating the Sorption of Organic Pesticide Compounds to Mineral Surfaces—cont'd

References	Sorbate	Mineral	Analysis Method
Sheals et al. (2002)	Glyphosate	Goethite	ATR-FTIR, XPS
Sheng et al. (2002)	4,6-Dinitro-*o*-cresol, dichlobenil	Montmorillonite	ATR-FTIR
Shimizu et al. (2010)	Monomethylarsenate, dimethylarsenate	Alumina (amorphous)	ATR-FTIR, EXAFS
Tofan-Lazar and Al-Abadleh (2012a)	Dimethylarsenate	Hematite	ATR-FTIR
Tofan-Lazar and Al-Abadleh (2012b)	Dimethylarsenate (w/phosphate)	Hematite	ATR-FTIR
Undabeytia et al. (2000)	Norflurazon	Montmorillonite, sepiollite	
Wu et al. (2011)	Isoxaflutole	Hydrous Fe-oxide, hydrous Al-oxide	ATR-FTIR, DRIFTS

QCC: quantum chemical calculations, TGA: thermogravimetric analysis, XPS: X-ray photoelectron spectroscopy, XRD: X-ray diffraction, ATR: attenuated total reflectance, FTIR, Fourier transform infrared, FTIR-PAS: FTIR photoacoustic spectroscopy, EXAFS: extended X-ray absorption fine structure spectroscopy, DRIFTS: diffuse reflectance infrared Fourier transform spectroscopy.

However, differences in position of the N–O bands were observed between mono- and divalent exchangeable cations with differing ionic radius and hydration enthalpy. In particular, the symmetric N–O stretching vibration at ~1350 cm^{-1} shifted to lower energy as hydration energy decreased (Johnston et al., 2002a). These changes suggest that the NO_2 group coordinates with metal cations in the clay interlayer, thus suggesting that the dinitrophenol herbicides adsorb to clay minerals through van der Waals interactions with neutral siloxane groups on the mineral surface and coordination with exchangeable cations (Johnston et al., 2002a). FTIR analyses also proved useful for determining mechanisms of carbaryl (1-naphthyl-N-methyl-carbamate) sorption to clay minerals and the importance of interlayer cation–carbonyl interactions for bonding strength (de Oliveira et al., 2005).

Others have used FTIR to investigate the interaction of anionic herbicides and herbicide degradation products with metal oxides to determine the types of complexes and structures formed upon adsorption. Celis et al. (1999) and Goyne et al. (2004) investigated mechanisms of 2,4-dichlorophenoxyacetic acid (2,4-D) sorption to metal oxide surfaces using transmission FTIR and ATR-FTIR, respectively. Both interpreted the acquired spectra as indication that 2,4-D sorbed to variable charge mineral surfaces via electrostatic interaction between the carboxylate group and ≡Metal–OH_2^+ surface functional groups on Al and Fe oxides. Wu et al. (2011) employed ATR-FTIR and DRIFTS spectroscopy to study the interactions of isoxaflutole degradates to hydrous aluminum and iron oxides. The ATR-FTIR spectra of the diketonitrile (DKN) and benzoic acid (BA) degradates of isoxaflutole adsorbed to the hydrous metal oxides provided no evidence of inner-sphere complex formation between the ketone carbonyl group of DKN or the carboxylate group of BA with mineral surfaces. In contrast, DRIFTS spectra of the BA-mineral complex suggested the formation of an inner-sphere complex upon freeze-drying based on a shift in the asymmetric COO^- stretch to a lower wavenumbers relative to the aqueous spectrum (Wu et al., 2011).

Adsorption of glyphosate [(N-phosphonomethyl)glycine], glyphosate degradates, and adsorbate surrogates of glyphosate to iron oxides have received considerable study using FTIR. Barja and dos Santos Afonso (1998) conducted ATR-FTIR studies as a function of pH and pD to identify particular bands in the glyphosate spectra and to evaluate changes in the glyphosate spectrum upon complexation with aqueous Fe(III). Three vibrations of the phosphonic group resided between 1320 and 979 cm^{-1} at pH 6–9, and four phosphonic group vibrations were observed in the range

of pH 2–4; carboxylic acid and amino vibrations were assigned to bands between 1736 and 1403 cm^{-1}. Coordination of the phosphonate group with aqueous Fe was indicated by a broad and unresolved band from 1200 to 950 cm^{-1} where stretching vibrations of the PO_2^- and PO_3^- are observed in the free ligand, and the absence of P=O and P-OH at 1400–1200 cm^{-1} and 917 cm^{-1}, respectively (Barja and dos Santos Afonso, 1998). Barja et al. (1999) employed methylphosophonic acid (MPA) as an adsorbate surrogate for glyphosate in adsorption studies with goethite. In situ CIR-FTIR spectra at low pH suggested that protonated MPA was bound through a monodentate complex between the phosphonate group and the goethite surface; whereas, a bridging bidentate complex was the proposed structure for MPA bonding at high pH. Sheals et al. (2002) and Barja and dos Santos Afonso (2005) studied glyphosate adsorption to goethite using ATR-FTIR and independently concluded that glyphosate sorbed to goethite as inner-sphere complexes similar to those proposed for MPA with no contribution from the carboxylic acid and amino groups.

Although herbicides have been an environmental concern for many decades, the widespread detection of pharmaceuticals and personal care products in the environment (e.g. Kolpin et al., 2002) has stimulated interest in the interactions of these contaminants with soil. Reactions of antibiotics at the solid–water interface have received particular attention and vibrational spectroscopy has improved understanding of antibiotic sorption processes to minerals. Reaction of minerals and antibiotics from the fluoroquinolone and tetracycline classes have been studied quite extensively using FTIR spectroscopy (e.g. Goyne et al., 2005; Gu and Karthikeyan, 2005a, b; Kulshrestha et al., 2004; Li et al., 2011). Lincosamide and β-lactam interactions with minerals have been studied as well but to a lesser extent (Chen et al., 2010; Peterson et al., 2009).

Fluoroquinolones form strong complexes with Fe and Al oxides via ligand exchange reactions, and ATR-FTIR studies have indicated the potential for two differing complexes to form with metal centers of the mineral. Spectra of ofloxacin sorbed to Al oxide in Goyne et al. (2005) were interpreted as indication of mononuclear bidentate complexation of Al with the ketone and carboxylate functional groups, and this assertion was supported by molecular modeling. Gu and Karthikeyan (2005b) also interpreted spectra of ciprofloxacin adsorbed to hydrous iron oxide as indication of ketone and carboxylate participation in the complex, although they proposed mononuclear monodentate complex formation between one of the oxygen in the carboxylate group and a metal center on hydrous aluminum

oxide. In contrast, Trivedi and Vasudevan (2007) observed spectroscopic evidence that ciprofloxacin complexes with iron atoms in goethite through a bidentate complex with both oxygen atoms in the carboxylate group. Molecular modeling by Aristilde and Sposito (2008) suggests that both types of bidentate complexes are possible. FTIR studies of fluoroquinolone interaction with 1:1 and 2:1 layer silicates have helped reveal differences in sorption between the layer silicates (e.g. intercalation vs external sorption), the influence of exchange cations on adsorption, participation of the carboxylate, ketone, and protonated N in the piperazinyl group in adsorption as a function of pH, and the influence of coadsorbing cations (Li et al., 2011; Nowara et al., 1997; Pei et al., 2010; Wang et al., 2011; Wu et al., 2010; Yan et al., 2012). Similar types of FTIR studies focused on tetracycline class antibiotic adsorption have proved useful in evaluating the mechanisms and the types of complexes formed between tetracyclines and minerals (Chang et al., 2009a, 2009b; Gu and Karthikeyan, 2005a; Kulshrestha et al., 2004; Li et al., 2010; Zhao et al., 2012b).

Organoarsenicals have been used historically as herbicides, insecticides, fungicides, and antibacterial compounds and their reaction with mineral surfaces have also been widely studies using vibrational spectroscopy (e.g. Cowen et al., 2008; Depalma et al., 2008; Shimizu et al., 2010). Although most instances of arsenic contamination can be attributed to weathering geologic sources, the industrial production of organoarsenicals, particularly for use in agriculture, is also of concern. Until recently *p*-arsanilic acid (and roxarsone) was commonly used as an additive to poultry feed and therefore an understanding of their interactions with soil minerals is important. ATR-FTIR spectroscopy was instrumental in determining that *p*-arsanilic acid formed inner-sphere complexes with iron (oxyhydr)oxide minerals (Chabot et al., 2009). And although this binding mechanism suggests limited transport of *p*-arsanilic acid in iron rich soils, this study also showed that aqueous phosphate can desorb *p*-arsanilic acid and thus has potential to enhance its transport, particularly important for poultry manure amended soils. Similar studies were also conducted using both ATR-FTIR spectroscopy and quantum chemical calculations to elucidate dimethylarsinic acid inner- and outer-sphere binding mechanisms to goethite (Adamescu et al., 2010). More recently, Tofan-Lazar and Al-Abadleh (Tofan-Lazar and Al-Abadleh, 2012a,b) have used ATR-FTIR to study the reaction kinetics of dimethylarsinic acid and phosphate (absence/presence of surface arsenic) sorption to hematite and goethite.

8.2 Inorganic Molecule Interactions with Mineral Surfaces

FTIR is a well-developed tool for probing the solid–solution interface to examine the processes of inorganic ion sorption. In particular, ATR-FTIR has proven to be a useful tool for determining the sorption mechanism (i.e. inner-sphere vs outer-sphere) of oxyanions to mineral surfaces, typically in cases where binding occurs and there is no change in the IR spectrum following reaction with the solid surface where outer-sphere sorption is taking place. However, the presence of new peaks or shifts in the wavenumbers of existing peaks is commonly attributed to inner-sphere coordination. Due to the fact that only molecules with a dipole moment (permanent or induced) are IR active, FTIR studies are best suited for oxyanions, which have relatively large dipole moments.

Of all the applications of vibrational spectroscopy in the area of soil chemistry, the use of FTIR to study inorganic ion sorption to mineral surfaces is the most complete and advances in recent years have somewhat slowed. As a result, prior review papers cover this area quite well. For example, Suarez et al. (1999) provide an excellent review of oxyanion (i.e. phosphate, borate, selenate, selenite) sorption mechanisms and present data showing inner-sphere coordination for arsenate and arsenite to amorphous Fe and Al oxides from ATR-FTIR and DRIFTS analysis. In addition, this review places an emphasis on pH and mineral surface charge [i.e. point of zero charge (pzc)] for oxyanion sorption coordination, in part through inclusion of electrophoretic mobility (EM) and titration data. In a slightly more recent review, Lefèvre (2004) provides a thorough and insightful article on ATR-FTIR theory and its application to studying inorganic ion sorption to metal oxides and hydroxides. In that review the adsorption of sulfate, carbonate, phosphate, nitrate, perchlorate, borate, selenite/selenate, and arsenate to metal oxides and hydroxides is addressed. Included in both of the aforementioned review papers are excellent tables summarizing FTIR band assignments for a number of dissolved and mineral-coordinated anions. In addition, a review of surface interactions of inorganic arsenic on mineral surfaces using a variety of spectroscopic techniques, including FTIR and Raman, is provided by Wang and Mulligan (2008). Due to the existence of these quality reviews, the study of inorganic ions on mineral surfaces will not be discussed in great detail here. Table 1.10 provides references for studies which probe inorganic ion sorption to soil minerals through vibrational spectroscopy.

Due largely to the common occurrence of elevated phosphate levels in agricultural soils, and concerns associated to its transport to surface waters

Table 1.10 Compiled List of Studies Investigating the Sorption of Inorganic Ions to Mineral Surfaces

References	Sorbate	Mineral	Analysis Method
Arai and Sparks (2001)	Phosphate	Ferrihydrite	ATR-FTIR
Arai et al. (2004)	Arsenate (w/carbonate)	Hematite	ATR-FTIR, XAS
Baltrusaitis et al. (2007)	Nitrate	Corundum, γ-alumina	Transmission FTIR, QCC
Bargar et al. (2005)	Carbonate	Hematite	ATR-FTIR, DFT
Beattie et al. (2008)	Sulfate, Cu^{II}	Goethite	ATR-FTIR
Connor and McQuillan (1999)	Phosphate	Titanium oxide	ATR-FTIR, Raman, CCM
Elzinga and Sparks (2007)	Phosphate	Hematite	ATR-FTIR
Elzinga and Kretzschmar (2013)	Phosphate (w/Cd^{II})	Hematite	ATR-FTIR
Goldberg and Johnston (2001)	Arsenite, arsenate	Fe-oxide (amorphous), Al-oxide (amorphous)	ATR-FTIR
Gong (2001)	Phosphate	Titanium oxide	ATR-FTIR
Guan et al. (2005)	Sodium pyrophosphate, sodium tripolyphosphate	Aluminum hydroxide (amorphous)	ATR-FTIR
Hug (1997)	Sulfate	Hematite	ATR-FTIR
Hug and Sulzberger (1994)	Sulfate	Anatase	ATR-FTIR, SVD
Johnston and Chrysochoou (2012)	Chromate	Ferrihydrite	ATR-FTIR, QCC
Luengo et al. (2006)	Phosphate	Goethite	ATR-FTIR
Luxton et al. (2008)	Silicate	Goethite	ATR-FTIR
McAuley and Cabaniss (2007)	Arsenate, sulfate, selenate	Goethite	ATR-FTIR
Michelmore et al. (2000)	Phosphate	Titanium oxide, silica	ATR-FTIR, Electrophoresis

Continued

Table 1.10 Compiled List of Studies Investigating the Sorption of Inorganic Ions to Mineral Surfaces—cont'd

References	Sorbate	Mineral	Analysis Method
Myneni et al. (1998)	Arsenate	Ettringite	ATR-FTIR
Ostergren et al. (2000)	Carbonate	Goethite	ATR-FTIR, EXAFS
Parfitt and Smart (1977)	Sulfate	Goethite	Transmission FTIR
	Sulfate	Goethite, akaganeite, lepidocrocite, hematite, amorphous Fe-hydroxide	Transmission FTIR
Parikh et al. (2008)	Arsenite, arsenate	Hydrous manganese oxide	ATR-FTIR
Parikh et al. (2010)	Arsenite, arsenate, phosphate	Hydrous manganese oxide, goethite	ATR-FTIR
Paul et al. (2005)	Sulfate	Hematite	ATR-FTIR, MO/DFT
Peak et al. (1999)	Sulfate	Goethite	ATR-FTIR
Pena et al. (2006)	Arsenite, arsenate	Titanium oxide	ATR-FTIR, EXAFS
Persson et al. (1996)	Phosphate	Goethite	DRIFTS
Roddick-Lanzilotta et al. (2002)	Arsenate	Hydrous Fe-oxide	ATR-FTIR
Suarez et al. (1999)	Arsenite, arsenate	Fe-oxide (amorphous), al-oxide (amorphous)	ATR-FTIR, DRIFTS
Su and Suarez (1995)	Boron	Fe-oxide, allophane, kaolinite	ATR-FTIR
Su and Suarez (1997a)	Boron	Allophane	DRIFTS
Su and Suarez (1997b)	Carbonate	Gibbsite, goethite, hydrous al-oxide, hydrous Fe-oxide	ATR-FTIR
Su and Suarez (2000)	Selenite, selenate	Goethite, Fe-oxide (amorphous)	ATR-FTIR, DRIFTS, Electrophoresis

Sun and Doner (1996)	Arsenite, arsenate	Goethite	ATR-FTIR, transmission FTIR
Sun and Doner (1998)	Arsenite	Goethite, birnessite	ATR-FTIR, XANES
Szlachta et al. (2012)	Arsenite, selenite	Fe–Mn hydrous oxide	DRIFTS, XPS
Tejedor-Tejedor and Anderson (1986)	Nitrate, perchlorate	Goethite	ATR-FTIR
Tejedor-Tejedor and Anderson (1990)	Phosphate	Goethite	ATR-FTIR
Tofan-Lazar and Al-Abadleh (2012b)	Phosphate (w/dimethylarsenate)	Hematite	ATR-FTIR
	Carbonate	Goethite	ATR-FTIR
Voegelin and Hug (2003)	Arsenite	Ferrihydrite	ATR-FTIR
Wijnja and Schulthess (1999)	Carbonate, nitrate	γ-Alumina	ATR-FTIR
Wijnja and Schulthess (2001)	Carbonate	Goethite	ATR-FTIR, DRIFTS, H^+ Coadsorption

XAS: X-ray absorption spectroscopy, QCC: quantum chemical calculations, DFT: density function theory, CCM: constant capacitance modeling, SVD: singular value decomposition, EXAFS: extended X-ray absorption fine structure spectroscopy, MO/DFT: molecular orbital/density function theory, XANES: X-ray absorption near-edge structure, XPS: X-ray photoelectron spectroscopy, ATR: attenuated total reflectance, FTIR, Fourier transform infrared, EXAFS: extended X-ray absorption fine structure spectroscopy, DRIFTS: diffuse reflectance infrared Fourier transform spectroscopy.

and subsequent impact on eutrophication, its interactions with soil minerals continue to be studied. Over the last 25 years FTIR spectroscopy has provided critical insight into the interactions of phosphate with various soil minerals. Some of the more impactful studies on phosphate sorption to iron oxides are found in Tejedor-Tejedor and Anderson (1990), Persson et al. (1996), and Arai and Sparks (2001), providing fundamental knowledge regarding the formation of inner-sphere phosphate complexes. Building on these studies, Elzinga and Sparks (2007) utilized the molecular-scale power of ATR-FTIR to examine the surface coordination of phosphate to hematite as a function of pH/pD (3.5–7.0). In this study, the authors compare spectra collected at various pH/pD values and suggest that multiple monoprotonated phosphate inner-sphere surface complexes (i.e. monodentate binuclear, monodentate mononuclear) are observed at the hematite–water interface. More recently, the impact of metal cations (i.e. Cd^{II}) on phosphate sorption to geoethite has been investigated using ATR-FTIR (Elzinga and Kretzschmar, 2013). In this study, phosphate sorption to goethite was enhanced in the presence of Cd^{II}, increasing with increased pH values. ATR-FTIR spectra indicated that Cd^{II} results in a distortion of the orthophosphate tetrahedron at low pH values, thus impacting phosphate protonation. This research demonstrates the importance of considering divalent metals, such as Cd^{II}, on the fate of phosphate in soil environments.

Lanfranco et al. (2003) successfully utilized Raman microspectroscopy to determine the presence of mixed-metal hydroxylapatites (Ca and Cd substituted) in manually doped soil at concentrations as low as 0.1% despite fluorescence interference. They were also able to determine the relative composition of the mixed-metal hydroxylapatites due to variance in Raman active bands as a function of the Cd content. This type of analysis illustrates the potential of Raman spectroscopy in the investigation of utilizing phosphates for remediation of metal contaminated soils. Several other studies have focused on using Raman spectroscopy to investigate phosphorus in soils (Bogrekci, 2006; Zheng et al., 2012). Zheng et al. (2012) recently used the technique to determine soil phosphorus concentrations and obtained a good correlation between the Raman signal and concentration (validation $R^2 = 0.937$). Application of Raman spectroscopy for this determination is significant as it enables simple and rapid determination of this soil nutrient comparable to other techniques such as UV-vis and NIR without interference from soil moisture, a major limitation of these techniques.

The coupling of FTIR with advanced modeling techniques for validation, and enhancement, of spectral interpretation also aids elucidation of

inorganic ion interactions at mineral surfaces. For example, Paul et al. (2005) utilized ATR-FTIR and molecular orbit/density functional theory (MO/DFT) to study sulfate sorption to hematite in aqueous and with subsequent dehydration. The results of this study reveal that sulfate binds at the mineral–water interface through a bidentate bridging or monodentate coordination, but following dehydration sulfate changes species to form a bidendate bridging or monodentate bisulfate complex. This study is an excellent example of the ability of vibrational spectroscopy to provide information regarding both sorption mechanisms and surface speciation information. These authors (Kubicki et al., 2007) also present an excellent theoretical (MO/DFT) study to model FTIR and extended X-ray absorption fine structure spectra of carbonate, phosphate, sulfate, arsenate, and arsenite on various Fe- and Al oxides. In another study, Bargar et al. (2005) used a similar approach to examine the speciation of adsorbed carbonate on hematite. Correlation between vibrational frequency calculations and experimental data suggested carbonate exists as both a monodentate binuclear inner-sphere complex and also fully or partially solvated species (i.e. outer-sphere) bound to the surface via hydrogen bonding. In a more recent study, chromate sorption to ferrihydrite was probed using this combined experimental and theoretical approach (Johnston and Chrysochoou, 2012). The authors conclude that at pH greater than pH 6.5 monodentate complexes are prevalent, whereas bidentate surface species are observed at $pH < 6$. The continuing advances in computer processing capabilities and affordability are making the use of molecular calculations accessible and providing significant advances to vibrational spectroscopy analysis on mineral surfaces.

Vibrational spectroscopy can also provide additional methodologies and insights for studying reaction kinetics of inorganic ions on mineral surfaces. The use of ATR-FTIR to monitor reaction kinetics has shown very good agreement with traditional batch approaches; for example, for phosphate sorption to goethite (Luengo et al., 2006, 2007). However, it was not until recent years that very rapid reactions could be studied using FTIR. Software and computing advances now permit rapid collection of data for vibrational spectroscopy and thus permit kinetic study or rapid sorption or transformation (e.g. redox) reactions. Reactions that occur on timescales of just minutes are difficult to observe in situ with most conventional techniques; however, the development of rapid-scan instrumentation and software opens up the possibilities for kinetic FTIR studies. The first application of a rapid-scan ATR-FTIR approach to study oxyanion sorption and transformation focused on the oxidative transformation of arsenite to arsenate on a hydrous

Mn oxide (HMO) mineral surface (Parikh et al., 2008). In that study, a temporal resolution of 2.55 s per scan was presented (24 scans, 8 cm^{-1} resolution) and revealed 50% of the oxidation reaction occurred within the first 1 min of reaction. It was additionally shown that following oxidation of arsenite, arsenate rapidly bound to the HMO surface leading to surface passivation. A follow-up study examined the impact of competing ions (i.e. phosphate), minerals (i.e. α-FeOOH), and bacteria (i.e. *Pseudomonas fluorescens, Alcaligenes faecalis*) on the rate and extent of arsenite oxidation via the same hydrous Mn oxide (Parikh et al., 2010) via batch and rapid-scan ATR-FTIR analysis. The data reveal that although the initial rates of oxidation are not greatly impacted, competing ions, biomolecules, and surfaces have a large impact on the extent of reaction via blocking of reactive surface sites and sorption of reaction products. These studies not only demonstrate the rapid nature of Mn oxide catalyzed oxidation of arsenite, but also highlight the importance of considering the heterogeneous nature of natural systems when studying environmental processes. In other studies examining inorganic redox transformations, SR-FTIR provided spatial and temporal resolution to reveal that microbial reduction of toxic Cr (VI) to less toxic Cr (III) from a heavy metal polluted site is stimulated via biodegradation of toluene (Holman et al., 1999). Holman et al. (2002) also used SR-FTIR to show that biodegradation rates of polycyclic aromatic hydrocarbons are enhanced by the presence of humic acids, suggesting that additional labile carbon sources can enhance bioremediation of contaminated soils.

8.3 Bacteria and Biomolecule Adhesion

The development of FTIR as a tool to examine bacteria and biomolecule samples has been critical for increasing our mechanistic understanding of bacteria and biomolecule adhesion on mineral surfaces. This application is particularly well suited to ATR-FTIR spectroscopy investigations as non-destructive in situ studies of bacteria, microbial biofilms, and biomolecules can be conducted in the presence of water biofilms (Nichols et al., 1985; Nivens et al., 1993a, 1993b; Schmitt and Flemming, 1998; Schmitt et al., 1995). In addition, overlapping IR bands arising from biological samples and the mineral substratum are reduced due to the differing "fingerprint" regions for organic and inorganic samples. Table 1.11 provides citations for a number of studies, which have utilized FTIR spectroscopy to study bacteria and biomolecule interactions with mineral surfaces.

The exterior surfaces of bacterial cells are complex, comprised of surface proteins, nucleic acids, EPS, LPS (Gram-negative bacteria), teichoic

Table 1.11 Compiled List of Studies Investigating the Sorption of Bacteria and Biomolecules on Mineral Surfaces

References	Sorbate	Mineral	Analysis Method
Borer et al. (2009)	Aerobactin (*E. coli*)	Lepidocrocite	ATR-FTIR
Brandes Ammann and Brandl (2011)	*Bacillus* sp. spores	Bentonite	Transmission FTIR, reflection FTIR
Bullen et al. (2008)	Microbial metabolites	Calcite	ATR-FTIR
Cao et al. (2011)	EPS (*Bacillus subtilis*)	Montmorillonite, kaolinite, goethite	ATR-FTIR
Deo et al. (2001)	*Paenibacillus polymyxa*	Hematite, corundum, Quarts	Transmission FTIR
	Shewanella putrefaciens	Hematite	ATR-FTIR
Gao and Chorover (2011)	*Cryptosporidium parvum* oocysts	Hematite	ATR-FTIR
Gao et al. (2009)	*Cryptosporidium parvum* oocysts	Hematite	ATR-FTIR
McWhirter et al. (2003)	*P. aeruginosa,* pyoverdine (*P. aeruginosa*)	Titanium oxide, iron oxide	ATR-FTIR
McWhirter et al. (2002)	*P. aeruginosa*	Titanium oxide	ATR-FTIR
Ojeda et al. (2008)	*P. putida*	Hematite	ATR-FTIR
Omoike and Chorover (2004)	EPS (*B. subtilis*)	Goethite	ATR-FTIR
Omoike and Chorover (2006)	EPS (*B. subtilis*)	Goethite	DRIFTS, transmission FTIR
Omoike et al. (2004)	EPS (*B. subtilis, P.aeruginosa*)	Goethite	ATR-FTIR, QCC
Parikh and Chorover (2006)	*S. oneidensis, P. aeruginosa, B. subtilis*	Hematite	ATR-FTIR
Parikh and Chorover (2008)	LPS (*P. aeruginosa*)	Corundum, hematite	ATR-FTIR
Rong et al. (2010)	*P. putida*	Kaolinite, montmorillonite	Transmission FTIR, SEM, ITC
Rong et al. (2010)	*P. putida*	Goethite	Transmission FTIR, SEM, ITC
Upritchard et al. (2011)	*E. coli*, enterobactin (*E. coli*)	Titanium oxide, boehmite	ATR-FTIR
Upritchard et al. (2007)	*P. aeruginosa*, pyoverdine (*P. aeruginosa*)	Titanium oxide, iron oxide, boehmite	ATR-FTIR
Vasiliadou et al. (2011)	*P. putida*	Kaolinite	ATR-FTIR, ^{1}H-NMR

QCC: quantum chemical calculations, SEM: scanning electron microscopy, ITC: isothermal titration calorimetry, NMR: nuclear magnetic resonance spectroscopy, ATR: attenuated total reflectance, FTIR, Fourier transform infrared, EXAFS: extended X-ray absorption fine structure spectroscopy, DRIFTS: diffuse reflectance infrared Fourier transform spectroscopy.

acids (Gram-positive bacteria), and other surface biosynthetic molecules that likely are involved in the adhesion process (Wingender et al., 1999). Through ATR-FTIR studies, it has been noted that a certain degree of universality of surface functional groups between bacteria (i.e. Gram-negative, Gram-positive) exists. FTIR spectra reveal that hydroxyl, carboxyl, phosphoryl, and amide groups are common among bacterial cell walls and that the negative charge of bacteria arises from the deprotonation of carboxylates and phosphates (Jiang et al., 2004). The charge of biomolecular functional groups on bacteria surfaces, and of the substratum, is certainly important for the adhesion process.

It is well established that bacteria and many environmental particles exhibit a net negative charge at environmental pH values (Rijnaarts et al., 1995). For example, silica is negatively charged at pH > 2.0 to 3.0 (Sposito, 1989). However, in weathering environments, many silicaceous surfaces become coated with a veneer of hydrous Al- and Fe- oxides, which can confer net positive charge even at circumneutral pH (Sposito, 1989). It is therefore significant that ATR-FTIR spectroscopy can be used to examine biomolecule–mineral interactions with surfaces of varying chemical composition and charge. Depending on the sample being studied, untreated IREs (e.g. ZnSe, diamond) can be used to collect spectrum of aqueous phase samples and Ge (GeO_2), due to similarity between the surface chemistry silica, is often used as a surrogate for studying interactions with siliceous minerals. ZnSe is a hydrophobic crystalline material (Reiter et al., 2002; Song et al., 1992) with a point of zero net proton charge (PZNPC) that is <4 (Tickanen et al., 1997). Ge, on the other hand, has a hydroxylated surface, similar to silica, and is relatively hydrophilic (Snabe and Petersen, 2002). A corresponding PZNPC for Ge was not found in the literature, however it is also presumed to be <4 when considering that the isoelectric point (IEP) of silica ranges from 2.0 to 2.5 (Gun'ko et al., 1998; Sparks, 1995) and that doping of SiO_2 up to 20% GeO_2 (by mass) had only minimal effects on the IEP (Gun'ko et al., 1998). ATR-FTIR experiments probing biomolecule interactions with other charged surfaces can be conducted using a variety of static and flow-through approaches in the presence of soil minerals. While some studies have examined interactions using mineral suspensions (e.g. Jiang et al., 2010; Parikh and Chorover, 2006; Rong et al., 2010; Vasiliadou et al., 2011), a number of studies have utilized mineral coatings (e.g. Fe-, Al-, Ti-oxides) on IREs in order to modify the surface chemistry of the substratum and examine sorption to a range of environmentally relevant surfaces (e.g. Elzinga et al., 2012; McWhirter et al., 2002; Ojeda et al., 2008; Parikh

and Chorover, 2006). With these approaches the interactions of bacteria and various biomolecules can be monitored in situ with ATR-FTIR to provide insight into their binding mechanisms with various surfaces.

FTIR studies have revealed that bacterial adhesion to clay minerals and other negatively charged surfaces are primarily mediated by interactions with proteins, such as extracellular enzymes, and hydrogen bonding. For example, under flow conditions using a cylindrical ZnSe IRE, *P. putida* (GB-1) biofilm growth corresponds to increased spectral absorbance in the amide I and II regions. Additionally, bacterial adhesion was inhibited when biogenic Mn-oxides were present on the cell exterior due to blocking of positively charged proteinaceous moieties and electrostatic repulsion between the ZnSe IRE and the negatively charged coated bacteria (Parikh and Chorover, 2005). As these experiments were performed with live bacteria it is not possible to conclusively distinguish between membrane-bound proteins and those in the EPS. Combined batch sorption and FTIR studies have demonstrated the preferential adsorption of proteinaceous constituents to montmorillonite and kaolinite, which are primarily negatively charged at environmental pH values (Cao et al., 2011). In this study numerous shifts in peaks associated with the vibrations of water molecules (e.g. 1634 to 1647 cm^{-1}), Si–O (e.g. 1124 to 992 cm^{-1}), and Al–OH (e.g. 906 to 913 cm^{-1}) indicate that the EPS sorption was mediated through hydrogen bonding. Similar nonelectrostatic forces are also involved in live bacterial interactions with these mineral surfaces. Following reaction of *P. putida* with kaolinite and montmorillonite shifts in the IR absorption bands of water molecules (e.g. 3450 to 3442 cm^{-1} and 1637 to 1647 cm^{-1} for kaolinite) are likewise attributed to hydrogen bonding—with much greater sorption observed to kaolinite (Rong et al., 2008). Hydrogen bonding has also been observed in the binding of the O-antigen from bacterial LPS (*E. coli*, *Citrobacter freundii, Stenotrophomonas maltophilia*) to TiO_2, SiO_2, and Al_2O_3 films on a ZnSe IRE (Jucker et al., 1997).

The ubiquity of negatively charged functional groups in EPS and on the surface of bacteria leads to favorable binding with positively charged mineral surfaces, such as Fe-, Al-, and Ti-oxides. The ability to coat IRE with these minerals makes FTIR a powerful approach for elucidating biomolecule and bacteria binding mechanisms. The collective data reveal that bacterial adhesion to metal oxide surfaces, which are typically positively charged at environmental pH values, is facilitated by carboxylate (Gao and Chorover, 2009; Gao et al., 2009; Ojeda et al., 2008), phosphate (Cao et al., 2011; Elzinga et al., 2012; Omoike et al., 2004; Parikh and Chorover, 2006), and catecholate (McWhirter et al., 2003; Upritchard et al., 2007, 2011)

groups associated with the EPS or cell surfaces. Of course, environmental factors such as pH and bacterial growth conditions have a large effect on these interactions.

Carboxyl groups are present within polysaccharides, amino acids, siderophores, and many other components of EPS, all of which can contribute to conditioning film formation and cell adhesion. Carboxyl groups can form both inner-sphere and outer-sphere complexes with metal oxides surfaces, with the inner-sphere complexes favored at acidic pH (Boily et al., 2000; Gao et al., 2009; Ha et al., 2008; Hwang and Lenhart, 2008). Substantial progress has been made in understanding bacterial adhesion processes through the use of model compounds. For example, elucidation of carboxylate binding mechanisms has been facilitated through FTIR experiments examining amino acids (Norén et al., 2008; Parikh et al., 2011; Roddick-Lanzilotta et al., 1998; Roddick-Lanzilotta and McQuillan, 2000) and model carboxylic acids (Boily et al., 2000; Deacon and Phillips, 1980; Ha et al., 2008; Norén and Persson, 2007). In fact, studies by Alcock and coauthors (1976) and later refined by others (Chu et al., 2004; Deacon and Phillips, 1980; Dobson and McQuillan, 1999), demonstrate that carboxyl binding mechanisms can be inferred through the separation differences ($\Delta\nu$) between the asymmetric carboxylate [$\nu_{as}(COO^-)$] and the symmetric carboxylate [$\nu_s(COO^-)$] stretching vibrations [i.e. $\Delta\nu = \nu_{as}(COO^-) - \nu_s(COO^-)$] as summarized in Table 1.6.

Following the spectral interpretations for model carboxylate compounds, there is evidence for carboxyl involvement during adhesion of *P. putida* to hematite (α-Fe_2O_3) under flow conditions, possibly forming bidentate bridging complexes to the mineral surface [$\nu_s(COO^-)$ shift from 1400 to 1415 cm^{-1}; $\Delta\nu \approx 150\ cm^{-1}$], with additional binding interactions through polysaccharides and phosphoryl groups (Ojeda et al., 2008). However, in this case the location of the $\nu_{as}(COO^-)$ is masked by the amide II band at 1550 cm^{-1} and some uncertainty in $\Delta\nu$ remains. In addition, the determination of surface coordination using this approach was developed for simple organic acids and interpretation of chemically heterogeneous systems such as this may require additional verification through chemical modeling studies. Therefore, although the shift of the $\nu_s(COO^-)$ is still indicative of inner-sphere coordination (Dobson and McQuillan, 1999; Duckworth and Martin, 2001; Ha et al., 2008), it is possible that other surface complexes exist.

Recent FTIR studies by Gao et al. (Gao and Chorover, 2011; Gao et al., 2009) highlight the importance of carboxyl groups in mediating the adhesion of *Cryptosporidium parvum* oocysts to a hematite (α-Fe_2O_3) surface, also by extending $\Delta\nu$ interpretation to more complex systems. In these experiments shifts of peaks corresponding to carboxyl groups splitting of

the $\nu_s(COO^-)$ were used to determine that in NaCl solutions oocysts bind to hematite primarily in monodendate complexes at low pH and in bidentate complexes with increased pH. However, it is noted that at pH values above the PZNPC for hematite, FTIR spectra closely resemble spectra corresponding to unbound oocysts and that outer-sphere coordination is observed. In this study, IR spectra were deconvoluted, permitting determination of $\nu_{as}(COO^-)$ peak location for calculation of $\Delta\nu$ to empirically determine the oocyst surface coordination.

Sideraphores, which are released from bacteria and found within EPS, provide additional functional groups of negative charge, which may mediate cell adhesion processes to metal oxides. Siderophores are a class of low molecular weight Fe^{3+} chelating compounds released by almost all bacteria, including *Pseudomonas* sp. and *E. coli,* in order to increase iron bioavailability (Crowley et al., 1991). The siderophore pyoverdine is produced by *Pseudomonas aeruginosa* and has carboxyl, hydroxyl, hydroxamate, and catecholate functional groups that can bind to Fe^{3+} (McWhirter et al., 2003; Upritchard et al., 2007). Enterobactin, the siderophore produced by *E. coli,* has both salicylate and catecholate binding sites (Upritchard et al., 2011). FTIR studies investigating these biomolecules suggest that pyoverdine and enterobactin play an important role in mediating cell adhesion to metal oxides surfaces (McWhirter et al., 2003; Upritchard et al., 2007, 2011), primarily through inner-sphere binding of catecholate groups to metal centers (e.g. Fe, Ti). These binding mechanisms were determined through analysis of IR spectra of bacteria, siderophores, and model catecholate compounds. For bacterial cells grown in minimal growth media and reacted with TiO_2 coated IREs, a peak at 1286 cm^{-1} for *P. aeruginosa* is consistent with pyoverdine and a peak around 1260 cm^{-1} for *E. coli* is consistent with enterobactin. Other FTIR studies with model siderophores (i.e. desferroxamine B, aerobactin) with lepidocrocite (γ-FeOOH) demonstrate possible inner-sphere sorption mechanisms through hydroxamate and outer-sphere coordination via carboxyl groups (Borer et al., 2009). The potential role of siderophores in mediating bacterial adhesion will be maximized in conditions of Fe scarcity, where siderophore production is the greatest (Crowley et al., 1991).

Due to the fact that most of the negative charge on bacterial cell walls are attributed to carboxyl and phosphoryl groups, the role of bacterial phosphate groups should also be considered. Due to the strong polarity of the P–O bond, FTIR spectroscopy is an ideal tool for examining phosphate binding to metal oxides. Phosphate groups originating from phospholipids, DNA, LPS, and other extracellular biomolecules provide potential binding sites to initiate bacterial adhesion to metal oxide surfaces. The binding of

phosphate with Fe oxide surfaces is well documented in numerous ATR-FTIR spectroscopic studies (Barja et al., 2001, 1999; Cagnasso et al., 2010; Tejedor-Tejedor and Anderson, 1990). Omoike et al. (2004) used a combined ATR-FTIR spectroscopy and modeling approach to demonstrate the occurrence of P–O–Fe bonds (1037 cm^{-1}) for extracted EPS reacted with goethite (α-FeOOH) (Figure 1.16). The complementary modeling calculated frequencies for phosphodiester clusters on α-FeOOH of 1045 cm^{-1} for a monodentate cluster [ν_s(FeO–PO)] and 1027 cm^{-1} for a bidentate cluster [ν_s(FeO–P–OFe)]. Due to the good correlation between experimental and calculated frequencies the authors suggest that phosphodiester bonds in DNA are involved in the binding of EPS to the mineral surface. Similarly,

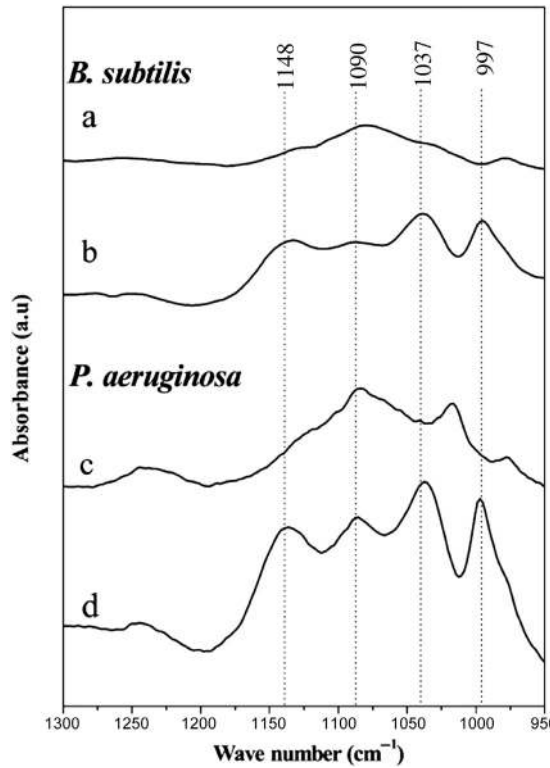

Figure 1.16 ATR-FTIR spectra (1300–950 cm^{-1}) of solution phase EPS and adsorbed EPS after 60 min reaction time: (a) *B. subtilis* EPS (free), (b) *B. subtilis* EPS after contact with goethite, (c) *P. aeruginosa* EPS (free), and (d) *P. aeruginosa* EPS after contact with goethite (17.9 mg L^{-1} EPS suspension, pH 6.0, and 10 mM NaCl). (ATR, attenuated total reflectance; FTIR, Fourier transform infrared; EPS, exopolysaccharide.) *Reprinted with permission from Omoike et al. (2004).*

another ATR-FTIR study revealed that phosphatidic acid (phospholipid) reaction with both Fe oxides and hematite (α-Fe_2O_3) produce Fe–O–P IR bands at 992 (α-Fe_2O_3) and 997 cm^{-1} (α-FeOOH) which are attributed to inner-sphere coordination of phosphate groups (Cagnasso et al., 2010).

The importance of bimolecular-P interactions with Fe oxides was also demonstrated with ATR-FTIR for live bacteria to α-Fe_2O_3 (Elzinga et al., 2012; Parikh and Chorover, 2006). When *Shewanella oneidensis, P. aeruginosa, and B. subtilis* cells were deposited in a ZnSe IRE coated with α-Fe_2O_3, FTIR peaks emerged at approximately 1020 and 1040 cm^{-1} and were attributed to inner-sphere coordination to the mineral surface (Parikh and Chorover, 2006). Elzinga et al. (2012) demonstrate the impact of pH and contact time for *Shewanella putrefaciens* adhesion to α-Fe_2O_3. The results of this study show that the initial binding of bacterial cells is mediated by bacterial phosphate groups; however, as bacterial contact times increase to 24 h, FTIR peaks corresponding to proteins and carboxyl groups become more apparent. Additionally, changes in pH impact the protonation of bacterial functional groups and thus impact their coordination to the hematite surface. Although corresponding studies with model compounds (i.e. phenylphophonic acid, adenosine 5—monophosphate, 2′-deoxyadenyl(3′→5′)-2′-deoxyadenosin, DNA) provide additional credence for an important role of bacterial phosphate groups (Parikh and Chorover, 2006), the precise source of phosphate in the EPS mixtures remains unclear.

9. REAL WORLD COMPLEXITY: SOIL ANALYSIS FOR MINERAL AND ORGANIC COMPONENTS

9.1 Soil Heterogeneity and Mineral Analysis

There has long been a desire to use FTIR spectroscopy to identify and quantify specific minerals in mineral/OM assemblages (Russell and Fraser, 1994). The potential utility and challenges for determining allophane/imogolite content in soils using FTIR have previously been noted; however, there are other significant challenges for analysis of soil minerals that must be considered as well. Russell and Fraser (1994) identify six factors that must be considered for quantitative determination of minerals using FTIR: (1) particle size of a sample should be <2 μm to minimize scattering and maximize sample absorption of radiation; (2) diligence must be expressed when weighing and transferring samples during sample preparation; (3) samples should be uniformly dispersed and thoroughly mixed when diluents are

employed (e.g. KBr) for sample preparation; (4) interference of bands from nontargeted minerals or OM should be minimized by choosing bands associated with the target mineral that are adequately isolated in the spectrum; (5) availability of specific minerals standards and the matching of standards to minerals in a sample (e.g. similar crystallinity, elemental composition), the latter is particularly challenging when little is known about the specimen being studied; and (6) the technique employed must generate highly reproducible results. Reeves et al. (2005) expand upon some of these issues and note that differences in methods of FTIR spectra collection (e.g. transmission vs. DRIFTS) may present challenges for utilizing mineral libraries to develop quantitative measures of minerals using FTIR.

Many studies investigating the utility of FTIR for mineral quantification have investigated artificially mixed mineral matrices to calibrate and validate a particular approach (Bertaux et al., 1998; Madejová et al., 2002; Matteson and Herron, 1993). Others have calibrated their approach using mineral assemblages and validated the approach using clays or rocks of known mineral composition as determined by XRD (Breen et al., 2008; Kaufhold et al., 2012). There have also been some who have applied models to quantify mineral content in soils (Bruckman and Wriessnig, 2013). Although mineral quantification with FTIR can be quite challenging, depending on the intended application the level of difficulty in quantification of soil mineral composition using FTIR may not present a significant issue. However, to achieve more widespread application, it is necessary to validate an MIR method using soils, which contain a complex assemblage of minerals and OM. An alternative approach to using MIR spectroscopy is visible/near-infrared (VNIR) spectroscopy, which has been demonstrated by Viscarra Rossel et al. (2009, 2006) to show some promise.

The presence of exploration rovers on Mars has increased interest in the use of vibration spectroscopy for identifying and quantifying specific minerals in mineral assemblages (Bishop et al., 2008, 2004; Villar and Edwards, 2006). For example, Bishop et al. (2004) demonstrated the use of VNIR and MIR spectroscopy for identifying hydrated sulfates in samples from acidic environments on Earth that may have application for identifying minerals in sulfate-rich rocks and soils on Mars. Villar and Edwards (2006) discuss and demonstrate the potential for the use of Raman spectroscopy for identifying minerals, such as carbonates, on Mars. Bishop et al. (2004) discuss phyllosilicate diversity in rock outcrops on Mars determined from VNIR data captured by the Mars Reconnaissance Orbiter/Compact Reconnaissance Imaging Spectrophotometer. Although soils of Mars are presumed to

lack extensive OM quantities (Summons et al., 2011), which would further convolute the vibrational spectra, it seems possible or even probable that significant advancements for accurately identifying and quantifying minerals in Earth's soil using vibrational spectroscopy may be associated with extraterrestrial exploration efforts.

9.2 Differentiating Mineral and Organic Spectral Absorbance

Soils contain organic C in a great variety of chemical forms. The soil C molecular structure is important, because it is one of the potential determinants of SOM recalcitrance, which has significant implications for soil and environmental quality. Soils contain a rich organic chemical diversity, from labile fatty acids, carbohydrates, and proteins, to more processed and condensed molecules, and highly insoluble, nonhydrolyzable forms of older C. Soil C molecular structure is an active area of research with many extraction methods and instrumentation technologies being evaluated. These approaches include combustion analyses, NMR spectroscopy, incubation and curve fitting, and pyrolysis molecular beam mass spectrometry (py-MBMS), among others. These methods are all contributing to our understanding of soil C quality, but MIR spectroscopy is a particularly valuable tool for soil scientists. This is especially true when different methodologies are used side-by-side, affording a more comprehensive picture of the chemical makeup of soil samples.

One of the challenges for soil scientists studying soil C chemistry via MIR data is identifying the spectral bands that can be fully or partially ascribed to organics, as opposed to the regions that are more affected by mineral absorption. Soils are predominantly mineral in nature, and even Histosols can have a substantial mineral content, which can hinder spectral interpretation (Reeves, 2012). Soil MIR spectra generally contain several regions that can be highly influenced by minerals. The presence of kaolinite, smectite, or illite clays will result in a peak near 3620 cm^{-1} due to hydroxyl stretching in aluminosilicate (Nguyen et al., 1991) (Figure 1.17). The region between 1790 and 2000 cm^{-1} often has three characteristic peaks due to silicates. It is not surprising then that absorbance within this region can correlate negatively with total soil C and N (Calderón et al., 2011a). Carbonates absorb in the region between 2995 and 2860 cm^{-1} and can cause a peak with a shoulder near 2520 cm^{-1}. The carbonate absorbance between 2995 and 2860 cm^{-1} will interfere with aliphatic CH bands, so it is beneficial to decalcify soil samples before scanning in order to rid the sample of carbonate interference (Reeves, 2012). Perhaps one of the most obvious mineral features in neat soil spectra is the "w"-shaped silicate inversion band

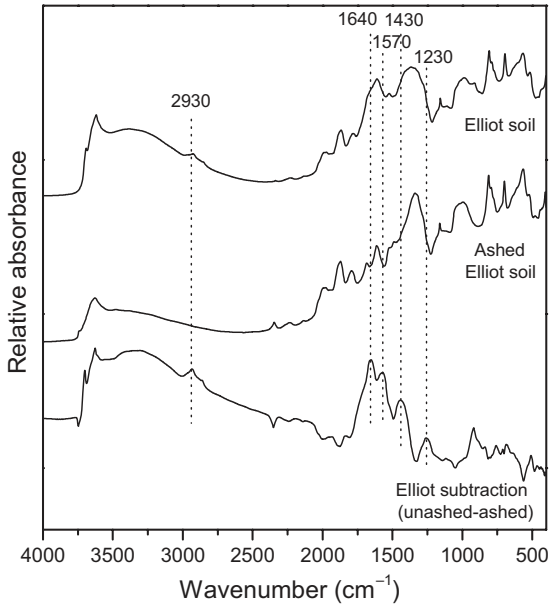

Figure 1.17 DRIFTS spectra of Elliott soil, ashed Elliott soil (550 °C for 3 h), and subtraction of the unashed-ashed spectra. Soil obtained from the International Humic Substances Society. (DRIFTS, diffuse reflectance Fourier transform infrared spectroscopy.)

that occurs between 1280 and 1070 cm^{-1} due to specular reflection (Figure 1.17). This inverted band may interfere with absorbance from carbonyls and other important functional groups. The inverted band is not present in KBr diluted samples (typically 5–10% soil or mineral), forming a broad peak instead, but the advantages of scanning a KBr–soil mixture need to be weighed against the convenience of scanning neat soils.

Studies on NMR spectroscopy of soils have used pretreatment with hydrofluoric acid (HF) in order to reduce the influence of minerals on the soil spectra, and that way enhance the resolution of organic signals (Rumpel et al., 2006). However, SOM molecular structure can be studied by DRIFTS on undiluted soils as long as mineral interferences and specular reflection are taken in account (Demyan et al., 2012) and there are no artifacts of HF treatment (e.g. Rumpel et al., 2006). Furthermore, the ability to detect mineral features (e.g. clays, sands, and carbonates) may be a benefit rather than a disadvantage, because soil texture and clay protection are important pieces of the puzzle in the study of SOC dynamics. Pretreated or whole soil spectra both hold important, albeit different kinds of information. It is all a matter of properly resolving the soil spectral traits that are relevant for a given research question.

Previous work has relied on ashing (e.g. 550 °C, 3 h) of the soil sample followed by the subtraction of the ashed soil spectrum from the intact soil spectrum. The ashing removes the organic C from the sample, so the subtraction helps to accentuate some of the organic bands in the spectrum (Calderón et al., 2011a,c; Sarkhot et al., 2007b). Figure 1.17 shows the ash subtracted spectrum, the intact soil spectrum, and the subtraction for a soil sample. The subtracted spectrum highlights several organic bands including the 2930–2830 cm^{-1} bands for aliphatic C–H (Haberhauer and Gerzabek, 1999). The peak at 1640 cm^{-1} is possibly C═O from amides, aromatic C═C, or carboxylates. The subtracted features at 1570 cm^{-1} (amide II band), 1430 cm^{-1} (C–O vibrations or C–H deformation), and 1230 cm^{-1} (aromatic ring C–H) also comprise organic absorbances.

Recently, it has been noted that these ashing subtractions need to be interpreted with caution because the heating of minerals can affect their spectral properties, and the removal of organics can cause artifacts due to altered specular reflection in the sample (Reeves, 2012). However, the aliphatic CH regions (3000–2800 cm^{-1}) and the region between 1750 and 1600 cm^{-1} are relatively free of those artifacts and can be accurately subtracted. This is significant because the range between 1750 and 1600 cm^{-1} is considered part of the fingerprint region that contains information about many important functional groups like amides, carboxylates, and aromatics that can be determinants of SOM quality. Subtractions outside these regions will need more judicious interpretation and involve assumptions that may or may not be met. While the accuracy of ashing subtraction spectra for analytical purposes may be limited, these spectra may still be useful when fingerprinting of soils is the chief objective, as in forensic studies (Cox et al., 2000). Additional discussion on removal of organic C from soil is provided in section 10.3.

For future studies, other modes of oxidation, such as hypochlorite treatment, should be investigated as alternatives to ashing-subtraction so that the effects of the heating of clays can be avoided. Another interesting approach will be to simply use wet chemistry extraction procedures to isolate different soil C pools and that way avoid the presence of mineral bands altogether. For example, HS can be obtained from soils and the characteristics of the humic and fulvic acids can be studied in detail via DRIFTS. Also, as previously mentioned, soils can be extracted with hot water and the dried extracts scanned directly to study the extracted carbon fraction, which is thought to contain labile organics (Demyan et al., 2012). Already a common FTIR-extract approach is DRIFTS of organics extracted sequentially by water and sodium pyrophosphate (He et al., 2012, 2011b; Kaiser and

Ellerbrock, 2005; Kaiser et al., 2007). Other possible fruitful approaches could include the analysis of nonhydrolyzable soil C, which has been shown to be old and recalcitrant (Follett et al., 2007). For the study of low mean residence time (MRT) SOM, density fractionation allows for the isolation of the LF (see below), a mostly organic material that consists of recently added plant residues (Calderón et al., 2011c).

Several studies have used ratios of specific spectral bands in environmental samples and soils to study the chemical composition of SOM (Artz et al., 2006; Calderón et al., 2006; Ellerbrock et al., 2005). Ellerbrock et al. (2005) related the wettability of soils to hydrophilic to hydrophobic band ratios. Artz et al. (2006) calculated the ratio of carboxylate to polysaccharide peak intensities and related it to the decomposability of organic soils. The band ratio approach can thus be used to minimize inorganic interferences and in effect normalize the data to resolve baseline issues. For example, Demyan et al. (2012) used the ratio of 1620–2930 cm^{-1} band areas as an index of SOM stability. This ratio is thought to measure the proportion of conjugated groups (aromatics, carboxylic acids, quinones) to aliphatic methyl groups, thus giving an index for SOM condensation. Assis et al. (2012) used the band ratio approach to determine hydrophobicity and condensation in SOM, which are related to the resistance to decomposition of SOM. The ratio 2929 to 1035 cm^{-1} represents apolar methyl groups to polar (C–O, –OH) groups. Similarly Matějková and Šimon (2012) used 3000–2800 cm^{-1} as an indicator of hydrophobic component, and 1740–1600 cm^{-1} to indicate hydrophilic components. Ding et al. (2002) calculated the ratios of labile (O-containing) to recalcitrant functional groups in humic acids. Oxygen containing groups are preferentially utilized by soil microbes, so absorbances such as 1727, 1650, 1160, 1127, 1050 cm^{-1} were considered labile, while absorbances at 2950, 2924, 2850, 1530, 1509, 1457, 1420, 779 cm^{-1} were considered resistant. Recently, Veum et al. (2014) used approaches similar to Demyan et al. (2012) and Ding et al. (2002) to study relationships between DRIFTS derived indices of decomposition stage (i.e. potentially reduced biological reactivity) and other measures of SOM lability. The authors noted all five decomposition indices (three relating aromatic to aliphatic moieties and two relating recalcitrant to O-containing functional groups) were negatively related to soil microbial dehydrogenase activity ($r = -0.63$ to -0.76; $p < 0.05$), potassium permanganate oxidizable-C ($r = -0.83$ to -0.95; $p < 0.001$), and water-extractable OC ($r = -0.66$ to -0.82; $p < 0.05$). Although the argument for using the lack of O-containing functional groups as an indicator/estimate of more resistant groups requires further testing (e.g. fatty acids rich in C–H

are relatively easily degraded by soil microbes), the work of Veum et al. (2014) demonstrates a linkage between DRIFTS measures of decomposition stage and microbial function.

10. FTIR SPECTROSCOPY FOR SOM ANALYSIS

Most soils are predominantly composed of minerals, from purely mineral soils to the outlier of 25% soil OC of Histosols (Woodwell, 1984). In general, surface horizons tend to contain more SOM (1–5% soil OC) and OC content in some subsoil horizons may be nearly undetectable. This relatively low OC content in soils presents a challenge for the spectroscopic study of OM, and the challenge is currently addressed by three broad experimental approaches. These FTIR spectroscopy approaches include: (1) whole soils, with low absorbance values for OM bands nonetheless quantified; (2) soil fractions enriched in OM, or SOM extracts with minor mineral components; and (3) calculation of subtraction or difference spectra, in which a spectrum of SOM is obtained indirectly by subtraction of an SOM removal treatment (e.g. combustion, oxidation).

10.1 SOM Analysis in Whole Soils

Some chemical insights of SOM can be gained from scans of whole soils. Meaningful quantification or even detection of SOM can be difficult due to the low intensity of organic absorbances relative to the dominance of mineral absorbances, in particular silicates [ν(Si–O) 1070–950 cm^{-1}]. Considerable overlap of SOM and mineral absorbances can occur, in particular 1400–400 cm^{-1}, making unambiguous assignments for mineral and organic moieties challenging (Calderón et al., 2011b). Advantages of using soil samples include minimal or no sample preparation, quantitative assessments of SOM, and additional data on the soil matrix (e.g. moisture content, soil mineralogy). For instance, whole soil samples have been employed in indices of hydrophobicity-hydrophilicity contributed to by OM (Ellerbrock and Gerke, 2004; Ellerbrock et al., 2005; Matejkova and Simon, 2012; Simon, 2007; Šimon et al., 2009; Simonetti et al., 2012). Areas of the aliphatic νs(C–H) band at 3000–2800 cm^{-1} as the hydrophobic region and a hydrophilic region of νs(C═O) at 1740–1600 cm^{-1} of whole soil spectra provided hydrophobic/hydrophilic ratios. Intensity of absorbance of these functionally defined regions was also employed to obtain indexes of hydrophobicity. These regions correspond to SOM components related to wettability (Ellerbrock et al., 2005). Previous work has established hydrophobic

components of FTIR absorbances (Capriel et al., 1995) and these as a function of management (Capriel, 1997).

Employing the same ratio of absorbances to track soil wettability and sorption properties, more recent studies have extended to different spatial scales and dimensions of SOM, from the three-dimensional microaspect of soil aggregates to landscapes. SOM hydrophobicity was evaluated with the aliphatic:carbonyl band ratios previously described over a chronosequence in the Swiss Alps (Egli et al., 2010). The same band ratio has been used for in situ FTIR mapping of soil physical structures, including pores, cracks, and earthworm tunnels, revealing significant heterogeneity in hydrophobicity and general SOM composition at the millimeter scale (Ellerbrock et al., 2009). It should be noted that in situ FTIR often requires untangling primary reflection, primary absorption, and diffuse reflection (i.e. Kubelk–Munk transformation) as a result of surface topology effects. A recent review addresses the physics of DRIFTS spectroscopy and the use of data transformation like Kubelk–Munk, to account for potentially interfering reflectance behaviors (Torrent and Barrón, 2008).

Performing FTIR of SOM with bulk soil on the same soil type is a strategy to control for mineral absorbances in order to highlight differences in SOM-based spectral features. This increases the sensitivity of organic bands with possible or partial mineral contributions, and is well suited for block treatment experiments (Demyan et al., 2012; Giacometti et al., 2013).

10.2 SOM Analysis via Fractions and Extracts

The dominance of FTIR spectra by mineral absorptions in whole soil samples typically prevents detailed investigation of SOM. As a result, researchers commonly use extractions of representative or C-enriched fractions in order to obtain detailed FTIR data on the organic component of soil (Simonetti et al., 2012). SOM fractions can be highly enriched in OM or are dominantly OM, allowing for better detection. This can be particularly useful for evaluating the effects of land-use, climate, and vegetation on SOM. The use of SOM fractions or extracts complements the theoretical approach to SOM as the sum of a number of pools of organic carbon, often overlapping at functional and structural levels. Moreover, these enriched OM fractions enable, greater FTIR detection of organic bands. FTIR of organic fractions can be used to track changes in SOM composition over time and in response to land management. Molecular resolution of SOM enhances the utility of these fractions beyond mass balance values and also allows controlling for potentially cofounding effects of composition variation within a fraction.

Chemical and physical fractionation of samples enriched in or composed of SOM allows comparative changes in chemical composition to be assessed from the increased resolution of organics compared to whole soils. Chemical and physical fractionation can be coupled to increase the specificity of FTIR data, as was done by Simonetti et al. by extracting humic acids from macroaggregates, micoraggregates, and the silt + clay fraction (Simonetti et al., 2012). FTIR analysis of SOM using chemical and physical fractionations are discussed below.

10.2.1 Chemical Extracts and Fractionation

In the literature, a number of chemical extracts of SOM have been analyzed by FTIR. Commonly studied fractions are dissolved organic matter (DOM) or water-extractable organic matter (WEOM) (He et al., 2011a, 2012; Kaiser and Ellerbrock, 2005; Kaiser et al., 2007; Peltre et al., 2011), and HS, which will be discussed shortly. Kaiser and He also report the use of pyrophosphate-extractable organic matter (PEOM) as an SOM fraction of intermediate stability suitable for FTIR characterization, using the ground freeze-dried extract to avoid water interference (He et al., 2011b; Kaiser and Ellerbrock, 2005). ^{14}C dating and greater carbonyl absorbance of ν(C═O) at 1710 and 1690 cm^{-1} in spectra of PEOM relative to WEOM suggests the former as an older, more stabilized fraction (Kaiser and Ellerbrock, 2005). FTIR characteristics of PEOM characterized were sensitive to soil type and crop rotation, unless fertilized by manure, which consistently increased carbonyl content of amide and carboxylate ν(C═O) at 1740–1700 and 1640–1600 cm^{-1}, respectively. The lower ν(C═O) absorbance of WEOM suggests PEOM as a more appropriate pool for evaluating organic amendments on SOM (Kaiser et al., 2007, 2008). Organic absorbances of WEOM extracts from potato cropping systems reflected irrigation treatment types through aliphatic ν(C–H) at 3020–2800 cm^{-1} and aromatic ν(C═C) at 1640–1600 cm^{-1}, in contrast to PEOM (He et al., 2011b). The high sensitivity of WEOM to labile organics make FTIR spectra of this fraction a means to track changes in aliphatic and proteinaceous material during municipal waste composting (He et al., 2011a).

10.2.2 HS: A Common SOM Extract for FTIR Analyses

The most common method of SOM fractionation for FTIR employs an OM pool referred to as HS. HS have been traditionally understood as a pool of stabilized, recalcitrant SOM (Kleber and Johnson, 2010; Schnitzer and Monreal, 2011). HS are an alkaline-soluble fraction of SOM, and FTIR is

performed on further fractions based on solubility in acid and base (Kerek et al., 2003; Mao et al., 2008; Senesi et al., 2007; Simonetti et al., 2012; Watanabe et al., 2007). These operationally defined components of HS include humic acids (HA), fulvic acids (FA) and humin, with similar postulated structures but differing and characteristic molecular weight, elemental composition, and functional group content (Khan, 1975). One of the early applications of FTIR in soil was the analysis of HS (e.g. Filip et al., 1974; Kodama and Schnitzer, 1971), and the FTIR characterization of HS composition from not only soils but also sediments and aquatic environments is well established. For this reason, discussion will focus on more recent advances in FTIR of HS and its applications in various contexts. For a review of FTIR analysis of HS readers are referred to Stevenson and Goh (1971).

FTIR spectroscopy of HS is particularly insightful when used in tandem with complementary molecular-level characterizations. FTIR provides information on functional groups, often coupled with ^{13}C NMR spectroscopy to corroborate observed distribution of carbon environments, or vice versa. The uniqueness of FTIR in these complementary approaches lies in its ability to provide molecular context to carbon environments measured by NMR. Additionally, noncarbon components of SOM and HA, such as sulfur and phosphate, can be simultaneously characterized with FTIR (Tatzber et al., 2008).

Along with NMR spectroscopy, elemental analysis is commonly coupled with FTIR for molecular-level analyses of HS (Tatzber et al., 2008). In the latter case, FTIR is used as a standard and non-destructive component of a spectroscopic toolkit to fully characterize HS, including UV–vis spectroscopy, fluorescence spectroscopy, electron spin resonance spectroscopy and NMR spectroscopy (Matilainen et al., 2011). Mass spectrometry methods are also common (e.g. Baglieri et al., 2012), and photochemical characterization has been suggested as an additional spectroscopic measurement (Uyguner-Demirel and Bekbolet, 2011).

FTIR spectra of HS have been frequently employed as a marker pool to monitor changes in the more recalcitrant portion of SOM. Though the utility of alkaline extracts as an SOM pool of functional significance is contested (Kleber and Johnson, 2010; Schmidt et al., 2011), these pools may find limited use as a standardized extract for monitoring SOM. Multiple FTIR studies on SOM employ HS, and direct comparisons of DRIFT and transmission (Baes and Bloom, 1989), and DRIFT and photoacoustic (PAS) FTIR (Du et al., 2013a) reveal that comparable spectra of HS are obtained across the varied sampling approaches.

FTIR has helped further understanding of HS chemistry, corroborating and revealing characteristics of HS fractions like functional group differences between HA and FA, and the variation of these as a function of environment. For instance, C–H bending vibrations at 1460 cm^{-1} suggest alkyl enrichment of FA relative to HA (Zhang et al., 2009), though aliphatic content of HS as measured by C–H stretching at 3000–2800 cm^{-1} can vary significantly as function of age and/or soil depth (Mafra et al., 2007; Marinari et al., 2010; Tatzber et al., 2007).

HS are particularly rich in functional groups detectable by FTIR such as carboxylic, carbonyl, and hydroxyl moieties that can interact with agrochemicals and heavy metals through complexation, ion exchange, and reduction (Sparks, 2002). FTIR has been used to understand sorption of Hg^{2+} to HA and FA, occurring through C═O (1628 cm^{-1}) and O-H (3446 cm^{-1}) groups (Zhang et al., 2009), quantify functional group differences between HA and FA to predict suitability for iron ore aggregation (Han et al., 2011), and reveal HA sorption and oxidative-mediation of Sb(III) to Sb (IV) of soils along highways (Ceriotti and Amarasiriwardena, 2009). Binding mechanisms with HS have been elucidated for cations like Cu^{2+} (Alvarez-Puebla et al., 2004; Piccolo and Stevenson, 1982), Pb^{2+}, Ca^{2+} (Piccolo and Stevenson, 1982), and Al^{3+} (Elkins and Nelson, 2002), and agrochemicals, including atrazine (Martin-Neto et al., 1994, Sposito, 1996), hydroxyatrazine (Martin-Neto et al., 2001), glyphosphate (Piccolo and Celano, 1994), paraquat and chlordimeform (Maqueda et al., 1993), and metribuzin (Landgraf et al., 1998).

The carboxyl groups that lend HS much of its characteristic properties, including pH-dependent structure and high chemical reactivity (e.g. metal complexation, pH buffering), can be studied by FTIR in great detail. Hay and Myneni found evidence of highly similar structures for HA of different origins using the carboxylate *va*(C–O) band as a sensitive indicator of structural environment (Hay and Myneni, 2007). ATR-FTIR of five HS obtained from the International Humic Substances Society revealed a common carboxylate *vs*(C–O) peak at 1578 cm^{-1} with similar narrow peak width, suggesting a high degree of structural similarity in carboxylate moieties of HS independent of source (e.g. soil, river). Comparison of the peak position of the carboxylate band of the five HS with a suite of carboxylate-containing model compounds suggested the presence of carboxyl structures similar to those of low molecular weight aliphatic acids of gluconate, D-lactate, methoxyacetate, acetoxyacetate, and malonate, and aromatic acids of salicylate and furancarboxylate. The strong pH-dependence

of the carboxylate band in FTIR spectra highlights increasing deprotonation of carboxylic acids with increasing pH (Gondar et al., 2005; Martin-Neto et al., 1994).

FTIR spectroscopy of HS can be used to evaluate agricultural management effects on SOM. Such studies commonly employ a handful of select absorbance bands and/or band ratios, and typically address the impact of the two main ways in which management can alter SOM quantity and quality: tillage and amendments. HA composition changes have been tracked by FTIR in agroecosystems as a function of amendments, including manure (Watanabe et al., 2007), organic waste (Brunetti et al., 2012), and fertilizers (Ferrari et al., 2011; Simonetti et al., 2012; Watanabe et al., 2007), cover crops (Ding et al., 2006) tillage, irrigation, and crop rotations (Ding et al., 2002; He et al., 2011b), or some combination thereof (Senesi et al., 2007; Verchot et al., 2011). However, some may question the use of FTIR data on HS to draw conclusions about the larger SOM pool. Though HS extracts are generally free of mineral absorbances, their recalcitrance as a stabilized OM pool can make them ineffective windows into SOM changes, even with extreme treatments or over many seasons. For instance, only at high manure addition rates (160 $Mg\,ha^{-1}\,yr^{-1}$) were the effects of continuous manure application reflected in HA composition (Watanabe et al., 2007). Spectra of HA across manure treatments were highly similar, and the absorbance intensity of the amide I band best discriminated among manure treatments, suggesting differences in peptidic or proteinaceous forms in soil organic N pools. Also unique to the HA spectra of high manure treatment was increased absorbance at the aliphatic C–H band 3000–2900 cm^{-1} and carbohydrate C–O band 1150–1040 cm^{-1}. Similarly, effects of high manure application have been observed in intermediately labile SOM fractions like PEOM as increased absorption of carbonyl C═O at 1710 cm^{-1} (Kaiser and Ellerbrock, 2005). Across a variety of land-use in the Philippines, including primary forest, restored forest, and plantations, there were no appreciable differences of HA and FA as characterized by FTIR, though differences were also not found by elemental analysis (Navarrete et al., 2010).

FTIR of HS has been used to evaluate differential tillage regimes on humification and SOM quality. In contrast to SOM as a nutrient reservoir, tillage may provide a more suitable context for FTIR of HS because soil disturbance is known to affect SOM dynamics and decomposition, including humification processes (Tatzber et al., 2008). This approach is often used to evaluate tillage practices, including no-till (Ding et al., 2002; González Pérez et al., 2004; Tatzber et al., 2007). Similarly, the effects of fallow and

amendment treatments have been tracked through changes in ^{14}C-labled HA functionalities over a 36-year experiment with FTIR and NMR. With manure vs straw treatment, and crop diversification and land cover (rotation vs. monoculture vs. fallow), general aromatic and carbonyl content decreased, with specific decreases in benzene and methyl absorbances, whereas amide bands and sulfone and/or ester absorbance increased (Ohno et al., 2009; Tatzber et al., 2009). HA functionalities sensitive to tillage and amendments include aromatic ν(C–H) at 3050 cm^{-1}, carbonyl ν(C═O) at 1700 cm^{-1}, amide ν(C═O) at 1650 cm^{-1} (amide I) amide νs(C–N) at 1420 cm^{-1} (amide III), sulfone νa(S═O) at 1315 cm^{-1} with possible ester contributions, aromatic out-of-plane b(C–H) at 873–728 cm^{-1}, and sp^3-CH_2 and mono-/di-substituted benzene rings at 766 cm^{-1}. FTIR of HS is also sensitive to climate, vegetation cover, and geologic features, allowing discrimination of HA by soil suborder level and humus type (Fernández-Getino et al., 2010).

FTIR for HS characterization extends beyond agricultural contexts and finds use in related areas like archeology, air and water quality, and compost production. FTIR has been used to study the mechanisms of HA formation in archeological samples (Ascough et al., 2011), analyze HA-like fractions from dust macromolecules (Zhao and Peng, 2011), and evaluate water fouling and treatment (Howe et al., 2002; Kanokkantapong et al., 2006). The use of FTIR for analyzing composition and quality of composts, industrial organic wastes, and sewage sludge, and their effects on SOM quality as soil amendments or disposed wastes, is well established (Martínez et al., 2012; Smidt and Meissl, 2007) and has been used to monitor humification during composting (Jouraiphy et al., 2008; Smidt and Schwanninger, 2005) as well as discerning compost quality as a function of feedstock and method (Carballo et al., 2008a; Fialho et al., 2010).

One HS-specific FTIR approach to monitor changes in recalcitrant or long MRT SOM involves two HA subfractions differentiated by cation-binding affinity: calcium-bound humic acid (CaHA) and noncalcium-bound, mobile humic acid (MHA) (Olk et al., 2000; Ve et al., 2004; Whitbread, 1994). MHA is younger and N-rich relative to CaHA, which is consequently less involved in nutrient cycling. Peptide enrichment of the MHA accounts for its greater ability to provision N (Mao et al., 2008). Notably, FTIR can only partly distinguish the increased peptide content of MHA relative to CaHA due to masking of peptide absorbances [amide ν(C═O), ν(C═N)] by aromatic signals [C–O–CH_3 1224 cm^{-1}, νa(COO^-)], illustrating a potential drawback in FTIR of heterogeneous organic samples. Yet

unlike NMR, FTIR was able to detect differences in phosphate [ν(P–O) 1075–1028 cm^{-1}], with partial overlap of alcohol ν(O–H) and ether ν(C–O) among HA subfractions and soils, reflecting known differences in soil P content. Phosphate P–O bonds at 1100–1000 cm^{-1} have been shown to be detectable in FTIR spectra of HS and correlate with phosphorus content of humic fractions (He et al., 2006). The MHA-CaHA FTIR method has also been used to assess N storage in soils for nutrient management in various crop systems, including lowland rice, legumes, and turfgrass (Kerek et al., 2003; Olk et al., 1999, 2000; Slepetiene et al., 2010).

10.2.3 SOM Analysis Following Physical Fractionation

Physical fractionation of soils according to settling properties and aggregate size affords a way of obtaining different types of SOM that vary in their chemistry, decomposability, and age (Assis et al., 2012; Calderón et al., 2011c). Physical fractionation of SOM is commonly performed to understand C cycling and SOM partitioning. These fractions, including soil aggregates, are particularly favorable for FTIR study because they provide distinct information on their own. FTIR characterization, which can be performed with little or no additional sample preparation to molecularly resolve these fractions. FTIR analysis of physical fractions can thus improve understanding of organomineral interactions that exert controls on SOM stabilization and turnover (Kögel-Knabner et al., 2008; Six et al., 2004; Wiseman and Püttmann, 2006). Physical aggregate fractions can serve as C-enriched soil samples with increased organic IR absorbance for improved SOM characterization. SOM composition among individual aggregate fractions and bulk soil allows detailed evaluation of the effect of different tillage and cropping regimes on soil chemistry and nutrient cycling (Calderón et al., 2011a; Davinic et al., 2012b; Tonon et al., 2010; Verchot et al., 2011). The use of FTIR for characterizing soil physical fractions is not limited to providing mean SOM composition on ground samples; surface and other spatial characterization is possible (Leue et al., 2010b).

While there are different fractionation schemes being used today, the fractions may consist of a LF that floats in a high-density solution, POM that is rich in organics but usually contains some sand, and finally the finer materials that separate by settling such as the clay-sized and silt-sized fractions (Haile-Mariam et al., 2008). Different fractionation procedures are also able to separate occluded soil C fractions or free fractions that occur inside and outside of soil aggregates (Assis et al., 2012). Aggregate classes in effect contain different forms of SOM that vary in their role in soil C

accrual. Intraaggregate microaggregates, for example, are thought to contain protected/recalcitrant C important for C sequestration. Macroaggregates, in turn, are responsive to tillage and contain some labile C (Oades, 1984). Sarkhot et al. (2007b) studied aggregate size fractions from a forested Spodosol and showed that polysaccharide bands in 250- to 150-μm aggregates could be indicative of aggregate binding agents secreted by microorganisms. One interesting aspect of physical fractionations is that clays and sands become enriched in different SOM chemical fractions and depleted in others, which needs to be taken into account during spectral interpretation (Fultz, 2012).

One advantage of soil physical fractions for FTIR is minimization of particle size effects on IR reflectance. Heterogeneous particle size of samples, like bulk soils, can produce inaccurate absorbances as a result of different reflectance patterns, in particular for DRIFTS. For instance, the homogeneity of textures within soil sets is thought to be partly responsible for the success of FTIR-calibrated models for soil C and N prediction (Cozzolino and Morón, 2006). Increased particle size homogeneity improves the consistency of diffuse reflectance (Dahm and Dahm, 2001). Absorbance is inversely proportional to particle size, such that soil samples containing a range of clay- to sand-sized particles may produce biases in FTIR data like disproportionally greater absorbance of sand-associated OM. The accuracy of FTIR quantification of soil C and N often varies by texture class within a given soil, and depending on the particular soil a texture fraction can have significantly different predictive accuracy (Cozzolino and Morón, 2006). For instance, soil C often strongly correlates with clay and silt C. In some cases correlations between C or N fractions and texture fractions are poor despite a theoretical expectation otherwise. For instance, stronger correlations can be found between soil C and fine sand C relative to coarse sand C (Cozzolino and Morón, 2006). In addition to confounding effects on reflectance, particle size heterogeneity can also encompass SOM variation that leads to absorbance bias by certain functional groups. Given the diversity of organic functional groups, components of SOM can differ in their absorbance of IR and thus be differentially sensitive to FTIR quantification. For instance, POM encompasses a range of humification products, generally increasing in humification with decreasing POM size. Large POM is thought to represent lightly processed litter (>1000 μm) whereas small POM contains humified SOM (<53 μm). The accuracy of FTIR measurements of soil C and N are lower for clay fractions compared to fractions of larger SOM size, mostly notable POM and sand-associated OM. This is thought to reflect the different sensitivity of FTIR to broad differences

in SOM quality, like nonhumified vs humified OM (Yang et al., 2012). Likewise, FTIR calibration models of SOM content have found improved predictions with decreasing particle size, which are thought to be the result of coarser particles (>20 μm) having more heterogeneous SOM distribution (Barthès et al., 2008).

The use of FTIR spectroscopy in conjunction with size fractionations has yielded good insights regarding the chemistry of different forms of C in soil. For example, spectral data shows that the LF and POM are possibly made up of partially decomposed plant residues of relatively short MRT. Calderón et al. (2011c) showed that spectral differences between the size fractions are maintained across soils from different locations from the Corn Belt. For example, the LF absorbs markedly at 3400 and 1750–1350 cm^{-1} (Figure 1.18). The POM also has relatively high absorbance at 1360 cm^{-1}. Long-term incubation shows that the LF loses absorbance at 3400 cm^{-1}, and 2920–2860 cm^{-1}, suggesting the decomposition of labile

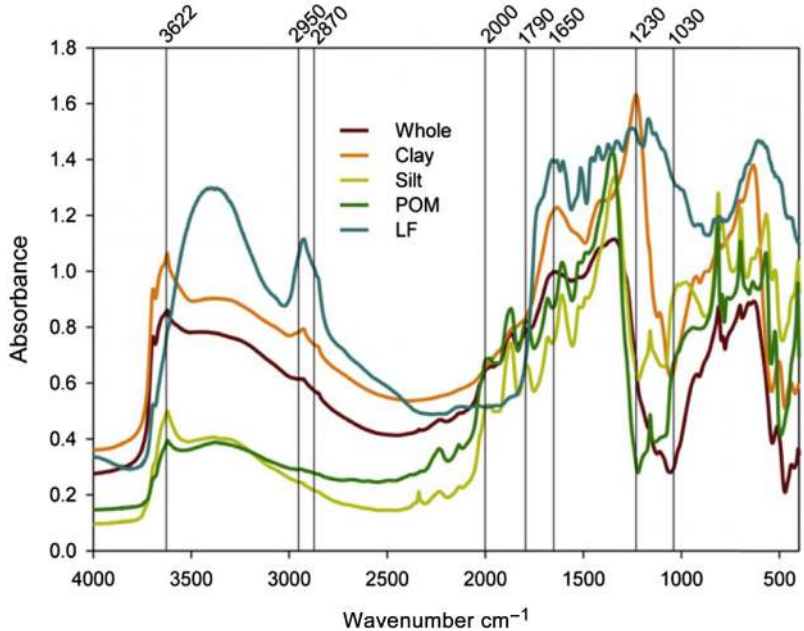

Figure 1.18 DRIFTS spectra of size and density fractions of SOM isolated in a clay loam (20 g C kg^{-1} soil) under long-term continuous maize cropping. Shown are spectra for whole soil, clay fraction, silt fraction, particulate organic matter (POM), and light fraction (LF). (DRIFTS, diffuse reflectance Fourier transform infrared spectroscopy; SOM, soil organic matter.) (For color version of this figure, the reader is referred to the online version of this book.) *Reprinted with permission from Calderón et al. (2011).*

residue C. In contrast, incubation increased the band at 1630 cm^{-1} indicating that this band represents more processed forms of plant-derived C. The study by Assis et al. (2012) shows that the LF from an oxisol can be separated into occluded and free fractions, and that the occluded material has a higher degree of condensation according to DRIFTS band ratios. This study also found that the free and occluded LF were affected differently by cultivation, showing that size fractionations can be a sensitive way to monitor the effects of agricultural management.

In physical aggregate fractions, the finer silt and clay fractions typically contain older, more processed C. The OC signal in these fine fractions is characterized by aromatic bands suggesting humification (Calderón et al., 2011c). The clay fraction contains more than half of the total soil C in many agricultural soils, so it is not surprising that high SOM soils have greater absorbance than low SOM soils at 1230 cm^{-1}, a band for aromatics and characteristic of clay minerals too. Future research should try to elucidate if absorbance at 1230 cm^{-1} is primarily due to organic or mineral absorbance in neat samples, because it is possible that the relationship of soil C with this band is a result of a correlation by proxy of C with clay mineral abundance. Clay fraction DRIFTS spectra do change during laboratory incubation (Calderón et al., 2011c), suggesting that soil C cycling dynamics can be very complex, with fractions that are thought to be old, but are not necessarily recalcitrant.

A classic example of the utility of FTIR for analysis of soil physical fractions involves examining SOM composition among soil aggregates as a function of management. For example, aggregate fractions (macro, >212 μm; meso, 212–53 μm; microaggregates 53–20 μm) of two mineralogically and texturally distinct soils (Ferralsol and Arenosol) were analyzed for organic absorbances (Verchot et al., 2011). Certain aggregate classes displayed a distinct FTIR signature with characteristic peaks independent of soil or management (e.g. tillage, crop type and rotation), whereas the SOM absorbances of other aggregate classes varied by site. Across soils and treatments, microaggregate spectra exhibited polysaccharide (C–O, 1018 cm^{-1}) enrichment and depletion of ketone and carboxyl (ν(C═O) 1778 cm^{-1}) and aromatic (C═C, 1635 cm^{-1}) moieties relative to mesoaggregate OM, for which opposite FTIR trends were observed. In contrast, macroaggregate OM composition varied by soil type. Comparison of macroaggregate with bulk soil spectra indicated that macroaggregates were poor in all but aliphatic C–H deformation (1370 cm^{-1}) and polysaccharide C–O in the clay-rich Ferralsol (420 g clay kg^{-1} soil), but poor in aliphatic C–H stretching (2930 cm^{-1})

and phenolic O–H (3435 cm^{-1}) in the Arenosol (180 g clay kg^{-1} soil). Similar aggregate characterization by additional FTIR studies suggest shared OM composition of aggregate classes within a range of edaphic factors, pointing to common mechanisms of organomineral stabilization and turnover by physical size. It is notable that despite the large range in soil C contents of these soils (5–24 g C kg^{-1} soil), bulk soil FTIR did not detect substantial differences among tillage (minimal vs. conventional) and crop rotation (continuous maize vs maize-legume vs maize-fallow), in contrast to aggregate FTIR. This illustrates the high suitability of C-enriched fractions and extracts for capturing SOM response to treatment effects, rather than bulk soil samples, with FTIR. These soil fractions can also provide the necessary resolution of SOM into various pools to track SOM cycling and responses to managements.

In another study using FTIR to examine physical fractions, Demyan et al. (2012) fractionated SOM from a Haplic Chernozem using a procedure that involved flotation, centrifugation, and heavy liquid density separation. They baseline-corrected band areas centered at 2930, 1620, 1530, and 1159 cm^{-1} in bulk soil and identified them as organic with minimal mineral interference. The lighter density SOM fractions correlated with bulk soil absorbance at 2930 cm^{-1}, while peak areas centered at 1620 cm^{-1} correlated with the denser SOM fractions, indicating that the SOM fractionation by density also resulted in a separation according to C stability.

Partial Least Squares (PLS) calibrations using FTIR for different POM size fractions at a field scale has also been developed (Bornemann et al., 2010). The PLS loadings, which show the spectral bands responsible for the calibration results, were used to identify the spectral bands that were useful to resolve the different POM fractions. Absorbance between 1000 and 1080 cm^{-1} was used as an indicator of cellulose in the POM classes. Hydroxyl and carbonyl groups (1320 and 1660 cm^{-1}, respectively) increased with decreasing POM size. Lignin, aliphatic C–H, aromatic, and cellulose bands allowed calibration for the different POM fractions. Besides the calibration analysis, this study gave insights about SOM spatial variability, and the role of the different fractions in SOM accumulation.

A recent study by Davinic et al. (2012a) incorporated two data-rich technologies to shed light into the relationship between SOM chemistry and microbiology. Nucleic acid pyrosequencing and DRIFTS were used to investigate soil bacterial communities and how they are associated with different soil C chemical attributes in macroaggregates, microaggregates,

silt, and clay fractions. Pyrosequencing showed that different microenvironments, such as macroaggregates and microaggregates, have distinct bacterial communities and ecological niches. DRIFTS was used to highlight spectral features that distinguished the different fractions, which included organic and mineral bands. With this approach, Davinic et al. (2012a) showed not only that each aggregate size fraction has a particular microbial composition, but that within each aggregate type different microbial taxa correlate with particular organic or mineral DRIFTS bands. Such combinations of DRIFTS with other soil microbiology analyses techniques will help us further our understanding of soil microbial ecology.

Physical fractions of acidic (pH 4.4) and alkaline (pH 7.8) forest soils at Rothamsted Research site revealed fraction-specific pH effects on SOM distribution and quality (Tonon et al., 2010). Less-processed 'light' fractions (free LF, intraaggregate LF) representing recent plant residue inputs accounted for a greater portion of total soil C in the acidic soil compared to the alkaline soil, with greater thermolabile SOM composition in the latter like lignin (guaiacyl lignin of softwoods at 1518 cm^{-1}). In contrast, no soil pH effect was observed for the quantitative distribution and quality of clay and silt-associated OM, 'heavy' fractions representing processed and stabilized SOM. A lack of these same thermolabile compounds and a dominance of absorbances consistent with NMR identification of aliphatics (e.g. C–H deformation 1460–1440 cm^{-1}) characterized the clay and silt SOM. In the acidic soil, increased absorbance of carboxylic acid ν(C═O) at 1724 cm^{-1} of LFs suggested greater protonation. The dominance of ν(O–H) at 3620 cm^{-1} from montmorillonite and kaolinite clays and low aliphatic absorbance area at $\nu a,s$(C–H) at 2950–2800 cm^{-1} was proposed to reflect mineral–organic interactions: hydrophobic association of aliphatic chains with clays lead to shielding of the latter. Another possible organomineral association detectable by FTIR was carboxylic acid ν(C═O) at 1724 cm^{-1} and carboxylate ν(C═O) at 1660 cm^{-1}. Present in LFs with limited or no stabilization by minerals, the carboxylic acid band was nonexistent in heavy fractions and the carboxylate band appeared to have shifted downfield to 1630–1620 cm^{-1}, suggesting carboxylate complexation with mineral surfaces. However, this assignment was not certain given the possible overlap of phyllosilicate interlayer water (b(O–H) 1660–1630 cm^{-1}). This suggests that one benefit of samples containing mineral components, in spite of possible interference with organic absorbances, is providing insight to interactions of organic and mineral constituents of soils.

10.3 SOM Analysis via Subtraction Spectra

A promising but less utilized approach to FTIR study of SOM is to remove mineral absorbances by subtraction of a mineral background. This may be thought of as a spectral correction, akin to correcting for water vapor or CO_2 contamination in extracts and the sample chamber (Kaiser et al., 2007, 2008), accounting for an interfering background (Ellerbrock and Gerke, 2004), or accentuating organic absorbances rather than providing a definite SOM spectrum (Sarkhot et al., 2007a). For instance, subtraction from bulk soil of the mineral component provides a difference or subtraction spectrum of SOM. Spectra of C enriched extracts or fractions, like humic acids and soil aggregates, can also be improved with respect to organic absorbances by subtracting a mineral background. The background or subtracted spectrum is most appropriately obtained by treating the sample to remove SOM (e.g. ashing, oxidation), though in model systems a pure mineral standard can be used. Subtraction of the treated sample spectrum from that of the bulk soil spectrum yields a subtraction spectrum representing the SOM removed during preparation of the background sample. In this regard, the subtraction method offers the possibility of calculating spectra of soil components isolated by fractionation, extractive or destructive.

Important considerations in the subtraction approach for FTIR of SOM include the type of SOM removal and possible treatment artifacts. It is necessary to know how the amount and kind of SOM was removed from the original sample for the subtraction background. Accordingly, using fractionations that isolate fractions of known function, vs largely operational fractions, makes subtraction spectra more useful for SOM characterization by FTIR. Certain fractionations may be better suited for subtraction approaches due to the effects of fractionation method (e.g. chemical oxidation by-products) on subtraction spectra quality. Artifacts of treatment in background samples can compromise the utility of subtraction spectra, though it has been argued that this depends on the overlap of affected regions and regions of interest (Reeves, 2012). For instance, soil ashing for SOM removal can alter mineral absorbances via phyllosilicate dehydration and collapse. One of the early uses of ashed subtraction spectra of total SOM was for obtaining sensitive fingerprints of soils for forensic purposes (Cox et al., 2000). Here the objective was not exact identification or quantitative analysis of SOM composition, but discrimination among soils using the putatively greater site-specificity of SOM composition as characterized by FTIR. The approach takes advantage of the high site-specificity of SOM and FTIR sensitivity to organic compounds to provide soil forensics with

a more sensitive means of fingerprinting soils. Thus, artifacts of treatment in subtraction spectra were not an unacceptable concern. This method has found continued use in soil forensics (Dawson and Hillier, 2010; Lorna et al., 2008).

An early application of the ashing subtraction method was for removing mineral absorbances from DRIFTS spectra of DOM fractions (Chefetz et al., 1998). It has been since used largely to calculate subtraction spectra of the total SOM pool, as well as to remove trace mineral absorbances in soil C extracts. There is great variation in the temperature and duration of ashing, ranging from 400 to 650 °C and 2–8 h (Calderón et al., 2011a,b; Cheshire et al., 2000; Kaiser et al., 2008; McCarty et al., 2010; Reeves et al., 2005, 2001; Sarkhot et al., 2007a,b; Simon, 2007) across a diversity of soil textures and mineralogies, suggesting the need to investigate upper limits of ashing conditions by soil type to avoid artifacts of subtraction that may result from mineral alteration. Theoretically, knowledge of a soil's mineral composition could inform ashing maximum temperatures. Alternatively, these conditions can be empirically established for a given soil by monitoring FTIR mineral bands sensitive to thermal alteration over a range of ashing conditions. For instance, Kaiser et al. (2007) evaluated ashing temperatures from 400 to 900 °C using changes in the intensity and position of the dominant silicate band of Si-O-Si stretching at 1100–1000 cm^{-1} as an indicator of mineral alteration unacceptable for calculating subtraction spectra. Ashing above 400 °C produced intensity changes and peak shifts in the silicate band (Kaiser et al., 2007, 2008). To ensure full SOM removal at this lower temperature, soils were ashed for 8 h. However, other soils may contain minerals that degrade at temperatures lower than 400 °C. As a precautionary measure, in the absence of information on the thermosensitivity of a soil, ashing for subtraction spectra should be performed at a default maximum of 400 °C.

Alternative methods exist for SOM removal with minimal collateral damage to minerals and consequentially insignificant, spectroscopically minimal, or well-defined artifacts in subtraction spectra. Methods for SOM removal have been developed for obtaining pure mineral samples for mineralogical analysis (Soukup et al., 2008) and particle size analysis (Gray et al., 2010; Leifeld and Kögel-Knabner, 2001; Vdović et al., 2010), including hydrogen peroxide, sodium hypochlorite, disodium peroxodisulfate, sodium dithionite, and sodium pyrophosphate, with varying C removal and sensitivity to mineralogy (Mikutta et al., 2005). Given their emphasis on maintaining mineral integrity, in particular with XRD, these methods are highly suitable for obtaining artifact-free mineral samples for subtraction spectra

of SOM. Less mineralogically sensitive reagents include hydrofluoric acid, hydrochloric acid, and potassium permanganate (Favilli et al., 2008; von Lützow et al., 2007).

Hydrogen peroxide has been suggested as an alternative to ashing for FTIR analysis of SOM (Reeves, 2012), though its efficacy depends on clay mineral type and content (Eusterhues et al., 2003) and it can dissolve mineral oxides (Mikutta et al., 2005), hence the use of hydrogen peroxide for field identification of Mn oxides. A comparative study of common oxidants for SOM removal developed a modified version of hypochlorite oxidation (Anderson, 1961) that maximizes OC loss while minimizing mineralogical changes, including relatively sensitive pedogenic oxides (Siregar et al., 2005). This has been corroborated by evaluation of SOM removal from the clay fraction by various oxidative and extractive methods (Cheshire et al., 2000; Favilli et al., 2008) (Figure 1.19). Different ranges of C loss by a single method within and among studies [e.g. hydrogen peroxide, (Leifeld and Kögel-Knabner, 2001; Plante et al., 2004; von Lützow et al., 2007)] suggest

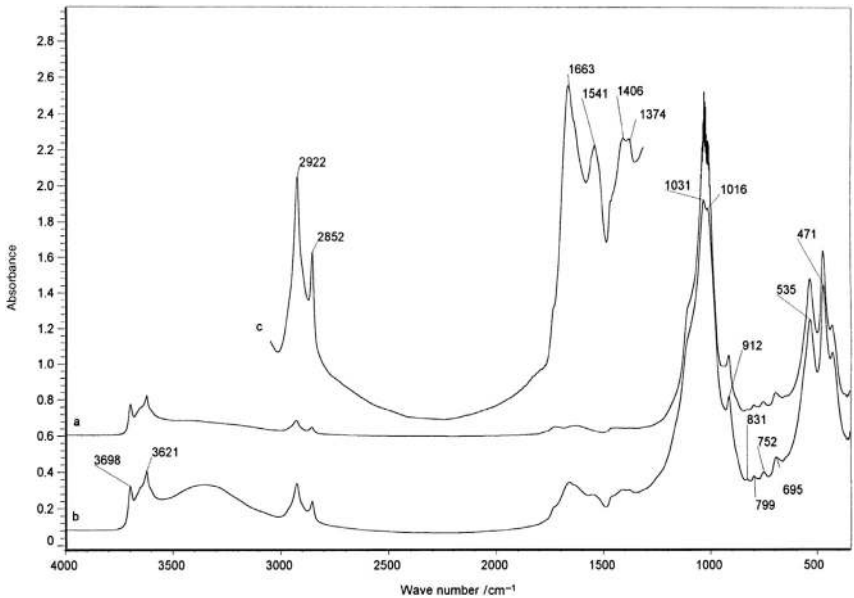

Figure 1.19 Subtraction spectra of SOM in the clay fraction of a pasture Spodosol surface horizon (56 g C kg^{-1} soil). Transmission FTIR spectrum of SOM (C) was calculated by subtraction of sodium hypochlorite-oxidized clay fraction spectrum (A), from the spectrum of the sodium pyrophosphate and sodium hydroxide extracted of this fraction (B). (SOM, soil organic matter; FTIR, Fourier transform infrared.) *Reprinted with permission from Cheshire et al. (2000).*

the influence of mineralogy, and SOM quality and quantity. Reagents may selectively remove distinct SOM pools of varying chemical thermostability and physical occlusion (Eusterhues et al., 2003; von Lützow et al., 2007), and combinations of oxidants and/or hydrolytic agents can obtain high SOM removal rates (Favilli et al., 2008). Alternative SOM removal methods include low-temperature ashing (LTA), in which radio frequency excites molecular oxygen at <100 °C to remove strongly absorbed OM from clay minerals (D'Acqui et al., 1999; Sullivan and Koppi, 1987), and potentially negative pressure treatments. FTIR and XRD comparative analysis of LTA and hydrogen peroxide treatments of bitumen and model clays found comparable loss of aliphatic C–H absorbance, but peroxide dissolution of siderite, confirmed by CEC measurements (Adegoroye et al., 2009).

Clearly, there is an abundance of soil C removal techniques for providing mineral backgrounds for SOM subtraction spectra. It should be noted that incomplete SOM removal is only a disadvantage when net SOM characterization is sought. These oxidative and hydrolytic treatments double as wet chemical methods for fractionating SOM by degree of physical protection, chemical stability, and MRT (von Lützow et al., 2007). They can be especially powerful when coupled to analytical techniques such as ^{14}C dating (e.g. Eusterhues et al., 2003, 2005). With the subtractive approach, FTIR can be used to characterize SOM to improve understanding of these fractions beyond MRT and C/N content. This approach extends beyond destructive fractionation and includes extractive fractionations, which offer the opportunity to cross-check subtractive data by direct FTIR analysis of the extract (in some cases purification is needed, via dialysis for removal of salts). For instance, comparison of SOM subtraction spectra of sodium hydroxide (i.e. HS), sodium pyrophosphate, and sodium hypochlorite treatments of soil clay fractions reveals significant differences in OM reflecting differences in the selectivity and reactivity of reagents (Cheshire et al., 2000).

10.4 Spectral Analysis through Addition of Organic Compounds

One way to validate IR band identification is to add a substance of known spectral properties to soil and then observe changes in absorbance patterns of the soil mixture. The differences can be visualized by subtracting the mixture spectrum from the pure soil spectrum, in which case the subtracted spectrum should show the spectral characteristic of the added substance. Figure 1.20 shows the spectra of soil, humic acid, soil plus humic acid mix, and the subtraction spectrum. The OH/NH region centered at 3400 cm^{-1}

does not show a prominent feature in the subtracted spectrum because absorbance in this band is not particularly different in soils and humic acids. The same can be said about the aliphatic C–H bands between 2930 and 2870 cm^{-1}. However, the regions where the humic acid and soil spectra are different are accentuated. For example, absorbance at 2540 cm^{-1}, which forms a slight rise in the humic acid spectrum but is negligible in pure soil, is shown as a prominent feature of the subtracted spectrum. This band is perhaps underutilized in soil analyses. It is due to overtones of the –COH stretch, and has been identified as important in the development of soil C calibrations (Janik et al., 2007). The humic acid also absorbs strongly at the 1750 cm^{-1} aromatic C=C band, which is characteristic of lignins and humic acids in general. Absorbance at 1750 cm^{-1} is greater in shallow soils than in deeper soils, so it could be used as a marker for SOM accretion in C sequestration scenarios (Calderón et al., 2011a). Absorbance at 1550, 1470, and 1230 cm^{-1} form smaller peaks in the subtraction spectrum due in part to the aromatic absorbance in the humic acid. It is interesting to note that the band at 1230 cm^{-1} falls within the silicate inversion band in neat soils, showing that spectral changes due to organics in this region can be amenable to subtraction and interpretation despite the inversion caused by reflection from sand particles.

Note that the 3630 cm^{-1} clay, 1890 cm^{-1} silica, 1370 cm^{-1} phenolic/carboxylate, 800 cm^{-1} silica, and 695 cm^{-1} silica bands were more intense on the soil spectrum and formed negative peaks in the subtracted spectrum (Figure 1.20). This suggests little interaction of the added humic acid with the soil in these regions and underscores the mineral character of these bands.

The argument could be made that the amendment-subtraction approach could be vulnerable to artifacts such as coating or matrix effects. It is possible that an added standard could coat the clay particles due to electrostatic attraction and shield the soil components from adequate exposure to the IR beam. This is especially true in the MIR range due to the higher energy and lower penetration of the IR energy. Also, it should be kept in mind that some of the older C in soil may be in close association with clays and not easily detected by DRIFTS. In contrast, the added substance should have a relatively good presentation to the IR beam due to its recent incorporation. Nevertheless, this approach can be seen mimicking a soil amendment such as compost addition to soil in the field. Future studies should explore which spectral bands will respond quantitatively according to Beer–Lambert law, and which spectral bands are more prone to artifacts derived from soil amendment interaction.

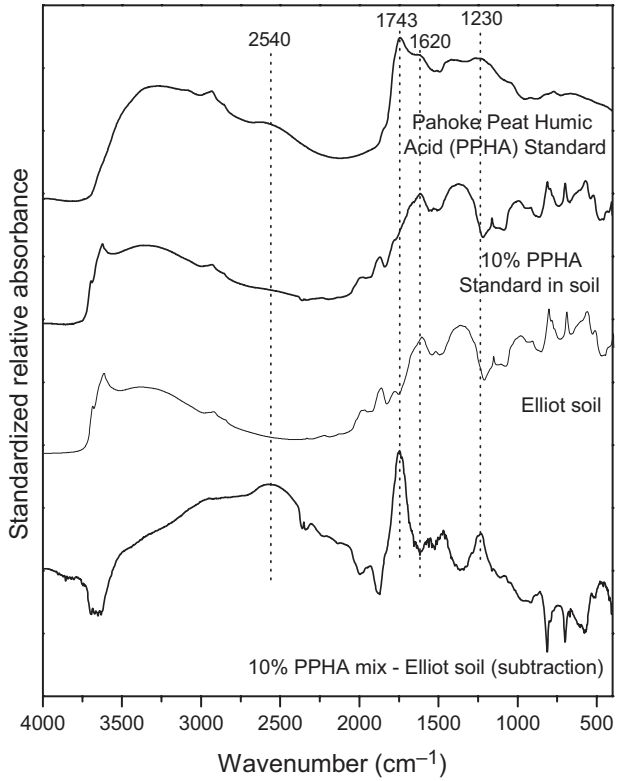

Figure 1.20 DRIFTS spectra of Elliott soil, Pahokee Peat Humic Acid Standard, soil-standard mixture (10% standard in soil by wt), and subtraction of the mix and pure soil spectra. The spectral data was standardized in order for the spectra to have the same mean and standard deviation. Soil and humic acid standards were obtained from the International Humic Substances Society. (DRIFTS, diffuse reflectance Fourier transform infrared spectroscopy; PPHA, Pahokee Peat Humic Acid.)

10.5 Quantitative Analysis of Soil Carbon and Nitrogen

Diffuse reflectance NIR spectroscopy has been used for decades to develop predictive calibrations for the analysis of grains, forages, and other agricultural materials (Roberts et al., 2004). IR calibrations are valuable because they can be used instead of expensive, complex, and time consuming chemical analyses. NIR and MIR spectroscopies have been used successfully to calibrate for soil parameters like soil C, N, as well as mineral features (Reeves, 2010). Given a sample set of adequate size and acceptable distribution of the C data, both NIR and MIR (i.e. DRIFTS) can produce calibrations for total soil C, although MIR often outperforms NIR (McCarty et al., 2010;

Mimmo et al., 2002; Reeves et al., 2005). One exception is when the soil samples are field moist, in which case DRIFTS calibrations fail due to its higher sensitivity to moisture (Reeves, 2010). Because of this, DRIFTS may be amenable for laboratory-based calibrations, but NIR has more potential for field on-site calibrations.

As with all calibrations of any kind, it is important to include a sample set that brackets the samples to be predicted in terms of C content and soil type (Reeves et al., 2012). Prediction accuracy benefits from having samples in the calibration set that are geographically proximate and compositionally similar to the samples to be predicted.

Soil C measurement was the original motive for developing calibrations with FTIR data. Indeed, MIR and NIR can be used to measure soil total C and N accurately (McCarty et al., 2002; Mimmo et al., 2002; Reeves et al., 2005, 2001). However, the last decade has seen a proliferation of calibration work for soil properties other than total C and N. DRIFTS has been used to predict alkyl, carbonyl, and aromatic C in soil and litter samples quantified via NMR (Ludwig et al., 2008). Recent work shows that we can potentially calibrate for other parameters in soil such as metals, carbonates (inorganic C), enzymes, potential nitrification, and pH (Du et al., 2013b; McCarty et al., 2002; Mimmo et al., 2002; Reeves et al., 2001; Siebielec et al., 2004). Because DRIFTS contains information related to organic and inorganic components that relate to texture and particle size distribution, calibrations can also be developed for soil physical attributes including moisture retention, bulk density, or hydraulic conductivity (Janik et al., 2007; Minasny et al., 2008; Tranter et al., 2008). For example, PLS regression coefficients show that absorbance at the 3630 cm^{-1} clay band, and at the 1640 cm^{-1} amide I or phenyl C–C band are important for calibrations for soil water retention (Tranter et al., 2008).

Sometimes predictions can be based on surrogate calibrations, meaning that an alternative to the analyte of interest is detected and a calibration is built inadvertently by correlation. For example, calibrations for pH could be based on the fact that the DRIFTS is measuring other soil qualities related to pH, such as carbonates, which have defined prominent features in the MIR (Reeves, 2010). Reeves et al. (2006) hypothesized that calibrations for $\delta^{13}C$ are possible due to a surrogate relationship of isotope ratios and soil C pool chemistry. It is important to note that surrogate calibrations can fall apart when the relationship between the analyte and the surrogate soil property changes, such as when the calibration is used to predict a soil sample with widely different parent material or geographic origin from the samples in the calibration set (Reeves, 2010).

11. SUMMARY

Vibrational spectroscopy can be a versatile and highly informative analytical tool for soil scientists. Although FTIR and Raman spectroscopies have great utility for characterization of pure samples, it is the continued development of computer science, sampling modules, and methodologies that continue to make vibrational spectroscopy a powerful approach for studying complex matrices such as soils. In particular, FTIR provides a relatively low cost approach for probing molecular composition and interactions on soil particles and at the mineral–liquid interface. The ability of FTIR to provide information on the chemical arrangement and composition of inorganic and organic moieties makes it somewhat unique and ideal analysis approach for soil scientists. Simultaneously providing information on soil minerals and OM composition or organic contaminant binding mechanisms is a benefit not provided by many other instrumental methods.

The existence of diverse methodologies that complement vibrational spectroscopy studies further enhance their potential impact. Studies of soil minerals benefit greatly by coupling FTIR and Raman spectroscopy with XRD to provide confirmation of mineral structures. Similarly, NMR spectroscopy is an excellent method to pair with FTIR for studies of SOM. Advanced synchrotron techniques, such as NEXAFS, also can be used in conjunction with FTIR to elucidate metal binding mechanisms on mineral surfaces. Additionally, the continued development of molecular modeling approaches is greatly improving spectral interpretations and providing detailed molecular-level information for molecular interactions on mineral and organic surfaces. These approaches highlight synergistic analytical methodologies which are becoming increasingly important tools for soil scientists.

Continued advances in the instrumentation and methodologies for vibrational spectroscopy hold great promise for soil science research. For example, advances in microfluidic sampling cells for SR-FTIR are making analysis in the presence of water possible. This will provide exciting capabilities for examining processes at the mineral–water interface with high spatial resolution. Confocal Raman microspectroscopy is another methodology with great potential to develop into a powerful tool for soil scientists. Using this approach sample depth profiling of soil aggregates or films on minerals could be probed with high spatial resolution.

Vibrational spectroscopy has provided a wealth of important data on soil chemical processes since it was first developed in the mid-1900s. Each

ensuing decade has witnessed significant advances in analytical capabilities, affording soil scientists with ever increasing tools to study soil minerals, OM, and their interactions. This review has highlighted some of the more recent applications and discoveries of vibrational spectroscopy, demonstrating a diverse set of approaches for studying important soil chemical processes. Future research efforts will benefit greatly from the continuing evolution of vibrational spectroscopy. It is anticipated that advances will provide new methodologies and provide exciting opportunities for studies of a variety of biogeochemical processes in soil.

ACKNOWLEDGMENTS

S.J. Parikh and K.W. Goyne acknowledge support from the United States Department of Agriculture (USDA) National Institute of Food and Agriculture (NIFA) for Hatch Formula Funding (provided to their respective institutions) and multistate regional project W-2082. A.J. Margenot acknowledges support from USDA NIFA Organic Agriculture Research and Education Initiative Award 2009-01415.

Disclaimer and EEO/Non-Discrimination statement

Mention of trade names or commercial products in this publication is solely for the purpose of providing specific information and does not imply recommendation or endorsement by the U.S. Department of Agriculture. USDA is an equal opportunity provider and employer.

REFERENCES

Adamescu, A., Mitchell, W., Hamilton, I.P., Al-Abadleh, H.A., 2010. Insights into the surface complexation of dimethylarsinic acid on iron (Oxyhydr)oxides from ATR-FTIR studies and quantum chemical calculations. Environ. Sci. Technol. 44, 7802–7807.

Adegoroye, A., Uhlik, P., Omotoso, O., Xu, Z., Masliyah, J., 2009. A comprehensive analysis of organic matter removal from clay-sized minerals extracted from oil sands using low temperature ashing and hydrogen peroxide. Energy & Fuels 23, 3716–3720.

Ajayan, P.M., 1999. Nanotubes from carbon. Chem. Rev. 99, 1787–1799.

Albrecht, M.G., Creighton, J.A., 1977. Anomalously intense Raman spectra of pyridine at a silver electrode. J. Am. Chem. Soc. 99, 5215–5217.

Alcock, N.W., Tracy, V.M., Waddington, T.C., 1976. Acetates and acetato-complexes. 2. spectroscopic studies. J. Chem. Dalt. Trans. 2243–2246.

Allen, B.L., Hajek, B.F., 1989. Mineral occurrence in soil environments. In: Dixon, J.B., Weed, S.B. (Eds.), Minerals in Soil Environments. Vol. SSSA Book Ser. 1. SSSA, Madison, WI.

Alvarez-Puebla, R.A., Valenzuela-Calahorro, C., Garrido, J.J., 2004. Cu(II) retention on a humic substance. J. Colloid Interface Sci. 270, 47–55.

Aminzadeh, A., 1997. Fluorescence bands in the FT-Raman spectra of some calcium minerals. Spectrochim. Acta Part A Mol. Biomol. Spectrosc. 53, 693–697.

Amir, S., Jouraiphy, A., Meddich, A., El Gharous, M., Winterton, P., Hafidi, M., 2010. Structural study of humic acids during composting of activated sludge-green waste: elemental analysis, FTIR and C-13 NMR. J. Hazard. Mater. 177, 524–529.

Amonette, J.E., 2002. Methods for determination of mineralogy and environmental availability. Vol. SSSA Book Ser. 7. In: Dixon, J.B., Schulze, D.G. (Eds.), Soil Mineralogy with Environmental Applications. SSSA, Madison, WI.

Anderson, J.U., 1961. An improved pretreatment for mineralogical analysis of samples containing organic matter. Clays Clay Miner. 10, 380–388.
Arai, Y., Sparks, D.L., 2001. ATR-FTIR spectroscopic investigation on phosphate adsorption mechanisms at the ferrihydrite-water interface. J. Colloid Interface Sci. 241, 317–326.
Arai, Y., Sparks, D.L., Davis, J.A., 2004. Effects of dissolved carbonate on arsenate adsorption and surface speciation at the hematite-water interface. Environ. Sci. Technol 38, 817–824.
Aranda, V., Ayora-Cañada, M.J., Domínguez-Vidal, A., Martín-García, J.M., Calero, J., Delgado, R., et al., 2011. Effect of soil type and management (organic vs. conventional) on soil organic matter quality in olive groves in a semi-arid environment in Sierra Mágina Natural Park (S Spain). Geoderma 164, 54–63.
Aristilde, L., Sposito, G., 2008. Molecular modeling of metal complexation by a fluoroquinolone antibiotic. Environ. Toxicol. Chem. 27, 2304–2310.
Aristilde, L., Marichal, C., Miéhé-Brendlé, J., Lanson, B., Charlet, L., 2010. Interactions of Oxytetracycline with a Smectite Clay: A Spectroscopic Study with Molecular Simulations. Environ. Sci. Technol. 44, 7839–7845.
Arocena, J.M., Pawluk, S., Dudas, M.J., Gajdostik, A., 1995. In situ investigation of soil organic matter aggregates using infrared microscopy. Can. J. Soil. Sci. 75, 327–332.
Artz, R.R.E., Chapman, S.J., Campbell, C.D., 2006. Substrate utilisation profiles of microbial communities in peat are depth dependent and correlate with whole soil FTIR profiles. Soil Biol. Biochem. 38, 2958–2962.
Artz, R.R.E., Chapman, S.J., Jean Robertson, A.H., Potts, J.M., Laggoun-Défarge, F., Gogo, S., et al., 2008. FTIR spectroscopy can be used as a screening tool for organic matter quality in regenerating cutover peatlands. Soil Biology and Biochemistry 40, 515–527.
Ascough, P.L., Bird, M.I., Francis, S.M., Lebl, T., 2011. Alkali extraction of archaeological and geological charcoal: evidence for diagenetic degradation and formation of humic acids. J. Archaeol. Sci. 38, 69–78.
Assis, C.P., Jucksch, I., Mendonca, E.S., Neves, J.C.L., Silva, L.H.M., Wendling, B., 2012. Distribution and quality of the organic matter in light and heavy fractions of a red Latosol under different uses and management practices. Commun. Soil Sci. Plant Anal. 43, 835–846.
Axe, K., Persson, P., 2001. Time-dependent surface speciation of oxalate at the water-boehmite (Gamma-AlOOH) interface: implications for dissolution. Geochim. Cosmochim. Acta 65, 4481–4492.
Axe, K., Vejgarden, M., Persson, P., 2006. An ATR-FTIR spectroscopic study of the competitive adsorption between oxalate and malonate at the water-goethite interface. J. Colloid Interface Sci. 294, 31–37.
Badireddy, A.R., Korpol, B.R., Chellam, S., Gassman, P.L., Engelhard, M.H., Lea, A.S., Rosso, K.M., 2008. Spectroscopic characterization of extracellular polymeric substances from *Escherichia coli* and *Serratia marcescens*: suppression using sub-inhibitory concentrations of Bismuth Thiols. Biomacromolecules 9, 3079–3089.
Baes, A.U., Bloom, P.R., 1989. Diffuse reflectance and transmission Fourier transform infrared (DRIFT) spectroscopy of humic and fulvic acids. Soil Sci. Soc. Am. J. 53, 695–700.
Baglieri, A., Gennari, M., Ioppolo, A., Leinweber, P., Nègre, M., 2012. Comparison between the humic acids characteristics of two andisols of different age by: FT-IR and 1H-NMR spectroscopy and py-FIMS. Geochem. Int. 50, 148–158.
Balan, E., Blanchard, M., Hochepied, J.-F., Lazzeri, M., 2008. Surface modes in the infrared spectrum of hydrous minerals: the OH stretching modes of bayerite. Phys. Chem. Minerals 35, 279–285.
Balan, E., Delattre, S., Guillaumet, M., Salje, E.K.H., 2010. Low-temperature infrared spectroscopic study of OH-stretching modes in kaolinite and dickite. Am. Mineral. 95, 1257–1266.

Balan, E., Lazzeri, M., Morin, G., Mauri, F., 2006. First-principles study of the OH-stretching modes of gibbsite. Am. Mineral. 91, 115–119.
Baltrusaitis, J., Schuttlefield, J., Jensen, J.H., Grassian, V.H., 2007. FTIR spectroscopy combined with quantum chemical calculations to investigate adsorbed nitrate on aluminium oxide surfaces in the presence and absence of co-adsorbed water. Phys. Chem. Chem. Phys. 9, 4970–4980.
Barer, R., Cole, A.R.H., Thompson, H.W., 1949. Infra-red spectroscopy with the reflecting microscope in physics, chemistry and biology. Nature 163, 198–201.
Bargar, J.R., Kubicki, J.D., Reitmeyer, R., Davis, J.A., 2005. ATR-FTIR spectroscopic characterization of coexisting carbonate surface complexes on hematite. Geochim. Cosmochim. Acta 69, 1527–1542.
Bargar, J.R., Persson, P., Brown Jr., G.E., 1999. Outer-sphere adsorption of Pb(II)EDTA on goethite. Geochim. Cosmochim. Acta 63, 2957–2969.
Barja, B.C., Afonso, M.D., 2005. Aminomethylphosphonic acid and glyphosate adsorption onto goethite: a comparative study. Environ. Sci. Technol. 39, 585–592.
Barja, B.C., dos Santos Afonso, M., 1998. An ATR−FTIR study of glyphosate and its Fe(III) complex in aqueous solution. Environ. Sci. Technol. 32, 3331–3335.
Barja, B.C., Herszage, J., Alfonso, M.D., 2001. Iron(III)-phosphonate complexes. Polyhedron 20, 1821–1830.
Barja, B.C., Tejedor-Tejedor, M.I., Anderson, M.A., 1999. Complexation of Methylphosphonic acid with the surface of goethite particles in aqueous solution. Langmuir 15, 2316–2321.
Barthès, B.G., Brunet, D., Hien, E., Enjalric, F., Conche, S., Freschet, G.T., d'Annunzio, R., Toucet-Louri, J., 2008. Determining the distributions of soil carbon and nitrogen in particle size fractions using near-infrared reflectance spectrum of bulk soil samples. Soil Biol. Biochem. 40, 1533–1537.
Beattie, D.A., Chapelet, J.K., Gräfe, M., Skinner, W.M., Smith, E., 2008. In Situ ATR FTIR Studies of SO4 Adsorption on Goethite in the Presence of Copper Ions. Environ. Sci. Technol. 42, 9191–9196.
Beauvais, A., Bertaux, J., 2002. In situ characterization and differentiation of kaolinites in lateritic weathering profiles using infrared microspectroscopy. Clays Clay Miner. 50, 314–330.
Beech, I., Hanjagsit, L., Kalaji, M., Neal, A.L., Zinkevich, V., 1999. Chemical and structural characterization of exopolymers produced by *Pseudomonas* sp NCIMB 2021 in continuous culture. Microbiology UK 145, 1491–1497.
Beech, I.B., Gubner, R., Zinkevich, V., Hanjangsit, L., Avci, R., 2000. Characterisation of conditioning layers formed by exopolymeric substances of *Pseudomonas* NCIMB 2021 on surfaces of AISI 316 stainless steel. Biofouling 16, 93–104.
Benetoli, L.O.B., de Souza, C.M.D., da Silva, K.L., Souza, I.G.D., de Santana, H., Paesano, A., et al., 2007. Amino acid interaction with and adsorption on clays: FT-IR and Mossbauer Spectroscopy and X-ray diffractometry investigations. Origins of Life and Evolution of Biospheres 37, 479–493.
Benning, L.G., Phoenix, V.R., Yee, N., Tobin, M.J., 2004. Molecular characterization of cyanobacterial silicification using synchrotron infrared micro-spectroscopy. Geochim. Cosmochim. Acta 68, 729–741.
Bersani, D., Lottici, P.P., Montenero, A., 1999. Micro-Raman investigation of iron oxide films and powders produced by sol–gel syntheses. J. Raman Spectrosc. 30, 355–360.
Bertaux, J., Frohlich, F., Ildefonse, P., 1998. Multicomponent analysis of FTIR spectra: quantification of amorphous and crystallized mineral phases in synthetic and natural sediments. J. Sediment. Res. 68, 440–447.
Bertsch, P.M., Hunter, D.B., 1998. Elucidating fundamental mechanisms in soil and environmental chemistry: the role of advanced analytical, spectroscopic, and microscopic methods. Future Prospects Soil Chem. SSSA Special Publ. 103–122.

Bigham, J.M., Fitzpatrick, R.W., Schulze, D.G., 2002. Iron oxides. Vol. SSSA Book Ser. 7. In: Dixon, J.B., Schulze, D.G. (Eds.), Soil Mineralogy with Environmental Applications. SSSA, Madison, WI.

Bish, D.L., Johnston, C.T., 1993. Rietveld refinement and Fourier-transform infrared spectroscopic study of the dickite structure at low-temperature. Clays Clay Miner. 41, 297–304.

Bishop, J.L., Dobrea, E.Z.N., McKeown, N.K., Parente, M., Ehlmann, B.L., Michalski, J.R., Milliken, R.E., Poulet, F., Swayze, G.A., Mustard, J.F., Murchie, S.L., Bibring, J.-P., 2008. Phyllosilicate diversity and past aqueous activity revealed at Mawrth Vallis, Mars. Science 321, 830–833.

Bishop, J.L., Dyar, M.D., Lane, M.D., Banfield, J.F., 2004. Spectral identification of hydrated sulfates on Mars and comparison with acidic environments on Earth. Int. J. Astrobiol. 3, 275–285.

Bishop, J.L., Murad, E., 2004. Characterization of minerals and biogeochemical markers on Mars: a Raman and IR spectroscopic study of montmorillonite. J. Raman Spectrosc. 35, 480–486.

Blanch, A.J., Quinton, J.S., Lenehan, C.E., Pring, A., 2008. The crystal chemistry of Al-bearing goethites: an infrared spectroscopic study. Mineral. Mag. 72, 1043–1056.

Blanchard, M., Lazzeri, M., Mauri, F., Balan, E., 2008. First-principles calculation of the infrared spectrum of hematite. Am. Mineral. 93, 1019–1027.

Blout, E.R., Mellors, R.C., 1949. Infrared spectra of tissues. Science 110, 137–138.

Bogrekci, I., Lee, W.S., 2006. The effect of particle size on sensing phosphorus by Raman spectroscopy. In: ASABE Annual Meeting.

Boily, J.-F., Nilsson, N., Persson, P., Sjöberg, S., 2000. Benzenecarboxylate surface complexation at the goethite (α-FeOOH)/water interface: I. A mechanistic description of pyromellitate surface complexes from the combined evidence of infrared spectroscopy, potentiometry, adsorption data, and surface complexation modeling. Langmuir 16, 5719–5729.

Boily, J.-F., Szanyi, J., Felmy, A.R., 2006. A combined FTIR and TPD study on the bulk and surface dehydroxylation and decarbonation of synthetic goethite. Geochim. Cosmochim. Acta 70, 3613–3624.

Borda, M.J., Strongin, D.R., Schoonen, M.A., 2003. A novel vertical attenuated total reflectance photochemical flow-through reaction cell for Fourier transform infrared spectroscopy. Spectrochimica Acta Part a-Molecular and Biomolecular Spectroscopy 59, 1103–1106.

Borer, P., Hug, S.J., Sulzberger, B., Kraemer, S.M., Kretzschmar, R., 2009. ATR-FTIR spectroscopic study of the adsorption of desferrioxamine B and aerobactin to the surface of lepidocrocite (gamma-FeOOH). Geochim. Cosmochim. Acta 73, 4661–4672.

Bornemann, L., Welp, G., Amelung, W., 2010. Particulate organic matter at the field scale: rapid acquisition using mid-infrared spectroscopy. Soil Sci. Soc. Am. J. 74, 1147–1156.

Bowen, J.M., Powers, C.R., Ratcliffe, A.E., Rockley, M.G., Hounslow, A.W., 1988. Fourier transform infrared and Raman spectra of dimethyl methylphosphonate adsorbed on montmorillonite. Environ. Sci. Technol. 22, 1178–1181.

Bowie, B.T., Chase, D.B., Griffiths, P.R., 2000. Factors affecting the performance of benchtop Raman spectrometers. Part II: effect of sample. Appl. Spectrosc. 54, 200A–207A.

Boyd, S.A., Johnston, C.T., Laird, D.A., Teppen, B.J., Li, H., 2011. Comprehensive study of organic contaminant adsorption by clays: methodologies, mechanisms, and environmental implications. In: Biophysico-chemical Processes of Anthropogenic Organic Compounds in Environmental Systems. John Wiley & Sons, Inc., pp. 51–71.

Brandenburg, K., 1993. Fourier-transform infrared-spectroscopy characterization of the lamellar and nonlamellar structures of free lipid-A and Re lipopolysaccharides from *Salmonella minnesota* and *Escherichia coli*. Biophys. J. 64, 1215–1231.

Brandenburg, K., Funari, S.S., Koch, M.H.J., Seydel, U., 1999. Investigation into the acyl chain packing of endotoxins and phospholipids under near physiological conditions by Waxs and FTIR spectroscopy. J. Struct. Biol. 128, 175–186.

Brandenburg, K., Jurgens, G., Muller, M., Fukuoka, S., Koch, M.H.J., 2001. Biophysical characterization of lipopolysaccharide and lipid A Inactivation by lactoferrin. Biol. Chem. 382, 1215–1225.

Brandenburg, K., Kusumoto, S., Seydel, U., 1997. Conformational studies of synthetic lipid A analogues and partial structures by infrared spectroscopy. Biochim. Biophys. Acta Biomembranes 1329, 183–201.

Brandenburg, K., Seydel, U., 1986. Orientation measurements on ordered multibilayers of phospholipids and sphingolipids from synthetic and natural origin by ATR Fourier-transform infrared-spectroscopy. Z. Naturforsch. C-A J. Biosci. 41, 453–467.

Brandenburg, K., Seydel, U., 1990. Investigation into the fluidity of lipopolysaccharide and free lipid-A membrane systems by fourier-transform infrared- spectroscopy and differential scanning calorimetry. Eur. J. Biochem. 191, 229–236.

Brandenburg, K., Seydel, U., 1996. Fourier transform infrared spectroscopy of cell surface polysaccharides. In: Mantsch, H.H., Chapman, D. (Eds.), Infrared Spectroscopy of Biomolecules. John Wiley and Sons, Inc., New York, pp. 203–237.

Brandenburg, K., Seydel, U., Schromm, A.B., Loppnow, H., Koch, M.H.J., Rietschel, E.T., 1996. Conformation of lipid A, the Endotoxic Center of Bacterial Lipopolysaccharide. J. Endotoxin Res. 3, 173–178.

Brandes Ammann, A., Brandl, H., 2011. Detection and differentiation of bacterial spores in a mineral matrix by Fourier transform infrared spectroscopy (FTIR) and chemometrical data treatment. BMC Biophys. 4, 14.

Brandes, J.A., Lee, C., Wakeham, S., Peterson, M., Jacobsen, C., Wirick, S., Cody, G., 2004. Examining marine particulate organic matter at sub-micron scales using scanning transmission X-ray microscopy and carbon X-ray absorption near edge structure spectroscopy. Mar. Chem. 92, 107–121.

Breen, C., Clegg, F., Herron, M.M., Hild, G.P., Hillier, S., Hughes, T.L., Jones, T.G.J., Matteson, A., Yarwood, J., 2008. Bulk mineralogical characterisation of oilfield reservoir rocks and sandstones using diffuse reflectance infrared Fourier transform spectroscopy and partial least squares analysis. J. Petroleum Sci. Eng. 60, 1–17.

Brewer, C.E., Schmidt-Rohr, K., Satrio, J.A., Brown, R.C., 2009. Characterization of biochar from fast pyrolysis and gasification systems. Environ. Prog. Sustain. Energy 28, 386–396.

Brewer, S.H., Anthireya, S.J., Lappi, S.E., Drapcho, D.L., Franzen, S., 2002. Detection of DNA Hybridization on gold surfaces by polarization modulation infrared reflection absorption spectroscopy. Langmuir 18, 4460–4464.

Brigatti, M.F., Lugli, C., Montorsi, S., Poppi, L., 1999. Effects of exchange cations and layer-charge location on cysteine retention by smectites. Clays Clay Miner. 47, 664–671.

Brody, R.H., Carter, E.A., Edwards, H.G.M., Pollard, A.M., 1999a. FT-Raman spectroscopy, applications. In: Editor-in-Chief: John, C.L. (Ed.), Encyclopedia of Spectroscopy and Spectrometry second ed. Academic Press, Oxford, pp. 732–740.

Brody, R.H., Carter, E.A., Edwards, H.G.M., Pollard, A.M., 1999b. FT-Raman spectroscopy, applications. In: Editor-in-Chief: John, C.L. (Ed.), Encyclopedia of Spectroscopy and Spectrometry, Elsevier, Oxford, pp. 649–657.

Bruckman, V.J., Wriessnig, K., 2013. Improved soil carbonate determination by FT-IR and X-ray analysis. Environ. Chem. Lett. 11, 65–70.

Brunetti, G., Farrag, K., Plaza, C., Senesi, N., 2012. Advanced techniques for characterization of organic matter from anaerobically digested grapemarc distillery effluents and amended soils. Environ. Monit. Assess. 184, 2079–2089.

Bullen, H.A., Oehrle, S.A., Bennett, A.F., Taylor, N.M., Barton, H.A., 2008. Use of attenuated total reflectance Fourier transform infrared spectroscopy to identify microbial metabolic products on carbonate mineral surfaces. Appl. Environ. Microbiol. 74, 4553–4559.

Busscher, W.J., Novak, J.M., Evans, D.E., Watts, D.W., Niandou, M.A.S., Ahmedna, M., 2010. Influence of Pecan Biochar on physical properties of a Norfolk Loamy sand. Soil Sci. 175, 10–14.

Cagnasso, M., Boero, V., Franchini, M.A., Chorover, J., 2010. ATR-FTIR studies of phospholipid vesicle interactions with alpha-FeOOH and alpha-Fe_2O_3 surfaces. Colloids Surf. B Biointerfaces 76, 456–467.

Caillaud, J., Proust, D., Righi, D., Martin, F., 2004. Fe-rich clays in a weathering profile developed from serpentinite. Clays Clay Miner. 52, 779–791.

Calderón, F.J., McCarty, G.W., Reeves, J.B., 2006. Pyrolisis-MS and FT-IR analysis of fresh and decomposed dairy manure. J. Anal. Appl. Pyrolysis 76, 14–23.

Calderón, F.J., Mikha, M.M., Vigil, M.F., Nielsen, D.C., Benjamin, J.G., Reeves III, J.B., 2011a. Diffuse-reflectance mid-infrared spectral properties of soils under alternative crop rotations in a semi-arid climate. Commun. Soil Sci. Plant Anal. 42, 2143–2159.

Calderón, F.J., Reeves, J.B., Collins, H.P., Paul, E.A., 2011b. Chemical differences in soil organic matter fractions determined by diffuse-reflectance mid-infrared spectroscopy (All rights reserved. No part of this periodical may be reproduced or transmitted in any form or by any means, electronic or mechanical, including photocopying, recording, or any information storage and retrieval system, without permission in writing from the publisher. Permission for printing and for reprinting the material contained herein has been obtained by the publisher) Soil Sci. Soc. Am. J. 75, 568–579.

Calderón, F.J., Reeves III, J.B., Collins, H.P., Paul, E.A., 2011c. Chemical differences in soil organic matter fractions determined by diffuse-reflectance mid-infrared spectroscopy. Soil Sci. Soc. Am. J. 75, 568–579.

Cambier, P., 1986a. Infrared study of goethites of varying crystallinity and particle size; I, interpretation of OH and lattice vibration frequencies. Clay Miner. 21, 191–200.

Cambier, P., 1986b. Infrared study of goethites of varying crystallinity and particle size; II, crystallographic and morphological changes in series of synthetic goethites. Clay Miner. 21, 201–210.

Campion, A., Kambhampati, P., 1998. Surface-enhanced Raman scattering. Chem. Soc. Rev. 27, 241–250.

Cançado, L.G., Jorio, A., Pimenta, M.A., 2007. Measuring the absolute Raman cross section of nanographites as a function of laser energy and crystallite size. Phys. Rev. B 76, 064304.

Cao, Y.Y., Wei, X., Cai, P., Huang, Q.Y., Rong, X.M., Liang, W., 2011. Preferential adsorption of extracellular polymeric substances from bacteria on clay minerals and iron oxide. Colloids Surf. B Biointerfaces 83, 122–127.

Capriel, P., 1997. Hydrophobicity of organic matter in arable soils: influence of management. Eur. J. Soil Sci. 48, 457–462.

Capriel, P., Beck, T., Borchert, H., Gronholz, J., Zachmann, G., 1995. Hydrophobicity of the organic matter in arable soils. Soil Biol. Biochem. 27, 1453–1458.

Carballo, T., Gil, M., Gómez, X., González-Andrés, F., Morán, A., 2008a. Characterization of different compost extracts using Fourier-transform infrared spectroscopy (FTIR) and thermal analysis. Biodegradation 19, 815–830.

Carballo, T., Gil, M.V., Gomez, X., Gonzalez-Andres, F., Moran, A., 2008b. Characterization of different compost extracts using Fourier-transform infrared spectroscopy (FTIR) and thermal analysis. Biodegradation 19, 815–830.

Carr, G.L., 2001. Resolution limits for infrared microspectroscopy explored with synchrotron radiation. Rev. Sci. Instrum. 72, 1613–1619.

Carrero, J.A., Goienaga, N., Olivares, M., Martinez-Arkarazo, I., Arana, G., Madariaga, J.M., 2012. Raman spectroscopy assisted with XRF and chemical simulation to assess the synergic impacts of guardrails and traffic pollutants on urban soils. J. Raman Spectrosc. 43, 1498–1503.
Case, S.D.C., McNamara, N.P., Reay, D.S., Whitaker, J., 2012. The effect of biochar addition on N_2O and CO_2 emissions from a sandy loam soil—the role of soil aeration. Soil Biol. Biochem. 51, 125–134.
Cécillon, L., Certini, G., Lange, H., Forte, C., Strand, L.T., 2012. Spectral fingerprinting of soil organic matter composition. Organic Geochemistry 46, 127–136.
Celis, R., Hermosin, M.C., Cox, L., Cornejo, J., 1999. Sorption of 2,4-dichlorophenoxyacetic acid by model particles simulating naturally occurring soil colloids. Environ. Sci. Technol. 33, 1200–1206.
Ceriotti, G., Amarasiriwardena, D., 2009. A study of antimony complexed to soil-derived humic acids and inorganic antimony species along a Massachusetts highway. Microchem. J. 91, 85–93.
Cervini-Silva, J., Fowle, D.A., Banfield, J., 2005. Biogenic dissolution of a soil cerium-phosphate mineral. Am. J. Sci. 305, 711–726.
Cesco, S., Nikolic, M., Römheld, V., Varanini, Z., Pinton, R., 2002. Uptake of ^{59}Fe from soluble ^{59}Fe-humate complexes by cucumber and barley plants. Plant Soil 241, 121–128.
Chabot, M., Hoang, T., Al-Abadleh, H.A., 2009. ATR-FTIR studies on the nature of surface complexes and desorption efficiency of p-arsanilic acid on iron (oxyhydr)oxides. Environ. Sci. Technol. 43, 3142–3147.
Chadwick, O.A., Chorover, J., 2001. The chemistry of pedogenic thresholds. Geoderma 100, 321–353.
Chalmers, J.M., Griffiths, P.R., 2002. Handbook of Vibrational Spectroscopy. J. Wiley.
Chang, P.-H., Li, Z., Jiang, W.-T., Jean, J.-S., 2009a. Adsorption and intercalation of tetracycline by swelling clay minerals. Appl. Clay Sci. 46, 27–36.
Chang, P.-H., Li, Z., Yu, T.-L., Munkhbayer, S., Kuo, T.-H., Hung, Y.-C., et al., 2009b. Sorptive removal of tetracycline from water by palygorskite. J. Hazard. Mater. 165, 148–155.
Chang, P.-H., Li, Z., Jean, J.-S., Jiang, W.-T., Wang, C.-J., Lin, K.-H., 2012. Adsorption of tetracycline on 2:1 layered non-swelling clay mineral illite. Applied Clay Science 67–68, 158–163.
Chefetz, B., Hader, Y., Chen, Y., 1998. Dissolved organic carbon fractions formed during composting of municipal solid waste: properties and significance. Acta Hydrochim. Hydrobiol. 26, 172–179.
Chen, H., He, X., Rong, X., Chen, W., Cai, P., Liang, W., et al., 2009. Adsorption and biodegradation of carbaryl on montmorillonite, kaolinite and goethite. Applied Clay Science 46, 102–108.
Chen, W.-R., Ding, Y., Johnston, C.T., Teppen, B.J., Boyd, S.A., Li, H., 2010. Reaction of lincosamide antibiotics with manganese oxide in aqueous solution. Environ. Sci. Technol. 44, 4486–4492.
Chen, Y.N., 2003. Nuclear magnetic resonance, infra-red and pyrolysis: application of spectroscopic methodologies to maturity determination of composts. Compost Sci. Util. 11, 152–168.
Chernyshova, I.V., Hochella Jr., M.F., Madden, A.S., 2007. Size-dependent structural transformations of hematite nanoparticles. 1. Phase transition. Phys. Chem. Chem. Phys. 9, 1736–1750.
Cheshire, M.V., Dumat, C., Fraser, A.R., Hillier, S., Staunton, S., 2000. The interaction between soil organic matter and soil clay minerals by selective removal and controlled addition of organic matter. Eur. J. Soil Sci. 51, 497–509.
Cheung, H.Y., Sun, S.Q., Sreedhar, B., Ching, W.M., Tanner, P.A., 2000. Alterations in extracellular substances during the biofilm development of *Pseudomonas aeruginosa* on aluminium plates. J. Appl. Microbiol. 89, 100–106.

Chia, C.H., Gong, B., Joseph, S.D., Marjo, C.E., Munroe, P., Rich, A.M., 2012. Imaging of mineral-enriched biochar by FTIR, Raman and SEM–EDX. Vib. Spectrosc. 62, 248–257.
Chittur, K.K., 1998a. FTIR/ATR for protein adsorption to biomaterial surfaces. Biomaterials 19, 357–369.
Chittur, K.K., 1998b. Surface techniques to examine the biomaterial-host interface: an introduction to the papers. Biomaterials 19, 301–305.
Choi, S., Crosson, G., Mueller, K.T., Seraphin, S., Chorover, J., 2005. Clay mineral weathering and contaminant dynamics in a caustic aqueous system - II. Mineral transformation and microscale partitioning. Geochim. Cosmochim. Acta 69, 4437–4451.
Chorover, J., Amistadi, M.K., 2001. Reaction of forest floor organic matter at goethite, birnessite and smectite surfaces. Geochim. Cosmochim. Acta 65, 95–109.
Chorover, J., Amistadi, M.K., Chadwick, O.A., 2004. Surface charge evolution of mineral-organic complexes during pedogenesis in Hawaiian basalt. Geochim. Cosmochim. Acta 68, 4859–4876.
Chu, H.A., Hillier, W., Debus, R.J., 2004. Evidence that the C-terminus of the D1 polypeptide of photosystem II is ligated to the manganese ion that undergoes oxidation during the S-1 to S-2 transition: an isotope-edited FTIR study. Biochemistry 43, 3152–3166.
Čičel, B., Komadel, P., 1997. Structural formulae of layer silicates. In: Amonette, J.E., Zelazny, L.W. (Eds.), Quantitative Methods in Soil Mineralogy. SSSA, Madison, WI, pp. 114–136.
Clarke, C.E., Aguilar-Carrillo, J., Roychoudhury, A.N., 2011. Quantification of drying induced acidity at the mineral-water interface using ATR-FTIR spectroscopy. Geochim. Cosmochim. Acta 75, 4846–4856.
Coblentz, W.W., 1911. Radiometric investigation of water of crystallisation, light filters and standard absorption bands. Bull. Bur. Stand. 7, 619–668.
Coleyshaw, E.E., Griffith, W.P., Bowell, R.J., 1994. Fourier-transform Raman spectroscopy of minerals. Spectrochim. Acta Part A Mol. Spectrosc. 50, 1909–1918.
Colthup, N.B., Daly, L.H., Wiberley, S.E., 1990. Introduction to Infrared and Raman Spectroscopy. Academic Press.
Connor, P.A., McQuillan, A.J., 1999. Phosphate adsorption onto TiO2 from aqueous solutions: An in situ internal reflection infrared spectroscopic study. Langmuir 15, 2916–2921.
Cooley, J.W., Tukey, J.W., 1965. An algorithm for machine calculation of complex Fourier series. Math. Comput. 19, 297.
Corrado, G., Sanchez-Cortes, S., Francioso, O., Garcia-Ramos, J.V., 2008. Surface-enhanced Raman and fluorescence joint analysis of soil humic acids. Anal. Chim. Acta 616, 69–77.
Cowen, S., Duggal, M., Hoang, T., Al-Abadleh, H.A., 2008. Vibrational spectroscopic characterization of some environmentally important organoarsenicals—a guide for understanding the nature of their surface complexes. Can. J. Chem. Rev. Can. Chim. 86, 942–950.
Cox, R.J., Peterson, H.L., Young, J., Cusik, C., Espinoza, E.O., 2000. The forensic analysis of soil organic by FTIR. Forensic Sci. Int. 108, 107–116.
Cozzolino, D., Morón, A., 2006. Potential of near-infrared reflectance spectroscopy and chemometrics to predict soil organic carbon fractions. Soil Tillage Res. 85, 78–85.
Crowley, D.E., Wang, Y.C., Reid, C.P.P., Szaniszlo, P.J., 1991. Mechanisms of iron acquisition from siderophores by microorganisms and plants. Plant Soil 130, 179–198.
Cuadros, J., Dudek, T., 2006. FTIR investigation of the evolution of the octahedral sheet of kaolinite-smectite with progressive kaolinization. Clays Clay Miner. 54, 1–11.
D'Acqui, L.P., Churchman, G.J., Janik, L.J., Ristori, G.G., Weissmann, D.A., 1999. Effect of organic matter removal by low-temperature ashing on dispersion of undisturbed aggregates from a tropical crusting soil. Geoderma 93, 311–324.
Dahlgren, R.A., 1994. Quantification of allophane and imogolite. In: Amonette, J.E., Zelazny, L.W. (Eds.), Quantitative Methods in Soil Mineralogy. SSSA, Madison, WI, pp. 430–451.

Dahm, D.J., Dahm, K.D., 2001. The Physics of Near Infrared Scattering. American Association of Cereal Chemists, St. Paul, Minnesota.
Das, R.S., Agrawal, Y.K., 2011. Raman spectroscopy: recent advancements, techniques and applications. Vib. Spectrosc. 57, 163–176.
Davies, J.E.D., Jabeen, N., 2002. The adsorption of herbicides and pesticides on clay minerals and soils. Part 1. Isoproturon. Journal of Inclusion Phenomena and Macrocyclic Chemistry 43, 329–336.
Davies, J.E.D., Jabeen, N., 2003. The adsorption of herbicides and pesticides on clay minerals and soils. Part 2. Atrazine. Journal of Inclusion Phenomena and Macrocyclic Chemistry 46, 57–64.
Davinic, M., Fultz, L.M., Acosta-Martinez, V., Calderón, F.J., Cox, S.B., Dowd, S.E., Allen, V.G., Zak, J.C., Moore-Kucera, J., 2012a. Pyrosequencing and mid-infrared spectroscopy reveal distinct aggregate stratification of soil bacterial communities and organic matter composition. Soil Biol. Biochem. 46, 63–72.
Davinic, M., Fultz, L.M., Acosta-Martinez, V., Calderón, F.J., Cox, S.B., Dowd, S.E., Allen, V.G., Zak, J.C., Moore-Kucera, J., 2012b. Pyrosequencing and mid-infrared spectroscopy reveal distinct aggregate stratification of soil bacterial communities and organic matter composition. Soil Biol. Biochem. 46, 63–72.
Dawson, L.A., Hillier, S., 2010. Measurement of soil characteristics for forensic applications. Surf. Interface Anal. 42, 363–377.
de Faria, D.L.A., Venâncio Silva, S., de Oliveira, M.T., 1997. Raman microspectroscopy of some iron oxides and oxyhydroxides. J. Raman Spectrosc. 28, 873–878.
de Oliveira, M.F., Johnston, C.T., Premachandra, G.S., Teppen, B.J., Li, H., Laird, D.A., Zhu, D.Q., Boyd, S.A., 2005. Spectroscopic study of carbaryl sorption on smectite from aqueous suspension. Environ. Sci. Technol. 39, 9123–9129.
Deacon, G.B., Phillips, R.J., 1980. Relationships between the carbon-oxygen stretching frequencies of carboxylato complexes and the type of carboxylate coordination. Coord. Chem. Rev. 33, 227–250.
Demyan, M.S., Rasche, F., Schulz, E., Breulmann, M., Mueller, T., Cadisch, G., 2012. Use of specific peaks obtained by diffuse reflectance Fourier transform mid-infrared spectroscopy to study the composition of organic matter in a Haplic Chernozem. Eur. J. Soil Sci. 63, 189–199.
Deo, N., Natarajan, K.A., Somasundaran, P., 2001. Mechanisms of adhesion of *Paenibacillus polymyxa* onto hematite, corundum and quartz. Int. J. Mineral Process. 62, 27–39.
Depalma, S., Cowen, S., Hoang, T., Al-Abadleh, H.A., 2008. Adsorption thermodynamics of p-arsanilic acid on iron (oxyhydr)oxides: In-situ ATR-FTIR studies. Environ. Sci. Technol. 42, 1922–1927.
Dickensheets, D.L., Wynn-Williams, D.D., Edwards, H.G.M., Schoen, C., Crowder, C., Newton, E.M., 2000. A novel miniature confocal microscope/Raman spectrometer system for biomolecular analysis on future Mars missions after Antarctic trials. J. Raman Spectrosc. 31, 633–635.
Ding, G., Liu, X., Herbert, S., Novak, J., Amarasiriwardena, D., Xing, B., 2006. Effect of cover crop management on soil organic matter. Geoderma 130, 229–239.
Ding, G., Novak, J.M., Amarasiriwardena, D., Hunt, P.G., Xing, B., 2002. Soil organic matter characteristics as affected by tillage management. Soil Sci. Soc. Am. J. 66, 421–429.
Dobson, K.D., McQuillan, A.J., 1999. In situ infrared spectroscopic analysis of the adsorption of aliphatic carboxylic acids to TiO_2, ZrO_2, Al_2O_3, and Ta_2O_5 from aqueous solutions. Spectrochim. Acta Part A Mol. Biomol. Spectrosc. 55, 1395–1405.
Dokken, K.M., Davis, L.C., Erickson, L.E., Castro-Diaz, S., Marinkovic, N.S., 2005a. Synchrotron Fourier transform infrared microspectroscopy: a new tool to monitor the fate of organic contaminants in plants. Microchem. J. 81, 86–91.
Dokken, K.M., Davis, L.C., Marinkovic, N.S., 2005b. Using SR-IMS to study the fate and transport of organic contaminants in plants. Spectroscopy 20, 14–18.

Dollish, F.R., Fateley, W.G., Bentley, F.F., 1974. Characteristic Raman frequencies of organic compounds. Wiley.
Dowding, C.E., Borda, M.J., Fey, M.V., Sparks, D.L., 2005. A new method for gaining insight into the chemistry of drying mineral surfaces using ATR-FTIR. J. Colloid Interface Sci. 292, 148–151.
Dresselhaus, M.S., Dresselhaus, G., Saito, R., Jorio, A., 2005. Raman spectroscopy of carbon nanotubes. Phys. Rep. Rev. Sect. Phys. Lett. 409, 47–99.
Du, C., He, Z., Zhou, J., 2013a. Characterization of soil humic substances using mid-infrared photoacoustic spectroscopy. In: Xu, J., Wu, J., He, Y. (Eds.), Functions of Natural Organic Matter in Changing Environment. Springer, Netherlands, pp. 43–47.
Du, C., Ma, Z., Zhou, J., Goyne, K.W., 2013b. Application of mid-infrared photoacoustic spectroscopy in monitoring carbonate content in soils. Sens. Actuators B Chem. 188, 1167–1175.
Duckworth, O.W., Martin, S.T., 2001. Surface complexation and dissolution of hematite by C-1-C-6 dicarboxylic acids at pH = 5.0. Geochim. Cosmochim. Acta 65, 4289–4301.
Dumas, P., Miller, L., 2003. Biological and biomedical applications of synchrotron infrared microspectroscopy. J. Biol. Phys. 29, 201–218.
Dumas, P., Sockalingum, G.D., Sulé-Suso, J., 2007. Adding synchrotron radiation to infrared microspectroscopy: what's new in biomedical applications? Trends Biotechnol. 25, 40–44.
Dünnwald, J., Otto, A., 1989. An investigation of phase transitions in rust layers using Raman spectroscopy. Corros. Sci. 29, 1167–1176.
Durand, J.-C., Jacquot, B., Salehi, H., Margerit, J., Cuisinier, F.G., 2012. Confocal Raman microscopy and SEM/EDS investigations of the interface between the zirconia core and veneering ceramic: the influence of a liner and regeneration firing. J. Mater. Sci. Mater. Med. 23, 1343–1353.
Eboigbodin, K.E., Biggs, C.A., 2008. Characterization of the extracellular polymeric substances produced by *Escherichia coli* using infrared spectroscopic, proteomic, and aggregation studies. Biomacromolecules 9, 686–695.
Edwards, H., Munshi, T., Scowen, I., Surtees, A., Swindles, G.T., 2012. Development of oxidative sample preparation for the analysis of forensic soil samples with near-IR Raman spectroscopy. J. Raman Spectrosc. 43, 323–325.
Efrima, S., Bronk, B.V., 1998. Silver colloids impregnating or coating bacteria. J. Phys. Chem. B 102, 5947–5950.
Egli, M., Mavris, C., Mirabella, A., Giaccai, D., 2010. Soil organic matter formation along a chronosequence in the Morteratsch proglacial area (Upper Engadine, Switzerland). CATENA 82, 61–69.
Elderfield, H., Hem, J.D., 1973. The development of crystalline structure in aluminum hydroxide polymorphs. Mineral. Mag. 39, 89–96.
Elkins, K.M., Nelson, D.J., 2002. Spectroscopic approaches to the study of the interaction of aluminum with humic substances. Coord. Chem. Rev. 228, 205–225.
Ellerbrock, R., Höhn, A., Gerke, H., 1999. Characterization of soil organic matter from a sandy soil in relation to management practice using FT-IR spectroscopy. Plant and Soil 213, 55–61.
Ellerbrock, R.H., Gerke, H.H., 2004. Characterizing organic matter of soil aggregate coatings and biopores by Fourier transform infrared spectroscopy. Eur. J. Soil Sci. 55, 219–228.
Ellerbrock, R.H., Gerke, H.H., Bachmann, J., Goebel, M.-O., 2005. Composition of organic matter fractions for explaining wettability of three forest soils. Soil Sci. Soc. Am. J. 69, 57–66.
Ellerbrock, R.H., Gerke, H.H., Boehm, C., 2009. In situ DRIFT characterization of organic matter composition on soil structural surfaces. Soil Sci. Soc. Am. J. 73, 531–540.
Ellery, A., Wynn-Williams, D., Parnell, J., Edwards, H.G.M., Dickensheets, D., 2004. The role of Raman spectroscopy as an astrobiological tool in the exploration of Mars. J. Raman Spectrosc. 35, 441–457.

Elzinga, E.J., Huang, J.-H., Chorover, J., Kretzschmar, R., 2012. ATR-FTIR spectroscopy study of the influence of pH and contact time on the adhesion of *Shewanella putrefaciens* bacterial cells to the surface of hematite. Environ. Sci. Technol. 46, 12848–12855.

Elzinga, E.J., Kretzschmar, R., 2013. In situ ATR-FTIR spectroscopic analysis of the co-adsorption of orthophosphate and Cd(II) onto hematite. Geochim. Cosmochim. Acta 117, 53–64.

Elzinga, E.J., Sparks, D.L., 2007. Phosphate adsorption onto hematite: an in situ ATR-FTIR investigation of the effects of pH and loading level on the mode of phosphate surface complexation. J. Colloid Interface Sci. 308, 53–70.

Epperson, P.M., Sweedler, J.V., Bilhorn, R.B., Sims, G.R., Denton, M.B., 1988. Applications of charge transfer devices in spectroscopy. Anal. Chem. 60, 327A–335A.

Ertlen, D., Schwartz, D., Trautmann, M., Webster, R., Brunet, D., 2010. Discriminating between organic matter in soil from grass and forest by near-infrared spectroscopy. Eur. J. Soil Sci. 61, 207–216.

Etchegoin, P.G., Le Ru, E.C., 2010. Basic electromagnetic theory of SERS. In: Surface Enhanced Raman Spectroscopy. Wiley-VCH Verlag GmbH & Co. KGaA, pp. 1–37.

Eusterhues, K., Rumpel, C., Kleber, M., Kögel-Knabner, I., 2003. Stabilisation of soil organic matter by interactions with minerals as revealed by mineral dissolution and oxidative degradation. Org. Geochem. 34, 1591–1600.

Eusterhues, K., Rumpel, C., Kögel-Knabner, I., 2005. Stabilization of soil organic matter isolated via oxidative degradation. Org. Geochem. 36, 1567–1575.

Ewald, M., Belin, C., Berger, P., Weber, J.H., 1983. Corrected fluorescence spectra of fulvic acids isolated from soil and water. Environ. Sci. Technol. 17, 501–504.

Falk, M., Hartman, K.A., Lord, R.C., 1963. Hydration of deoxyribonucleic acid. 3. A spectroscopic study of effect of hydration on structure of deoxyribonucleic acid. J. Am. Chem. Soc. 85, 391–394.

Farmer, V.C., 1958. The infra-red spectra of talc, saponite, and hectorite. Mineral. Mag. 31, 829–845.

Farmer, V.C., 1974a. The anhydrous oxide minerals. Vol. Mineral. Soc. Monograph 4. In: Farmer, V.C. (Ed.), The Infrared Spectra of Minerals. Mineral. Soc., London, UK, pp. 183–204.

Farmer, V.C., 1974b. The Infrared Spectra of Minerals. Mineralogical Society, London.

Farmer, V.C., 1974c. The layer silicates. Vol. Mineral. Soc. Monograph 4. In: Farmer, V.C. (Ed.), The Infrared Spectra of Minerals. Mineral. Soc., London, UK, pp. 331–363.

Farmer, V.C., 2000. Transverse and longitudinal crystal modes associated with OH stretching vibrations in single crystals of kaolinite and dickite. Spectrochim. Acta Part A 56, 927–930.

Farmer, V.C., Fraser, A.R., Russell, J.D., Yoshinaga, N., 1977. Recognition of imogolite structures in allophanic clays by infrared spectroscopy. Clay Miner. 12, 55–57.

Favilli, F., Egli, M., Cherubini, P., Sartori, G., Haeberli, W., Delbos, E., 2008. Comparison of different methods of obtaining a resilient organic matter fraction in Alpine soils. Geoderma 145, 355–369.

Fernández-Getino, A.P., Hernández, Z., Piedra Buena, A., Almendros, G., 2010. Assessment of the effects of environmental factors on humification processes by derivative infrared spectroscopy and discriminant analysis. Geoderma 158, 225–232.

Ferrari, A.C., Meyer, J.C., Scardaci, V., Casiraghi, C., Lazzeri, M., Mauri, F., Piscanec, S., Jiang, D., Novoselov, K.S., Roth, S., Geim, A.K., 2006. Raman spectrum of graphene and graphene layers. Phys. Rev. Lett. 97.

Ferrari, A.C., Robertson, J., 2000. Interpretation of Raman spectra of disordered and amorphous carbon. Phys. Rev. B 61, 14095–14107.

Ferrari, E., Francioso, O., Nardi, S., Saladini, M., Ferro, N.D., Morari, F., 2011. DRIFT and HR MAS NMR characterization of humic substances from a soil treated with different organic and mineral fertilizers. J. Mol. Struct. 998, 216–224.

Ferraro, J.R., 1967. Advances in Raman instrumentation and sampling techniques. In: Szymanski, H. (Ed.), Raman Spectroscopy. Springer, US, pp. 44–81.
Ferraro, J.R., 2003. Introductory Raman Spectroscopy, second ed. Academic Press, Amsterdam.
Ferreira, A.R., Martins, M.J.F., Konstantinova, E., Capaz, R.B., Souza, W.F., Chiaro, S.S.X., Leitão, A.A., 2011. Direct comparison between two structural models by DFT calculations. J. Solid State Chem. 184, 1105–1111.
Fialho, L.L., Lopes da Silva, W.T., Milori, D.M.B.P., Simões, M.L., Martin-Neto, L., 2010. Characterization of organic matter from composting of different residues by physicochemical and spectroscopic methods. Bioresour. Technol. 101, 1927–1934.
Filip, Z., Haider, K., Beutelspacher, H., Martin, J.P., 1974. Comparisons of IR-spectra from melanins of microscopic soil fungi, humic acids and model phenol polymers. Geoderma 11, 37–52.
Fitts, J.P., Persson, P., Brown, G.E., Parks, G.A., 1999. Structure and bonding of Cu(II)-glutamate complexes at the gamma-Al2O3-water interface. J. Colloid Interface Sci. 220, 133–147.
Fleischmann, M., Hendra, P.J., McQuillan, A.J., 1974. Raman spectra of pyridine adsorbed at a silver electrode. Chem. Phys. Lett. 26, 163–166.
Follett, R.F., Paul, E.A., Pruessner, E.G., 2007. Soil carbon dynamics during a long-term incubation study involving C-13 and C-14 measurements. Soil Sci. 172, 189–208.
Foriel, J., Philippot, P., Susini, J., Dumas, P., Somogyi, A., Salomé, M., Khodja, H., Ménez, B., Fouquet, Y., Moreira, D., López-García, P., 2004. High-resolution imaging of sulfur oxidation states, trace elements, and organic molecules distribution in individual microfossils and contemporary microbial filaments. Geochim. Cosmochim. Acta 68, 1561–1569.
Forrester, S.T., Janik, L.J., McLaughlin, M.J., Soriano-Disla, J.M., Stewart, R., Dearman, B., 2013. Total Petroleum Hydrocarbon Concentration Prediction in Soils Using Diffuse Reflectance Infrared Spectroscopy. Soil Sci. Soc. Am. J 77, 450–460.
Foucher, F., Lopez-Reyes, G., Bost, N., Rull-Perez, F., Rüßmann, P., Westall, F., 2013. Effect of grain size distribution on Raman analyses and the consequences for in situ planetary missions. J. Raman Spectrosc. 44, 916–925.
Francioso, O., Ciavatta, C., Sànchez-Cortés, S., Tugnoli, V., Sitti, L., Gessa, C., 2000. Spectroscopic characterization of soil organic matter in long-term amendment trials. Soil Sci. 165, 495–504.
Francioso, O., Sànchez-Cortés, S., Tugnoli, V., Marzadori, C., Ciavatta, C., 2001. Spectroscopic study (DRIFT, SERS and 1H NMR) of peat, leonardite and lignite humic substances. J. Mol. Struct. 565–566, 481–485.
Francioso, O.S.-C., S., Tugnoli, V., Ciavatta, C., Sitti, L., Gessa, C., 1996. Infrared, Raman, and nuclear magnetic resonance (^{1}H, ^{13}C, and ^{31}P) spectroscopy in the study of fractions of peat humic acids. Appl. Spectrosc. 50, 1165–1174.
Fries, M., Steele, A., 2011. Raman Spectroscopy and Confocal Raman Imaging in Mineralogy and Petrography. In: Dieing, T., Hollricher, O., Toporski, J. (Eds.), Confocal Raman Microscopy, vol. 158. Springer Berlin Heidelberg, pp. 111–135.
Fringeli, U.P., Günthard, H.H., 1981. Infrared membrane spectroscopy. In: Grell, E. (Ed.), Membrane Spectroscopy. Springer-Verlag, Berlin, pp. 270–332.
Frost, R.L., Bahfenne, S., Čejka, J., Sejkora, J., Plášil, J., Palmer, S.J., 2010a. Raman and infrared study of phyllosilicates containing heavy metals (Sb, Bi): bismutoferrite and chapmanite. J. Raman Spectrosc. 41, 814–819.
Frost, R.L., Bahfenne, S., Čejka, J., Sejkora, J., Plášil, J., Palmer, S.J., 2010b. Raman spectroscopic study of the hydrogen-arsenate mineral pharmacolite Ca(AsO3OH)·2H2O—implications for aquifer and sediment remediation. J. Raman Spectrosc. 41, 1348–1352.
Frost, R.L., Palmer, S.J., 2011. Raman spectroscopic study of the minerals diadochite and destinezite $Fe^{3+}_2(PO_4,SO_4)_2(OH)\cdot 6H_2O$: implications for soil science. J. Raman Spectrosc. 42, 1589–1595.

Frost, R.L., Thu Ha, T., Kristof, J., 1997. FT-Raman spectroscopy of the lattice region of kaolinite and its intercalates. Vib. Spectrosc. 13, 175–186.
Fuentes, M., Baigorri, R., Gonzalez-Gaitano, G., Garcia-Mina, J.M., 2007. The complementary use of H-1 NMR, C-13 NMR, FTIR and size exclusion chromatography to investigate the principal structural changes associated with composting of organic materials with diverse origin. Org. Geochem. 38, 2012–2023.
Fuertes, A.B., Arbestain, M.C., Sevilla, M., Macia-Agullo, J.A., Fiol, S., Lopez, R., Smernik, R.J., Aitkenhead, W.P., Arce, F., Macias, F., 2010. Chemical and structural properties of carbonaceous products obtained by pyrolysis and hydrothermal carbonisation of corn stover. Aust. J. Soil. Res. 48, 618–626.
Fultz, L.M., 2012. Dynamics of Soil Aggregation, Organic Carbon Pools, and Greenhouse Gases in Integrated Crop-Livestock Agroecosystems in the Texas High Plains. Tech University, Texas.
Gao, X., Chorover, J., 2009. In-situ monitoring of cryptosporidium parvum oocyst surface adhesion using ATR-FTIR spectroscopy. Colloids Surf. B Biointerfaces 71, 169–176.
Gao, X., Chorover, J., 2011. Amphiphile disruption of pathogen attachment at the hematite (α-Fe_2O_3)−Water interface. Langmuir 27, 5936–5943.
Gao, X., Metge, D.W., Ray, C., Harvey, R.W., Chorover, J., 2009. Surface complexation of carboxylate adheres cryptosporidium parvum oocysts to the hematite-water interface. Environ. Sci. Technol. 43, 7423–7429.
Garidel, P., Boese, M., 2007. Non-invasive Fourier transform infrared microspectroscopy and imaging techniques. In: Méndez-Vilas, A., Diaz, J. (Eds.), Basic Principles and Application, in Modern Research and Educational Topics in Microscopy.
Ghosh, U., Gillette, J.S., Luthy, R.G., Zare, R.N., 2000. Microscale location, characterization, and association of polycyclic aromatic hydrocarbons on harbor sediment particles. Environ. Sci. Technol. 34, 1729–1736.
Giacometti, C., Demyan, M.S., Cavani, L., Marzadori, C., Ciavatta, C., Kandeler, E., 2013. Chemical and microbiological soil quality indicators and their potential to differentiate fertilization regimes in temperate agroecosystems. Appl. Soil Ecol. 64, 32–48.
Glaser, B., 2007. Prehistorically modified soils of central Amazonia: a model for sustainable agriculture in the twenty-first century. Philos. Trans. Roy. Soc. B: Biol. Sci. 362, 187–196.
Glaser, B., Lehmann, J., Zech, W., 2002. Ameliorating physical and chemical properties of highly weathered soils in the tropics with charcoal—a review. Biol. Fertil. Soils 35, 219–230.
Glaser, B., Woods, W.I., 2004. Amazon Dark Earths: Explorations in Space and Time. Springer, Berlin.
Glotch, T.D., Rossman, G.R., 2009. Mid-infrared reflectance spectra and optical constants of six iron oxide/oxyhydroxide phases. Icarus 204, 663–671.
Goienaga, N., Arrieta, N., Carrero, J.A., Olivares, M., Sarmiento, A., Martinez-Arkarazo, I., Fernández, L.A., Madariaga, J.M., 2011. Micro-Raman spectroscopic identification of natural mineral phases and their weathering products inside an abandoned zinc/lead mine. Spectrochim. Acta Part A Mol. Biomol. Spectrosc. 80, 66–74.
Goldberg, S., Johnston, C.T., 2001. Mechanisms of arsenic adsorption on amorphous oxides evaluated using macroscopic measurements, vibrational spectroscopy, and surface complexation modeling. J. Colloid Interface Sci. 234, 204–216.
Gondar, D., Lopez, R., Fiol, S., Antelo, J.M., Arce, F., 2005. Characterization and acid–base properties of fulvic and humic acids isolated from two horizons of an ombrotrophic peat bog. Geoderma 126, 367–374.
Gong, W., 2001. A real time in situ ATR-FTIR spectroscopic study of linear phosphate adsorption on titania surfaces. Int. J. Miner. Process 63, 147–165.
González Pérez, M., Martin-Neto, L., Saab, S.C., Novotny, E.H., Milori, D.M.B.P., Bagnato, V.S., Colnago, L.A., Melo, W.J., Knicker, H., 2004. Characterization of humic acids from a Brazilian Oxisol under different tillage systems by EPR, ^{13}C NMR, FTIR and fluorescence spectroscopy. Geoderma 118, 181–190.

Gore, R.C., 1949. Infrared spectrometry of small samples with the reflecting microscope. Science 110, 710–711.
Goyne, K.W., Brantley, S.L., Chorover, J., 2006. Effects of organic acids and dissolved oxygen on apatite and chalcopyrite dissolution: Implications for using elements as organomarkers and oxymarkers. Chem. Geol. 234, 28–45.
Goyne, K.W., Brantley, S.L., Chorover, J., 2010. Rare earth element release from phosphate minerals in the presence of organic acids. Chem. Geol. 278, 1–14.
Goyne, K.W., Chorover, J., Kubicki, J.D., Zimmerman, A.R., Brantley, S.L., 2005. Sorption of the antibiotic ofloxacin to mesoporous and nonporous alumina and silica. J. Colloid Interface Sci. 283, 160–170.
Goyne, K.W., Chorover, J., Zimmerman, A.R., Komarneni, S., Brantley, S.L., 2004. Influence of mesoporosity on the sorption of 2,4-dichlorophenoxyacetic acid onto alumina and silica. J. Colloid Interface Sci. 272, 10–20.
Gray, A.B., Pasternack, G.B., Watson, E.B., 2010. Hydrogen peroxide treatment effects on the particle size distribution of alluvial and marsh sediments. The Holocene 20, 293–301.
Gregoriou, V.G., Rodman, S.E., 2002. Quantitative depth profile analysis of micrometer-thick multilayered thin coatings using step-scan FT-IR photoacoustic spectroscopy. Anal. Chem. 74, 2361–2369.
Griffiths, P.R., de Haseth, J.A., 1986. Fourier Transform Infrared Spectrometry. John Wiley and Sons, NY.
Griffiths, P.R., de Haseth, J.A., 2006. Sampling the interferogram. In: Fourier Transform Infrared Spectrometry. John Wiley & Sons, Inc, pp. 57–74.
Gu, B.H., Schmitt, J., Chen, Z., Liang, L.Y., Mccarthy, J.F., 1995. Adsorption and desorption of different organic-matter fractions on iron-oxide. Geochim. Cosmochim. Acta 59, 219–229.
Gu, C., Karthikeyan, K.G., 2005a. Interaction of tetracycline with aluminum and iron hydrous oxides. Environ. Sci. Technol. 39, 2660–2667.
Gu, C., Karthikeyan, K.G., 2005b. Sorption of the antimicrobial ciprofloxacin to aluminum and iron hydrous oxides. Environ. Sci. Technol. 39, 9166–9173.
Guan, X.H., Liu, Q., Chen, G.H., Shang, C., 2005. Surface complexation of condensed phosphate to aluminum hydroxide: An ATR-FTIR spectroscopic investigation. J. Colloid Interface Sci. 289, 319–327.
Gun'ko, V.M., Zarko, V.I., Turov, V.V., Leboda, R., Chibowski, E., Gun'ko, V.V., 1998. Aqueous suspensions of highly disperse silica and germania/silica. J. Colloid Interface Sci. 205, 106–120.
Gulley-Stahl, H., Hogan, P.A., Schmidt, W.L., Wall, S.J., Buhrlage, A., Bullen, H.A., 2010. Surface Complexation of Catechol to Metal Oxides: An ATR-FTIR, Adsorption, and Dissolution Study. Environ. Sci. Technol. 44, 4116–4121.
Ha, J., Hyun Yoon, T., Wang, Y., Musgrave, C.B., Brown, J.G.E., 2008. Adsorption of organic matter at mineral/water interfaces: 7. ATR-FTIR and quantum chemical study of lactate interactions with hematite nanoparticles. Langmuir 24, 6683–6692.
Haberhauer, 1998. Comparison of the composition of forest soil litter derived from three different sites at various decompositional stages using FTIR spectroscopy. Geoderma 83, 331–342.
Haberhauer, G., Gerzabek, M.H., 1999. Drift and transmission FT-IR spectroscopy of forest soils: an approach to determine decomposition processes of forest litter. Vib. Spectrosc. 19, 413–417.
Haile-Mariam, S., Collins, H.P., Wright, S., Paul, E.A., 2008. Fractionation and long-term laboratory incubation to measure soil organic matter dynamics. Soil Sci. Soc. Am. J. 72, 370–378.
Haley, L.V., Wylie, I.W., Koningstein, J.A., 1982. An investigation of the lattice and interlayer water vibrational spectral regions of muscovite and vermiculite using Raman microscopy. A Raman microscopic study of layer silicates. J. Raman Spectrosc. 13, 203–205.

Han, G., Jiang, T., Li, G., Huang, Y., Zhang, Y., 2011. Investigation on modified humic substances based Binders for iron ore agglomeration. J. Eng. Mater. Technol. 134, 010901.
Harsh, J., Chorover, J., Nizeyimana, E., 2002. Allophane and imogolite. In: Dixon, J.B., Schulze, D.G. (Eds.), Soil Mineralogy with Environmental Applications. SSSA, Madison, WI, pp. 291–322. Vol. SSSA Book Ser. 7.
Hart, T.R., Adams, S.B., Tempkin, H., 1976. Flammarion Sciences, Paris.
Hay, M.B., Myneni, S.C.B., 2007. Structural environments of carboxyl groups in natural organic molecules from terrestrial systems. Part 1: Infrared spectroscopy. Geochim. Cosmochim. Acta 71, 3518–3532.
Hayes, M.H.B., Malcolm, R.L., 2001. Considerations of compositions and of aspects of the structures of humic substances. Humic Subst. Chem. Contam. Access Publ. 3–39.
Hazen, R.M., Sverjensky, D.A., 2010. Mineral surfaces, geochemical complexities, and the origins of life. Cold Spring Harb. Perspect. Biol. 2.
He, X., Xi, B., Wei, Z., Guo, X., Li, M., An, D., Liu, H., 2011a. Spectroscopic characterization of water extractable organic matter during composting of municipal solid waste. Chemosphere 82, 541–548.
He, Z., Honeycutt, C.W., Zhang, H., 2011b. Elemental and Fourier transform-infrared spectroscopic analysis of water- and pyrophosphate-extracted soil organic matter. Soil Sci. 176, 183–189. http://dx.doi.org/10.1097/SS.0b013e318212865c.
He, Z., Honeycutt, C.W., Olanya, O.M., Larkin, R.P., Halloran, J.M., Frantz, J.M., 2012. Comparison of soil phosphorus status and organic matter composition in potato fields with different crop rotation systems. In: He, Z., Larkin, R., Honeycutt, W. (Eds.), Sustainable Potato Production: Global Case Studies. Springer, Netherlands, pp. 61–79.
He, Z., Ohno, T., Cade-Menun, B.J., Erich, M.S., Honeycutt, C.W., 2006. Spectral and chemical characterization of phosphates associated with humic substances trade or manufacturers' names mentioned in the paper are for information only and do not constitute endorsement, recommendation, or exclusion by the USDA-ARS. Soil Sci. Soc. Am. J. 70, 1741–1751.
Heymann, K., Lehmann, J., Solomon, D., Schmidt, M.W.I., Regier, T., 2011. C 1s K-edge near edge X-ray absorption fine structure (NEXAFS) spectroscopy for characterizing functional group chemistry of black carbon. Org. Geochem. 42, 1055–1064.
Hibben, J.H., 1939. The Raman Effect and Its Chemical Applications. Reinhold Publishing Corp., New York, NY.
Hind, A.R., Bhargava, S.K., McKinnon, A., 2001. At the solid/liquid interface: FTIR/ATR - the tool of choice. Adv. Colloid Interface Sci. 93, 91–114.
Hirschfeld, T., Chase, B., 1986. FT-Raman spectroscopy: development and justification. Appl. Spectrosc. 40, 133–137.
Hirschmugl, C.J., 2002. Frontiers in infrared spectroscopy at surfaces and interfaces. Surf. Sci. 500, 577–604.
Holman, H.-Y.N., 2010. Chapter 4-Synchrotron infrared spectromicroscopy for studying chemistry of microbial activity in geologic materials. In: Balwant, S., Markus, G. (Eds.), Developments in Soil Science, vol. 34. Elsevier, pp. 103–130.
Holman, H.-Y.N., Bechtel, H.A., Hao, Z., Martin, M.C., 2010. Synchrotron IR spectromicroscopy: chemistry of living cells. Anal. Chem. 82, 8757–8765.
Holman, H.-Y.N., Miles, R., Hao, Z., Wozei, E., Anderson, L.M., Yang, H., 2009. Real-time chemical imaging of bacterial activity in biofilms using open-channel microfluidics and synchrotron FTIR spectromicroscopy. Anal. Chem. 81, 8564–8570.
Holman, H.-Y.N., Nieman, K., Sorensen, D.L., Miller, C.D., Martin, M.C., Borch, T., McKinney, W.R., Sims, R.C., 2002. Catalysis of PAH biodegradation by humic acid shown in synchrotron infrared studies. Environ. Sci. Technol. 36, 1276–1280.
Holman, H.N., Perry, D.L., Martin, M.C., Lamble, G.M., McKinney, W.R., Hunter-Cevera, J.C., 1999. Real-time characterization of biogeochemical reduction of Cr(VI) on Basalt surfaces by SR-FTIR imaging. Geomicrobiol. J. 16, 307–324.

Holman, H.Y.N., Martin, M.C., 2006. Synchrotron radiation infrared spectromicroscopy: a noninvasive chemical probe for monitoring biogeochemical processes. In: Donald, L.S. (Ed.), Advances in Agronomy, vol. 90. Academic Press, pp. 79–127.
Horwath, W.R., 2007. Carbon cycling and formation of soil organic matter. In: Paul, E.A. (Ed.), Soil Microbiology, Ecology, and Biochemistry. Academic Press, San Diego, CA.
Howe, K.J., Ishida, K.P., Clark, M.M., 2002. Use of ATR/FTIR spectrometry to study fouling of microfiltration membranes by natural waters. Desalination 147, 251–255.
Hsu, J.-H., Lo, S.-L., 1999. Chemical and spectroscopic analysis of organic matter transformations during composting of pig manure. Environ. Pollut. 104, 189–196.
Huang, P.M., Wang, M.K., Kämpf, N., Schultze, D.G., 2002. Aluminum hydroxides. Vol. SSSA Book Ser. 7. In: Dixon, J.B., Schulz, L.A. (Eds.), Soil Mineralogy with Environmental Applications. SSSA, Madison, WI, pp. 261–289.
Huang, Q.J., Li, X.Q., Yao, J.L., Ren, B., Cai, W.B., Gao, J.S., Mao, B.W., Tian, Z.Q., 1999. Extending surface Raman spectroscopic studies to transition metals for practical applications: III. Effects of surface roughening procedure on surface-enhanced Raman spectroscopy from nickel and platinum electrodes. Surf. Sci. 427–428, 162–166.
Huang, W.E., Griffiths, R.I., Thompson, I.P., Bailey, M.J., Whiteley, A.S., 2004. Raman microscopic analysis of single microbial cells. Anal. Chem. 76, 4452–4458.
Huang, W.E., Li, M., Jarvis, R.M., Goodacre, R., Banwart, S.A., 2010. Chapter 5-Shining light on the microbial World: the application of Raman microspectroscopy. In: Allen, I.L., Sima, S., Geoffrey, M.G. (Eds.), Advances in Applied Microbiology, vol. 70. Academic Press, pp. 153–186.
Hübner, W., Blume, A., 1998. Interactions at the lipid–water interface. Chem. Phys. Lipids 96, 99–123.
Hug, S.J., 1997. In situ Fourier transform infrared measurements of sulfate adsorption on hematite in aqueous solutions. J. Colloid Interface Sci. 188, 415–422.
Hug, S.J., Bahnemann, D., 2006. Infrared spectra of oxalate, malonate and succinate adsorbed on the aqueous surface of rutile, anatase and lepidocrocite measured with in situ ATR-FTIR. J. Electron Spectrosc. Relat. Phenom. 150, 208–219.
Hug, S.J., Sulzberger, B., 1994. In-situ fourier-transform infrared spectroscopic evidence for the formation of several different surface complexes of oxalate on TiO_2 in the aqueous-phase. Langmuir 10, 3587–3597.
Hugo, R.C., Cady, S.L., 2004. Preparation of geological and biological TEM specimens by embedding in sulfur. Microsc. Today 12, 28–30.
Hwang, Y.S., Lenhart, J.J., 2008. Adsorption of C4-dicarboxylic acids at the hematite/water interface. Langmuir 24, 13934–13943.
Ikoma, T., Kobayashi, H., Tanaka, J., Walsh, D., Mann, S., 2003. Physical properties of type I collagen extracted from fish scales of *Pagrus major* and *Oreochromis niloticas*. Int. J. Biol. Macromol. 32, 199–204.
Ibarra, J., Muñoz, E., Moliner, R., 1996. FTIR study of the evolution of coal structure during the coalification process. Organic Geochemistry 24, 725–735.
Inbar, Y., Chen, Y., Hadar, Y., 1991. Carbon-13 CPMAS NMR and FTIR Spectroscopic analysis of organic-matter transformations during composting of solid-wastes from wineries. Soil Sci. 152, 272–282.
Ivnitski, D., Abdel-Hamid, I., Atanasov, P., Wilkins, E., 1999. Biosensors for detection of pathogenic bacteria. Biosens. Bioelectron. 14, 599–624.
Janik, L.J., Merry, R.H., Skjemstad, J.O., 1998. Can mid infrared diffuse reflectance analysis replace soil extractions? Australian Journal of Experimental Agriculture 38, 681–696.
Janik, L.J., Skjemstad, J.O., Shepherd, K.D., Spouncer, L.R., 2007. The prediction of soil carbon fractions using mid-infrared-partial least square analysis. Aust. J. Soil Res. 45, 73–81.
Jawhari, T., Roid, A., Casado, J., 1995. Raman spectroscopic characterization of some commercially available carbon black materials. Carbon 33, 1561–1565.

Jeanmaire, D.L., Van Duyne, R.P., 1977. Surface raman spectroelectrochemistry: Part I. Heterocyclic, aromatic, and aliphatic amines adsorbed on the anodized silver electrode. J. Electroanal. Chem. Interfacial Electrochem. 84, 1–20.

Jiang, W., Saxena, A., Song, B., Ward, B.B., Beveridge, T.J., Myneni, S.C.B., 2004. Elucidation of functional groups on gram-positive and gram-negative bacterial surfaces using infrared spectroscopy. Langmuir 20, 11433–11442.

Jiang, W., Yang, K., Vachet, R.W., Xing, B.S., 2010. Interaction between oxide nanoparticles and biomolecules of the bacterial cell envelope as examined by infrared spectroscopy. Langmuir 26, 18071–18077.

Johnson, S.B., Yoon, T.H., Kocar, B.D., Brown, G.E., 2004. Adsorption of Organic Matter at Mineral/Water Interfaces. 2. Outer-Sphere Adsorption of Maleate and Implications for Dissolution Processes. Langmuir 20, 4996–5006.

Johnston, C.P., Chrysochoou, M., 2012. Investigation of chromate coordination on ferrihydrite by in situ ATR-FTIR spectroscopy and theoretical frequency calculations. Environ. Sci. Technol. 46, 5851–5858.

Johnston, C.T., 2010. Probing the nanoscale architecture of clay minerals. Clay Miner. 45, 245–279.

Johnston, C.T., Agnew, S.F., Bish, D.L., 1990. Polarized single-crystal Fourier-transform infrared microscopy of Ouray dickite and Keokuk kaolinite. Clays Clay Miner. 38, 573–588.

Johnston, C.T., Aochi, Y.O., 1996. Fourier transform infrared and Raman spectroscopy. Vol. SSSA Book Ser. 5. In: Methods of Soil Analysis. Part 3. Chemical Methods. SSSA, Madison, WI, pp. 269–321.

Johnston, C.T., Kogel, J.E., Bish, D.L., Kogure, T., Murray, H.H., 2008. Low-temperature FTIR study of kaolin-group minerals. Clays Clay Miner. 56, 470–485.

Johnston, C.T., Sheng, G., Teppen, B.J., Boyd, S.A., De Oliveira, M.F., 2002a. Spectroscopic study of dinitrophenol herbicide sorption on smectite. Environ. Sci. Technol. 36, 5067–5074.

Johnston, C.T., Sposito, G., Earl, W.L., 1993. Characterization of environmental particles by Fourier transform infrared and nuclear magnetic resonance spectroscopy. In: Buffle, J., van Leeuwen, H.P. (Eds.), Environmental Particles, vol. 2. Lewis Publishers., Boca Raton, FL.

Johnston, C.T., Sposito, G., Erickson, C., 1992. Vibrational probe studies of water interactions with montmorillonite. Clays Clay Miner. 40, 722–730.

Johnston, C.T., Stone, D.A., 1990. Influence of hydrazine on the vibrational-modes of kaolinite. Clays Clay Miner. 38, 121–128.

Johnston, C.T., Wang, S.-L., Bish, D.L., Dera, P., Agnew, S.F., Kenney, J.W., 2002b. Novel pressure-induced phase transformations in hydrous layered materials. Geophys. Res. Lett. 29, 17-1–17-4.

Jorio, A., 2012. Raman spectroscopy in graphene-based systems: prototypes for nanoscience and nanometrology. ISRN Nanotechnol. 16.

Jorio, A., Ribeiro-Soares, J., Cançado, L.G., Falcão, N.P.S., Dos Santos, H.F., Baptista, D.L., Martins Ferreira, E.H., Archanjo, B.S., Achete, C.A., 2012. Microscopy and spectroscopy analysis of carbon nanostructures in highly fertile Amazonian anthrosoils. Soil Tillage Res. 122, 61–66.

Joseph, S.D., Camps-Arbestain, M., Lin, Y., Munroe, P., Chia, C.H., Hook, J., van Zwieten, L., Kimber, S., Cowie, A., Singh, B.P., Lehmann, J., Foidl, N., Smernik, R.J., Amonette, J.E., 2010. An investigation into the reactions of biochar in soil. Aust. J. Soil Res. 48, 501–515.

Jouraiphy, A., Amir, S., Winterton, P., El Gharous, M., Revel, J.C., Hafidi, M., 2008. Structural study of the fulvic fraction during composting of activated sludge–plant matter: elemental analysis, FTIR and ^{13}C NMR. Bioresour. Technol. 99, 1066–1072.

Joussein, E., Petit, S., Churchman, J., Theng, B., Righi, D., Delvaux, B., 2005. Halloysite clay minerals—a review. Clay Miner. 40, 383–426.

Jucker, B.A., Harms, H., Hug, S.J., Zehnder, A.J.B., 1997. Adsorption of bacterial surface polysaccharides on mineral oxides is mediated by hydrogen bonds. Colloids Surf. B Biointerfaces 9, 331–343.

Julien, C.M., Massot, M., Poinsignon, C., 2004. Lattice vibrations of manganese oxides—Part 1. Periodic structures. Spectrochim. Acta Part A Mol. Biomol. Spectrosc. 60, 689–700.

Kahraman, M., Yazici, M.M., Sahin, F., Bayrak, O.F., Culha, M., 2007. Reproducible surface-enhanced Raman scattering spectra of bacteria on aggregated silver nanoparticles. Appl. Spectrosc. 61, 479–485.

Kaiser, M., Ellerbrock, R.H., 2005. Functional characterization of soil organic matter fractions different in solubility originating from a long-term field experiment. Geoderma 127, 196–206.

Kaiser, M., Ellerbrock, R.H., Gerke, H.H., 2007. Long-term effects of crop rotation and fertilization on soil organic matter composition. Eur. J. Soil Sci. 58, 1460–1470.

Kaiser, M., Ellerbrock, R.H., Gerke, H.H., 2008. Cation exchange capacity and composition of soluble soil organic matter fractions (All rights reserved. No part of this periodical may be reproduced or transmitted in any form or by any means, electronic or mechanical, including photocopying, recording, or any information storage and retrieval system, without permission in writing from the publisher. Permission for printing and for reprinting the material contained herein has been obtained by the publisher) Soil Sci. Soc. Am. J. 72, 1278–1285.

Kamnev, A.A., Antonyuk, L.P., Matora, L.Y., Serebrennikova, O.B., Sumaroka, M.V., Colina, M., Renou-Gonnord, M.F., Ignatov, V.V., 1999. Spectroscopic characterization of cell membranes and their constituents of the plant-associated soil bacterium *Azospirillum brasilense*. J. Mol. Struct. 481, 387–393.

Kang, S., Xing, B., 2007. Adsorption of dicarboxylic acids by clay minerals as examined by in situ ATR-FTIR and ex situ DRIFT. Langmuir 23, 7024–7031.

Kang, S.H., Amarasiriwardena, D., Xing, B.S., 2008. Effect of dehydration on dicarboxylic acid coordination at goethite/water interface. Colloids Surf. A Physicochem. Eng. Aspects 318, 275–284.

Kanokkantapong, V., Marhaba, T.F., Panyapinyophol, B., Pavasant, P., 2006. FTIR evaluation of functional groups involved in the formation of haloacetic acids during the chlorination of raw water. J. Hazard. Mater. 136, 188–196.

Katon, J.E., 1996. Infrared microspectroscopy. A review of fundamentals and applications. Micron 27, 303–314.

Katrin, K., Harald, K., Irving, I., Ramachandra, R.D., Michael, S.F., 2002. Surface-enhanced Raman scattering and biophysics. J. Phys. Condens. Matter 14, R597.

Katti, K.S., Katti, D.R., 2006. Relationship of swelling and swelling pressure on silica-water interactions in montmorillonite. Langmuir 22, 532–537.

Kaufhold, S., Hein, M., Dohrmann, R., Ufer, K., 2012. Quantification of the mineralogical composition of clays using FTIR spectroscopy. Vib. Spectrosc. 59, 29–39.

Keiluweit, M., Nico, P.S., Johnson, M.G., Kleber, M., 2010. Dynamic molecular structure of plant biomass-derived black carbon (Biochar). Environ. Sci. Technol. 44, 1247–1253.

Kerek, M., Drijber, R.A., Gaussoin, R.E., 2003. Labile soil organic matter as a potential nitrogen source in golf greens. Soil Biol. Biochem. 35, 1643–1649.

Kerscchbaum, F.P., 1914. Instrumentenk 34, 43.

Khan, S.U., 1975. Soil Organic Matter. Elsevier Science.

Kim, P., Johnson, A., Edmunds, C.W., Radosevich, M., Vogt, F., Rials, T.G., Labbé, N., 2011. Surface functionality and carbon structures in lignocellulosic-derived biochars produced by fast pyrolysis. Energy & Fuels 25, 4693–4703.

Kizewski, F., Liu, Y.-T., Morris, A., Hesterberg, D., 2011. Spectroscopic Approaches for phosphorus speciation in soils and other environmental systems (All rights reserved. No part of this periodical may be reproduced or transmitted in any form or by any means,

electronic or mechanical, including photocopying, recording, or any information storage and retrieval system, without permission in writing from the publisher) J. Environ. Qual. 40, 751–766.
Kleber, M., Johnson, M.G., 2010. Advances in understanding the molecular structure of soil organic matter: implications for interactions in the environment. In: Donald, L.S. (Ed.), Advances in Agronomy, vol. 106. Academic Press, pp. 77–142.
Kodama, H., Schnitzer, M., 1971. Evidence for interlamellar adsorption of organic matter by clay in a podzol soil. Can. J. Soil. Sci. 51, 509–512.
Kögel-Knabner, I., Guggenberger, G., Kleber, M., Kandeler, E., Kalbitz, K., Scheu, S., Eusterhues, K., Leinweber, P., 2008. Organo-mineral associations in temperate soils: Integrating biology, mineralogy, and organic matter chemistry. J. Plant Nutr. Soil. Sci. 171, 61–82.
Kolpin, D.W., Furlong, E.T., Meyer, M.T., Thurman, E.M., Zaugg, S.D., Barber, L.B., Buxton, H.T., 2002. Pharmaceuticals, hormones, and other organic wastewater contaminants in US streams, 1999–2000: a national reconnaissance. Environ. Sci. Technol. 36, 1202–1211.
Komadel, P., Bujdak, J., Madejová, J., Sucha, V., Elsass, F., 1996. Effect of non-swelling layers on the dissolution of reduced-charge montmorillonite in hydrochloric acid. Clay Miner. 31, 333–345.
Kookana, R.S., Sarmah, A.K., Van Zwieten, L., Krull, E., Singh, B., 2011. Chapter three—biochar application to soil: agronomic and environmental benefits and unintended consequences. In: Donald, L.S. (Ed.), Advances in Agronomy, vol. 112. Academic Press, pp. 103–143.
Kramar, S., Urosevic, M., Pristacz, H., Mirtič, B., 2010. Assessment of limestone deterioration due to salt formation by micro-Raman spectroscopy: application to architectural heritage. J. Raman Spectrosc. 41, 1441–1448.
Kubicki, J.D., Kwon, K.D., Paul, K.W., Sparks, D.L., 2007. Surface complex structures modelled with quantum chemical calculations: carbonate, phosphate, sulphate, arsenate and arsenite. Eur. J. Soil Sci. 58, 932–944.
Kubicki, J.D., Mueller, K.T., 2010. Computational spectroscopy in environmental chemistry. In: Grunenberg, J. (Ed.), Computational Spectroscopy: Methods, Experiments and Applications. Wiley-VCH Verlag GmbH & Co. KGaA, Weinheim, Germany, pp. 323–351.
Kubicki, J.D., Schroeter, L.M., Itoh, M.J., Nguyen, B.N., Apitz, S.E., 1999. Attenuated total reflectance fourier-transform infrared spectroscopy of carboxylic acids adsorbed onto mineral surfaces. Geochim. Cosmochim. Acta 63, 2709–2725.
Kulshrestha, P., Giese, R.F., Aga, D.S., 2004. Investigating the molecular interactions of oxytetracycline in clay and organic matter: Insights on factors affecting its mobility in soil. Environ. Sci. Technol. 38, 4097–4105.
Lackovic, K., Johnson, B.B., Angove, M.J., Wells, J.D., 2003. Modeling the adsorption of citric acid onto Muloorina illite and related clay minerals. J. Colloid Interface Sci. 267, 49–59.
Laird, D.A., Fleming, P., Davis, D.D., Horton, R., Wang, B., Karlen, D.L., 2010. Impact of biochar amendments on the quality of a typical Midwestern agricultural soil. Geoderma 158, 443–449.
Laird, D.A., Yen, P.Y., Koskinen, W.C., Steinheimer, T.R., Dowdy, R.H., 1994. Sorption of atrazine on soil clay components. Environ. Sci. Technol. 28, 1054–1061.
Landgraf, M.D., da Silva, S.C., Rezende, M. O. de O., 1998. Mechanism of metribuzin herbicide sorption by humic acid samples from peat and vermicompost. Anal. Chim. Acta 368, 155–164.
Lanfranco, A.M., Schofield, P.F., Murphy, P.J., Hodson, M.E., Mosselmans, J.F.W., Valsami-Jones, E., 2003. Characterization and identification of mixed-metal phosphates in soils: the application of Raman spectroscopy. Mineral. Mag. 67, 1299–1316.
Lang, P.L., 2006. Microspectroscopy. In: Encyclopedia of Analytical Chemistry. John Wiley & Sons, Ltd.

Lawrence, J.R., Hitchcock, A.P., 2011. Synchrotron-based X-ray and FTIR absorption spectromicroscopies of organic contaminants in the environment. In: Biophysico-chemical Processes of Anthropogenic Organic Compounds in Environmental Systems. John Wiley & Sons, Inc., pp. 341–368.

Lefèvre, G., 2004. In situ Fourier-transform infrared spectroscopy studies of inorganic ions adsorption on metal oxides and hydroxides. Adv. Colloid Interface Sci. 107, 109–123.

Lefèvre, G., Preočanin, T., Lützenkirchen, J., 2012. Attenuated total reflection - infrared spectroscopy applied to the study of mineral - aqueous electrolyte solution interfaces: a general overview and a case study. In: Grunenberg, J. (Ed.), Computational Spectroscopy: Methods, Experiments and Applications. Wiley-VCH Verlag GmbH & Co. KGaA, Weinheim, Germany.

Legal, J.M., Manfait, M., Theophanides, T., 1991. Applications of FTIR spectroscopy in structural studies of cells and bacteria. J. Mol. Struct. 242, 397–407.

Lehmann, J., Joseph, S. (Eds.), 2009. Biochar for Environmental Management: Science and Technology. Earthscan Ltd, London, UK.

Lehmann, J., Kinyangi, J., Solomon, D., 2007. Organic matter stabilization in soil microaggregates: implications from spatial heterogeneity of organic carbon contents and carbon forms. Biogeochemistry 85, 45–57.

Lehmann, J., Liang, B.Q., Solomon, D., Lerotic, M., Luizao, F., Kinyangi, J., Schafer, T., Wirick, S., Jacobsen, C., 2005. Near-edge X-ray absorption fine structure (NEXAFS) spectroscopy for mapping nano-scale distribution of organic carbon forms in soil: application to black carbon particles. Glob. Biogeochem. Cycles 19.

Lehmann, J., Solomon, D., 2010. Chapter 10-Organic carbon chemistry in soils observed by synchrotron-based spectroscopy. In: Balwant, S., Markus, G. (Eds.), Developments in Soil Science, vol. 34. Elsevier, pp. 289–312.

Leifeld, J., Kögel-Knabner, I., 2001. Organic carbon and nitrogen in fine soil fractions after treatment with hydrogen peroxide. Soil Biol. Biochem. 33, 2155–2158.

Leite, R.C.C., Porto, S.P.S., 1966. Enhancement of Raman cross section in CdS due to resonant absorption. Phys. Rev. Lett. 17, 10–12.

Leue, M., Ellerbrock, R.H., Gerke, H.H., 2010a. DRIFT mapping of organic matter composition at intact soil aggregate surfaces. Vadose Zone J. 9, 317–324.

Leue, M., Ellerbrock, R.H., Gerke, H.H., 2010b. DRIFT mapping of organic matter composition at intact soil aggregate surfaces (All rights reserved. No part of this periodical may be reproduced or transmitted in any form or by any means, electronic or mechanical, including photocopying, recording, or any information storage and retrieval system, without permission in writing from the publisher) Vadose Zone J. 9, 317–324.

Levenson, E., Lerch, P., Martin, M.C., 2008. Spatial resolution limits for synchrotron-based infrared spectromicroscopy. Infrared Phys. Technol. 51, 413–416.

Levine, S., Stevenson, H.J.R., Chambers, L.A., Kenner, B.A., 1953. Infrared spectrophotometry of enteric bacteria. J. Bacteriol. 65, 10–15.

Lewis, D.G., Farmer, V.C., 1986. Infrared-absorption of surface hydroxyl-groups and lattice-vibrations in lepidocrocite (gamma-FeOOH) and boehmite (gamma-AlOOH). Clay Miner. 21, 93–100.

Lewis, I.R., Edwards, H.G.M., 2001. Handbook of Raman Spectroscopy: From the Research Laboratory to the Process Line. Marcel Dekker.

Leyton, P., Córdova, I., Lizama-Vergara, P.A., Gómez-Jeria, J.S., Aliaga, A.E., Campos-Vallette, M.M., Clavijo, E., García-Ramos, J.V., Sanchez-Cortes, S., 2008. Humic acids as molecular assemblers in the surface-enhanced Raman scattering detection of polycyclic aromatic hydrocarbons. Vib. Spectrosc. 46, 77–81.

Li-Chan, E., Chalmers, J.M., Griffiths, P., 2010. Applications of Vibrational Spectroscopy in Food Science. John Wiley & Sons, Ltd, West Sussex, UK.

Li, H., Sheng, G.Y., Teppen, B.J., Johnston, C.T., Boyd, S.A., 2003. Sorption and desorption of pesticides by clay minerals and humic acid-clay complexes. Soil Sci. Soc. Am. J. 67, 122–131.
Li, X., Hayashi, J.-i., Li, C.-Z., 2006. FT-Raman spectroscopic study of the evolution of char structure during the pyrolysis of a Victorian brown coal. Fuel 85, 1700–1707.
Li, J., Li, Y., Lu, J., 2009. Adsorption of herbicides 2,4-D and acetochlor on inorganic–organic bentonites. Applied Clay Science 46, 314–318.
Li, Z., Hong, H., Liao, L., Ackley, C.J., Schulz, L.A., MacDonald, R.A., Mihelich, A.L., Emard, S.M., 2011. A mechanistic study of ciprofloxacin removal by kaolinite. Colloids Surf. B Biointerfaces 88, 339–344.
Li, Z., Kolb, V.M., Jiang, W.-T., Hong, H., 2010. FTIR and XRD investigations of tetracycline intercalation in smectites. Clays Clay Miner. 58, 462–474.
Liang, B., Lehmann, J., Solomon, D., Kinyangi, J., Grossman, J., O'Neill, B., Skjemstad, J.O., Thies, J., Luizao, F.J., Petersen, J., Neves, E.G., 2006. Black carbon increases cation exchange capacity in soils. Soil Sci. Soc. Am. J. 70, 1719–1730.
Liang, B., Lehmann, J., Solomon, D., Sohi, S., Thies, J.E., Skjemstad, J.O., Luizão, F.J., Engelhard, M.H., Neves, E.G., Wirick, S., 2008. Stability of biomass-derived black carbon in soils. Geochim. Cosmochim. Acta 72, 6069–6078.
Liang, E.J., Yang, Y., Kiefer, W., 1999. Surface-enhanced raman spectra of fulvic and humic acids adsorbed on copper electrodes. Spectrosc. Lett. 32, 689–701.
Liang, E.J., Yang, Y.H., Kiefer, W., 1996. Surface–enhanced Raman spectra of fulvic and humic acids on silver nitrate–modified Fe–C–Cr–Ni surface. J. Environ. Sci. Health. Part A Environ. Sci. Eng. Toxicol. 31, 2477–2486.
Liu, T.-T., Lin, Y.-H., Hung, C.-S., Liu, T.-J., Chen, Y., Huang, Y.-C., Tsai, T.-H., Wang, H.-H., Wang, D.-W., Wang, J.-K., Wang, Y.-L., Lin, C.-H., 2009. A high speed detection platform based on surface-enhanced raman scattering for monitoring antibiotic-induced chemical changes in bacteria cell Wall. PLoS One 4, e5470.
Livingston, D., 1973. The Master of Light: A Biography of Albert A. Michelson. University of Chicago Press, Chicago, IL.
Lombardi, J.R., Birke, R.L., 2009. A unified view of surface-enhanced Raman scattering. Acc. Chem. Res. 42, 734–742.
Lombi, E., Hettiarachchi, G.M., Scheckel, K.G., 2011. Advanced in situ spectroscopic techniques and their applications in environmental biogeochemistry: introduction to the special section. J. Environ. Qual. 40, 659–666.
Long, D.A., 1977. Raman Spectroscopy. McGraw-Hill.
Long, D.A., 2002. The Raman Effect: A Unified Treatment of the Theory of Raman Scattering by Molecules. Wiley.
Lorna, D., Colin, C., Stephen, H., Mark, B., 2008. Methods of characterizing and fingerprinting soils for forensic application. In: Soil Analysis in Forensic Taphonomy. CRC Press, pp. 271–315.
Lu, S., Chunfeng, H., Sakka, Y., Qing, H., 2012. Study of phase transformation behaviour of alumina through precipitation method. J. Phys. Appl. Phys. 45. 215302 (6 pp.)–215302 (6 pp.).
Ludwig, B., Nitschke, R., Terhoeven-Urselmans, T., Michel, K., Flessa, H., 2008. Use of mid-infrared spectroscopy in the diffuse-reflectance mode for the prediction of the composition of organic matter in soil and litter. J. Plant Nutr. Soil Sci. Z. Pflanzenernahrung Bodenkunde 171, 384–391.
Luengo, C., Brigante, M., Antelo, J., Avena, M., 2006. Kinetics of phosphate adsorption on goethite: comparing batch adsorption and ATR-IR measurements. J. Colloid Interface Sci. 300, 511–518.
Luengo, C., Brigante, M., Avena, M., 2007. Adsorption kinetics of phosphate and arsenate on goethite. A comparative study. J. Colloid Interface Sci. 311, 354–360.
Luxton, T.P., Eick, M.J., Rimstidt, D.J., 2008. The role of silicate in the adsorption/desorption of arsenite on goethite. Chem. Geol. 252, 125–135.

Lyon, L.A., Keating, C.D., Fox, A.P., Baker, B.E., He, L., Nicewarner, S.R., Mulvaney, S.P., Natan, M.J., 1998. Raman spectroscopy. Anal. Chem. 70, 341–362.
Madejová, J., 2003. FTIR techniques in clay mineral studies. Vib. Spectrosc. 31, 1–10.
Madejová, J., Keckes, J., Paalkova, H., Komadel, P., 2002. Identification of components in smectite/kaolinite mixtures. Clay Miner. 37, 377–388.
Madejová, J., Komadel, P., 2001. Baseline studies of the Clay minerals society source clays: infrared methods. Clays Clay Miner. 49, 410–432.
Maes, E., Vielvoye, L., Stone, W., Delvaux, B., 1999. Fixation of radiocaesium traces in a weathering sequence mica→vermiculite→hydroxy interlayered vermiculite. Eur. J. Soil Sci. 50, 107–115.
Mafra, A.L., Senesi, N., Brunetti, G., Miklós, A.A.W., Melfi, A.J., 2007. Humic acids from hydromorphic soils of the upper Negro river basin, Amazonas: chemical and spectroscopic characterisation. Geoderma 138, 170–176.
Major, J., Steiner, C., Downie, A., Lehmann, J., 2009. Biochar effects on nutrient leaching. In: Joseph, J.L.A.S. (Ed.), Biochar for Environmental Management—Science and Technology. Earthscan, London, pp. 227–249.
Mao, J., Olk, D.C., Fang, X., He, Z., Schmidt-Rohr, K., 2008. Influence of animal manure application on the chemical structures of soil organic matter as investigated by advanced solid-state NMR and FT-IR spectroscopy. Geoderma 146, 353–362.
Mao, Y., Daniel, L.N., Whittaker, N., Saffiotti, U., 1994. DNA binding to crystalline silica characterized by Fourier-transform infrared spectroscopy. Environ. Health Perspect. 102, 165–171.
Maqueda, C., Morillo, E., Martin, F., Undabeytia, T., 1993. Interaction of pesticides with the soluble fraction of natural and artificial humic substances. J. Environ. Sci. Health Part B 28, 655–670.
Maquelin, K., Kirschner, C., Choo-Smith, L.P., Ngo-Thi, N.A., Van Vreeswijk, T., Stammler, M., Endtz, H.P., Bruining, H.A., Naumann, D., Puppels, G.J., 2003. Prospective study of the performance of vibrational spectroscopies for rapid identification of bacterial and fungal pathogens recovered from blood cultures. J. Clin. Microbiol. 41, 324–329.
Maquelin, K., Kirschner, C., Choo-Smith, L.P., van den Braak, N., Endtz, H.P., Naumann, D., Puppels, G.J., 2002. Identification of medically relevant microorganisms by vibrational spectroscopy. J. Microbiol. Methods 51, 255–271.
Mariey, L., Signolle, J.P., Amiel, C., Travert, J., 2001. Discrimination, classification, identification of microorganisms using FTIR spectroscopy and chemometrics. Vib. Spectrosc. 26, 151–159.
Marinari, S., Dell'Abate, M.T., Brunetti, G., Dazzi, C., 2010. Differences of stabilized organic carbon fractions and microbiological activity along Mediterranean Vertisols and Alfisols profiles. Geoderma 156, 379–388.
Martin-Neto, L., Traghetta, D.G., Vaz, C.M.P., Crestana, S., Sposito, G., 2001. On the interaction mechanisms of atrazine and hydroxyatrazine with humic substances. J. Environ. Qual. 30, 520–525.
Martin-Neto, L., Vieira, E.M., Sposito, G., 1994. Mechanism of atrazine sorption by humic acid: a spectroscopic study. Environ. Sci. Technol. 28, 1867–1873.
Martin, M.C., McKinney, W.R., 2001. The first synchrotron infrared beamlines at the advanced light source: spectromicroscopy and fast timing. Ferroelectrics 249, 1–10.
Martínez, E.J., Fierro, J., Sánchez, M.E., Gómez, X., 2012. Anaerobic co-digestion of FOG and sewage sludge: study of the process by Fourier transform infrared spectroscopy. Int. Biodeterior. Biodegrad. 75, 1–6.
Matejkova, S., Simon, T., 2012. Application of FTIR spectroscopy for evaluation of hydrophobic/hydrophilic organic components in arable soil. Plant Soil Environ. 58, 192–195.
Matilainen, A., Gjessing, E.T., Lahtinen, T., Hed, L., Bhatnagar, A., Sillanpää, M., 2011. An overview of the methods used in the characterisation of natural organic matter (NOM) in relation to drinking water treatment. Chemosphere 83, 1431–1442.

Matteson, A., Herron, M.M., 1993. Quantitative mineral analysis by Fourier transform infrared spectroscopy. Soc. Core Anal. Conf. Pap. 9308, 1–15.
McAuley, B., Cabaniss, S.E., 2007. Quantitative detection of aqueous arsenic and other oxoanions using attenuated total reflectance infrared spectroscopy utilizing iron oxide coated internal reflection elements to enhance the limits of detection. Analytica Chimica Acta 581, 309–317.
McCarty, G.W., Reeves Iii, J.B., Gurel, S., Katkat, A.V., 2010. Evaluation of methods for measuring soil organic carbon in West African soils. Afr. J. Agric. Res. 5, 2169–2177.
McCarty, G.W., Reeves, J.B., Reeves, V.B., Follett, R.F., Kimble, J.M., 2002. Mid-infrared and near-infrared diffuse reflectance spectroscopy for soil carbon measurement. Soil Sci. Soc. Am. J. 66, 640–646.
McMillan, P.F., Hofmeister, A.M., 1988. Infrared and Raman spectroscopy. In: Hawthorne, F.C. (Ed.), Review in Mineralogy: Spectroscopic methods in mineralogy and geology, vol. 18. pp. 99–159(Miner. Soc. Am).
McWhirter, M.J., Bremer, P.J., Lamont, I.L., McQuillan, A.J., 2003. Siderophore-mediated covalent bonding to metal (oxide) surfaces during biofilm initiation by *Pseudomonas aeruginosa* bacteria. Langmuir 19, 3575–3577.
McWhirter, M.J., McQuillan, A.J., Bremer, P.J., 2002. Influence of ionic strength and pH on the first 60 min of Pseudomonas aeruginosa attachment to ZnSe and to TiO2 monitored by ATR-IR spectroscopy. Colloids Surf. B Biointerfaces 26, 365–372.
Mendive, C.B., Bredow, T., Blesa, M.A., Bahnemann, D.W., 2006. ATR-FTIR measurements and quantum chemical calculations concerning the adsorption and photoreaction of oxalic acid on TiO2. Physical Chemistry Chemical Physics 8, 3232–3247.
Messerschmidt, R.G., Chase, D.B., 1989. FT-Raman microscopy: discussion and preliminary results. Appl. Spectrosc. 43, 11–15.
Michelmore, A., Gong, W.Q., Jenkins, P., Ralston, J., 2000. The interaction of linear polyphosphates with titanium dioxide surfaces. Physical Chemistry Chemical Physics 2, 2985–2992.
Mikutta, R., Kleber, M., Kaiser, K., Jahn, R., 2005. Review. Soil Sci. Soc. Am. J. 69, 120–135.
Mimmo, T., Reeves, J.B., McCarty, G.W., Galletti, G., 2002. Determination of biological measures by mid-infrared diffuse reflectance spectroscopy in soils within a landscape. Soil Sci. 167, 281–287.
Minasny, B., McBratney, A.B., Tranter, G., Murphy, B.W., 2008. Using soil knowledge for the evaluation of mid-infrared diffuse reflectance spectroscopy for predicting soil physical and mechanical properties. Eur. J. Soil Sci. 59, 960–971.
Mirabella, F.M.J., 1985. Internal reflection spectroscopy. Appl. Spectrosc. Rev. 21, 45–78.
Morris, P.M., Wogelius, R.A., 2008. Phthalic acid complexation and the dissolution of forsteritic glass studied via in situ FTIR and X-ray scattering. Geochim. Cosmochim. Acta 72, 1970–1985.
Moskovits, M., 1985. Surface-enhanced spectroscopy. Rev. Mod. Phys. 57, 783–826.
Moskovits, M., 2005. Surface-enhanced Raman spectroscopy: a brief retrospective. J. Raman Spectrosc. 36, 485–496.
Mukome, F.N.D., Zhang, X., Sillva, L.C.R., Six, J., Parikh, S.J., 2013. Use of chemical and physical characteristics to investigate trends in biochar feedstocks. J. Agric. Food Chem. 61, 2196–2204.
Mulvaney, R.L., Yaremych, S.A., Khan, S.A., Swiader, J.M., Horgan, B.P., 2004. Use of diffusion to determine soil cation-exchange capacity by ammonium saturation. Commun. Soil Sci. Plant Anal. 35, 51–67.
Muniz-Miranda, M., Gellini, C., Salvi, P.R., Pagliai, M., 2010. Surface-enhanced Raman micro-spectroscopy of DNA/RNA bases adsorbed on pyroxene rocks as a test of in situ search for life traces on Mars. J. Raman Spectrosc. 41, 12–15.

Myneni, S.C.B., Traina, S.J., Waychunas, G.A., Logan, T.J., 1998. Vibrational spectroscopy of functional group chemistry and arsenate coordination in ettringite. Geochim. Cosmochim. Acta 62, 3499–3514.

Naja, G., Bouvrette, P., Hrapovic, S., Luong, J.H.T., 2007. Raman-based detection of bacteria using silver nanoparticles conjugated with antibodies. Analyst 132, 679–686.

Nara, M., Torii, H., Tasumi, M., 1996. Correlation between the vibrational frequencies of the carboxylate group and the types of its coordination to a metal ion: an ab initio molecular orbital study. J. Phys. Chem. 100, 19812–19817.

Naumann, D., Fijala, V., Labischinski, H., Giesbrecht, P., 1988. The rapid differentiation and identification of pathogenic bacteria using Fourier transform infrared spectroscopic and multivariate statistical analysis. J. Mol. Struct. 174, 165–170.

Naumann, D., Helm, D., Labischinski, H., 1991. Microbiological characterizations by FT-IR spectroscopy. Nature 351, 81–82.

Naumann, D., Keller, S., Helm, D., Schultz, C., Schrader, B., 1995. FT-IR spectroscopy and FT-Raman spectroscopy are powerful analytical tools for the non-invasive characterization of intact microbial cells. J. Mol. Struct. 347, 399–405.

Naumann, D., Schultz, C.P., Helm, D., 1996. What can infrared spectroscopy tell us about the structure and composition of intact bacterial cells? In: Mantch, H.H., Chapman, D. (Eds.), Infrared Spectroscopy of Biomolecules. John Wiley and Sons, New York, pp. 279–310.

Navarrete, I.A., Tsutsuki, K., Navarrete, R.A., 2010. Humus composition and the structural characteristics of humic substances in soils under different land uses in Leyte, Philippines. Soil Sci. Plant Nutr. 56, 289–296.

Nguyen, T.T., Janik, L.J., Raupach, M., 1991. Diff use reflectance infrared fourier transform (DRIFT) spectroscopy in soil studies. Aust. J. Soil Res. 29, 49–67.

Nichols, P.D., Henson, J.M., Guckert, J.B., Nivens, D.E., White, D.C., 1985. Fourier transform-infrared spectroscopic methods for microbial ecology - analysis of bacteria, bacteria-polymer mixtures and biofilms. J. Microbiol. Methods 4, 79–94.

Niemeyer, J., Chen, Y., Bollag, J.M., 1992. Characterization of humic acids, composts, and peat by diffuse reflectance Fourier-transform infrared-spectroscopy. Soil Sci. Soc. Am. J. 56, 135–140.

Nivens, D.E., Schmitt, J., Sniatecki, J., Anderson, T.R., Chambers, J.Q., White, D.C., 1993a. Multichannel ATR/FT-IR spectrometer for on-line examination of microbial biofilms. Appl. Spectrosc. 47, 668–671.

Nivens, D.E., Chambers, J.Q., Anderson, T.R., Tunlid, A., Smit, J., White, D.C., 1993. Monitoring Microbial Adhesion and Biofilm Formation by Attenuated Total Reflection Fourier-Transform Infrared- Spectroscopy. J. Microbiol. Methods 17, 199–213.

Norén, K., Loring, J.S., Persson, P., 2008. Adsorption of alpha amino acids at the water/goethite interface. J. Colloid Interface Sci. 319, 416–428.

Norén, K., Persson, P., 2007. Adsorption of monocarboxylates at the water/goethite interface: the importance of hydrogen bonding. Geochim. Cosmochim. Acta 71, 5717–5730.

Novak, J.M., Busscher, W.J., Laird, D.L., Ahmedna, M., Watts, D.W., Niandou, M.A.S., 2009. Impact of biochar amendment on fertility of a Southeastern Coastal Plain soil. Soil Sci. 174, 105–112.

Nowara, A., Burhenne, J., Spiteller, M., 1997. Binding of fluoroquinolone carboxylic acid derivatives to clay minerals. J. Agric. Food Chem. 45, 1459–1463.

O'Reilly, J.M., Mosher, R.A., 1983. Functional groups in carbon black by FTIR spectroscopy. Carbon 21, 47–51.

Oades, J.M., 1984. Soil organic matter and structural stability: mechanisms and implications for management. Plant Soil 76, 319–337.

Ohno, T., He, Z., Tazisong, I.A., Senwo, Z.N., 2009. Influence of tillage, cropping, and nitrogen source on the chemical characteristics of humic acid, fulvic acid, and water-soluble soil organic matter fractions of a long-term cropping system study. Soil Sci. 174, 652–660. http://dx.doi.org/10.1097/SS.0b013e3181c30808.

Ojeda, J.J., Romero-Gonzalez, M.E., Pouran, H.M., Banwart, S.A., 2008. In situ monitoring of the biofilm formation of *Pseudomonas putida* on hematite using flow-cell ATR-FTIR spectroscopy to investigate the formation of inner-sphere bonds between the bacteria and the mineral. Mineral. Mag. 72, 101–106.

Olk, D.C., Brunetti, G., Senesi, N., 1999. Organic matter in double-cropped lowland rice soils: chemical and spectroscopic properties. Soil Sci. 164, 633–649.

Olk, D.C., Brunetti, G., Senesi, N., 2000. Decrease in humification of organic matter with intensified lowland rice cropping a wet chemical and spectroscopic investigation. Soil Sci. Soc. Am. J. 64, 1337–1347.

Omoike, A., Chorover, J., 2004. Spectroscopic study of extracellular polymeric substances from *Bacillus subtilis*: aqueous chemistry and adsorption effects. Biomacromolecules 5, 1219–1230.

Omoike, A., Chorover, J., 2006. Adsorption to goethite of extracellular polymeric substances from *Bacillus subtilis*. Geochim. Cosmochim. Acta 70, 827–838.

Omoike, A., Chorover, J., Kwon, K.D., Kubicki, J.D., 2004. Adhesion of bacterial exopolymers to α-FeOOH: inner-sphere complexation of phosphodiester groups. Langmuir 20, 11108–11114.

Ostergren, J.D., Trainor, T.P., Bargar, J.R., Brown, G.E., Parks, G.A., 2000. Inorganic ligand effects on Pb(II) sorption to goethite (alpha-FeOOH) - I. Carbonate. J. Colloid Interface Sci. 225, 466–482.

Otto, A., Mrozek, I., Grabhorn, H., Akemann, W., 1992. Surface-enhanced Raman scattering. J. Phys. Condens. Matter 4, 1143.

Otto, C., Pully, V.V., 2012. Hyperspectral Raman microscopy of the living cell. In: Ghomi, M. (Ed.), Applications of Raman Spectroscopy to Biology, Vol. 5. Ios Press Inc., pp. 148–173.

Ouatmane, A., Provenzano, M.R., Hafidi, M., Senesi, N., 2000. Compost maturity assessment using calorimetry, spectroscopy and chemical analysis. Compost Sci. Util. 8, 124.

Özçimen, D., Ersoy-Meriçboyu, A., 2010. Characterization of biochar and bio-oil samples obtained from carbonization of various biomass materials. Renewable Energy 35, 1319–1324.

Parfitt, R.L., Smart, R.S.C., 1977. Infrared spectra from binuclear bridging complexes of sulphate adsorbed on goethite ([small alpha]-FeOOH). Journal of the Chemical Society, Faraday Transactions 1: Physical Chemistry in Condensed Phases 73, 796–802.

Parfitt, R.L., Smart, R.S.C., 1978. Mechanism of sulfate adsorption on iron-oxides. Soil Science Society of America Journal 42, 48–50.

Parikh, S.J., Chorover, J., 2005. FTIR spectroscopic study of biogenic Mn-oxide formation by *Pseudomonas putida* GB-1. Geomicrobiol. J. 22, 207–218.

Parikh, S.J., Chorover, J., 2006. ATR-FTIR spectroscopy reveals bond formation during bacterial adhesion to iron oxide. Langmuir 22, 8492–8500.

Parikh, S.J., Chorover, J., 2007. Infrared spectroscopy studies of cation effects on lipopolysaccharides in aqueous solution. Colloids Surf. B Biointerfaces 55, 241–250.

Parikh, S.J., Chorover, J., 2008. ATR-FTIR study of lipopolysaccharides at mineral surfaces. Colloids Surf. B Biointerfaces 62, 188–198.

Parikh, S.J., Kubicki, J.D., Jonsson, C.M., Jonsson, C.L., Hazen, R.M., Sverjensky, D.A., Sparks, D.L., 2011. Evaluating glutamate and aspartate binding mechanisms to rutile (α-TiO_2) via ATR-FTIR spectroscopy and quantum chemical calculations. Langmuir 27, 1778–1787.

Parikh, S.J., Lafferty, B.J., Meade, T.G., Sparks, D.L., 2010. Evaluating environmental influences on AsIII oxidation kinetics by a poorly crystalline Mn-oxide. Environ. Sci. Technol. 44, 3772–3778.

Parikh, S.J., Lafferty, B.J., Sparks, D.L., 2008. An ATR-FTIR spectroscopic approach for measuring rapid kinetics at the mineral/water interface. J. Colloid Interface Sci. 320, 177–185.

Paul, K.W., Borda, M.J., Kubicki, J.D., Sparks, D.L., 2005. Effect of dehydration on sulfate coordination and speciation at the Fe−(Hydr)oxide−water interface: a molecular orbital/density functional theory and Fourier transform infrared spectroscopic investigation. Langmuir 21, 11071–11078.

Paul, T., Machesky, M.L., Strathmann, T.J., 2012. Surface Complexation of the Zwitterionic Fluoroquinolone Antibiotic Ofloxacin to Nano-Anatase TiO2 Photocatalyst Surfaces. Environ. Sci. Technol. 46, 11896–11904.

Peak, D., Ford, R.G., Sparks, D.L., 1999. An in situ ATR-FTIR investigation of sulfate bonding mechanisms on goethite. J. Colloid Interface Sci. 218, 289–299.

Pei, Z., Shan, X.-Q., Kong, J., Wen, B., Owens, G., 2010. Coadsorption of ciprofloxacin and Cu(II) on montmorillonite and kaolinite as affected by solution pH. Environ. Sci. Technol. 44, 915–920.

Pelletier, M.J., 1999. Analytical Applications of Raman Spectroscopy. Wiley.

Pellow-Jarman, M.V., Hendra, P.J., Lehnert, R.J., 1996. The dependence of Raman signal intensity on particle size for crystal powders. Vib. Spectrosc. 12, 257–261.

Peltre, C., Thuriès, L., Barthès, B., Brunet, D., Morvan, T., Nicolardot, B., Parnaudeau, V., Houot, S., 2011. Near infrared reflectance spectroscopy: a tool to characterize the composition of different types of exogenous organic matter and their behaviour in soil. Soil Biol. Biochem. 43, 197–205.

Pemberton, J.E., Sobocinski, R.L., Sims, G.R., 1990. The effect of charge traps on Raman spectroscopy using a Thomson-CSF charge coupled device detector. Appl. Spectrosc. 44, 328–330.

Pena, M., Meng, X.G., Korfiatis, G.P., Jing, C.Y., 2006. Adsorption mechanism of arsenic on nanocrystalline titanium dioxide. Environ. Sci. Technol. 40, 1257–1262.

Peng, X., Ye, L.L., Wang, C.H., Zhou, H., Sun, B., 2011. Temperature- and duration-dependent rice straw-derived biochar: characteristics and its effects on soil properties of an Ultisol in southern China. Soil Tillage Res. 112, 159–166.

Pereira, M.R., Yarwood, J., 1994. Depth-profiling of polymer laminates using Fourier-transform infrared (ATR) spectroscopy—the barrier film technique. J. Polym. Sci. Part B Polym. Phys. 32, 1881–1887.

Pérez-Sanz, A., Lucena, J.J., Graham, M.C., 2006. Characterization of Fe–humic complexes in an Fe-enriched biosolid by-product of water treatment. Chemosphere 65, 2045–2053.

Pershina, A., Sazonov, A., Ogorodova, L., 2009. Investigation of the interaction between DNA and cobalt ferrite nanoparticles by FTIR spectroscopy. Russ. J. Bioorg. Chem. 35, 607–613.

Persson, P., Axe, K., 2005. Adsorption of oxalate and malonate at the water-goethite interface: molecular surface speciation from IR spectroscopy. Geochim. Cosmochim. Acta 69, 541–552.

Persson, P., Karlsson, M., Ohman, L.O., 1998. Coordination of acetate to Al(III) in aqueous solution and at the water-aluminum hydroxide interface: A potentiometric and attenuated total reflectance FTIR study. Geochim. Cosmochim. Acta 62, 3657–3668.

Persson, P., Nilsson, N., Sjoberg, S., 1996. Structure and bonding of orthophosphate ions at the iron oxide aqueous interface. J. Colloid Interface Sci. 177, 263–275.

Peterson, J.W., O'Meara, T.A., Seymour, M.D., Wang, W., Gu, B., 2009. Sorption mechanisms of cephapirin, a veterinary antibiotic, onto quartz and feldspar minerals as detected by Raman spectroscopy. Environ. Pollut. 157, 1849–1856.

Petit, S., Righi, D., Madejová, J., Decarreau, A., 1998. Layer charge estimation of smectites using infrared spectroscopy. Clay Miner. 33, 579–591.

Petit, S., Righl, D., Madejová, J., 2006. Infrared spectroscopy of NH(4)(+)-bearing and saturated clay minerals: a review of the study of layer charge. Appl. Clay Sci. 34, 22–30.

Petry, R., Schmitt, M., Popp, J., 2003. Raman spectroscopy—a prospective tool in the life sciences. ChemPhysChem 4, 14–30.

Piccolo, A., Celano, G., 1994. Hydrogen-bonding interactions between the herbicide glyphosate and water-soluble humic substances. Environ. Toxicol. Chem. 13, 1737–1741.
Piccolo, A., Stevenson, F.J., 1982. Infrared spectra of Cu^{2+} Pb^{2+} and Ca^{2+} complexes of soil humic substances. Geoderma 27, 195–208.
Piccolo, A., Zaccheo, P., Genevini, P.G., 1992. Chemical characterization of humic substances extracted from organic-waste-amended soils. Bioresource Technology 40, 275–282.
Plante, A.F., Chenu, C., Balabane, M., Mariotti, A., Righi, D., 2004. Peroxide oxidation of clay-associated organic matter in a cultivation chronosequence. Eur. J. Soil Sci. 55, 471–478.
Popp, J., Kiefer, W., 2006. Raman scattering, fundamentals. In: Encyclopedia of Analytical Chemistry. John Wiley & Sons, Ltd.
Popp, J., Schmitt, M., 2004. Raman spectroscopy breaking terrestrial barriers! J. Raman Spectrosc. 35, 429–432.
Porto, S.P.S., Tell, B., Damen, T.C., 1966. Near-forward Raman scattering in zinc oxide. Phys. Rev. Lett. 16, 450–452.
Potter, R.M., Rossman, G.R., 1979. Tetravalent manganese oxides—identification, hydration, and structural relationships by infrared-spectroscopy. Am. Mineral. 64, 1199–1218.
Prost, R., Dameme, A., Huard, E., Driard, J., Leydecker, J.P., 1989. Infrared study of structural oh in kaolinite, dickite, nacrite, and poorly crystalline kaolinite at 5-K to 600-K. Clays Clay Miner. 37, 464–468.
Puppels, G.J., de Mul, F.F.M., Otto, C., Greve, J., Robert-Nicoud, M., Arndt-Jovin, D.J., Jovin, T.M., 1990. Studying single living cells and chromosomes by confocal Raman microspectroscopy. Nat. Commun. 347, 301–303.
Pusino, A., Braschi, I., Gessa, C., 2000. Adsorption and degradation of triasulfuron on homoionic montmorillonites. Clays Clay Miner. 48, 19–25.
Pusino, A., Gelsomino, A., Fiori, M.G., Gessa, C., 2003. Adsorption of Two Quinolinecarboxylic Acid Herbicides on Homoionic Montmorillonites. Clays Clay Miner. 51, 143–149.
Quiles, F., Burneau, A., Keiding, K., 1999. In situ ATR-FTIR Characterization of organic macromolecules aggregated with metallic colloids. In: Berthelin, J., Huang, P.M., Bollag, J.-M., Andreuz, F. (Eds.), Effect of Mineral-Organic Microorganism Interactions on Soil and Freshwater Environments. Klumer Academic / Plenum Publishers, New York, pp. 133–142.
Raab, T.K., Vogel, J.P., 2004. Ecological and agricultural applications of synchrotron IR microscopy. Infrared Phys. Technol. 45, 393–402.
Rakshit, S., Elzinga, E.J., Datta, R., Sarkar, D., 2013a. In Situ Attenuated Total Reflectance Fourier-Transform Infrared Study of Oxytetracycline Sorption on Magnetite. J. Environ. Qual. 42, 822–827.
Rakshit, S., Sarkar, D., Elzinga, E.J., Punamiya, P., Datta, R., 2013b. Mechanisms of ciprofloxacin removal by nano-sized magnetite. J. Hazard. Mater 246–247, 221–226.
Raman, C.V., Krishnan, K.S., 1928. A new type of secondary radiation. Nat. Commun. 121, 501–502.
Rank, D.H., Douglas, A.E., 1948. Light scattering in optical glass. J. Opt. Soc. Am. 38, 966–970.
Reeves, J.B., Francis, B.A., Hamilton, S.K., 2005. Specular reflection and diffuse reflectance spectroscopy of soils. Appl. Spectrosc. 59, 39–46.
Reeves III, J.B., 2010. Near- versus mid-infrared diffuse reflectance spectroscopy for soil analysis emphasizing carbon and laboratory versus on-site analysis: where are we and what needs to be done? Geoderma 158, 3–14.
Reeves III, J.B., 2012. Mid-infrared spectral interpretation of soils: is it practical or accurate? Geoderma 189, 508–513.
Reeves III, J.B., McCarty, G.W., Calderón, F.J., Hively, H.D., 2012. Advances in Spectroscopic Methods for Quantifying Soil Carbon, first ed. (Coordinated Agricultural Research through GRACEnet to Address our Changing Climate).

Reeves III, J.B., Follett, R.F., McCarty, G.W., Kimble, J.M., 2006. Can near or mid-infrared diffuse reflectance spectroscopy be used to determine soil carbon pools? Commun. Soil. Sci. Plant Anal. 37, 2307–2325.

Reeves, J.B., McCarty, G.W., Reeves, V.B., 2001. Mid-infrared diffuse reflectance spectroscopy for the quantitative analysis of agricultural soils. J. Agric. Food Chem. 49, 766–772.

Reiter, G., Siam, M., Falkenhagen, D., Gollneritsch, W., Baurecht, D., Fringeli, U.P., 2002. Interaction of a bacterial endotoxin with different surfaces investigated by in situ Fourier transform infrared attenuated total reflection spectroscopy. Langmuir 18, 5761–5771.

Riddle, J.W., Kabler, P.W., Kenner, B.A., Bordner, R.H., Rockwood, S.W., Stevenson, H.J.R., 1956. Bacterial identification by infrared spectrophotometry. J. Bacteriol. 72, 593–603.

Rijnaarts, H.H.M., Norde, W., Bouwer, E.J., Lyklema, J., Zehnder, A.J.B., 1995. Reversibility and mechanism of bacterial adhesion. Colloids Surf. B Biointerfaces 4, 5–22.

Rinaudo, C., Roz, M., Boero, V., Franchini-Angela, M., 2004. FT-Raman spectroscopy on several di- and trioctahedral T—O–T phyllosilicates. Neues Jahrb. Mineral. Monatsh. 537–554.

Rintoul, L., Fredericks, P.M., 1995. Infrared microspectroscopy of Bauxitic Pisoliths. Appl. Spectrosc. 49, 1608–1616.

Roberts, C.A., Workman, J., Reeves III, J.B., 2004. Near-infrared Spectroscopy in Agriculture. American Societies of Agronomy, Crop and Soil Science, Madison, WI.

Roddick-Lanzilotta, A.D., Connor, P.A., McQuillan, A.J., 1998. An in situ infrared spectroscopic study of the adsorption of lysine to TiO_2 from an aqueous solution. Langmuir 14, 6479–6484.

Roddick-Lanzilotta, A.D., Mcquillan, A.J., 1999. An in Situ Infrared Spectroscopic Investigation of Lysine Peptide and Polylysine Adsorption to Tio2 From Aqueous Solutions. J. Colloid Interface Sci 217, 194–202.

Roddick-Lanzilotta, A.D., McQuillan, A.J., 2000. An in situ infrared spectroscopic study of glutamic acid and of aspartic acid adsorbed on TiO_2: Implications for the biocompatibility of titanium. J. Colloid Interface Sci. 227, 48–54.

Roddick-Lanzilotta, A.J., McQuillan, A.J., Craw, D., 2002. Infrared spectroscopic characterisation of arsenate (V) ion adsorption from mine waters, Macraes mine, New Zealand. Applied Geochemistry 17, 445–454.

Roldán, M.L., Corrado, G., Francioso, O., Sanchez-Cortes, S., 2011. Interaction of soil humic acids with herbicide paraquat analyzed by surface-enhanced Raman scattering and fluorescence spectroscopy on silver plasmonic nanoparticles. Anal. Chim. Acta 699, 87–95.

Rong, X., Chen, W., Huang, Q., Cai, P., Liang, W., 2010. Pseudomonas putida adhesion to goethite: studied by equilibrium adsorption, SEM, FTIR and ITC. Colloids Surf. B Biointerfaces 80, 79–85.

Rong, X., Huang, Q., He, X., Chen, H., Cai, P., Liang, W., 2008. Interaction of Pseudomonas putida with kaolinite and montmorillonite: a combination study by equilibrium adsorption, ITC, SEM and FTIR. Colloids Surf. B Biointerfaces 64, 49–55.

Rosenqvist, J., Axe, K., Sjoberg, S., Persson, P., 2003. Adsorption of Dicarboxylates on Nano-Sized Gibbsite Particles: Effects of Ligand Structure on Bonding Mechanisms. Colloid Surf. A-Physicochem. Eng. Asp. 220, 91–104.

Rotzinger, F.P., Kesselman-Truttmann, J.M., Hug, S.J., Shklover, V., Gratzel, M., 2004. Structure and vibrational spectrum of formate and acetate adsorbed from aqueous solution onto the TiO2 rutile (110) surface. Journal of Physical Chemistry B 108, 5004–5017.

Ruan, H.D., Frost, R.L., Kloprogge, J.T., 2001. The behavior of hydroxyl units of synthetic goethite and its dehydroxylated product hematite. Spectrochim. Acta Part A Mol. Biomol. Spectrosc. 57, 2575–2586.

Ruan, H.D., Frost, R.L., Kloprogge, J.T., Duong, L., 2002a. Infrared spectroscopy of goethite dehydroxylation. II. Effect of aluminium substitution on the behaviour of hydroxyl units. Spectrochim. Acta Part A Mol. Biomol. Spectrosc. 58, 479–491.

Ruan, H.D., Frost, R.L., Kloprogge, J.T., Duong, L., 2002b. Infrared spectroscopy of goethite dehydroxylation: III. FT-IR microscopy of in situ study of the thermal transformation of goethite to hematite. Spectrochim. Acta Part A Mol. Biomol. Spectrosc. 58, 967–981.

Rumpel, C., Rabia, N., Derenne, S., Quenea, K., Eusterhues, K., Koegel-Knabner, I., Mariotti, A., 2006. Alteration of soil organic matter following treatment with hydrofluoric acid (HF). Org. Geochem. 37, 1437–1451.

Russell, J.D., Fraser, A.R., 1994. Infrared methods. In: Wilson, M.J. (Ed.), Clay Mineralogy: Spectroscopic and Chemical Determinative Methods. Chapman & Hall, London, UK, pp. 11–67.

Russell, J.D., Parfitt, R.L., Fraser, A.R., Farmer, V.C., 1974. Surface structures of gibbsite goethite and phosphated goethite. Nature 248, 220–221.

Sadezky, A., Muckenhuber, H., Grothe, H., Niessner, R., Pöschl, U., 2005. Raman microspectroscopy of soot and related carbonaceous materials: spectral analysis and structural information. Carbon 43, 1731–1742.

Sánchez-Cortés, S., Francioso, O., Ciavatta, C., García-Ramos, J.V., Gessa, C., 1998. pH-dependent adsorption of fractionated peat humic substances on different silver colloids studied by surface-enhanced Raman spectroscopy. J. Colloid Interface Sci. 198, 308–318.

Sanchez-Cortes, S.C.G., Trubetskaya, O.E., Trubetskoj, O.A., Hermosin, B., Saiz-Jimenez, C., 2006. Surface-enhanced Raman spectroscopy of chernozem humic acid and their fractions obtained by coupled size exclusion chromatography-polyacrylamide gel electrophoresis (SEC-PAGE). Appl. Spectrosc. 60, 48–53.

Sánchez- Monedero, M.A., Roig, A., Cegarra, J., Bernal, M.P., Paredes, C., 2002. Effects of HCl–HF purification treatment on chemical composition and structure of humic acids. European Journal of Soil Science 53, 375–381.

Sarkhot, D.V., Comerford, N.B., Jokela, E.J., Reeves, J.B., Harris, W.G., 2007a. Aggregation and aggregate carbon in a forested southeastern coastal plain spodosol (All rights reserved. No part of this periodical may be reproduced or transmitted in any form or by any means, electronic or mechanical, including photocopying, recording, or any information storage and retrieval system, without permission in writing from the publisher. Permission for printing and for reprinting the material contained herein has been obtained by the publisher) Soil Sci. Soc. Am. J. 71, 1779–1787.

Sarkhot, D.V., Comerford, N.B., Jokela, E.J., Reeves III, J.B., Harris, W.G., 2007b. Aggregation and aggregate carbon in a forested southeastern coastal plain spodosol. Soil Sci. Soc. Am. J. 71, 1779–1787.

Schenzel, K., Fischer, S., 2001. NIR FT Raman Spectroscopy–a Rapid Analytical Tool for Detecting the Transformation of Cellulose Polymorphs. Cellulose 8, 49–57.

Scherrer, S., Diniz, I., Morais, H., 2010. Climate and host plant characteristics effects on lepidopteran caterpillar abundance on Miconia ferruginata DC. and Miconia pohliana Cogn (Melastomataceae). Brazilian Journal of Biology 70, 103–109.

Schmidt, M.W.I., Skjemstad, J.O., Jager, C., 2002. Carbon isotope geochemistry and nanomorphology of soil black carbon: black chernozemic soils in central Europe originate from ancient biomass burning. Glob. Biogeochem. Cycles 16.

Schmidt, M.W.I., Torn, M.S., Abiven, S., Dittmar, T., Guggenberger, G., Janssens, I.A., Kleber, M., Kogel-Knabner, I., Lehmann, J., Manning, D.A.C., Nannipieri, P., Rasse, D.P., Weiner, S., Trumbore, S.E., 2011. Persistence of soil organic matter as an ecosystem property. Nature 478, 49–56.

Schmitt, J., Flemming, H.C., 1998. FTIR-spectroscopy in microbial and material analysis. Int. Biodeterior. Biodegrad. 41, 1–11.

Schmitt, J., Flemming, H.C., 1999. Water binding in biofilms. Water Sci. Technol. 39, 77–82.

Schmitt, J., Nivens, D., White, D.C., Flemming, H.C., 1995. Changes of biofilm properties in response to sorbed substances—an FTIR-ATR study. Water Sci. Technol. 32, 149–155.

Schnitzer, M., Monreal, C.M., 2011. Chapter three—Quo Vadis soil organic matter research? A biological link to the chemistry of humification. In: Donald, L.S. (Ed.), Advances in Agronomy, vol. 113. Academic Press, pp. 143–217.
Schrader, B., Hoffmann, A., Keller, S., 1991. Near-infrared Fourier transform Raman spectroscopy: facing absorption and background. Spectrochim. Acta Part A Mol. Spectrosc. 47, 1135–1148.
Schrader, B., Schulz, H., Andreev, G.N., Klump, H.H., Sawatzki, J., 2000. Non-destructive NIR-FT-Raman spectroscopy of plant and animal tissues, of food and works of art. Talanta 53, 35–45.
Schuttlefield, J.D., Cox, D., Grassian, V.H., 2007. An investigation of water uptake on clays minerals using ATR-FTIR spectroscopy coupled with quartz crystal microbalance measurements. J. Geophys. Res. Atmos. 112.
Schwertmann, U., Cornell, R.M., 1991. Iron Oxides in the Laboratory: Preparation and Characterization, second ed. Wiley-VCH, Weinheim.
Schwertmann, U., Cornell, R.M., 2000. Iron Oxides in the Labrotory. Wiley-VCH, Weinheim, Germany.
Schwertmann, U., Taylor, R.M., 1989. Iron oxides. In: Klute, A. (Ed.), Methods of Soil Analysis, Part 1—Physical and Mineralogical Methods, vol. 5. SSSA, Madison, WI, pp. 379–438.
Senesi, N., D'Orazio, V., Ricca, G., 2003. Humic acids in the first generation of EUROSOILS. Geoderma 116, 325–344.
Senesi, N., Plaza, C., Brunetti, G., Polo, A., 2007. A comparative survey of recent results on humic-like fractions in organic amendments and effects on native soil humic substances. Soil Biol. Biochem. 39, 1244–1262.
Sham, T.K., Rivers, M.L., 2002. A brief overview of synchrotron radiation. Rev. Mineral. Geochem. 49, 117–147.
Sharma, B.K., 2004. Instrumental Methods of Chemical Analysis. Goel Publishing House, Meerut, India.
Sharma, R.K., Wooten, J.B., Baliga, V.L., Lin, X., Geoffrey Chan, W., Hajaligol, M.R., 2004. Characterization of chars from pyrolysis of lignin. Fuel 83, 1469–1482.
Sheals, J., Sjoberg, S., Persson, P., 2002. Adsorption of glyphosate on goethite: molecular characterization of surface complexes. Environ. Sci. Technol. 36, 3090–3095.
Shearer, J.C., Peters, D.C., 1987. Fourier transform infrared microspectrophotometry as a failure analysis tool. In: Roush, P.B. (Ed.), The design, sample handling, and applications of infrared microscopes. ASTM Committee E-13 on Molecular Spectroscopy Federation of Analytical Chemistry Spectroscopy Societies.
Sheng, G.Y., Johnston, C.T., Teppen, B.J., Boyd, S.A., 2002. Adsorption of dinitrophenol herbicides from water by montmorillonites. Clays Clay Miner. 50, 25–34.
Shimizu, M., Ginder-Vogel, M., Parikh, S.J., Sparks, D.L., 2010. Molecular scale assessment of methylarsenic sorption on aluminum oxide. Environ. Sci. Technol. 44, 612–617.
Siebielec, G., McCarthy, G.W., Stuczynski, T.I., Reeves, J.B., 2004. Near- and mid-infrared diffuse reflectance spectroscopy for measuring soil metal content. J. Environ. Qual. 33, 2056–2069.
Simon, 2007. Quantitative and qualitative characterization of soil organic matter in the long-term fallow experiment with different fertilization and tillage. Archives Agronomy Soil Sci. 53, 241–251.
Šimon, T., Javůrek, M., Mikanová, O., Vach, M., 2009. The influence of tillage systems on soil organic matter and soil hydrophobicity. Soil Tillage Res. 105, 44–48.
Simonetti, G., Francioso, O., Nardi, S., Berti, A., Brugnoli, E., Francesco Morari, E.L., 2012. Characterization of humic carbon in soil aggregates in a long-term experiment with manure and mineral fertilization. Soil Sci. Soc. Am. J. 76, 880–890.

Singh, B., Singh, B.P., Cowie, A., 2010. Characterisation and evaluation of biochars for their application as a soil amendment. Aust. J. Soil Res. 48, 516–525.
Siregar, A., Kleber, M., Mikutta, R., Jahn, R., 2005. Sodium hypochlorite oxidation reduces soil organic matter concentrations without affecting inorganic soil constituents. Eur. J. Soil Sci. 56, 481–490.
Six, J., Bossuyt, H., Degryze, S., Denef, K., 2004. A history of research on the link between (micro)aggregates, soil biota, and soil organic matter dynamics. Soil Tillage Res. 79, 7–31.
Slepetiene, A., Liaudanskiene, I., Slepetys, J., Velykis, A., 2010. The influence of reduced tillage, winter crops and ecologically managed long-term mono- and multi-component swards on soil humic substances. Chem. Ecol. 26, 97–109.
Smith, E., Dent, G., 2005. "Modern Raman spectroscopy: A practical approach," Hoboken, NJ, J. Wiley.
Smidt, E., Meissl, K., 2007. The applicability of Fourier transform infrared (FT-IR) spectroscopy in waste management. Waste Manag. 27, 268–276.
Smidt, E., Schwanninger, M., 2005. Characterization of waste materials using FTIR spectroscopy: process monitoring and quality assessment. Spectrosc. Lett. 38, 247–270.
Smith, B., 2011. Fundamentals of Fourier Transform Ifrared Spectroscopy. CRC PRess, Boca Raton.
Smith, E., 2005. Modern Raman Spectroscopy: A Practical Approach. J. Wiley, Hoboken, NJ.
Smith, N.J.H., 1980. Anthrosols and human carrying capacity in Amazonia*. Ann. Assoc. Am. Geogr. 70, 553–566.
Snabe, T., Petersen, S.B., 2002. Application of infrared spectroscopy (attenuated total reflection) for monitoring enzymatic activity on substrate films. J. Biotechnol. 95, 145–155.
Sobkowiak, M., Painter, P., 1992. Determination of the aliphatic and aromatic CH contents of coals by FT-i.r.: studies of coal extracts. Fuel 71, 1105–1125.
Sockalingum, G.D., Bouhedja, W., Pina, P., Allouch, P., Mandray, C., Labia, R., et al., 1997. ATR-FTIR Spectroscopic Investigation of Imipenem-Susceptible and -Resistant *Pseudomonas aeruginosa* Isogenic Strains. Biochem. Biophys. Res. Commun. 232, 240–246.
Sohi, S.P., Krull, E., Lopez-Capel, E., Bol, R., 2010. Chapter 2-A review of biochar and its use and function in soil. In: Donald, L.S. (Ed.), Advances in Agronomy, vol. 105. Academic Press, pp. 47–82.
Solomon, D., Lehmann, J., Kinyangi, J., Liang, B.Q., Schafer, T., 2005. Carbon K-edge NEXAFS and FTIR-ATR spectroscopic investigation of organic carbon speciation in soils. Soil Sci. Soc. Am. J. 69, 107–119.
Solomon, D., Lehmann, J., Kinyangi, J., Amelung, W., Lobe, I., Pell, A., Riha, S., Ngoze, S., Verchot, L.O.U., Mbugua, D., Skjemstad, J.A.N., Schäfer, T., 2007a. Long-term impacts of anthropogenic perturbations on dynamics and speciation of organic carbon in tropical forest and subtropical grassland ecosystems. Glob. Change Biol. 13, 511–530.
Solomon, D., Lehmann, J., Thies, J., Schäfer, T., Liang, B., Kinyangi, J., Neves, E., Petersen, J., Luizão, F., Skjemstad, J., 2007b. Molecular signature and sources of biochemical recalcitrance of organic C in Amazonian Dark Earths. Geochim. Cosmochim. Acta 71, 2285–2298.
Solomon, D., Lehmann, J., Wang, J., Kinyangi, J., Heymann, K., Lu, Y., Wirick, S., Jacobsen, C., 2012. Micro- and nano-environments of C sequestration in soil: a multi-elemental STXM–NEXAFS assessment of black C and organomineral associations. Sci. Total Environ. 438, 372–388.
Sombroek, W., Ruivo, M.L., Fearnside, P.M., Glaser, B., Lehmann, J., 2003. Amazonian Dark Earths as carbon stores and sinks. In: Lehmann, J., Kern, D.C., Glaser, B., Woods, W.I. (Eds.), Amazonian Dark Earths: Origin, Properties, Management. Kluwer Academic Publishers, The Netherlands, pp. 125–139.
Sombroek, W.G., 1966. Amazon Soils a Reconnaissance of the Soils of the Brazilian Amazon Region.

Song, Y.P., Yarwood, J., Tsibouklis, J., Feast, W.J., Cresswell, J., Petty, M.C., 1992. Fourier-transform infrared spectroscopic studies on alternate-layer Langmuir–Blodgett-films with nonlinear optical-properties. Langmuir 8, 262–266.
Song, Z., Chouparova, E., Jones, K.W., Feng, H., Marinkovic, N.S., 2001. FTIR Investigation of Sediments from NY/NJ Harbor, San Diego Bay, and the Venetian Lagoon. NSLS(Activity Report).
Soukup, D.A., Buck, B.J., Harris, W., 2008. Preparing soils for mineralogical analyses. In: Ulery, A.L., Drees, L.R. (Eds.), Methods of Soil Analysis, Part 5-Mineralogical Methods. Soil Science Socity of America, Madison, WI.
Sparks, D.L., 1995. Environmental Soil Chemistry. Academic Press, Inc., San Diego, CA.
Sparks, D.L., 2002. Environmental Soil Chemistry. Elsevier Science.
Spath, R., Flemming, H.C., Wuertz, S., 1998. Sorption properties of biofilms. Water Sci. Technol. 37, 207–210.
Spedding, F.H., Stamm, R.F., 1942. The Raman spectra of the sugars in the solid state and in solution I. The Raman spectra of alpha- and beta-D-glucose. J. Chem. Phys. 10, 176–183.
Specht, C.H., Frimmel, F.H., 2001. An in Situ ATR-FTIR Study on the Adsorption of Dicarboxylic Acids Onto Kaolinite in Aqueous Suspensions. Physical Chemistry Chemical Physics 3, 5444–5449.
Sposito, G., 1989. The Chemsitry of Soils. Oxford University Press, New York.
Sposito, G., 2004. The Surface Chemistry of Natural Particles. Oxford University Press, New York.
Sposito, G., Martin-Neto, L., Yang, A., 1996. Atrazine Complexation by Soil Humic Acids. J. Environ. Qual. 25, 1203–1209.
Starsinic, M., Taylor, R.L., Walker Jr., P.L., Painter, P.C., 1983. FTIR studies of Saran chars. Carbon 21, 69–74.
Steinbeiss, S., Gleixner, G., Antonietti, M., 2009. Effect of biochar amendment on soil carbon balance and soil microbial activity. Soil Biol. Biochem. 41, 1301–1310.
Stenberg, B., Viscarra Rossel, R.A., Mouazen, A.M., Wetterlind, J., 2010. Chapter five—visible and near infrared spectroscopy in soil science. In: Donald, L.S. (Ed.), Advances in Agronomy, vol. 107. Academic Press, pp. 163–215.
Stevenson, F.J., Goh, K.M., 1971. Infrared spectra of humic acids and related substances. Geochim. Cosmochim. Acta 35, 471–483.
Stiles, P.L., Dieringer, J.A., Shah, N.C., Van Duyne, R.P., 2008. Surface-enhanced Raman spectroscopy. Annu. Rev. Anal. Chem. 1, 601–626.
Stokes, D.L., Wullschleger, S., Martin, M., Vo-Dinh, T., 2003. Raman Spectroscopy and Instrumentation for Monitoring Soil Carbon Systems. Environmental Sciences Division Oak Ridge National Laboratory.
Strojek, J.W., Mielczar, J.A., 1974. Internal-reflection spectroscopy for investigations of sorption on powders. Rocz. Chem. 48, 1747–1751.
Stuart, B., 2000. Infrared spectroscopy. In: Kirk-Othmer Encyclopedia of Chemical Technology. John Wiley & Sons, Inc.
Su, C., Suarez, D.L., 1995. Coordination of Adsorbed Boron: A FTIR Spectroscopic Study. Environ. Sci. Technol. 29, 302–311.
Su, C.M., Suarez, D.L., 1997a. Boron sorption and release by allophane. Soil Science Society of America Journal 61, 69–77.
Su, C.M., Suarez, D.L., 1997b. In situ infrared speciation of absorbed carbonate on aluminum and iron oxide. Clays Clay Miner. 45, 814–825.
Su, C., Suarez, D.L., 2000. Selenate and Selenite Sorption on Iron Oxides An Infrared and Electrophoretic Study Soil Sci. Soc. Am. J 64, 101–111.
Suarez, D.L., Goldberg, S., Su, C., 1999. Evaluation of oxyanion adsorption mechanisms on oxides using FTIR spectroscopy and electrophoretic mobility. In: Mineral-Water Interfacial Reactions, vol. 715, American Chemical Society, pp. 136–178.

Suci, P.A., Vrany, J.D., Mittelman, M.W., 1998. Investigation of interactions between antimicrobial agents and bacterial biofilms using attenuated total reflection Fourier transform infrared spectroscopy. Biomaterials 19, 327–339.

Sullivan, L.A., Koppi, A.J., 1987. In-situ soil organic matter studies using scanning electron microscopy and low temperature ashing. Geoderma 40, 317–332.

Summons, R.E., Amend, J.P., Bish, D., Buick, R., Cody, G.D., Des Marais, D.J., Dromart, G., Eigenbrode, J.L., Knoll, A.H., Sumner, D.Y., 2011. Preservation of martian organic and environmental records: final report of the Mars biosignature working group. Astrobiology 11, 157–181.

Sun, X.H., Doner, H.E., 1996. An investigation of arsenate and arsenite bonding structures on goethite by FTIR. Soil Science 161, 865–872.

Sun, X.H., Doner, H.E., 1998. Adsorption and oxidation of arsenite on goethite. Soil Science 163, 278–287.

Szabó, L., Leopold, L., Cozar, B., Leopold, N., Herman, K., Chiş, V., 2011. SERS approach for Zn(II) detection in contaminated soil. Central Eur. J. Chem. 9, 410–414.

Szlachta, M., Gerda, V., Chubar, N., 2012. Adsorption of arsenite and selenite using an inorganic ion exchanger based on Fe–Mn hydrous oxide. J. Colloid Interface Sci. 365, 213–221.

Tandy, S., Healey, J.R., Nason, M.A., Williamson, J.C., Jones, D.L., Thain, S.C., 2010. FT-IR as an alternative method for measuring chemical properties during composting. Bioresour. Technol. 101, 5431–5436.

Tapia, Y., Cala, V., Eymar, E., Frutos, I., Gárate, A., Masaguer, A., 2010. Chemical characterization and evaluation of composts as organic amendments for immobilizing cadmium. Bioresour. Technol. 101, 5437–5443.

Tatzber, M., Stemmer, M., Spiegel, H., Katzlberger, C., Haberhauer, G., Gerzabek, M.H., 2008. Impact of different tillage practices on molecular characteristics of humic acids in a long-term field experiment—an application of three different spectroscopic methods. Sci. Total Environ. 406, 256–268.

Tatzber, M., Stemmer, M., Spiegel, H., Katzlberger, C., Haberhauer, G., Mentler, A., Gerzabek, M.H., 2007. FTIR-spectroscopic characterization of humic acids and humin fractions obtained by advanced NaOH, $Na_4P_2O_7$, and Na_2CO_3 extraction procedures. J. Plant Nutr. Soil. Sci. 170, 522–529.

Tatzber, M., Stemmer, M., Spiegel, H., Katzlberger, C., Zehetner, F., Haberhauer, G., Garcia-Garcia, E., Gerzabek, M.H., 2009. Spectroscopic behaviour of ^{14}C-labeled humic acids in a long-term field experiment with three cropping systems. Soil Res. 47, 459–469.

Tejedor-Tejedor, M.I., Anderson, M.A., 1986. *In situ* attenuated total reflection Fourier-transform infrared studies of the goethite (α-FeOOH)-aqueous solution interface. Langmuir 2, 203–210.

Tejedor-Tejedor, M.I., Anderson, M.A., 1990. Protonation of phosphate on the surface of goethite as a studied by CIR-FTIR and electrophoretic mobility. Langmuir 6, 602–611.

Tejedor-Tejedor, M.I., Yost, E.C., Anderson, M.A., 1992. Characterization of benzoic and phenolic complexes at the goethite aqueous-solution interface using cylindrical internal-reflection fourier-transform infrared-spectroscopy. 2. Bonding structures. Langmuir 8, 525–533.

Tejedor-Tejedor, M.I., Yost, E.C., Anderson, M.A., 1990. Characterization of benzoic and phenolic complexes at the goethite aqueous-solution interface using cylindrical internal-reflection Fourier-transform infrared-spectroscopy. 1. Methodol. Langmuir 6, 979–987.

Thibeau, R.J., Brown, C.W., Heidersbach, R.H., 1978. Raman spectra of possible corrosion products of iron. Appl. Spectrosc. 32, 532–535.

Tickanen, L.D., Tejedor-Tejedor, M.I., Anderson, M.A., 1997. Quantitative characterization of aqueous suspensions using variable-angle ATR-FTIR spectroscopy: determination of optical constants and absorption coefficient spectra. Langmuir 13, 4829–4836.

Tofan-Lazar, J., Al-Abadleh, H.A., 2012a. ATR-FTIR studies on the adsorption/desorption kinetics of dimethylarsinic acid on iron–(oxyhydr)oxides. J. Phys. Chem. A 116, 1596–1604.

Tofan-Lazar, J., Al-Abadleh, H.A., 2012b. Kinetic ATR-FTIR studies on phosphate adsorption on iron (oxyhydr)oxides in the absence and presence of surface arsenic: molecular-level insights into the ligand exchange mechanism. J. Phys. Chem. A 116, 10143–10149.

Tomić, Z., Makreski, P., Gajić, B., 2010. Identification and spectra–structure determination of soil minerals: Raman study supported by IR spectroscopy and X-ray powder diffraction. J. Raman Spectrosc. 41, 582–586.

Tonon, G., Sohi, S., Francioso, O., Ferrari, E., Montecchio, D., Gioacchini, P., Ciavatta, C., Panzacchi, P., Powlson, D., 2010. Effect of soil pH on the chemical composition of organic matter in physically separated soil fractions in two broadleaf woodland sites at Rothamsted, UK. Eur. J. Soil Sci. 61, 970–979.

Torrent, J., Barrón, V., 2008. Diffuse reflectance spectroscopy. In: Ulery, A.L., Drees, L.R. (Eds.), Methods of Soil Analysis, Part 5-Mineralogical Methods. Soil Science Society of America, Madison, WI.

Tranter, G., Minasny, B., McBratney, A.B., Viscarra Rossel, R.A., Murphy, B.W., 2008. Comparing spectral soil inference systems and mid-infrared spectroscopic predictions of soil moisture retention. Soil. Sci. Soc. Am. J. 72, 1394–1400.

Trivedi, P., Vasudevan, D., 2007. Spectroscopic investigation of ciprofloxacin speciation at the goethite-water interface. Environ. Sci. Technol. 41, 3153–3158.

Tsuboi, M., 1961. Infrared spectra and secondary structure of deoxyribonucleic acid. Prog. Theor. Phys. Suppl. 17, 99–107.

Undabeytia, T., Nir, S., Rubin, B., 2000. Organo-clay formulations of the hydrophobic herbicide norflurazon yield reduced leaching. Journal of Agricultural and Food Chemistry 48, 4767–4773.

Upritchard, H.G., Yang, J., Bremer, P.J., Lamont, I.L., McQuillan, A.J., 2007. Adsorption to metal oxides of the *Pseudomonas aeruginosa* siderophore pyoverdine and implications for bacterial biofilm formation on metals. Langmuir 23, 7189–7195.

Upritchard, H.G., Yang, J., Bremer, P.J., Lamont, I.L., McQuillan, A.J., 2011. Adsorption of enterobactin to metal oxides and the role of siderophores in bacterial adhesion to metals. Langmuir 27, 10587–10596.

Usher, C.R., Paul, K.W., Narayansamy, J., Kubicki, J.D., Sparks, D.L., Schoonen, M.A.A., Strongin, D.R., 2005. Mechanistic aspects of pyrite oxidation in an oxidizing gaseous environment: an in situ HATR-IR isotope study. Environ. Sci. Technol. 39, 7576–7584.

Uyguner-Demirel, C.S., Bekbolet, M., 2011. Significance of analytical parameters for the understanding of natural organic matter in relation to photocatalytic oxidation. Chemosphere 84, 1009–1031.

Vasiliadou, I.A., Papoulis, D., Chrysikopoulos, C.V., Panagiotaras, D., Karakosta, E., Fardis, M., Papavassiliou, G., 2011. Attachment of *Pseudomonas putida* onto differently structured kaolinite minerals: a combined ATR-FTIR and H-1 NMR study. Colloids Surf. B Biointerfaces 84, 354–359.

Vdović, N., Obhođaš, J., Pikelj, K., 2010. Revisiting the particle-size distribution of soils: comparison of different methods and sample pre-treatments. Eur. J. Soil Sci. 61, 854–864.

Ve, N.B., Olk, D.C., Cassman, K.G., 2004. Nitrogen mineralization from humic acid fractions in rice soils depends on degree of humification Journal Series No. 14403 from the Agricultural Research Division, Univ. of Nebraska. Soil Sci. Soc. Am. J. 68, 1278–1284.

Verchot, L.V., Dutaur, L., Shepherd, K.D., Albrecht, A., 2011. Organic matter stabilization in soil aggregates: understanding the biogeochemical mechanisms that determine the fate of carbon inputs in soils. Geoderma 161, 182–193.

Verhejien, F., Jeddery, S., Bastos, A., van der Velde, C.M., Diafas, I., 2010. Biochar Application to Soils. Institute for Environment and Sustainability, European Communities.

Vergnoux, A., Guiliano, M., Di Rocco, R., Domeizel, M., Théraulaz, F., Doumenq, P., 2011. Quantitative and mid-infrared changes of humic substances from burned soils. Environmental Research 111, 205–214.
Veum, J., Goyne, K., Kremer, R., Miles, R., Sudduth, K., 2014. Biological indicators of soil quality and soil organic matter characteristics in an agricultural management continuum. Biogeochemistry 117, 81–99.
Villanueva, U., Raposo, J.C., Castro, K., de Diego, A., Arana, G., Madariaga, J.M., 2008. Raman spectroscopy speciation of natural and anthropogenic solid phases in river and estuarine sediments with appreciable amount of clay and organic matter. J. Raman Spectrosc. 39, 1195–1203.
Villalobos, M., Leckie, J.O., 2001. Surface complexation modeling and FTIR study of carbonate adsorption to goethite. J. Colloid Interface Sci. 235, 15–32.
Villar, S.E.J., Edwards, H.G.M., 2006. Raman spectroscopy in astrobiology. Anal. Bioanal. Chem. 384, 100–113.
Viscarra Rossel, R.A., Cattle, S.R., Ortega, A., Fouad, Y., 2009. In situ measurements of soil colour, mineral composition and clay content by vis-NIR spectroscopy. Geoderma 150, 253–266.
Viscarra Rossel, R.A., McGlynn, R.N., McBratney, A.B., 2006. Determing the composition of mineral-organic mixes using UV-vis-NIR diffuse reflectance spectroscopy. Geoderma 137, 70–82.
Voegelin, A., Hug, S.J., 2003. Catalyzed oxidation of arsenic(III) by hydrogen peroxide on the surface of ferrihydrite: An in situ ATR-FTIR study. Environ. Sci. Technol 37, 972–978.
Vogel, E., Geßner, R., Hayes, M.H.B., Kiefer, W., 1999. Characterisation of humic acid by means of SERS. J. Mol. Struct. 482–483, 195–199.
von Lützow, M., Kögel-Knabner, I., Ekschmitt, K., Flessa, H., Guggenberger, G., Matzner, E., Marschner, B., 2007. SOM fractionation methods: relevance to functional pools and to stabilization mechanisms. Soil Biol. Biochem. 39, 2183–2207.
Wan, J., Tyliszczak, T., Tokunaga, T.K., 2007. Organic carbon distribution, speciation, and elemental correlations within soil microaggregates: applications of STXM and NEXAFS spectroscopy. Geochim. Cosmochim. Acta 71, 5439–5449.
Wang, A., Freeman, J.J., Jolliff, B.L., Chou, I.M., 2006. Sulfates on Mars: a systematic Raman spectroscopic study of hydration states of magnesium sulfates. Geochim. Cosmochim. Acta 70, 6118–6135.
Wang, C.-J., Li, Z., Jiang, W.-T., Jean, J.-S., Liu, C.-C., 2010. Cation exchange interaction between antibiotic ciprofloxacin and montmorillonite. J. Hazard. Mater. 183, 309–314.
Wang, C.J., Li, Z., Jiang, W.T., 2011. Adsorption of ciprofloxacin on 2:1 dioctahedral clay minerals. Appl. Clay Sci. 53, 723–728.
Wang, H., Hollywood, K., Jarvis, R.M., Lloyd, J.R., Goodacre, R., 2010. Phenotypic characterization of Shewanella oneidensis MR-1 under aerobic and anaerobic growth conditions by using Fourier transform infrared spectroscopy and high-performance liquid chromatography analyses. Appl. Environ. Microbiol. 76, 6266–6276.
Wang, S., Mulligan, C.N., 2008. Speciation and surface structure of inorganic arsenic in solid phases: a review. Environ. Int. 34, 867–879.
Wang, S.L., Johnston, C.T., 2000. Assignment of the structural OH stretching bands of gibbsite. Am. Mineral. 85, 739–744.
Wang, Y.S., Muramatsu, A., Sugimoto, T., 1998. FTIR analysis of well-defined alpha-Fe_2O_3 particles. Colloids Surf. A Physicochem. Eng. Aspects 134, 281–297.
Watanabe, A., Kawasaki, S., Kitamura, S., Yoshida, S., 2007. Temporal changes in humic acids in cultivated soils with continuous manure application. Soil. Sci. Plant Nutr. 53, 535–544.
Weisz, A.D., Regazzoni, A.E., Blesa, M.A., 2001. ATR-FTIR study of the stability trends of carboxylate complexes formed on the surface of titanium dioxide particles immersed in water. Solid State Ionics 143, 125–130.

Weisz, A.D., Rodenas, L.G., Morando, P.J., Regazzoni, A.E., Blesa, M.A., 2002. FTIR study of the adsorption of single pollutants and mixtures of pollutants onto titanium dioxide in water: oxalic and salicylic acids. Catal. Today 76, 103–112.

Wershaw, R.L., Leenheer, J.A., Kennedy, K.R., Noyes, T.I., 1996. Use of ^{13}C NMR and FTIR for elucidation of degradation pathways during natural litter decomposition and composting I. Early stage leaf degradation. Soil Sci. 161, 667–679.

Whitbread, A., 1994. Soil organic matter: its fractionation and role in soil structure. In: Lefroy, R., Blair, G., Craswell, E. (Eds.), Soil Organic Matter Management for Sustainable Agriculture, vol. 56. ACIAR, Canberra, pp. 124–130 (ACT, Ubon, Thailand).

Wilkinson, T.J., Perry, D., McKinney, M., Martin, M.Z., 2002. Physics and forensics. In: Physics World, Vol. 15, pp. 43–46.

Wingender, J., Neu, T.R., Flemming, H.C., 1999. What are bacterial extracellular polymeric substances? In: Wingender, J., Neu, T.R., Flemming, H.C. (Eds.), Microbial Extracellular Polymeric Substances: Characterization, Structure, and Function. Springer, Berlin, pp. 1–15.

Wingender, J., Strathmann, M., Rode, A., Leis, A., Flemming, H.-C., 2001. Isolation and biochemical characterization of extracellular polymeric substances from *Pseudomonas aeruginosa*. In: Doyle, R.J. (Ed.), Microbial Growth in Biofilms, Part A: development and molecular biological aspects, vol. 336. Academic Press, New York, pp. 303–314.

Wijnja, H., Schulthess, C.P., 1999. ATR-FTIR and DRIFT spectroscopy of carbonate species at the aged gamma-Al2O3/water interface. Spectrochimica Acta Part a-Molecular and Biomolecular Spectroscopy 55, 861–872.

Wijnja, H., Schulthess, C.P., 2001. Carbonate adsorption mechanism on goethite studied with ATR-FTIR, DRIFT, and proton coadsorption measurements. Soil Science Society of America Journal 65, 324–330.

Wiseman, C.L.S., Püttmann, W., 2006. Interactions between mineral phases in the preservation of soil organic matter. Geoderma 134, 109–118.

Wolf, E.E., Yuh, S.J., 1984. Kinetic and FTIR studies of steam gasification of coal chars catalyzed by alkali salts. Abstr. Pap. Am. Chem. Soc. 187, 43. FUEL.

Woodwell, G.M., 1984. The Role of Terrestrial Vegetation in the Global Carbon Cycle: Measurement by Remote Sensing. Published on behalf of the Scientific Committee on Problems of the Environment (SCOPE) of the International Council of Scientific Unions (ICSU) by Wiley, New York.

Wu, H., Yip, K., Tian, F., Xie, Z., Li, C.-Z., 2009. Evolution of char structure during the steam gasification of biochars produced from the pyrolysis of various Mallee biomass components. Ind. Eng. Chem. Res. 48, 10431–10438.

Wu, Q., Li, Z., Hong, H., Yin, K., Tie, L., 2010. Adsorption and intercalation of ciprofloxacin on montmorillonite. Appl. Clay Sci. 50, 204–211.

Wu, S.H., Goyne, K.W., Lerch, R.N., Lin, C.-H., 2011. Adsorption of isoxaflutole degradates to aluminum and iron hydrous oxides. J. Environ. Qual. 40, 528–537.

Wu, Q., Li, Z., Hong, H., 2013a. Adsorption of the quinolone antibiotic nalidixic acid onto montmorillonite and kaolinite. Applied Clay Science 74, 66–73.

Wu, Q., Li, Z., Hong, H., Li, R., Jiang, W.-T., 2013b. Desorption of ciprofloxacin from clay mineral surfaces. Water Res. 47, 259–268.

Wullschleger, S.D., Martin, M.Z., Vo-Dinh, T., Griffin, G.D., Stokes, D.L., Wintenberg, A.L., 2003. Advanced Instrumentation for In Situ Field Monitoring of Soil Carbon Sequestration. Oak Ridge National Laboratory.

Xie, C., Li, Y.-q, 2003. Confocal micro-Raman spectroscopy of single biological cells using optical trapping and shifted excitation difference techniques. J. Appl. Phys. 93, 2982–2986.

Yan, W., Hu, S., Jing, C., 2012. Enrofloxacin sorption on smectite clays: effects of pH, cations, and humic acid. J. Colloid Interface Sci. 372, 141–147.

Yang, X.M., Xie, H.T., Drury, C.F., Reynolds, W.D., Yang, J.Y., Zhang, X.D., 2012. Determination of organic carbon and nitrogen in particulate organic matter and particle size fractions of Brookston clay loam soil using infrared spectroscopy. Eur. J. Soil Sci. 63, 177–188.

Yang, Y.-h., Li, B.-n., Tao, Z.-y., 1994. Characterization of humic substances by laser Raman spectroscopy. Spectrosc. Lett. 27, 649–660.

Yang, Y.-h., Wang, T., 1997. Fourier transform Raman spectroscopic characterization of humic substances. Vib. Spectrosc. 14, 105–112.

Yang, Y., Chase, H.A., 1998. Applications of Raman and surface-enhanced raman scattering techniques to humic substances. Spectrosc. Lett. 31, 821–848.

Yoon, T.H., Johnson, S.B., Musgrave, C.B., Brown, G.E., 2004a. Adsorption of organic matter at mineral/water interfaces: I. ATR-FTIR spectroscopic and quantum chemical study of oxalate adsorbed at boehmite/water and corundum/water interfaces. Geochim. Cosmochim. Acta 68, 4505–4518.

Yoon, T.H., Johnson, S.B., Brown, G.E., 2004b. Adsorption of Suwannee River fulvic acid on aluminum oxyhydroxide surfaces: An in situ ATR-FTIR study. Langmuir 20, 5655–5658.

Yu, C., Irudayaraj, J., 2005. Spectroscopic characterization of microorganisms by Fourier transform infrared microspectroscopy. Biopolymers 77, 368–377.

Zhang, J., Dai, J., Wang, R., Li, F., Wang, W., 2009. Adsorption and desorption of divalent mercury (Hg^{2+}) on humic acids and fulvic acids extracted from typical soils in China. Colloids Surf. A Physicochem. Eng. Aspects 335, 194–201.

Zhao, J., Peng, P.A., Song, J., Ma, S., Sheng, G., Fu, J., 2011. Characterization of macromolecular organic matter in atmospheric dust from Guangzhou, China. Atmos. Environ. 45, 5612–5620.

Zhao, W., Liu, F., Feng, X., Tan, W., Qiu, G., Chen, X., 2012a. Fourier transform infrared spectroscopy study of acid birnessites before and after Pb^{2+} adsorption. Clay Miner. 47, 191–204.

Zhao, Y., Gu, X., Gao, S., Geng, J., Wang, X., 2012b. Adsorption of tetracycline (TC) onto montmorillonite: cations and humic acid effects. Geoderma 183, 12–18.

Zheng, L., Lee, W.S., Li, M., Katti, A., Yang, C., Li, H., Sun, H., 2012. Analysis of Soil Phosphorus Concentration Based on Raman Spectroscopy. 852718–852718.

Zhou, Y., Li, Y., 2004. Studies of interaction between poly(allylamine hydrochloride) and double helix DNA by spectral methods. Biophys. Chem. 107, 273–281.

Zimba, C.G., Hallmark, V.M., Swalen, J.D., Rabolt, J.F., 1987. Fourier-transform Raman-spectroscopy of long-chain molecules containing strongly absorbing chromophores. Appl. Spectrosc. 41, 721–726.

Zimmerman, A.R., Gao, B., Ahn, M.-Y., 2011. Positive and negative carbon mineralization priming effects among a variety of biochar-amended soils. Soil Biol. Biochem. 43, 1169–1179.